Polyyne Rotaxanes

Levon D. Movsisyan

Hertford College

University of Oxford

A thesis submitted in partial fulfillment of the requirements for the degree of

Doctor of Philosophy

Trinity Term 2014

Polyyne Rotaxanes

Levon D. Movsisyan, Hertford College, University of Oxford

D.Phil. Thesis, Trinity Term 2014

This thesis describes the synthesis of polyyne rotaxanes and an investigation of their excited state photophysical properties. The threading of dumbbell-shaped carbon chains with macrocyclic components is a way to mechanically insulate and control the environment around the carbon chains. The resulting polyyne rotaxanes can serve as model compounds for insulated carbyne. Different strategies have been tested for the synthesis of polyyne rotaxanes with different topologies and structures. Study of rotaxanes in the excited states reveals strong electronic communication between an acetylenic thread and a macrocycle.

Chapter 1 summarizes the field of acetylene scaffolding, introducing some recent achievements in acetylene chemistry. General synthetic methods for polyynes are discussed, and an introduction to active-metal template synthesis of rotaxanes is given.

Chapter 2 describes the synthesis of a family of polyyne rotaxanes with different axle lengths and macrocycles, prepared by homocoupling of terminal alkynes. Synthesis of hexayne rotaxane with functional pyridine end-group is presented and a number of crystal structures of polyyne rotaxanes are analyzed.

Chapter 3 demonstrates the use of acetylene cross-coupling in the synthesis of rotaxanes. Synthesis of rotaxanes with different topological structure is provided.

Chapter 4 details the excited state properties of polyynes studied by time-resolved spectroscopy. The complexes of rhenium(I) carbonyls with rotaxanes is presented and the excited state energy transfer in rotaxanes is studied.

Chapter 5 explores new synthetic strategies for polyyne rotaxanes, using "masked" precursors. It also highlights the potential of carbenoid rearrangement of alkylidenes for the construction of linear and cyclic architectures.

Chapter 6 is the summary of the project and general discussion of future directions.

There are two appendices in the end of thesis: *Appendix A* covers the photophysics of rhenium tricarbonyl complex of the hexayne rotaxane with a small macrocycle and *Appendix B* reports work towards the synthesis of rotaxanes with platinum(II)-alkyne complexes.

Acknowledgments

I want to thank my supervisor Harry who trusted me with a project in his group and for his support, patient guidance throughout my studies in Oxford.

The study presented here would not be possible to carry out without the contribution that collaborators had in the project. My gratitude to Prof. Rik R. Tykwinski for hosting me in the University of Erlangen-Nuremberg, Germany, and giving me an opportunity to learn the fascinating synthetic chemistry of polyynes in his laboratory. Thank you to Michael Franz for being three years in a direct collaboration with me cross the border and greatly supporting the successful start of the project.

I express my gratitude to Prof. Tony Parker, Prof. Mike Towrie and Dr. Greg Greetham, (Central Laser Facilities at Harwell) for the spent intense time on TR spectroscopy experiments, late night brainstormings in the lab and intriguing conversations over the coffee breaks.

Dr. Amber L. Thompson (Oxford Crystallography) helped me with many crystal structures. My thanks to Dr. Barbara Odell (Oxford NMR) for NMR experimental support, Dr Steve Goldup (University of Southampton) for collaboration on rotaxanes.

I want to thank to my high school chemistry teacher Mr. Norayr Poghosyan for showing me the beauty of chemistry, my previous supervisors Dr Robert Karapetyan and Dr Tigran Kurtikyan who guided my early steps in the chemistry laboratory, and also all former and present members of Anderson group for having joyful time and assistance inside and outside of lab. Thanks to Dima for supervising my first year in Oxford, Cecile, Sophie and Julien for proofreading my thesis. Thanks to G2&G1 guys, particularly Igor, Karolina, Phil, Pengpeng, James, Nun, Pati, Martin, Christiane and Rene for sharing together sunny and rainy days.

I want to thank my friends outside the lab. Aleksandr for your encouragement to apply to University of Oxford and for your endless motivation. Tigran and Hayk for sport and so many go outs in Oxford. Haykaz, Boris, Vahe for just being of my friends.

In the end I want to thank my parents Mam, Dad and my sister Lilit for their priceless love, support and encouragement throughout my years of being abroad.

Table of Contents

List of symbols and abbreviations

Å	Angstrom
δ	chemical shift
Δ	absorption difference
ε	molar extinction coefficient
λ	wavelength
μ	micro
ν	vibrational mode, frequency
τ	time constant
ϕ	angle
aq	aqueous
AFM	atomic force microscopy
Ar	aryl
bipy	4,4'-bipyridine
BLA	bond length alternation
BQ	1,4-benzpquinone
Bu	butyl
CCDC	Cambridge Crystallographic Data Centre
cm	centimeter(s)
d	doublet
Da	Dalton
DCM	dichloromethane
DMF	*N*,*N*-dimethylformamide
DMSO	dimethylsulfoxide
ECL	effective conjugation length
EI MS	electron impact mass spectroscopy
ESI	electrospray ionization
Et	ethyl
EtOAc	ethyl acetate
eq.	equivalent(s)
EET	excitation energy transfer
eV	electron volts
FBW	Fritsch-Buttenberg-Wiechell
FTIR	Fourier transform infrared spectroscopy
FVP	flash-vacuum-pyrolysis
g	gram(s)
h	hour(s)
HOMO	highest occupied molecular orbital
HRMS	high resolution mass spectrometry
Hz	Hertz
i	iso
IC	internal conversion
ISC	intersystem crossing
IR	infrared
J	coupling constant
L	liter
LDA	lithium diisopropylamine
LUMO	lowest unoccupied molecular orbital
m	multiplet
M	molar
MALDI	matrix-assisted laser desorption ionization
Me	methyl
mg	milligram(s)
MHz	megaHertz
mL	milliliter(s)
mmol	millimole(s)
mol	mole(s)
Mp	melting point
MS	mass spectroscopy
m/z	mass-to-charge ratio
n-BuLi	*n*-butyllithium
NBS	*N*-bromosuccinimide
NIR	near infared
nm	nanometer(s)
NMR	nuclear magnetic resonance
NOE	nuclear Overhauser effect
ns	nanosecond
p	*para*

Ph	phenyl
PCC	pyridinium chlorochromate
ppm	parts per million
Pr	propyl
ps	picosecond
Py	pyridine
q	quartet
R_f	retention factor
ROESY	Rotating-frame nuclear Overhauser effect correlation spectroscopy singlet
SEC	size exclusion chromatography
t	triplet
t	tertiary
TA	transient absorption
TBAF	tetrabutyl ammonium fluoride
TEM	transmission electron microscopy
THF	tetraydrofuran
TIPS	triisopropylsilyl
TLC	thin layer chromatography
TMEDA	*N*,*N*,*N*′ ,*N*′-tetramethylethylenediamine
TMS	trimethylsilyl
TOF	time-of-flight
tol	tolyl
TR	time-resolved
Tr*	supertrityl [tris(3,5-di-*t*-butylphenyl)methyl]
UV	ultraviolet
UV-Vis	ultraviolet-visible
vw	very weak
w	weak

To my family

Chapter 1. General Introduction

1.1 Carbon-rich materials and acetylene scaffolding

Carbonaceous materials play an important role in a wide range of technological fields and have prompted intense research efforts among scientists across various disciplines.[1] The allotropes diamond and graphite have been known for thousands of years, but the constant search for novel materials with new and improved properties has led to a variety of investigations into the field of carbon-rich materials.[2] Particularly, carbon materials, like zero-dimensional fullerenes, one-dimensional carbon nanotubes (CNTs), two-dimensional graphene, and three-dimensional nanocrystalline diamond films (Figure 1.1) have been used in various applications as novel energy sources and storage materials, high performance construction and organic electronic materials.[2,3]

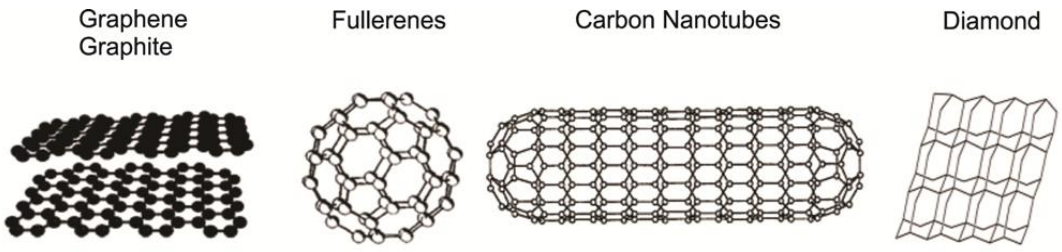

Figure 1.1 Known allotropes of carbon.

Although it would be impossible to review advances in carbonaceous materials exhaustively in this introductory chapter, it is useful to discuss a selection of relevant examples. For instance, one extensively researched field is the use of carbon materials as insertion electrodes in rechargeable lithium batteries.[4] Reversible formation of lithium-carbon intercalation complexes plays a central role in the operation of lithium batteries, where many properties of battery electrodes depend on the crystallinity and micromorphology of the carbonaceous materials. Furthermore, carbonaceous nanostructured materials such as carbon fibers, due to their high tensile strength, low density (1800 kg/m^3) and high chemical inertness have been used for fabrication of carbon fiber reinforced polymers and other composites.[5] The demand for carbon fiber composites is increasing constantly and is expected to reach US$18.6 billion by 2015.[6] These two examples are among numerous applications of carbonaceous materials, the technological importance of which sparked interest in the development of new carbon allotropes and carbon-rich analogs. One of the main problems on the route to carbon composites is the production cost of large quantities of pure materials. Typical preparative methods have recently been reviewed[7] and include arc-

discharge methods,[8] laser ablation techniques,[9] oxidative combustion[10] and chemical vapour deposition.[11] These methods are based on harsh reaction conditions, do not allow the preservation of chemical functionalities and typically yield significant amounts of impurities, like catalyst contamination, amorphous carbon materials or structural defects. This major drawback has motivated organic chemists to develop stepwise synthetic approaches toward molecular carbon nanostructures. For example, a tremendous advancement has been achieved in synthetic organic methods for the postsynthetic functionalization of fullerenes,[7b] whereas the chemical stability and low solubility of CNTs creates challenges for their functionalization.[7c] While a number of purification and functionalization procedures for CNTs have been reported,[7d] the lack of control over the aggregation of the resulting carbon species, and structural changes during the functionalization are still a major problem.

The acetylene motif is a very interesting chemical group for the bottom-up synthesis of carbon-rich materials. Remarkable advancements have been achieved in preparative alkyne chemistry, and a plethora of novel sp^1 carbon-based compounds have been generated during the last 30 years by means of stepwise chemical reactions.[12] For example, one of the impressive achievements of stepwise synthesis of acetylene nanostructures was reported by Diederich and co-workers, who used a small, simple, differentially silyl-protected tris(alkynyl)methyl methyl ether **1.1** as a building block to construct an expanded octa(methoxy)-cubane **1.2** through four steps (Scheme1.1).[13] This extended version of cubane is interesting for its physical properties, in particular, for the thermochemical quantities as a cage compound.

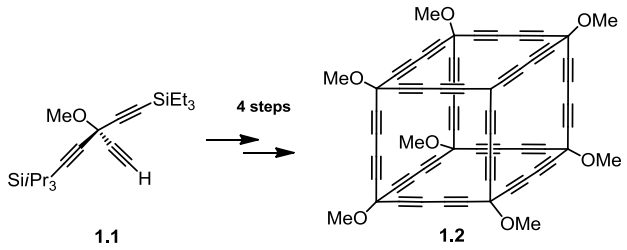

Scheme 1.1 Differentially silyl-protected tris(alkynyl)methyl methyl ether **1.1** as a corner module in the synthesis of expanded cubane **1.2** with a central C56 core.[13]

The preparation of simple carbon-rich building blocks to assemble various acetylenic frameworks via coupling reactions has been intensively investigated for the acetylenic scaffolding in one, two, and three dimensions. (*E,Z*)-1,2-Diethynylethenes (DEEs),[14] tetraethynylethenes (TEEs)[15] and tetraethynylmethane (TEM)[16] (Chart 1.1) served as starting materials for the construction of well-defined, carbon-rich molecular architectures and advanced functional materials.

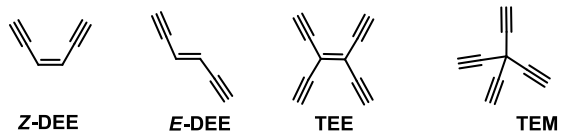

Chart 1.1 Carbon-rich building blocks for acetylene scaffolding.

Feldman and co-workers reported the synthesis of TEM in 1993.[16] In the solid state it decomposes rapidly at room temperature, even in inert atmosphere. Due to the tetrahedral alignment of ethynyl groups, TEM might serve as a simple building block for 3D structures called 'superdiamondoid', the simplest of which is the elusive hexadecaethynyladamantane (Scheme 1.2).[2b]

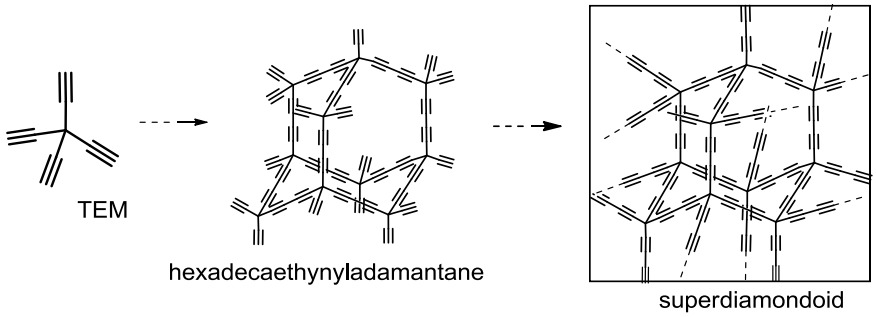

Scheme 1.2 TEM is a possible precursor for elusive hexadecaethynyladamantane and superdiamondoid.[2b]

Another interesting example of the use of acetylene building blocks was the cyclization of the (Z)-DEE under oxidative Glaser-Eglinton[17] coupling which afforded the dodecadehydro[18]annulene **1.3** (Scheme 1.3).[18] [18]Annulene was exclusively obtained in this cyclization, without formation of higher cyclic oligomers.

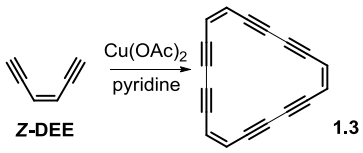

Scheme 1.3 Synthesis of dodecadehydro[18]annulene **1.3**.[18]

The name "annulenes" describes fully conjugated cyclic polyenes, with the ring size indicated by a number in brackets. In dehydroannulenes some of double bonds are substituted with triple bonds, and in benzannulenes the benzoid ring is fused with annulenes. Dehydroannulenes and benzannulenes have received considerable interest recently because of their potential applications as optoelectronic, liquid-crystalline, and sensing materials.[19] A variety of benzo- and dehydroannulenes have been prepared, inspiring the design of many interesting acetylene scaffoldings, such as the ethylene glycol substituted triangular macrocycle **1.**4a,[20] which self-assembles from water/chloroform mixture into bilayer vesicles

(Figure 1.2). This was the first demonstration of vesicle self-assembly from discotic liquid-crystalline molecules.

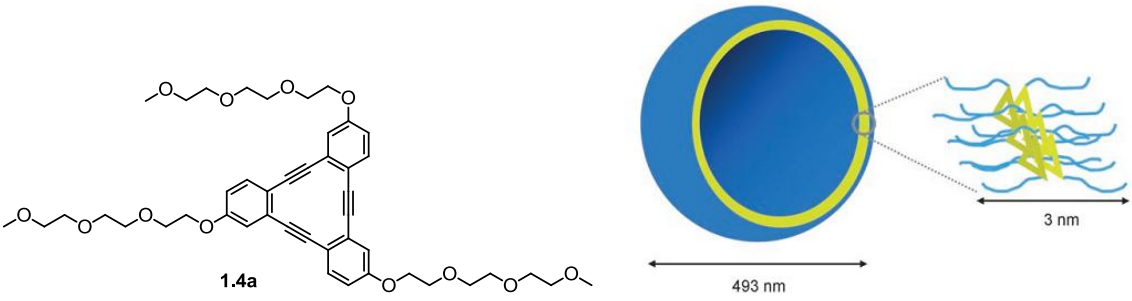

Figure 1.2 Structure of **1.4a** and a schematic illustration of the bilayered unilamellar vesicle characterized by AFM and TEM images.[20]

Benzannulenes, such as **1.4b**[21] and **1.5**,[22] could be potential precursors for 2D networks, like elusive graphyne[23] (Scheme 1.4). With their large number of sp^1-carbon atoms, the dehydroannulenes and 2D networks act as a potent electron acceptors, the experimental and theoretical investigation of which is important to understand the aromaticity and delocalisation of π electrons.[24]

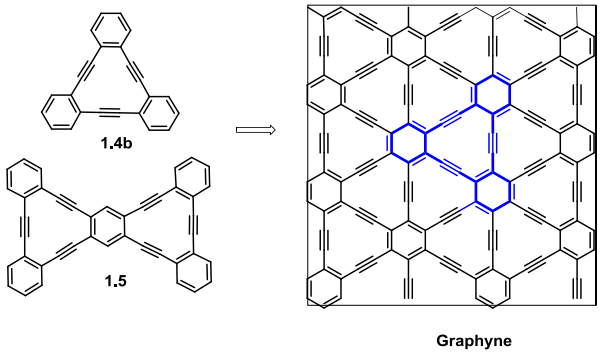

Scheme 1.4 Benzannulated dehydroannulene-derived molecules **1.4** and **1.5** have been prepared as potential precursors to the 2D all-carbon network graphyne.

Another member of the family, the octadehydrodibenzo[12]annulene **1.7**, synthesized via Hay coupling[25] of precursor **1.6** (Scheme 1.5), formed self-assembled monolayers on graphite surfaces.[26] The structure of the 2D networks of **1.7** depends on the length of the alkyl chain, and incorporation of a C18 alkyl chain led to molecular alignment in a parallel fashion forming a lamellar structure. Although the closest contact between the diacetylenic units in **1.7** ($R=OC_{18}H_{37}$) is only slightly greater than the typical distances necessary for topochemical polymerization to produce **1.8**, no evidence for polymerization on the surface was observed.

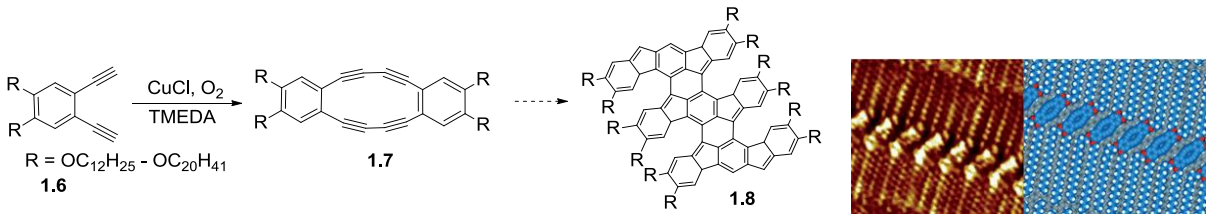

Scheme 1.5 Synthesis of **1.7** and STM image of a 2D molecular network (R=$OC_{18}H_{37}$) with a tentative network model of the lamellar structure.[26] (TMEDA=N,N,N',N'-tetramethylethylenediamine)

Another simple acetylene building block from the series of DEEs is *gem*-DEE[27] (Chart 1.2), which is a precursor for the preparation of radialenes. Radialenes are a series of exocyclic all-methylidene-substituted cycloalkanes of molecular formula C_nH_n. Upon formal insertion of ethynediyl or buta-1,3-diynediyl moieties into the cyclic framework, the carbon-rich homologous series of expanded radialenes with the molecular formulas $C_{2n}H_n$ and $C_{3n}H_n$, respectively, can be obtained (Chart 1.2).

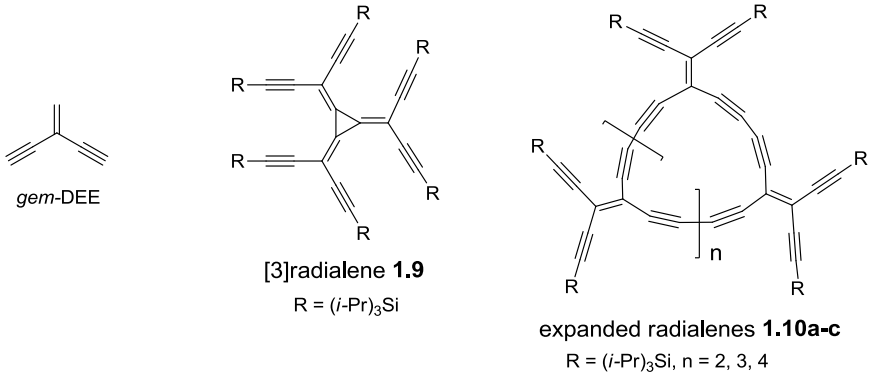

Chart 1.2 Structure of *gem*-DEE,[27] [3]radialene **1.9**[28] and expanded radialenes **1.10a-c**.[29]

The [3]radialene **1.9** can be readily reduced in CH_2Cl_2 in two reversible, one-electron transfers, occurring at –0.52 and –1.09 V (vs Ag/AgCl). The easy electron uptake was explained by an aromaticity enhancement upon reduction.[30] For another series of expanded radialenes **1.10a-c**, the optical lowest absorption remains almost constant, and is not dependent on the ring size. These radialenes displayed strong charge transfer (CT) transitions with absorptions extending to 575 nm. The electron acceptor nature of the cyclic core was also proved electrochemically. These radialenes exhibit a strong ability to accommodate electrons upon reduction, and the radical anions are very stable, in particularly those of the expanded [3]- and [4]-radialenes, which might be explained by gain of aromaticity upon reduction.[30]

Tobe et al. prepared the expanded radialenes **1.11a-d** with bicyclo[4.3.1]decatriene units.[31] Interestingly, in negative mode laser desorption time-of-flight mass spectra, the radialene **1.11d** (*n* = 4) lost the aromatic indane fragments in a stepwise manner, and exhibited peaks assignable to the

corresponding cyclo[n]carbon anions (n = 36) which supposedly isomerize to the corresponding cyclocarbons. (Scheme 1.6).

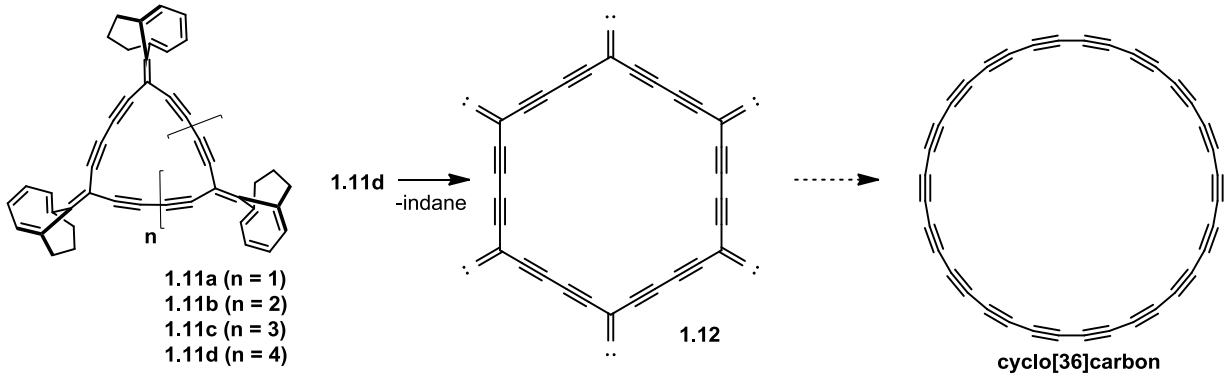

Scheme 1.6 Extended radialenes **1.11a-d** and the proposed formation of cyclo[36]carbon via vinylidene intermediate **1.12**.

The interest in new allotropes of carbon originates from 1960s, when Hoffmann proposed that some cyclo[n]carbons could be stabilized from aromaticity of two orthogonal [4n + 2] π-electron systems.[32] Since then, a couple of protocols to prepare cyclocarbons starting from different macrocyclic dehydroannulenes and expanded radialenes were explored, one of which is shown in Scheme 1.6. However, the formation of cyclocarbon was observed only in the gas phase and bulk quantities of this long-anticipated material have not been isolated yet.[31,33,2b]

Investigations towards 2D carbon networks like graphyne or ribbons like **1.8**, as well as 3D carbon networks such as superdiamondoid, were stimulated by important discoveries in the field of carbon nanomaterials from fullerenes to graphene. However, the preparative challenge for the aforementioned 2D and 3D networks exceeds the current synthetic availability, but the active generation of precursors for these networks has led to a renaissance of annulene, radialene and other acetylene-derivative chemistry.

Perhaps the most studied field of acetylene chemistry remains the chemistry of polyynes. Polyynes, which are made up of alternating triple and single bonds, possess a very efficiently conjugated system because there is very little or no loss in this conjugation due to conformational effects (bond rotation), in contrast to double bonds. Due to their 1D linear structure and high degree of conjugation they are often referred to as 'molecular wires'. Efficient conjugation and rigid linearity are reasons that polyyne materials are potentially useful in many optical and electronic applications. However, most investigations concerning polyyns have explicitly aimed at the preparation of stable derivatives as model compounds for the hypothetical, one-dimensional *sp*-hybridized carbon allotrope 'carbyne' $(C{\equiv}C)_{\infty}$. (Chart 1.3)

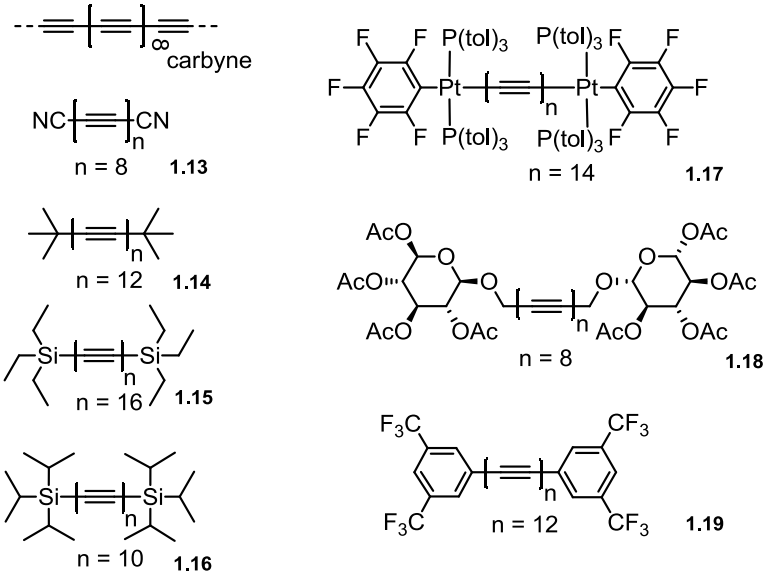

Chart 1.3 The elusive carbyne and various polyynes synthesized so far on the way to carbyne. The nitrile-capped series of oligo(ethynylene)s **1.13**[34] were reported by Hirsch and co-workers. Tykwinski and co-workers reported the synthesis of tert-butyl-functionalized dodecaynes **1.14**.[35] and the TIPS-terminated decayne **1.16**.[36] In the early 1970's Walton and co-workers synthesized TES-terminated C36 polyyne **1.15** in solution using oxidative coupling of terminal acetylenes.[37] Metal-terminated dodecayne **1.17** was synthesized by Gladysz and co-workers.[38] Glycosylated octayne **1.18** was prepared by Hoheisel and Frauenrath.[39] Cox and coworkers have reported the synthesis of the aryl-endcapped dodecayne **1.19** via β-chlorovinylsilane elimination.[40]

The thermodynamic stability of polyynes decreases with the length of the carbon chain. For example, butadiyne rapidly polymerizes above 0 °C, while neat hexatriyne is reported to be explosive.[41] However, long polyynes can be kinetically stabilized by capping the two ends of the carbon chain with bulky end-groups. Using this approach it became possible to synthesize series of polyynes with different lengths and end-groups (Chart 1.3),[42] and many of them have been crystallographically characterized.[43] Nitrile-capped oligoynes with up to 8 conjugated triple bonds (compound **1.13**, Chart 1.3) have been synthesized by vaporization of graphite under Kratscluner-Huffman conditions[44] in the presence of cyanogen $(CN)_2$.[34] This convenient method enables facile access to gram quantities of molecules having different numbers of triple bonds in one reaction step, and avoids acetylene coupling, protection, and activation sequences involving unstable intermediates, which would be required for a conventional synthesis.

Tykwinski and co-workers reported the synthesis of a series of *t*-butyl-capped polyynes with up to 10 triple bonds (compound **1.14**, Chart 1.3).[35] The X-ray structural data showed a distinct reduction in the bond-length alternation as a function of the polyyne length, but this trend appeared to saturate before a cumulenic-like structure could be achieved. Another series of polyynes, this time terminated with TIPS-groups, was prepared by Tykwinski et al. and studied for non-linear optical properties.[36] They observed that the nonresonant molecular second hyperpolarizabilities increase exponentially as a function of

molecular length with an exponent that is larger than the observed exponent for polyenes and polyenynes.[36]

From a historical point of view, the early steps towards extended oligoacetylenes are connected with the names of T. R. Johnson, D. R. M. Walton, and R. Eastmond, all of whom worked in the UK, at the University of Sussex, who used TES (triethylsilyl) end-groups to protect the polyyne chain during the chain-doubling reaction using a copper(I)-TMEDA complex.[37] Via a stepwise chain elongation technique it became possible to obtain polyynes with up to 8 triple bonds in the solid state, and with up to 16 triple bonds in hexane.

One of the outstanding synthetic achievements was reported by Zheng and Gladysz who prepared Pt-capped polyynes with up to 14 triple bonds.[38] Another interesting example was reported from the Frauenrath group. A copper-free heterocoupling protocol based on the Negishi[45] reaction was used for the preparation of symmetrically diglycosylated oligoynes up to the octayne **1.18**.[39] These compounds are intermediates in the preparation of carbon-rich amphiphiles to be used as potential molecular precursors for hierarchically structured carbon materials. Later, the same group reported the 'wet-chemical' preparation of carbon nanostructures at room temperature with controlled nanoscopic morphology and surface chemistry, using oligoyne **1.20** as a reactive molecular carbon precursor (Figure 1.3).[45] In the same work, the importance of low temperature preparation of labile carbon nanostructures, such as carbon-coated inorganic nanoparticles was highlighted as a convenient route for the preparation of electrode materials in lithium batteries.[47]

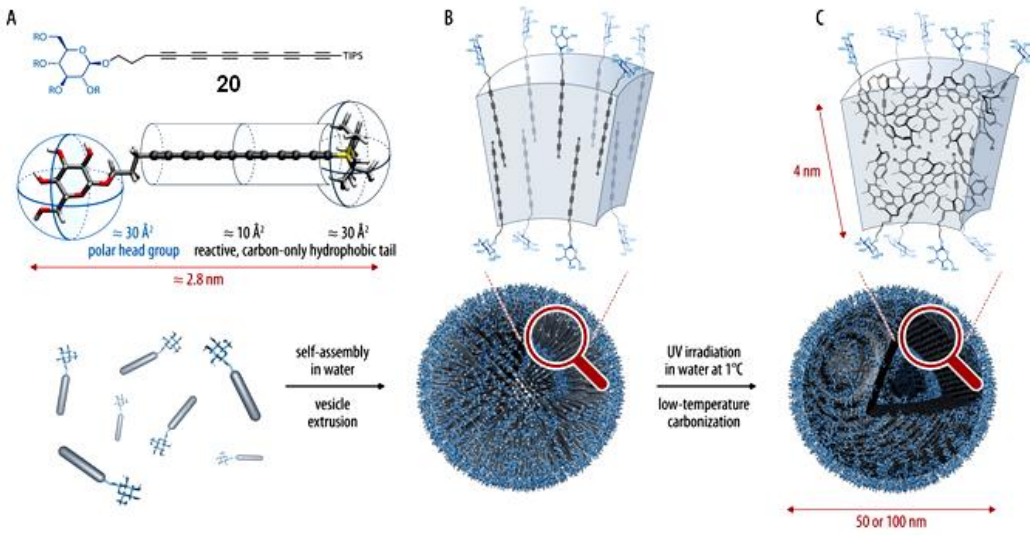

Figure 1.3 Wet-chemical preparation of carbon nanostructures with controlled morphology and surface chemistry. After the deprotection of **1.20** and self-assembly of the carbon-rich amphiphiles in water and vesicle extrusion, carbonization takes place under UV irradiation below room temperature in water.[45]

Recently, a synthetic breakthrough was reported by Tykwinski and Chalifoux[48] who used the supertrityl moiety (referred to as Tr*) as a stabilizing end-group and prepared a series of polyynes with up to 44 sp^1 carbon atoms length (Figure 1.4, compound **1.21**), which is the longest known polyyne up to date. This challenging molecule was synthesized by applying the Glaser-Eglinton-Hay coupling protocol. Surprisingly, **1.21** was not particularly sensitive to light, moisture or oxygen, and could be handled under normal laboratory conditions. The ^{13}C NMR and UV-vis analysis reveal that the carbon framework is composed of alternating single and triple bonds (non-cumulenic structure) even for **1.21**. Another distinct trend in this series of polyynes was the estimation of a finite gap between the highest occupied molecular orbital (HOMO) and the lowest unoccupied molecular orbital (LUMO) for carbyne, which is estimated to be ~2.56 eV (predicted saturation after 30 triple bonds).

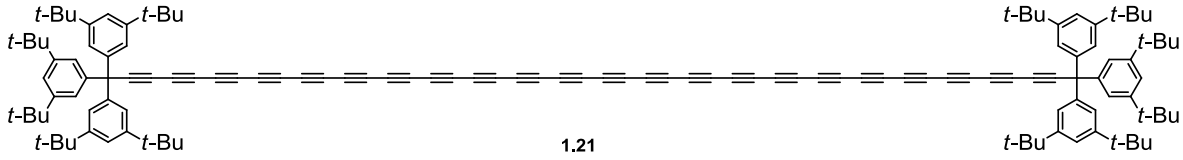

Figure 1.4 The structure of the longest known polyyne **1.21**.[48]

Carbyne has been proposed (unconvincingly) to exist in interstellar dust,[49] meteorites[50] and as a by-product of shock-fused graphite.[51] While carbyne may or may not exist as a new allotrope material of carbon, the active investigation of polyynes as a model for carbyne led to numerous fascinating discoveries and still remains at the centre of attention of organic and physical chemists.

1.2 Polyyne synthesis: General considerations

The laboratory synthesis of polyynes mostly relies on a number of methods which include the homo- or heterocoupling of acetylenic precursors,[52] as well as the elimination[53] or extrusion[31] of functional subunits to assemble the linear framework of the polyyne in the last step of the synthesis. The lability of the terminal proton plays an important role in the rich chemistry of acetylenes. Terminal acetylenes can be readily deprotonated under different conditions due to the higher electronegativity of sp^1 carbons compared to sp^2 or sp^3 ones (higher proportion of *s* character of the molecular orbital).[54] The ability of terminal acetylenes to undergo metalation is crucial in several coupling reactions.

The first polyyne synthesis was reported by Carl Glaser in 1869, who performed an oxidative dimerization of copper(I) phenylacetylide in the presence of air producing diphenylbutadiyne (Scheme 1.7).[55]

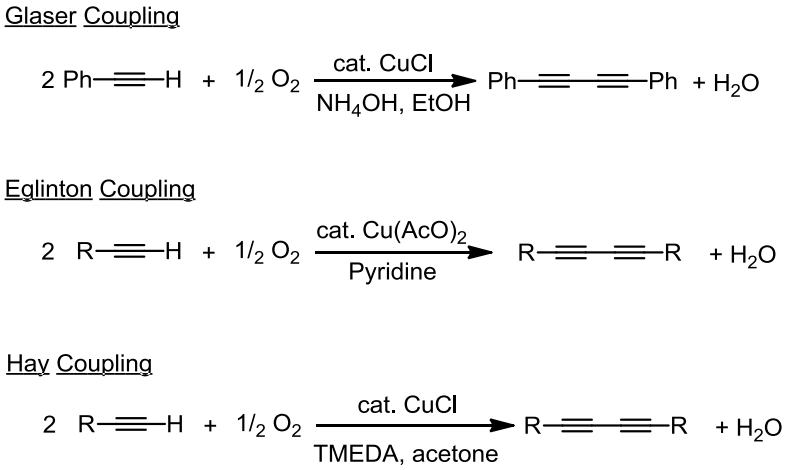

Scheme 1.7 Classic Cu-mediated acetylene homocoupling reactions.

Subsequently, different methodologies have been developed, significantly improving the Glaser homocoupling reaction. For example, in 1956 Eglinton and Galbraith reported the oxidative homocoupling of acetylenes using $Cu(OAc)_2$ in the presence of pyridine (Scheme 1.7).[17] Another breakthrough was reported in 1962 by Hay[25] where CuCl was used as an catalyst in the presence of TMEDA and O_2 as an oxidant (Scheme 1.7). The commonly used solvents in this reaction include acetone or CH_2Cl_2, and the method turned out to be very effective. Another modification in the alkyne homocoupling reactions was the use of Pd catalysis instead of the traditional Cu(I)/Cu(II) system (Scheme 1.8).[56] Pd catalysis can substitute effectively the Cu catalyst in cases when the latter becomes ineffective.[57] The preparation of alkyne-based compounds through palladium catalysis has been reviewed recently.[58]

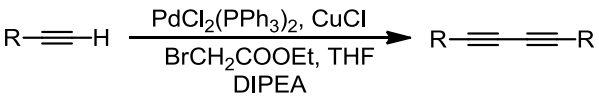

Scheme 1.8 A novel pathway for the Pd-catalyzed homocoupling reaction. During the reaction a PdBr(enolate) intermediate is formed. This intermediate can undergo double transmetalation with an alkynyl copper reagent, and reductive elimination produces a diyne. DIPEA = diisopropylethylamine.[56]

Although Cu- or Pd-mediated homocoupling reactions typically give satisfactory results for the synthesis of symmetrical polyynes, they are often unsuitable for the formation of unsymmetrical derivatives. Three methods are commonly used to address this problem: the Cadiot-Chodkiewicz reaction,[59] the Negishi protocol,[45] and the Sonogashira cross-coupling reaction (Scheme 1.9).[60]

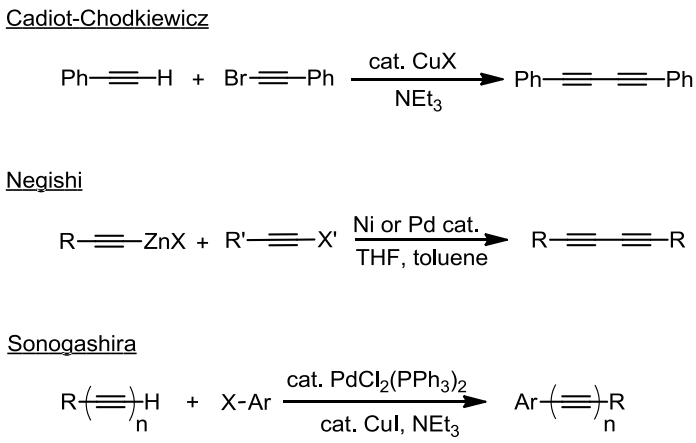

Scheme 1.9 Classic cross-coupling reactions of alkynes.

In the Cadiot-Chodkiewicz cross-coupling the terminal alkynes react with 1-haloacetylenes in the presence of a copper(I) salt and a suitable amine (Scheme 1.9). The most used coupling partners in this reaction are 1-bromoacetylenes, while iodoalkynes have been used to a minor extent, and chloroacetylenes do not have practical importance because of their low reactivity and their tendency to undergo self-coupling.[52]

On the other hand, the Negishi cross-coupling (Scheme 1.9)[45] between *in situ* prepared Zn-acetylides (formed by lithiation of silyl protected acetylenes followed by transmetalation with $ZnCl_2$) and terminal acetylene bromides can be a suitable method for the synthesis of polyynes.[39]

In the Sonogashira cross-coupling reaction a Pd catalyst is used with a combination of Cu co-catalyst to form a carbon–carbon bond between a terminal acetylene and an aryl or vinyl halide (Scheme 1.9).[60] The combination of Cu and Pd catalysts increases the reactivity of the reagents and allows the reaction to be carried out at room temperature, making the Sonogashira cross-coupling a very useful reaction.[61]

In general, due to the decrease in stability of long conjugated acetylene units, the synthesis of extended polyynes becomes problematic. One of the approaches to avoid the use of long, very reactive deprotected polyyne precursors is the formation of the polyyne framework in the last step of the synthesis. In 1894 Fritsch, Buttenberg and Wiechell demonstrated that the carbenoid intermediate **B**, formed from *geminal* dibromoolefins, can collapse to an alkyne via 1,2-migration of a pendant functional group (Scheme 1.10).[62] During the 2000's the Tykwinski group intensively developed this strategy, commonly referred to as Fritsch-Buttenberg-Wiechell (FBW) rearrangement, for the synthesis of polyynes and acetylene derivatives.[63]

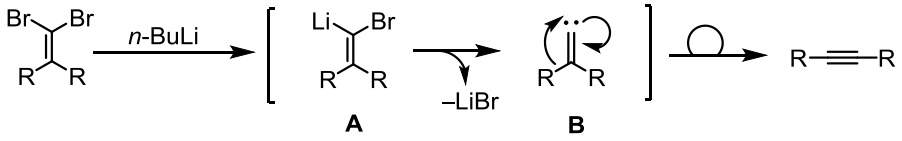

Scheme 1.10 Triple bond formation through Fritsch-Buttenberg-Wiechell (FBW) rearrangement.

Tobe and co-workers designed a new method to form polyynes through 1,2-migration of an alkynyl moiety in alkylidene intermediates.[31,64] The precursor **1.22** is synthesized readily from dehydroindane. By the photolysis of **1.22** indane is eliminated through [2+1] cheletropic reaction resulting in the free alkylidene carbene **1.23** (Scheme 1.11). Subsequent migration of one of the alknyl moieties gives the desired triyne **1.24**. This reaction was used to prepare longer polyynes, for example pentayne **1.24b**.

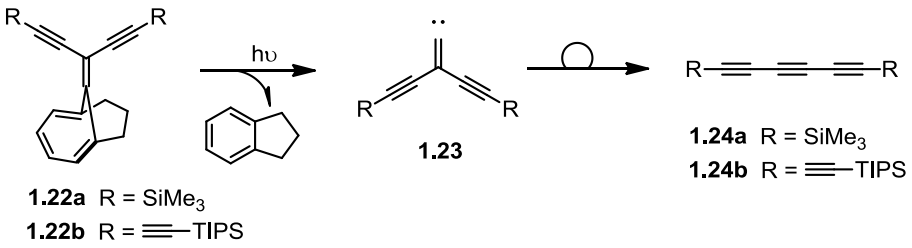

Scheme 1.11 Tobe's reported alkylidene carbene rearrangement.

Another approach to synthesize TIPS-terminated pentayne **1.24b** was reported by Diederich.[65] This time the pentayne framework was constructed in the last step of the synthesis by flash vacuum pyrolysis (FVP) of the precursor **1.25** (Scheme 1.12).

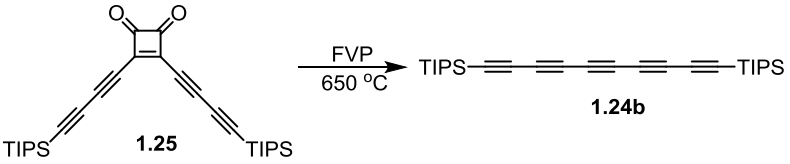

Scheme 1.12 Synthesis of pentayne **24b** by flash vacuum pyrolysis.[65]

However, the harsh conditions of FVP make the method unacceptable towards the synthesis of long polyynes. Moreover, an alternative for the synthesis of pentayne **1.24b** using FBW rearrangement proved to be very successful. It allowed the preparation of TIPS terminated octayne **1.27** via two-fold carbenoid rearrangement in one step (Scheme 1.13).[36]

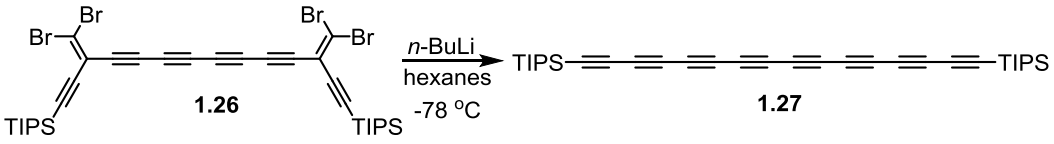

Scheme 1.13 Synthesis of the octayne **1.27** by Tykwinski et al.[36]

Recently, Cox and co-workers have reported an innovative strategy for the construction of polyyne chains by elimination of chlorovinylsilane groups (Scheme 1.14).[40] For example, dodecayne **1.19** (Chart 1.3) initially was assembled in the form of a masked dodecayne **1.28** through a series of oxidative homocoupling reactions. The final polyyne was formed through exhaustive elimination using TBAF. The identity of compound **1.19** was confirmed by UV-visible spectroscopy and 'matrix free' MALDI-TOF mass spectrometry.

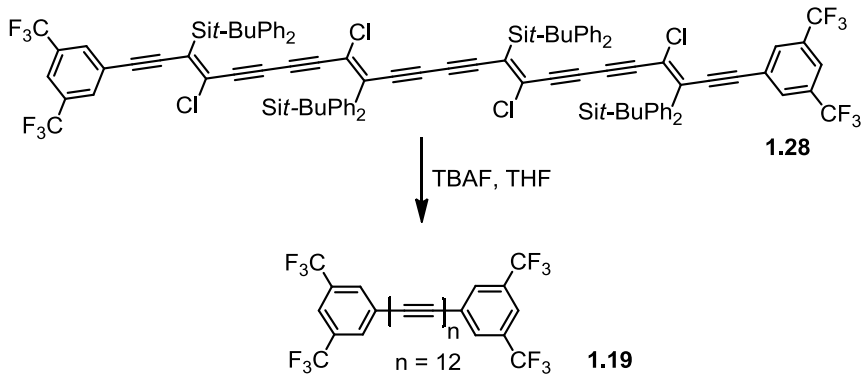

Scheme 1.14 Cox's synthesis of dodecayne **1.19** from the masked precursor **1.28**.

Surface reactions recently gained special interest for construction of conjugated polymeric materials and graphene nanoribbons.[66] Particularly, Fuchs et al. presented the on-surface Glaser coupling of various arylalkynes, without "capping" ions, as an efficient 2D reaction at various metal surfaces (Figure 1.4).[67] The Glaser coupling was tested on Ag(111), Au(111) and Cu(111) surfaces. The surface acts as a 2D supporting system allowing the molecules to adsorb and orient in two-dimensional space, and it also likely mediates the reactions. This interesting technique generates linear oligomer/polymer chains in spatial confinement at surfaces, which is impossible in conventional solution schemes. Furthermore, the same research group reported the light-induced Glaser homocoupling of aryl-alkynes at metal surfaces without thermal activation of the precursor building blocks.[67b]

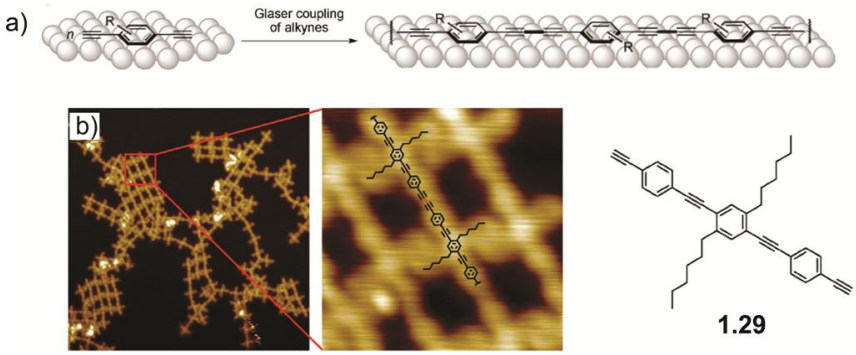

Figure 1.4 a) General outline of the 2D Glaser coupling at surfaces. (b) STM images of alkyne **1.29** on Ag(111) after on-surface oligomerization (2 V, 10 pA, 40 nm x 40 nm, area of inset 5 nm x 5 nm).[67]

The topochemical polymerization of polyynes is another interesting aspect of the diverse chemistry of acetylene. While 1,4-polymerization of diacetylenes was discovered in 1972,[68] the 1,6-polymerization of a triacetylene was achieved by supramolecular (host-guest) control.[69] The structural parameters for a topochemical triacetylene polymerization requires that the monomeric units must be preorganized with a defined interatomic (C1-C6) distance of 3.5 Å, close to the van der Waals contact, a condition that should maximize the chances of polymerization. The needed preorganization was accomplished using hydrogen bonding to prepare the host-guest complex **1.30** (Figure 1.5). The irradiation of the host-guest crystals with ^{60}Co γ-radiation resulted in polymerization. The structure of the host-guest complex and final polymer was confirmed by X-ray crystallography. This interesting result shows a natural evolution of synthetic polyyne chemistry from the molecular to the supramolecular level.

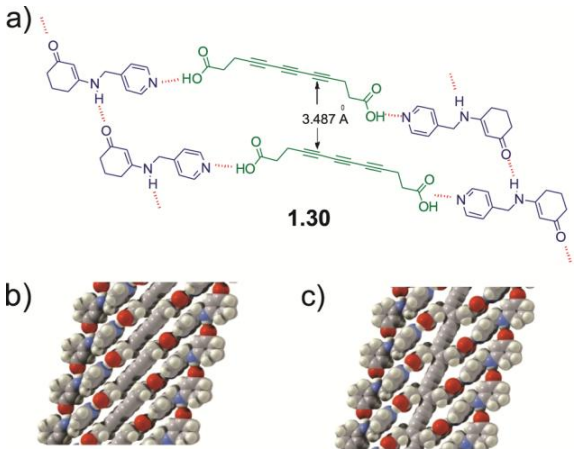

Figure 1.5 (a) A part of the molecular structure of vinylogous amide (purple) and triacetylene (green) host-guest complex **1.30** suitable for the topochemical preparation of a polytriacetylene (hydrogen bonds are coloured in red). X-ray crystallographic structures of (b) the host-guest triacetylene monomer and (c) the resulting triacetylene polymer.[69]

1.3 Active-metal template synthesis of rotaxanes

Despite the tremendous amount of research in acetylene chemistry, one interesting aspect of the supramolecular polyyne chemistry, that is polyyne based rotaxane chemistry, has not gained as much attention as other areas. It has been suggested that threading of polyynes through macrocycles to form rotaxanes or polyrotaxanes could stabilize them,[70] however until recently polyyne rotaxanes with axles longer than butadiynes had not been reported.[71]

Here, the active-metal template strategy of rotaxane synthesis[72] is introduced, as it has been used intensively for the synthesis of polyyne rotaxanes, described in this thesis.[73]

Rotaxanes belong to the family of mechanically interlocked (or topologically linked) architectures (Figure 1.6). In mechanically locked architectures molecules are not linked together through a covalent bond, but through their shape: often this kind of link is referred to as a "mechanical bond".[74] When two rings are interlinked the resulting architecture is called a catenane. Rotaxanes are another type of interlinked structure, however here a macrocycle is threaded on a linear axle. A system where such a ring can still slip out from its axle is called a pseudorotaxane (Figure 1.6).[74] In supramolecular species the assembled structures can be disconnected by different stimuli, while in mechanically interlocked molecules the cleavage of one covalent bond is necessary to separate the constituent parts.[74]

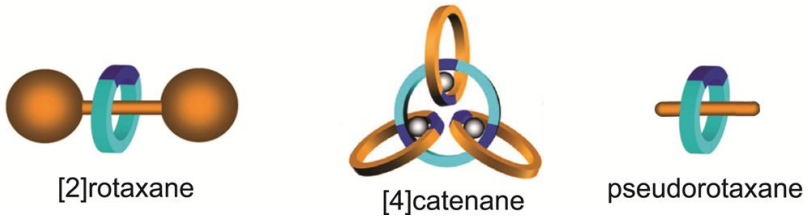

Figure 1.6 Schematic representation of a [2]rotaxane, [4]catenane and pseudorotaxane.[74f] In the case of the [4]catenane the coordinated metal template is shown as brown spheres.

Before discussing the active-metal template strategy it is worth introducing the classic approach of 'passive' metal templating of rotaxanes.[74] In this strategy, a complexation of two or more ligands to one or more metal ions takes place in the first step of the synthesis. In this way the organic building blocks are held together in such an orientation that a subsequent covalent bond forming reaction can be used to mechanically capture the ligand components. The metal ion generally stays passive during the formation of the mechanically interlocked structure.[74]

Early examples of passive-metal template rotaxane synthesis were reported by the Gibson[75] and Sauvage groups.[76] For instance, Gibson used the tetrahedral geometry of the Cu(I) ion (in form of $[Cu(CH_3CN)_4]BF_4$ salt) to glue together 1,10-phenanthroline-based macrocycle **1.31** and 1,10-phenanthroline-based axle **1.32** (Scheme 1.15). In the next step, the formed pseudorotaxane architecture was capped with bulky stoppers **1.33**. In the nomenclature of rotaxanes the numbers in brackets indicate the number of locked molecular components.

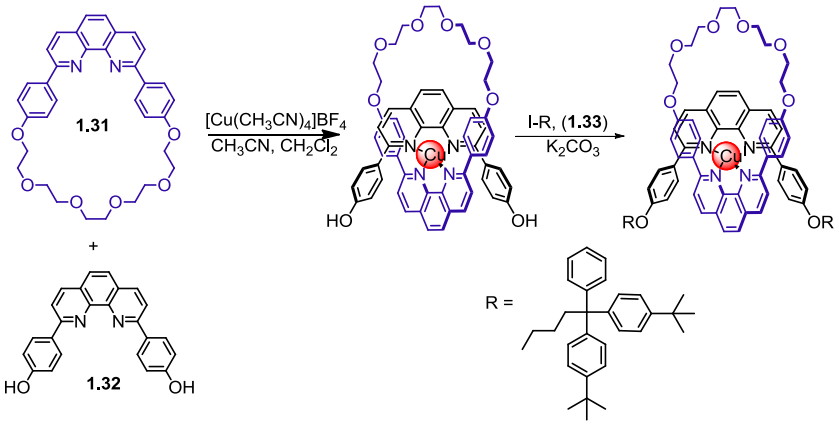

Scheme 1.15 Gibson's synthesis of rotaxane using passive-metal template strategy.[76]

Passive template strategy requires, as a rule, a stoichiometric quantity of the metal template and permanent coordination sites on each of the components. In contrast, in active metal template synthesis the metal ion acts as a template and catalyzes a covalent bond formation between molecular components resulting in a interlocked structure.[72]

The metal ion must be capable of coordinating to the macrocycle and then of promoting a covalent bond formation between two suitably functionalised ‘‘half-thread’’ units of the dumbbell shaped axle of the rotaxane (Scheme 1.16). The catalytic process thus takes place within the cavity of the macrocycle leading to the formation of a new mechanical bond. The active-metal template process can be stoichiometric (relies on the use of one equivalent of template) or catalytic (substoichiometric amount of the metal turns over during the reaction). The lack of requirement for permanent recognition elements on each component of the interlocked product, and, in some cases, use of sub-stoichiometric amounts of the template-catalyst with high applicability to vary transition metal-catalysed reactions makes the application of active metal template more diverse and flexible.

The first [2]rotaxane synthesized through an active-metal template strategy was reported in 2006.[76] Using the copper(I)-catalysed terminal alkyne–azide 1,3-cycloaddition (CuAAC),[77] Leigh and co-workers

assembled a [2]rotaxane **1.37** by stirring of an equimolar mixture of pyridine macrocycle **1.34**, alkyne **1.35** and azide **1.36** (Scheme 1.16). The reaction turned out to be very efficient when alkyne **1.35** and azide **1.36** were used in 5-fold excess. The authors also demonstrated that in the presence of pyridine the template can be used in substoichiometric amounts. A possible mechanism of the reaction was also proposed, which is presented in Scheme 1.16.

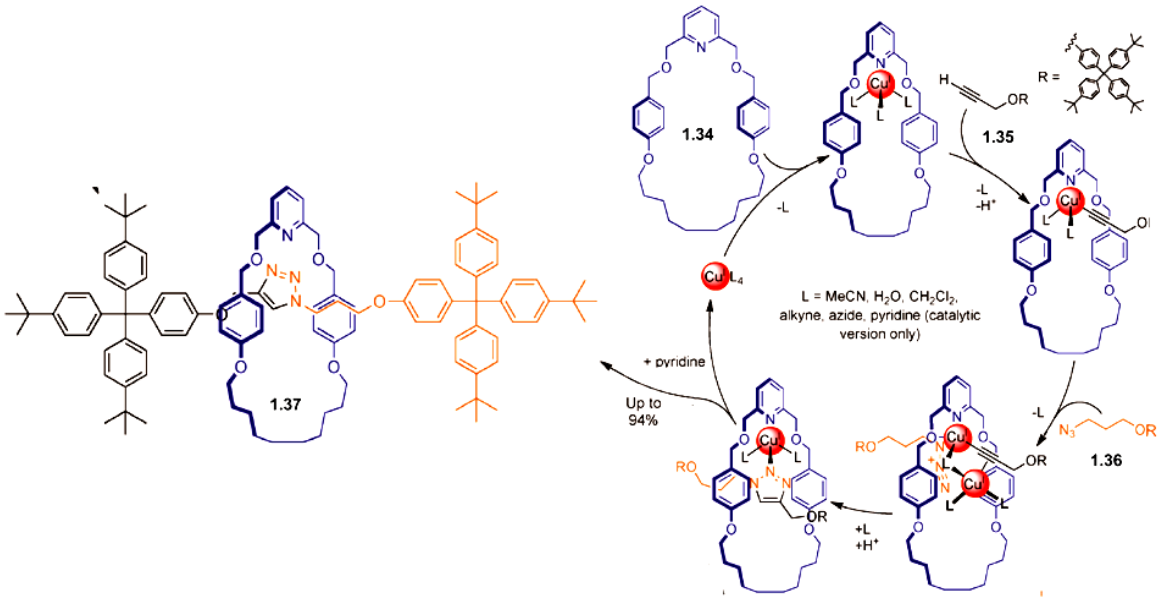

Scheme 1.16 [2]Rotaxane 1.37 synthesis through active-metal template CuAAC reaction in the presence of stoichiometric (94 % yield) or sub-stoichiometric (20 mol % Cu(I), 82 % yield) quantities of Cu(I).

Later, the same group extended this work into broad mechanistic studies, testing the effect of different macrocycle structure, reaction conditions, the nature and the effect of catalytic and stoichiometric amounts of Cu(I) on the rotaxane formation.[78] Surprisingly, when high ratios of macrocycle:Cu(I) were applied, the formation of double-threaded [3]rotaxane was detected. The proposed mechanism of this unusual threading reaction is presented in Scheme 1.17.

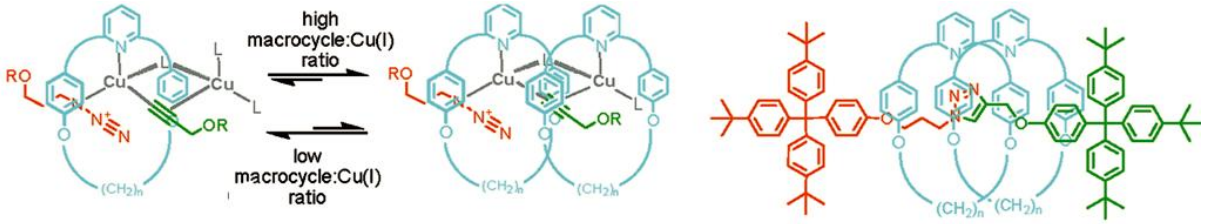

Scheme 1.17 The proposed mechanism of formation of [3]rotaxane via active-metal template 'CuAAC' reaction.[78]

Active-metal template rotaxane formation via Glaser coupling[58] of the arylalkyne **1.38** was for the first time reported by Saito and co-workers (Scheme 1.18).[79] The phenanthroline-based macrocycle **M1** and stoichiometric quantities of Cu(I) were used to give the corresponding rotaxane **1.39** in 72 % yield.

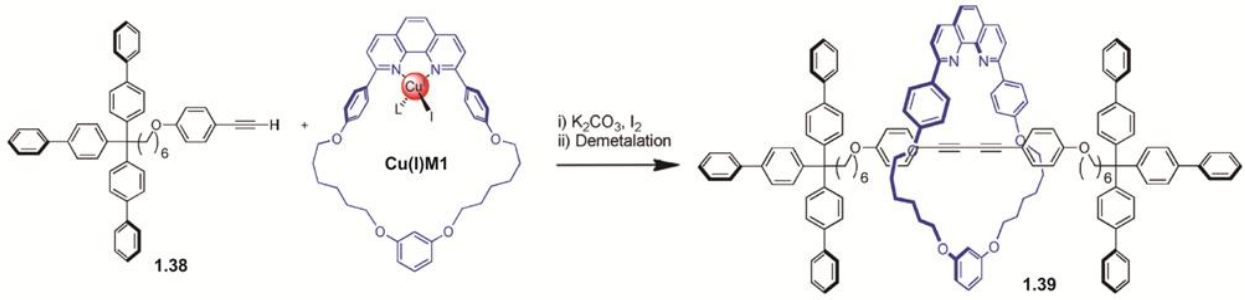

Scheme 1.18 Saito's synthesis of [2]rotaxane **1.39** via active-metal template Glaser coupling of arylakyne.[79]

As in the case of polyyne synthesis,[58] the use of Pd as the catalyst for alkyne–alkyne bond formation can be useful for rotaxane preparation. Thus, the Leigh group reported the Pd(II) catalyzed homocoupling of alkynes using substoichiometric amounts of the active-template metal ion (Scheme 1.19).[80]

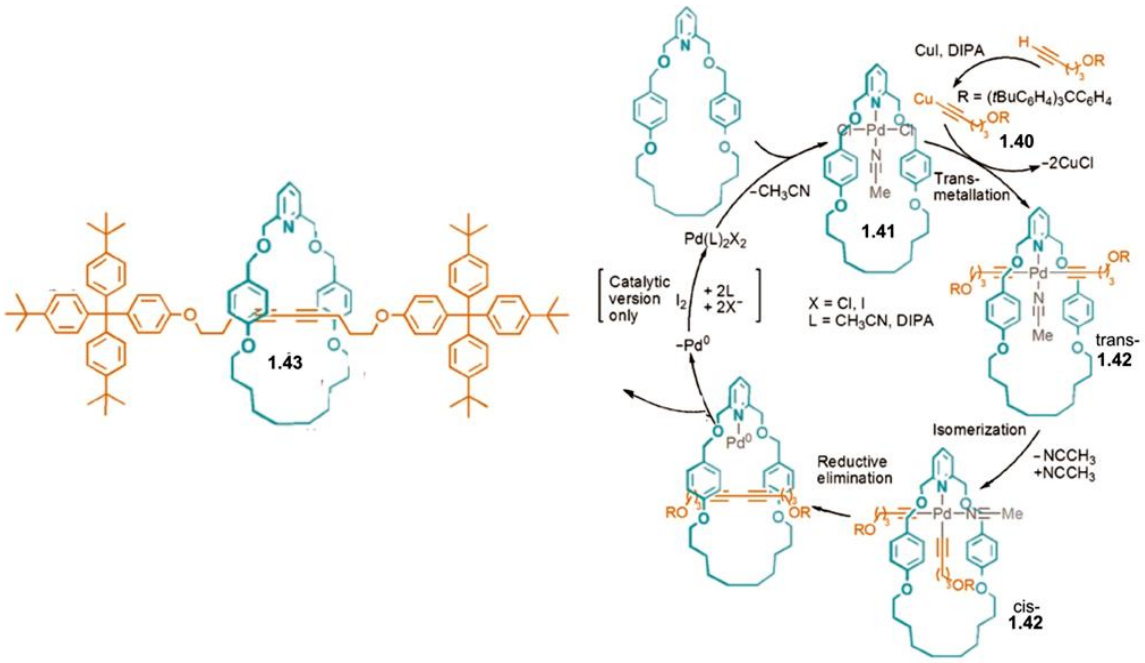

Scheme 1.19 Synthesis of rotaxane **1.43** via active template Pd(II)-catalyzed homo-coupling of alkyne. DIPA=diisopropylamine.

Conditions which employ 5-10 mol% of Pd(II) and iodine to oxidize Pd(0) back to Pd(II) resulted in higher yields of [2]rotaxane compared to the stoichiometric reaction. According to the proposed reaction mechanism, transmetalation takes place between copper-acetylide complex **1.40** and macrocycle-Pd(II) complex **1.41**. A concerted trans–cis isomerization of **1.42** in which the ligands do not detach from the Pd(II) center maintains the geometry, which allows for C-C bond formation by reductive elimination of cis-**1.42** to form [2]rotaxane **1.43** (Scheme 1.19).

Polyynes have a rich chemistry and alluring potential in material science, serving as precursors for 1D, 2D and 3D materials. So far, little has been done towards the fabrication of polyynes in advanced materials, mainly due to lack of control in the reactivity in bulk materials. This is an area where supramolecular chemistry can have a real impact on the application of polyynes, particularly, the rotaxination of polyyne chains. This aspect of the polyynes will be discussed throughout this thesis.

1.4 References

1. (a) *Carbon Materials for Advanced Technologies*, editor: Burchell, T.D. Elsevier, UK, **1999**. (b) Hoheisel, T. N.; Schrettl, S.; Szilluweit, R.; Frauenrath, H. *Angew. Chem. Int. Ed.* **2010**, *49*, 6496–6515.

2. (a) *Carbon-Rich Compounds: From Molecules to Materials*, Editors: Haley, M. M.; Tykwinski, R. R. Wiley-VHC, Weinheim, Germany, **2006**. (b) Diederich, F. *Nature* **1994**, *369*, 199–207. (c) Novoselov, K. S.; Geim, A. K.; Morozov, S. V.; Jiang, D.; Zhang, Y.; Dubonos, S. V.; Grigorieva, I. V.; Firsov, A. A. *Science* **2004**, *306*, 666–669 (d) Smalley, R. E. *Angew. Chem.***1997**, 109, 1666–1669; *Angew. Chem. Int. Ed. Engl.***1997**, *36*, 1594–1601. (e) Ajayan, P. M. *Chem. Rev.***1999**, 99, 1787–1800. (f) Avouris, P.; Chen, Z.; Perebeinos, V. *Nat. Nanotechnol*. **2007**, *2*, 605–615.

3. (a) *Science of Fullerenes and Carbon Nanotubes.* Dresselhaus, M. S.; Dresselhaus, G.; Eklund, P. C. Academic Press, San Diego, **1996**. (b) Scott, L. T.; Boorum, M. M.; McMahon, B. J.; Hagen, S.; Mack, J.; Blank, J.; Wegner, H.; de Meijere, A. *Science* **2002,** *295*, 1500–1503. (c) Aricò, A. S.; Bruce, P.; Scrosati, B.; Tarascon,' J.-M.; van Schalkwijk, W. *Nature Materials* **2005**, *4*, 366–377. (d) Prasek, J.; Drbohlavova, J.; Chomoucka, J.; Hubalek, J.; Jasek, O.; Adam, V.; Kizek, R.; *J. Mater. Chem.* **2011**, *21*, 15872–15884.

4. (a) Winter, M.; Besenhard, J. O.; Spahr, M. E.; Novak, P. *Adv. Mater*. **1998**, *10*, 725–763 (b) Fauteux, D.; Koksbang, R. *J. Appl. Electrochem*. **1993**, *23*, 1–10.

5. Minus, M. L.; Kumar, S.; Min. J. *Met. Mater. Soc.* **2005**, *57*, 52–58. (b) Liu, J.; Yue, Z.; Fong, H. *Small* **2009**, *5*, 536–542.

6. *Market Report: Global Carbon Fiber Composite Market*. Acmite Market Intelligence, **2014**

7. (a) Dervishi, E.; Li, Z.; Xu, Y.; Saini, V.; Biris, A. R.; Lupu, D.; Biris, A. S. *Part. Sci. Technol*. **2009**, *27*, 107–125. (b) Cousseau, J.; Allard, E.; Chopin, S. *C. R. Chim.* **2006**, *9*, 1051–1057. (c) Hirsch, A. *Angew. Chem*. **2002**, *114*, 1933–1939; *Angew. Chem. Int. Ed*. **2002**, *41*, 1853–1859. (d) Duesberg, G. S.; Muster, J.; Krstic, V.; Burghard, M.; Roth, S. *Appl. Phys. A* **1998**, *67*, 117–119.

8. (a) Iijima, S. *Nature* **1991**, *354*, 56–58. (b) Ebbesen, T. W.; Ajayan, P. M. *Nature* **1992**, *358*, 220–222.

9. (a) Guo, T.; Nikolaev, P.; Thess, A.; Colbert, D. T.; Smalley, R. E. *Chem. Phys. Lett*. **1995**, *243*, 49–54. (b) Zhang, Y.; Iijima, S. *Appl. Phys. Lett*. **1999**, 75, 3087–3089.

10. Howard, J. B.; Lafleur, A. L.; Makarovsky, Y.; Mitra, S.; Pope, C. J.; Yadav, T. K. *Carbon* **1992**, *30*, 1183–1201.

11. (a) Li, W. Z.; Xie, S. S.; Qian, L. X.; Chang, B. H.; Zou, B. S.; Zhou, W. Y.; Zhao, R. A.; Wang, G. *Science* **1996**, *274*, 1701–1703. (b) Lee, C. J.; Park, J.; Huh, Y.; Lee, J. Y.; *Chem. Phys. Lett*. **2001**, *343*, 33–38.

12. (a) Moonen, N. N. P.; Boudon, C.; Gisselbrecht, J. P.; Seiler, P.; Gross, M.; Diederich, F. *Angew. Chem. Int. Ed.* **2002**, *41*, 3044–3447. (b) Stahl, J.; Bohling, J. C.; Bauer, E. B.; Peters, T. B.; Mohr, W.; Martin-Alvarez, J. M.; Hampel, F.; Gladysz, J. A. *Angew. Chem. Int. Ed.* **2002**, *41*, 1871–1876. (c) Iyoda, M.; Yamakawa, J.; Rahman, J. M. . *Angew. Chem. Int. Ed.* **2011**, *50*, 10522–10553. (d) Kivala, M.; Diederich, F. *Pure Appl. Chem.* **2008**, *80*, 411–427. (e) Edelmann, M. J.; Estermann, M. A.; Gramlich, V.; Diederich, F. *Helv. Chim. Acta* **2001**, *84*, 473–480. (f) Nielsen, M. B.; Diederich. F. *Chem. Rev*. **2005**, *105*, 1837–1867. (g) Bunz, U. H. F.; Rubin, Y.; Tobe, Y. *Chem. Soc. Rev*. **1999**, 28, 107–119.

13. Manini, .P.; Amrein, W.; Gramlich, V.; Diederich, F. *Angew. Chem. Int. Ed.* **2002**, *41*, 4339–4343.

14. (a) Okamura, W. H.; Sondheimer, F. *J. Am. Chem. Soc.* **1967**, *89*, 5991. (b) Vollhardt, K. P. C.; Bergman, R. G. *J. Am. Chem. Soc*. **1973**, *95*, 7538–7539.

15. Anthony, J.; Boldi, A. M.; Rubin, Y.; Hobi, M.; Gramlich, V.; Knobler, C. B.; Seiler, P.; Diederich, F. *Helv. Chim. Acta* **1995**, *78*, 13–45.

16. Feldman, K. S.; Kraebel, S. M.; Parvez, M. *J. Am. Chem. Soc*. **1993**, *115*, 3846–3847.

17. (a) Eglinton, G.; Galbraith, A. R. *Chem. Ind.* (London) **1956**, 737–738 (b) Eglinton G.; Galbraith,A. R. *J. Chem. Soc.* 1**959**, 889–896.

18. Okamura, W. H.; Sondheimer, F. *J. Am. Chem. Soc.* **1967**, *89*, 5991–5992.

19. (a) Moore, J. S. *Acc. Chem. Res.***1997**, *30*, 402–413. b) Kivala, M.; Mitzel, F.; Boudon, C.; Gisselbrecht, J.-P.; Seiler, P.; Gross, M.; Diederich, F. *Chem. Asian J*. **2006**, *1*, 479–489. (c) Ojima, J.; Fujita, S.; Masumoto, M.; Ejiri, E.; Kato, T.; Kuroda, S.; Nozawa, Y.; Tatemitsu, H. *J. Chem. Soc*. *Chem. Commun*. **1987**, 534–536. (d) Ajami, D.; Oeckler, O.; Simon, A.; Herges, R. *Nature* **2003**, *426*, 819–821.

20. Seo, S. H.; Chang, J. Y.; Tew, G. N. *Angew. Chem.* **2006**, *118*, 7688–7962; *Angew. Chem. Int. Ed*. **2006**, *45*, 7526–7530.

21. Sondheimer, F.; Wolovsky, R. *J. Am. Chem. Soc.* **1962**, *84*, 260–270.

22. (a) Kehoe, J. M.; Kiley, J. H.; English, J. J.; Johnson, C. A.; Petersen, R. C.; Haley, M. M. *Org. Lett.* **2000**, *2*, 969–972 (b) O. S. Miljanic ´, K. P. C. Vollhardt, G. D. Whitener, *Synlett*. **2003**, 29–34.

23. M. M. Haley, *Pure Appl. Chem.* **2008**, *80*, 519–532.

24. (a) Baughman, R. H.; Eckhardt, H.; Kertesz, M. *J. Chem. Phys*. **1987**, *87*, 6687–6699. b) Li, G.; Li, Y.; Liu, H.; Guo, Y.; Li, Y.; Zhu, D. *Chem. Commun.* **2010**, *46*, 3256–3258.

25. Hay, A. S. *J. Org. Chem.* **1962**, *27*, 3320–3221.

26. Tahara, K.; Inukai, K.; Hara, N.; Johnson II, C. A.; Haley, M. M.; Tobe, Y. *Chem. Eur. J.* **2010**, *16*, 8319–8329.

27. Alberts, A. H. *J. Am. Chem. Soc*. **1989**, *111*, 3093–3094.

28. Lange, T.; Gramlich, V.; Amrein, W.; Diederich, F.; Gross, M.; Boudon, C.; Gisselbrecht, J.-P. *Angew. Chem., Int. Ed.* **1995**, 34, 805–809.

29. Boldi, A. M.; Diederich, F. *Angew. Chem. Int. Ed.* **1994**, *33*, 468–471.

30. Lepetit, C.; Nielsen, M. B.; Diederich, F.; Chauvin, R. *Chem. Eur. J*. **2003**, *9*, 5056–5066.

31. (a) Tobe, Y.; Fujii, T.; Matsumoto, H.; Naemura, K. *Pure Appl. Chem.* **1996**, *68*, 239–242. (b) Tobe, Y.; Umeda, R.; Iwasa, N.; Sonoda, M. *Chem. Eur. J.* **2003**, *9*, 5549–5559.

32. Hoffmann, R. *Tetrahedron* **1966**, *22*, 521–538.

33. (a) Diederich, F.; Rubin, Y.; Knobler, C. B.; Whetten, R. L.; Schriver, K. E.; Houk, K. N.; Li, Y. *Science* **1989**, *245*, 1088–1090. (b) Diederich, F.; Rubin, Y.; Chapman, O. L.; Goroff, N. S. *Helv. Chim. Acta* **1994**, *77*, 1441–1457.

34. (a) Griisser, T.; Hirsch, A. *Angew,. Chem*. **1993**, *105*. 1390–1392; *Angew. Chem. Int. Ed.* **1993**, *32*, 1340–1342. (b) Schermann, G.; Grsser, T.; Hampel, F.; Hirsch, A. *Chem. Eur. J.* **1997**, *3*, 1105–1112.

35. Chalifoux, W. A.; MacDonald, R.; Ferguson, M. J.; Tykwinski, R. R. *Angew. Chem. Int. Ed.* **2009**, *48*, 7915–7919.

36. Eisler, S.; Slepkov, A. D.; Elliott, E.; Luu, T.; McDonald, R.; Hegmann, F. A.; Tykwinski, R. R. *J. Am. Chem. Soc.* **2005**, *127*, 2666–2676.

37. (a) Johnson, T. R.; Walton, D. R. M. *Tetrahedron* **1972**, *28*, 5221–5236. (b) Eastmond, R.; Johnson, T. R.; Walton, D. R. M. *Tetrahedron* **1972**, *28*, 4601–4616.

38. Zheng, Q.; Gladysz, J. A. *J. Am. Chem. Soc*. **2005**, *127*, 10508–10509.

39. Hoheisel, T. N.; Frauenrath, H. *Org. Lett.* **2008**, *10*, 4525 - 4528.

40. Simpkins, S. M. E.; Weller, M. D.; Cox, L. R. *Chem. Comm.* **2007**, 4035–4037.

41. Armitage, B.; Entwistle, N.; Jones, E. R. H.; Whiting, M. C. *J. Chem. Soc*. **1954**, 147–154.

42. W. A. Chalifoux, R. R. Tykwinski, *C. R. Chim.* **2009**, *12*, 341–358.

43. Szafert, S.; Gladysz, J. A. *Chem. Rev*. **2006**, *106*, PR1–PR33.

44. Kratscluner, W.; Lamb, L. D.; Fostiropoulos, K.; Huffman. D. R. *Nature*, **1990**, *347*, 354–358.

45. Métay, E.; Hu, Q.; Negishi, E.-i. *Org. Lett.* **2006**, *8*, 5773–5776.

46. Szilluweit, R.; Hoheisel, T. N.; Fritzsche, M.; Ketterer, B.; Morral, A. F.; Demurtas, D.; Laporte, V.; Verel, R.; Bolisetty, S.; Mezzenga, R.; Frauenrath H. *Nano Lett*. **2012**, *12*, 2573−2578.

47. Wang, Y.; Wang, Y.; Hosono, E.; Wang, K.; Zhou, H. *Angew. Chem. Int. Ed.* **2008**, *47*, 7461−7465.

48. Chalifoux, W. A.; Tykwinski, R. R. *Nat. Chem.* **2010**, *2*, 967–971.

49. Webster, A. *Mon. Not. R. Astron. Soc*. **1980**, *192*, 7–9.

50. Hayatsu, R., Scott, R. G., Studier, M. H., Lewis, R. S.; Anders, E. *Science*, **1980**, *209*, 1515–1518.

51. El Goresy, A.; Donnay, G. *Science* **1968**, *161*, 363–364.

52. Siemsen, P.; Livingston, R. C.; Diederich, F. *Angew. Chem. Int. Ed.* **2000**, *39*, 2632–2657.

53. (a) Weller, M. D.; Cox, L. R. *C. R. Chimie* **2009**, *12*, 366–377. (b) Orita, A.; Otera, J. *Chem. Rev.* **2006**, *106*, 5387–5412.

54. Clayden, J.; Greeves, N.; Warren, S.; Wothers, P. *Organic chemsitry*. Oxford University Press, Oxford, **2001**, pp 181–207.

55. Glaser, C. *Ber. Dtsch. Chem. Ges.* **1869**, *2*, 422–424.

56. Lei, A.; Srivastava, M.; Zhang, X. *J. Org. Chem.* 2002, *67*, 1969–1971.

57. Marsden, J. A.; Miller, J. J.; Haley, M. M. *Angew. Chem. Int. Ed.* **2004**, *43*, 1694–1697.

58. Chinchilla, R.; Najera, C. *Chem. Rev.* **2014**, *114*, 1783–1826.

59. Cadiot, P.; Chodkiewicz, W. In *Chemistry of Acetylenes*; Viehe, H. G., Ed; Dekker: New York, 1969; pp 597–647.

60. Sonogashira, K. *J. Organomet. Chem.* **2002**, *653*, 46–49.

61. Chinchilla, R.; Najera, C. *Chem. Soc. Rev.* **2011**, *40*, 5084–5121.

62. (a) Buttenberg, W. P. *Liebigs Ann. Chem.* **1894**, *279*, 324–337. (b) Fritsch, P. *Liebigs Ann. Chem.* **1894**, *279*, 319–324. (c) Wiechell, H. *Liebigs Ann. Chem.* **1894**, *279*, 337–344.

63.(a) Eisler, S.; Tykwinski, R. R. *J. Am. Chem. Soc*. **2000**, *122*, 10736–10737. (b) Eisler, S.; Chahal, N.; McDonald, R.; Tykwinski, R. R. *Chem. Eur. J.* **2003**, *9*, 2542–2550. (c) Kendall, J.; McDonald, R.; Ferguson, M. J.; Tykwinski, R. R. *Org. Lett.* **2008**, *10*, 2163–2166. (d) Luu, T.; Shi, W.; Lowary, T. L.; Tykwinski, R. R. *Synthesis* **2005**, 3167–3177. (e) Spantulescu, A.; Luu, T.; Zhao, Y.; McDonald, R.; Tykwinski, R. R. *Org. Lett.* **2008**, *10*, 609–612.

64. Tobe, Y.; Iwasa, R.; Umeda, R.; Sonoda, M.; *Tetrahedron Lett.* **2001**, *42*, 5485–5488.

65. Rubin, Y.; Lin, S. S.; Knobler, C. B.; Anthony, J.; Boldi, M.; Diederich, F. *J. Am. Chem. Soc.* **1991**, *113*, 6943–6949.

66. a) Grill, L.; Dyer, M.; Lafferentz, L.; Persson, M.; Peters, M. V.; Hecht, S. *Nat. Nanotechnol*. **2007**, *2*, 687–691. b) Lafferentz L.; Ample, F.; Yu, H.; Hecht, S.; Joachim, C.; Grill, L. *Science* **2009**, *323*, 1193–1197. c) Saywell, A.; Schwarz, J.; Hecht, S.; Grill, L. *Angew. Chem.* **2012**, *124*, 5186–5190; *Angew. Chem. Int. Ed*. **2012**, *51*, 5096–5100. (d) Bieri, M.; Blankenburg, S.; Kivala, M.; Pignoli, C. A.; Ruffieux, P.; Müllen, K.; Fasel, R. *Chem. Commun*. **2011**, *47*, 10239–10241. (e) Cai, J.; Ruffieux, P.; Jaafar ,R.; Bieri, M.; Braun, T.; Blankenburg, S.; Muoth, M.; Seitsonen, A. P.; Saleh, M.; Feng, X.; Müllen, K.; Fasel, R. *Nature* **2010** , *466*, 470–473.

67. (a) Gao, H.-Y.; Wagner, H.; Zhong, D.; Franke, J.-H.; Studer, A.; Fuchs, H. *Angew. Chem. Int. Ed*. **2013**, *52*, 4024–4028. (b) Gao, H.-Y.; Franke, J.-H.; Wagner, H.; Zhong, D.; Held, P.-A.; Studer, A.; Fuchs, H. *J. Phys. Chem. C***2013**, *117*,18595–18602.

68. Kiji, J.; Kaiser, J.; Wegner, G.; Schulz, R. C. *Polymer* **1973**, *14*, 433–439.

69. Xiao, J.; Yang, M.; Lauher, J. W.; Fowler, F. W. *Angew. Chem. Int. Ed*. **2000**, *39*, 2132–2135.

70. (a) Huuskonen, J.; Buston, J. E. H.; Scotchmer, N. D.; Anderson, H. L. *New J. Chem.* **1999**, *23*, 1245–1252. (b) Simpkins, S. M. E.; Kariuki, B. M.; Cox, L. R. *J. Organomet. Chem.* **2006**, *691*, 5517–5523. (c) Sugiyama, J.; Tomita, I. *Eur. J. Org. Chem.* **2007**, 4651–4653. (d) Shir, I. B.; Sasmal, S.; Mejuch, T.; Sinha, M. K.; Kapon, M.; Keinan, E. *J. Org. Chem.* **2008**, *73*, 8772–8779.

71. (a) Langton, M. J.; Matichak, J. D.; Thompson, A. L.; Anderson, H. L. *Chem. Sci.* **2011**, *2*, 1897–1901.

72. Crowley, J. D.; Goldup, S. M.; Lee, A-L.; Leigh, D. A.; McBurney, R. T. *Chem. Soc. Rev*. **2009**, *38*, 1530–1541.

73. Later, we and others reported the first synthesis of polyyne rotaxanes: Movsisyan, L. D.; Kondratuk, D. V.; Franz, M.; Thompson, A. L.; Tykwinski, R. R.; Anderson, H. L. *Org. Lett.* **2012**, *14*, 3424–3426. Weisbach, N.; Baranová, Z.; Gauthier, S.; Reibenspies, J. H.; Gladysz, J. A. *Chem. Commun*. **2012**, *48*, 7562–7564.

74. (a) *Catenanes, Rotaxanes and Knots*. Academic Press, Shill, G. New York, **1971**. (b) Dichtel, W. R. ; Miljanić, O. Š.; Zhang, W. ; Spruell, J. M.; Patel, K.; Aprahmian, I.; Heath, J. R.; Stoddart, J. F. *Acc. Chem. Res.* **2008**, *41*, 1750–1761. (c) Fang, L.; Olson, M. A.; Benı´tez, D.; Tkatchouk, E.; Goddard III, W. A.; Stoddart, J. F. *Chem. Soc. Rev*. **2010**, *39*, 17–29. (d) Stoddart, J. F. *Chem. Soc. Rev.* **2009**, *38*, 1802–1820. (e) *Molecular Catenanes, Rotaxanes and Knots*. Editors: Sauvage, J.-P.; Dietrich-Buchecker, C. O. Wiley-VCH, Weinheim, **1999**. (f) Beves, J. E.; Blight, B. A.; Campbell, C. J.; Leigh, D. A.; McBurney, R. T. *Angew. Chem. Int. Ed*. **2011**, *50*, 9260–9327.

75. Wu, C.; Lecavalier, P. R.; Shen, Y. X.; Gibson, H. W. *Chem. Mater*. **1991**, *3*, 569–572.

76. Solladié, N.; Chambron, J.-C.; Sauvage, J.-P. *J. Am. Chem. Soc*. **1999**, *121*, 3684–3692.

77. Aucagne, V.; Hänni, K. D.; Leigh, D. A.; Lusby, P. J.; Walker, D. B. *J. Am. Chem. Soc.* **2006**, *128*, 2186–2187.

77. (a) Kolb, H. C.; Finn, M. G.; Sharpless, K. B. *Angew. Chem., Int. Ed*. **2001**, *40*, 2004–2021. (b) Wang, Q.; Chittaboina, S.; Barnhill, H. N. *Lett. Org. Chem.* **2005**, *2*, 293–301.

78. Aucagne, V.; Bern, J.; Crowley, J. D.; Goldup, S. M.; Hänni, K. D.; Leigh, D. A.; Lusby, P. J.; Ronaldson, V. E. Slawin, A. M. Z.; Viterisi, A.; Walker, D. B. *J. Am. Chem. Soc*. **2007**, *129*, 11950–11963.

79. Saito, S.; Takahashi, E.; Nakazono, K. *Org. Lett*. **2006**, *8*, 5133–5136.

80. Goldup, S. M.; Leigh, D. A.; Lusby, P. J.; McBurney, R. T.; Slawin, A. M. Z. *Angew. Chem*. **2008**, *120*, 3429–3432; *Angew. Chem. Int. Ed*. **2008**, *47*, 3381–3384.

Chapter 2

Mechanical but still organic, How to connect two nanoscale electrodes, When length and size become important

Chapter 2. Synthesis of Rotaxanes via Active Metal Template Homocoupling of Polyynes

2.1 Introduction[1]

One of the main problems in the synthesis of polyynes is the stability, which decreases substantially as a function of length.[1] It was shown that large, sterically demanding end-capping groups stabilize longer polyynes.[2,3] For instance, the utilization of the bulky tris(3,5-di-*t*-butylphenyl)methyl end-group (Tr*, referred here as 'supertrityl', Figure 2.1) enabled the synthesis of polyynes with up to 22 triple bonds, the longest known polyyne to date.[4] The influence of the terminal groups on the properties and stability of a polyyne is expected to decrease as the polyyne becomes longer. Several authors have suggested that polyynes could be stabilized by threading them through macrocycles to form rotaxanes or polyrotaxanes.[5] In the Anderson group rotaxination of organic molecules has been widely used as a valuable strategy for modifying the properties of long conjugated π-systems, by generating 'insulated molecular wires'.[6] Previously, other groups have shown that polyynes can be encapsulated by forming double-helical 'bean-pole'complexes,[7] by co-crystallization with planar mercury(II) complexes,[8] and by trapping them inside carbon nanotubes.[9] The homocoupling of terminal acetylene has been proved as a convenient reaction to assemble rotaxanes, catenanes and knots,[10] and in some cases the coupling of acetylene was catalyzed by active Cu(I)-template.10mnug In the active template synthesis the metal acts as both template controlling the position of the building blocks during the reaction and catalyst forming a covalent bond and mechanically locking the final building compartments. The Anderson group recently showed that an active-metal template synthesis strategy can be utilized to make two different [2]rotaxanes with porphyrin stoppers and a butadiyne linker.[11] This work was the only reported example of polyyne rotaxanes with the axle entirely consisting of butadiyne linker.[12] Therefore, we were interested in the investigation of the synthesis of rotaxanes with extended polyyne chain. The Cu(I)-catalyzed active-metal template synthesis of rotaxanes was chosen to achieve the molecular insulation of polyynes. This chapter describes the preparation of a family of rotaxanes threaded with different macrocycles and up to 12 triple bonds in axle using bulky supertrityl end-capped polyynes under active-metal template homocoupling reaction conditions.

[1] A part of this chapter has been published. Movsisyan, L. D.; Kondratuk, D. V.; Franz, M.; Thompson, A. L.; Tykwinski, R. R.; Anderson, H. L. *Org. Lett.* **2012**, *14*, 3424–3426.

2.2 Synthesis of polyynes

The synthesis of polyynes **2.1**, **2.2** and **2.5** with a tris(3,5-di-*tert*-butylphenyl)methyl (supertrityl = Tr*) end-group (Figure 2.1) was carried out as described in literature.[4] The **2.3** and **2.4** polyynes were generously provided by Michael Franz from the Tykwinski group (Friedrich-Alexander-Universität, Erlangen, Germany). The Tr* end-group (~14 Å in diameter) is bulky enough to prevent the slippage of the macrocycle (cavity size ~9×7 Å) from the dumbbell-like thread.

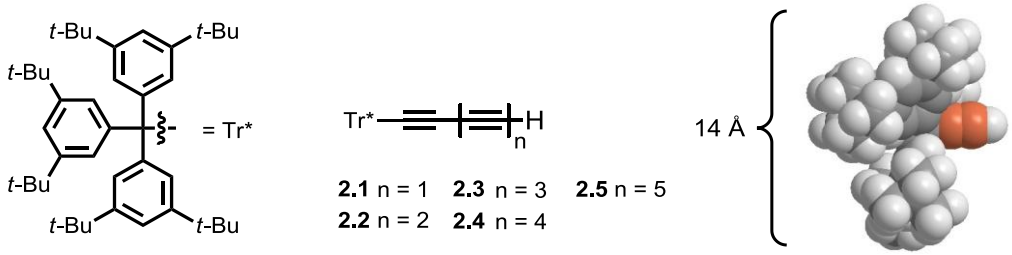

Figure 2.1 The supertrityl polyynes. The size of Tr* group is calculated from the reported X-ray structure.[4]

The supertrityl end-group was synthesized using cheap, commercially available starting materials. A three-fold Friedel-Craft alkylation of benzene with 2-chloro-2-methylpropane at –20 °C gave 1,3,5-tri-*t*-butylbenzene (**2.6**) in 71% yield (Scheme 2.1).[14] The substitution one *t*-butyl group with bromine in the presence of iron turnings at 0 °C afforded a mono-substituted product **2.7** in 85% yield.[15] Formation of the Grignard, followed by addition to diethyl carbonate, yielded supertritylalcohol **2.8** in 94% yield.[4] The alcohol (**2.8**) was converted to the supertrityl chloride (**2.9**) using oxalyl chloride in THF, then the addition of ethynylmagnesium bromide gave supertritylacetylene (**2.10**) in 88% yield over the two steps.[16] The supertritylacetylene (**2.10**) was used as feedstock for all supertrityl polyynes and precursors.

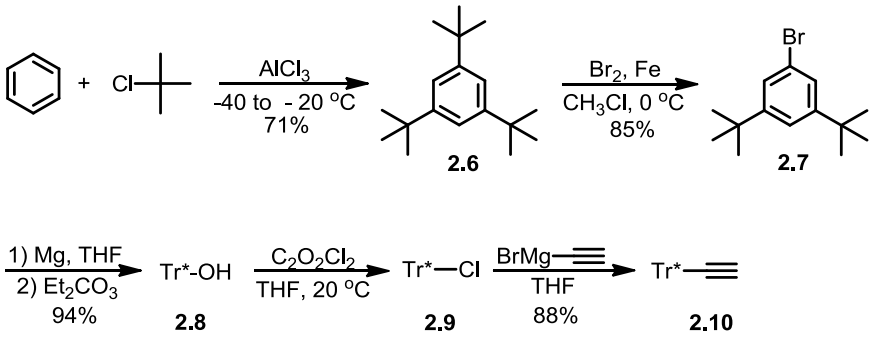

Scheme 2.1 The synthesis of supertritylacetylene **2.10**.

The next target in the synthesis of polyyne series was the supertrityl terminal diyne **2.1**. It was shown that **2.1** is readily accessible via Fritsch-Buttenberg-Wiechell (FBW) carbenoid rearrangement of the

dibromolefine **2.12** (Scheme 2.2). This route was preferred, as it did not generate unwanted by-products which would be generated during the synthesis of asymmetrical butadiynes under Glaser coupling conditions.[4] The reaction of *n*-BuLi with supertritylacetylene **2.10** in THF at –78 °C, followed by the addition of DMF resulted in an aldehyde **2.11** in 88% yield. Dibromoolefination under Ramirez conditions led to **2.7** in 87% yield.[17] Finally, the FBW rearrangement of **2.7** in THF via addition of *n*-BuLi at –78 °C yielded terminal diyne **2.1** in 90%.[4]

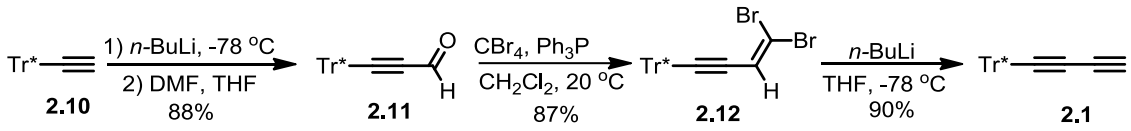

Scheme 2.2 The synthesis of supertrityl diyne **2.1**.

The synthesis of **2.2** was accomplished using the procedure based on the FBW rearrangement as it was shown to be the most efficient for the synthesis of Tr*-triyne **2.2**.[18] Supertritylacetylene **2.10** was lithiated by *n*-BuLi at –78 °C in THF. The solution was then transferred to a THF solution of triisopropylsilyl propargylic aldehyde **2.13**[18] to afford alcohol **2.14** in 90% yield (Scheme 2.3). Oxidation of alcohol **2.14** to ketone **2.15** using pyridinium clorocromate (PCC) proceeded smoothly with 96% yield. Dibromoolefination of **2.15** to give **2.16** (96%) followed by a FBW rearrangement (88%) led to the TIPS-protected triyne **2.17**. The desilylation of **2.17**, carried out in cold THF using TBAF, afforded the terminal triyne **2.2** in 86% yield.

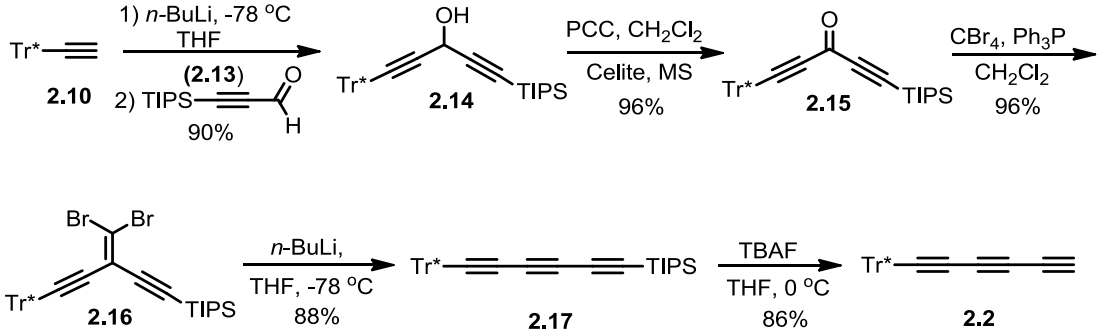

Scheme 2.3 Synthesis of supertrityl triyne **2b**.

The TIPS protected precursor of pentayne **2.4** was obtained using a modified Glaser-Eglinton-Hay[19-22] coupling, optimized by Chalifoux,[4] where a mixture of deprotected supertrityldiyne **2.1** and 1-TIPS-6-TMS-hexa-1,3,5-triyne **2.18** was cross-coupled (Scheme 2.4). The TMS group underwent *in situ* proto-desilylation, producing the active mono-free acetylene polyyne coupling partner. The reaction was

complete after 12 h stirring, yielding the product **2.19** in 71%. The homocoupling of 1-TIPS-hexa-1,3,5-triyne proceeds easier then the cross-coupling with **2.1**, and since **2.1** is the more precious partner, the TIPS precursor was used in a five-fold excess, and the 1,12-bis(TIPS)-hexayne was the main by-product (The yield of 1,12-bis(TIPS)-hexayne was not calculated as it was not separated as a pure compound). The products of this reaction were easily separated by column chromatography (silica, hexanes), due to higher polarity of the TIPS-capped compared to the Tr*-capped polyynes. The deprotection of pentayne **2.19** was carried out in mild conditions using CsF in the mixture of THF/H_2O affording the product **2.4** quantitatively (98% yield).

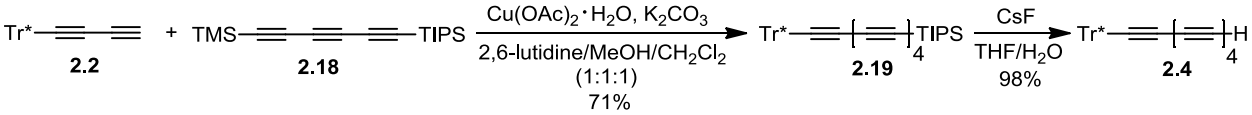

Scheme 2.4 Synthesis of supertrityl pentayne **2.4**.

2.3 Synthesis of macrocycle M1

In the active template synthesis of rotaxanes the macrocycle must be able to bind the metal ion, since it acts both as template and catalyst.[23] 1,10-Phenanthrolines bind strongly with Cu(I) ions, which makes them ideal for Cu(I)-catalyzed active-template Glaser coupling.[23,13] 1,10-Phenanthroline-based macrocycles are one of the broadly utilized molecules in the synthesis of rotaxanes and catenanes.[24] The successful use of a 33-membered 1,10-phenanthroline macrocycles in the Cu(I) catalyzed Glaser coupling by Saito,[13] and later by Langton,[11] served as a good milestone to test the synthesis of polyyne rotaxanes.

We prepared a 33-membered phenanthroline macrocycle **M1** from 2,9-bis(4-hydroxyphenyl)-1,10-phenanthroline (**2.20**) and 1,3-bis(bromohexyloxy)benzene (**2.21**).[11] First, bromoanisole was lithiated by *t*-BuLi and then added to a suspension of 1,10-phenanthroline in dry toluene. Subsequent oxidation of the reduced product with manganese(IV) dioxide resulted in the 2,9-aryl-substituted phenanthroline **2.22** in 55% yield (Scheme 2.5). The demethylation of **2.22** was carried out in a mixture of pyridine/conc. HCl at 140 °C yielding the product **2.20** quantitatively (99%). The demethylation reaction was very sensitive to the trace amount of moisture, therefore water was distilled first from the reaction mixture at 210 °C. At the end of the distillation, the pressure was lowered (100 mbar), which guaranteed effective removal of moisture. The macrocycle synthesis was carried out in diluted DMSO to minimize the formation of the linear by-products from intermolecular side-reactions. After column chromatography on silica followed by

recrystalization from CH_2Cl_2/CH_3OH the product **M1** was isolated in 49% yield. Changing from K_2CO_3 to Cs_2CO_3 and from DMSO to DMF did not affect the macrocycle formation yield significantly.

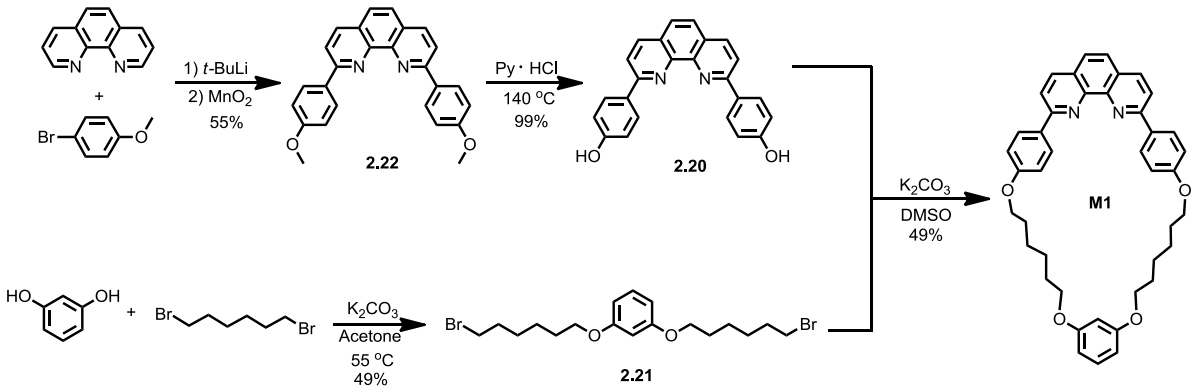

Scheme 2.5 Synthesis of macrocycle **M1**.

2.4 The synthesis of polyyne rotaxane 2b⊂M1

Supertrityl triyne **2.2** was identified as a candidate for rotaxane synthesis as the length of three triple bonds was considered optimal compared to the diyne, where steric factors due to the shortness of the polyyne chain could harm the reaction. With the macrocycle **M1** in hands, we decided to test the active metal template synthesis of polyyne rotaxane under Cu(I) catalyzed Glaser coupling conditions reported by Saito and coworkers.[22] In this work the threading of a butadiyne axle with macrocycle was carried out in the presence of **M1**·Cu(I) complex, where the active Cu(I) can coordinate two terminal acetylenes and catalyze the formation of C–C bond within the macrocycle cavity (Scheme 2.6). In that work, the rotaxane was synthesized in toluene at 110 °C, conditions that could be too harsh for our aims considering the tendency of the triyne **2.2** to decompose at high temperatures. In a modified version of this procedure, reported by Langton, porphyrin rotaxanes were synthesized in 1:1 mixture of toluene/THF at lower temperature (60 °C).[11] These conditions were chosen for a test reaction (Scheme 2.6). As oxidant, one equivalent I_2 was used and the reaction was monitored by TLC and MALDI mass spectrometry. After 5 days of stirring the TLC confirmed the reaction completion and the rotaxane **2b⊂M1** was isolated after aquaous KCN workup, followed by column chromatography in 6.7% yield.

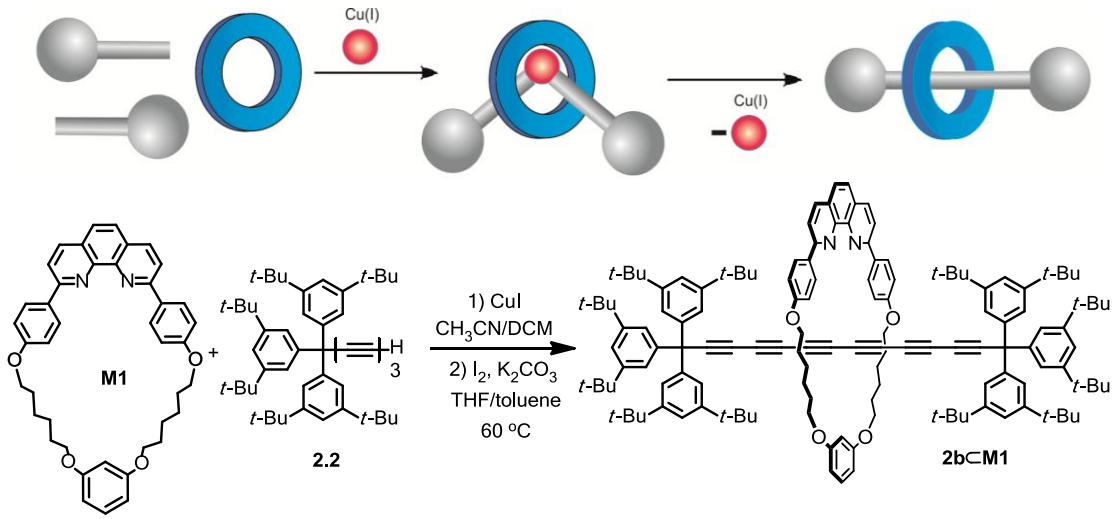

Scheme 2.6 The schematic view of the active metal template synthesis of polyyne rotaxanes and the synthesis of **2b⊂M1** rotaxane.

This result was encouraging, since it showed that our strategy of the synthesis for supertrityl hexayne rotaxane was fruitful. The next logical goal was the optimization of the rotaxane yield. In this test reaction, we prepared the **M1**·CuI complex in CH_2Cl_2/CH_3CN 1:1 solution using 1.0 equivalent CuI and 1.5 equivalent **M1** macrocycle (Table 2.1, entry 1) as initially reported by Langton.[11] This ratio of Cu(I) and **M1** was chosen, as it was envisioned that the excess macrocycle would suppress the formation of free hexayne dumbbell through homocoupling of terminal acetylene by free Cu(I) resulting from the dissociation of the **M1**·CuI complex. The triyne **2.2** was used in stoichiometric amount (2 equivalent) and the reaction was carried out in an air-saturated solution. In the next step we increased the amount of I_2 by a factor of 2, which gave small increase in rotaxane yield (8.5%, Table 2.1 entry 2), indicating that excess oxidant is beneficial. Later, we always used the oxidant in a slight excess (1.25 eq.). We were aware that additional amounts of iodine should not harm polyynes as it was shown before that polyynes reversibly form inclusion complexes with molecular iodine in hexane under UV-irradiation, but no irreversible reaction was reported.[25]

Mechanistic studies of active-template reactions involving the closely related Cu(I) catalyzed CuAAC "click" reactions, suggest that the reaction proceeds via a bimetallic intermediate.[26] If this is the case with active metal template Glaser homocoupling of polyynes, the excess macrocycle could interfere with the formation of Cu···Cu catalytic centers and lower the product yield. Thus, we prepared the **M1**·CuI complex in a 1:1 ratio, which under the previously tested conditions gave the rotaxane **2b⊂M1** in 12.6% (Table 2.1, entry 3). The two-fold increase in product yield is in an agreement with the suggested

hypothesis, however it would be too bold to deduce the reaction mechanism from only this experimental result.[27] The reaction was complete after 5 days and an obvious way to increase the reaction rate could be the investigation of higher temperatures. Having this idea in mind, we carried out the reaction in toluene under reflux (Table 2.1, entry 4). However, the result was disappointing as after 5 days of stirring the TLC showed complete consumption of the starting acetylene, but no rotaxane was formed. One of the reasons of the reaction failure could be insolubility of the K_2CO_3 in toluene. To test this hypothesis, organic N,N-diisopropylethylamine (DIPEA) base was used instead of K_2CO_3 (Table 2.1, entry 5), but again TLC did not show rotaxane formation after 5 days of stirring at 110 °C. Another explanation for this negative result could be the decomposition of the triyne **2.2** at 110 °C. Interestingly, when the reaction was carried out at 100 °C in toluene, in the presence of K_2CO_3 the rotaxane was separated in 8.4% yield (Table 2.1, entry 6). The reaction was complete after 24 h stirring, which was a significant improvement, even if the reaction yield was still relatively low. Another possible optimization was the choice of the oxidant. In previous test experiments, we used I_2 (E^0 = +0.54 V) which is readily soluble in toluene and THF. In organic chemistry, 1,4-benzoquinone (BQ) is one of the most widely used organic oxidant, despite the fact that its redox potential is highly dependent on the reaction conditions.[28] BQ was tested to substitute iodine in the synthesis of **2b⊂M1** rotaxane. At the same time the amount of **2.2** triyne was increased to 2.5 equivalents. TLC analysis of the reaction mixture showed the consumption of acetylene after 5 days, yielding the rotaxane **2b⊂M1** in 15.2% yield (Table 2.1, entry 7). BQ proved to be equally as good oxidant as iodine with slightly better rotaxane yield, which could be result of excess acetylene rather the effect of the BQ. Thus, the use of iodine was still preferred as the separation of BQ and its reduced products from the reaction mixture could be challenging.

Table 2.1. Summery of reaction conditions of the synthesis of **2b⊂M1**.

	CuI, *eq.*	**M1**, *eq.*	**2.2**, *eq.*	Oxidant, *eq.*	Solvent	T, °C	Yield	Time	Base
1	1	1,5	2.0	I_2, 1	THF/toluene	60	6.7%	5 days	K_2CO_3
2	1	1.5	2.0	I_2, 2	THF/toluene	60	8.5%	5 days	K_2CO_3
3	1	1	2.0	I_2, 1.25	toluene	60	12.6%	5 days	K_2CO_3
4	1	1	2.0	I_2, 1.25	toluene	110	-	5 days	K_2CO_3
5	1	1	2.0	I_2, 1.25	toluene	110	-	5 days	DIPEA
6	1	1	2.0	I_2, 1.25	toluene	100	8.4%	1 day	K_2CO_3
7	1	1	2.5	BQ, 1.25	toluene	100	15.2%	5 days	K_2CO_3
8	1	1	2.5	I_2, 1.25	THF	60	32%	10 h	K_2CO_3

BQ–1,4-benzoquinone; DIPEA-diisopropylethylamine; Rotaxane yields are calculated referring to the amount of the macrocycle.

Finally, the last optimization was to change the solvent to THF and decrease the temperature to 60 °C, which surprisingly afforded rotaxane in 32% yield (Table 2.1, entry 8) and shortened the reaction time down to 10 h. The reason of the increased rotaxane yield in THF was not clear. It is possible that THF decreases the energy of the transition state through better solvation. In all experiments, we did not detect the formation of free hexayne resulting from the homocoupling of **2.2** outside the macrocycle (TLC). Upon silica chromatography column, a yellow fraction with poor solubility in hexanes was collected before the rotaxane fraction. The UV-Vis spectrum of this fraction showed a broad absorption and no indication of any polyyne chain (distinct absorption pattern, *vide infra*). We did not pursue further investigation of the nature of this by-product.

The unthreaded macrocycle **M1** collected from column chromatography was not pure, and a second silica column and recrystallization were needed to purify it back to reagent grade. Due to some loss of material during the purification procedures, the collected amounts of macrocycle were always less than expected.

Finally, to explore the effect of atmospheric oxygen, in one test reaction the reaction mixture was degassed through three cycles of freeze-pump-thaw, saturated with nitrogen and stirred under the conditions pointed in the entry 8, Table 2.1. The yield of rotaxane was similar in air- and N_2-saturated THF.

2.5 The synthesis of polyyne rotaxanes 2a⊂M1, 2c⊂M1, 2d⊂M1 and 2e⊂M1.

With improved conditions for the synthesis of polyyne rotaxane **2b⊂M1**, we moved towards the synthesis of other polyyne rotaxanes, being curious which would be the longest and shortest polyyne that could be threaded with the macrocycle **M1**.

The reaction of supertrityl diyne **2.1** with macrocyclic Cu(I) complex under the optimized conditions was complete after 24 h, and gave the product **2a⊂M1** in 34% yield (Scheme 2.7). Attempts to prepare the corresponding shorter C4 rotaxane from the terminal acetylene **2.5** were not successful, and it seems that the polyyne chain needs at least 8 *sp* carbon atoms to accommodate the macrocycle. Interestingly, in the porphyrin-capped rotaxanes it was possible to thread the butadiyne linker using the same macrocycle and homocoupling reaction.[11]

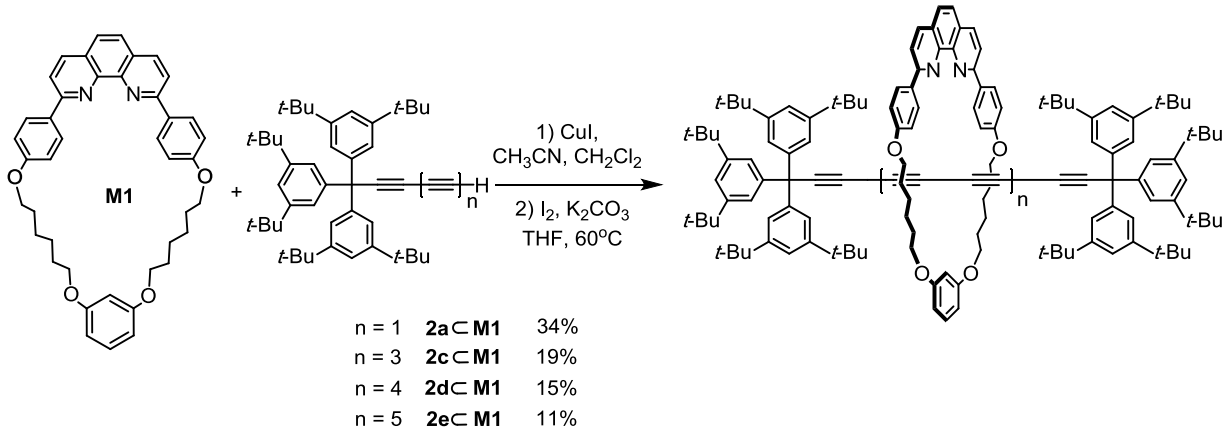

Scheme 2.7 The synthesis of polyyne rotaxanes **2a⊂M1**, **2c⊂M1**, **2d⊂M1** and **2e⊂M1**.

In the next step supertrityl tetrayne **2.3** was injected under rotaxane synthesis conditions. After 40 h, the product **2c⊂M1** was isolated in 19% yield. For the synthesis of the C_{20} rotaxane the TIPS-protected precursor **2.19** was desilylated in a mild condition by CsF immediately before the rotaxane synthesis. The mixture with terminal pentayne was passed through silica plug (hexanes/CH_2Cl_2) and **2.4** was used as obtained for the rotaxane synthesis. After 36 h stirring of the reaction mixture, followed by workup, the product **2d⊂M1** was isolated in 15% yield.

The synthesis procedure for the **2e⊂M1** rotaxane was similar to **2d⊂M1**. The reaction was complete after 2 days and gave rotaxane **2e⊂M1** in 11% yield. A clear trend here was the decrease of the rotaxane yield and increase of the reaction time when polyyne gets longer. Lower yields can be explained considering the enhanced instability of the long acetylene precursors at 60 °C. The electronegativity of the terminal carbon atom and the polarity of the C–H bond increases with elongation of the polyyne chain, so we expected that longer polyynes must be more reactive requiring shorter reaction time, and supposedly better rotaxane yields. However, experiments showed that the product yield decreases with elongation of polyyne chain; this could be due to instability of long polyynes at 60 °C.

While ^{1}H NMR of **2e⊂M1** rotaxane was clean, the ^{13}C NMR showed minor signals accompanying to the resonances of C24 chain in the region of polyyne carbons (Figure 2.2). These signals belong to rotaxanes with shorter C22 and C20 carbon chains, which was confirmed by MALDI spectrometry. Previously, it was reported that for homocoupling of polyynes with 4 or more triple bonds there was loss of acetylene(s). This process was observed, for example, during the synthesis of decayne from **2.4** under Hay conditions, where a considerable amount of the nonayne was formed.[18] In the case of the synthesis of

dodecayne from **2.5** undecayne and decayne were formed.[4,18] The nature of the acetylene loss under Hay conditions is still not understood but has been reported in a number of other cases.[29] Thus, we identified this side reaction to be a problem for the polyyne rotaxane synthesis too. To purify the **2e⊂M1** rotaxane, the mixture in toluene was passed through SEC column (Bio-Beads-SX1). The UV-vis spectra of compound before and after SEC column clearly indicated a satisfactory purification (Figure 2.2). The final pure product was collected after couple of SEC column cycles and its purity was confirmed by ^{13}C NMR (Figure 2.2).

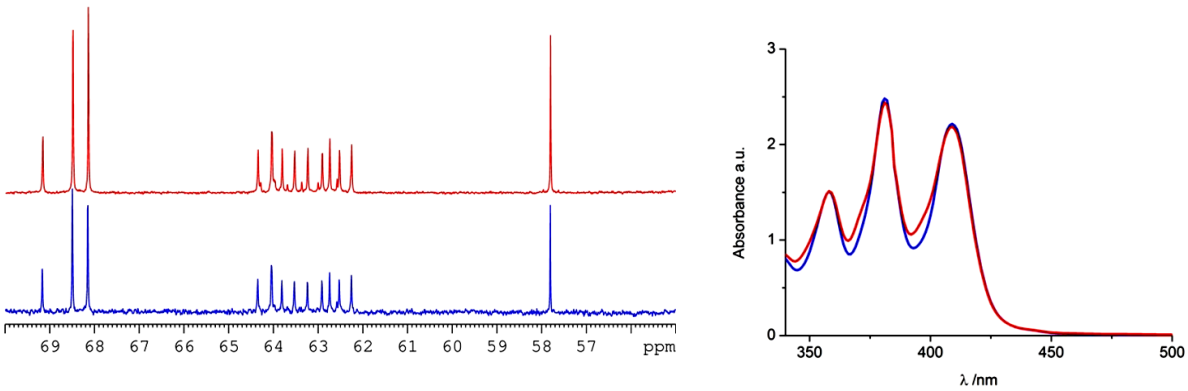

Figure 2.2 ^{13}C NMR (CD_2Cl_2, 125 MHz, 298 K) and UV-Vis absorption spectra (toluene) of rotaxane **2e⊂M1** before (red) and after SEC column (blue).

It seems, the synthesis of longer polyyne rotaxanes ($(C{\equiv}C)_n$, n > 12) becomes troublesome and attempts to synthesize rotaxane from supertrityl octayne were futile. The instability of extended polyynes at 60 °C was the main challenge. We tested the synthesis of **2b⊂M1** rotaxane in the THF at 45 °C, however, the reaction progress was incredibly slow (three days stirring the reaction did not get to completion with traces of rotaxane on TLC). This failed attempt indicates the limitation of current reaction conditions for preparation of longer rotaxanes.

2.6 Threading hexayne chain with different macrocycles

The supertrityl end-group is large enough to prevent the slippage of the relatively large macrocycle **M1**. The large cavity of the macrocycle limits the choice of stoppering groups preventing the use of simple, smaller end-groups. This disadvantage reduces the potential number of polyyne rotaxanes which could be synthesized and studied. Additionally, in many rotaxanes the macrocycle mechanically protects the thread from the environment, like in prodrugs and natural products,[30] mechanically protected dyes[31] and insulated molecular wires,[32] and a "tight" fit between macrocycle and thread is preferable. Therefore

stabilization of polyyne chain through tight molecular insulation is promising to access longer polyyne chains. Following this idea, the decision was made to test, under homocoupling conditions, series of macrocycles with smaller cavity. The triyne **2.2** was chosen for rotaxane synthesis since it is obtained in high yield, it is stable in its unprotected form at room temperature and its three triple bonds are long enough to eliminate steric factors imposed from the Tr* end-group.

First, the size of macrocycle **M1** was reduced by shortening the alkyl linker between phenanthroline and resorcinol moieties. New 29-member macrocycle **M2** was synthesized in 34% yield (Scheme 2.8) and the corresponding rotaxane **2b⊂M2** was isolated in 28% yield.

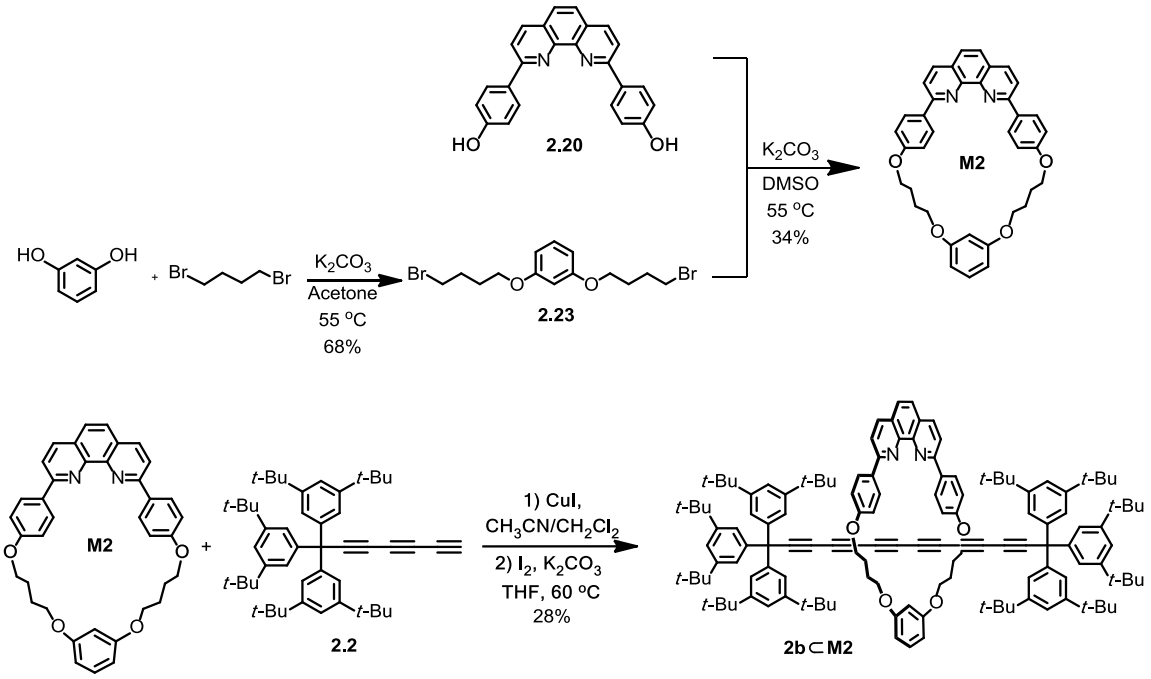

Scheme 2.8 Synthesis of macrocycle **M2** and hexayne rotaxanes **2b⊂M2**.

To further tighten the macrocycle, the cavity of the phenanthroline moiety was encycled with an alkyl strap. The new macrocycle **M3** was prepared from the reaction of **2.14** with 1,10-dibromodecane yielding the product in 29% yield. The corresponding rotaxane **2b⊂M3** was synthesized under active-metal Glaser homocoupling conditions in 17 % yield (Scheme 2.9).

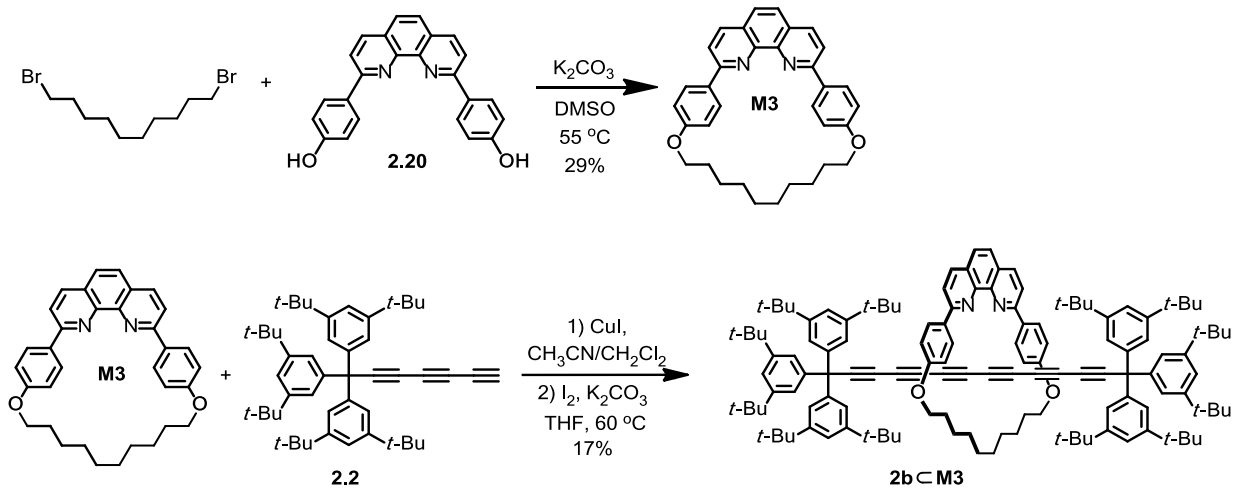

Scheme 2.9 Synthesis of macrocycle **M3** and hexayne rotaxanes **2b⊂M3**.

The decyl chain in the 26-membered macrocycle **M3** is smaller than macrocycle **M2.** Simple CPK modeling showed that further shortening of the strap, for example, by encycling the phenanthroline with an octane chain may be impossible, as the distance between phenolic OH groups of phenanthroline is slightly less then the length of the octyl chain. Moreover, for efficient protection of the polyyne chain the alkyl strap is not bulky enough and we decided to look for other possible condidates. In the literature, there was a report of another 27-member phenanthroline based macrocycle with a para-tolyl ether linker.[33] This macrocycle **M4** was considered as a good candidate for its small cavity and bulky *p*-tolyl ether linker. The macrocycle **M4** was synthesized in 50% yield, and the coupling of the triyne **2.2** under active metal Glaser homocoupling conditions resulted rotaxane **2b⊂M4** in 23% yield (Scheme 2.10).

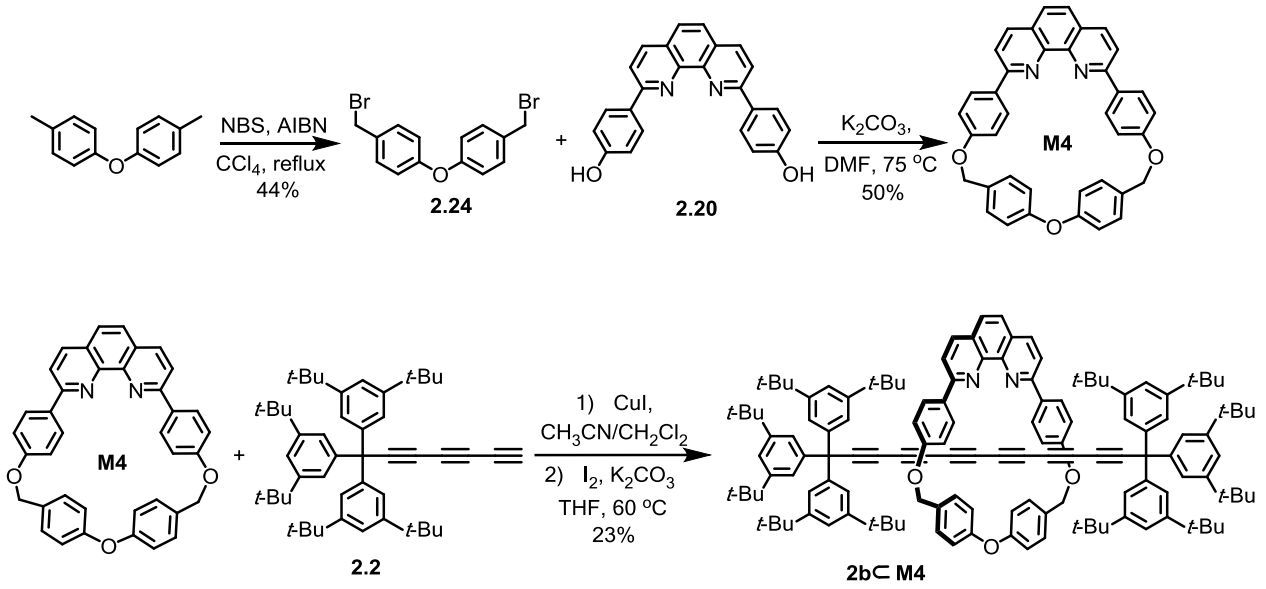

Scheme 2.10 Synthesis of macrocycle **M4** and hexayne rotaxanes **2b⊂M4**.

All macrocycles used for polyyne rotaxane synthesis were based on planar, rigid 1,10-phenanthroline. At the same time a number of 2,2'-bipyridine-based (bpy) macrocycles were utilized successfully in the synthesis of various rotaxanes,[34] but to our knowledge there was not a example of polyyne rotaxanes with a bpy-based macrocycle. The bipyridine moiety is more flexible than phenanthroline and could be less strained while being mechanically interlocked with polyynes. To test the rotaxination of hexayne chain with a bpy macrocycle, a 26-member macrocycle **M5** was generously provided by Dr Stephen Goldup from the Queen Mary University of London. The reaction of **M5** with **2.2** gave the rotaxane **2b⊂M5** in 23% yield under standard conditions (Scheme 2.11).

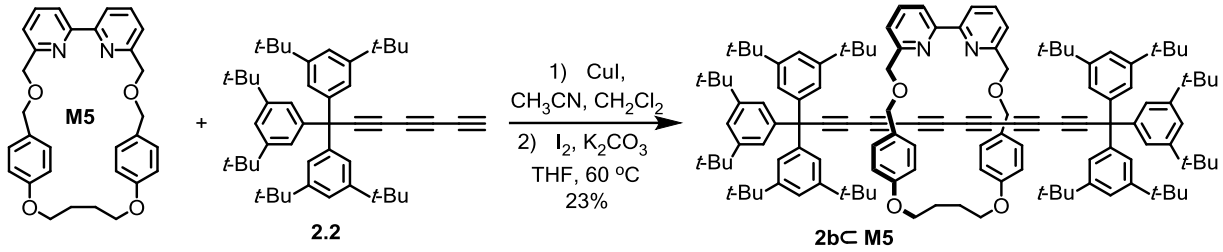

Scheme 2.11 Synthesis of hexayne rotaxanes **2b⊂M5**.

The yields of **2b⊂M4** and **2b⊂M5** rotaxanes are similar, and it seems there is not much difference between phenanthroline- and bpy-based macrocycles in term of product yields. The yields of all macrocycles and corresponding rotaxanes are summarized in Table 2.2.

Table 2.2. Summary of the yields of macrocycles formation and their corresponding hexayne rotaxanes **2b⊂M2**, **2b⊂M3**, **2b⊂M4** and **2b⊂M5**.

Macrocycle	Yield	Rotaxane	Yield
M2	34%	**2b⊂M2**	28%
M3	29%	**2b⊂M3**	17%
M4	50%	**2b⊂M4**	23%
M5	12%*	**2b⊂M5**	23%

*The yield is taken from ref. 34a. Yields are calculated referring to the amount of the macrocycles.

2.7. Synthesis of pyridine-capped hexayne rotaxane

Polyynes are very attractive molecules for electron transport through the carbon-rich backbone.[35] The almost cylindrical conjugation over the alternating single and triple bonds of the one-dimensional *sp*-backbone leads to proposed applications as molecular wires.[36] Theoretical studies suggest that polyynes could show metallic-like charge-transport characteristics when connected between two metal or graphene electrodes.[37] To connect polyynes to a metal surface (i.e. gold electrodes) proper anchoring groups must be design. So far, sulfur and nitrogen functionalized polyynes have been studied using single molecule

conductance techniques,[38] and shown that the electron transferring properties are almost independent from the length of carbon chain.[35] However, the synthesis of oligoynes encounters problems as the stability decreases rapidly with the increasing number of the triple bonds in the backbone: Due to instability, the number of triple bonds in differently capped polyynes never exceeded 4. Consequently, we were interested in the synthesis of longer polyyne molecular wires with enhanced stability, which might be achieved by the rotaxination of longer polyynes. The molecular insulation would not only enable to study the charge conducting properties of longer (-(C≡C)$_n$, n >2) chains, but also be the first example of molecularly insulated polyyne wires (Figure 2.3).

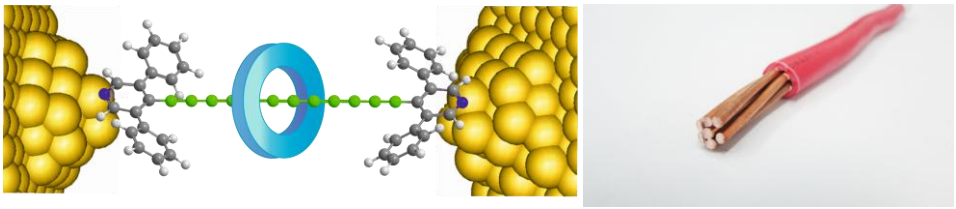

Figure 2.3. Ilustretion of the polyyne based insulated molecular wires between two gold electrodes and the analogy with metallic insulated wire.

To test the rotaxination, pyridine-functionalized, TIPS-protected triyne **Py1**, generously provided by Maximilian Krempe, from the Tykwinski group, was deprotected by adding TBAF. The free triyne was purified by passing the reaction mixture through a neutral alumina plug (EtOAc). The solution was concentrated and THF was added. This procedure was repeated couple of times without drying the sample until all EtOAc was removed, and the sample was proceeded for rotaxane synthesis using **M4** macrocycle. After 24 h stirring at 60 °C, followed by workup the product **Py2⊂M4** was isolated in disappointingly low 2% yield (Scheme 2.12). However, we managed to characterize the compound by ^{1}H and ^{13}C NMR and MALDI techniques.

Single molecule conductance studies of **Py2⊂M4** might help to better understand the nature of carbyne and utilize polyynes in atomic-scale nanodevices,[39] and are currently under investigation (Professor R. J. Nichols group, University of Liverpool).

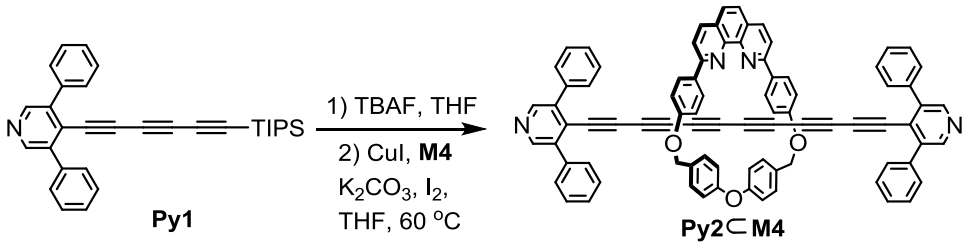

Scheme 2.12 Synthesis of hexayne rotaxane **Py2⊂M4**.

2.8 UV-Vis absorption and NMR spectroscopy of rotaxanes

The optoelectronic properties of polyynes are of special interest due to their nonlinear optical properties and charge-transport behavior, which may be exploited to create functional carbon-rich materials.[35,40] Absorption spectroscopy serves as a diagnostic tool to characterize polyynes because these molecules display very distinct, signature spectra, with well resolved fine structure.[40]

The threading of a polyyne chain in rotaxanes has not changed the basic electronics compared to the corresponding free dumbbells, synthesis of which is reported by Tykwinski et al. (Figure 2.4).[4]

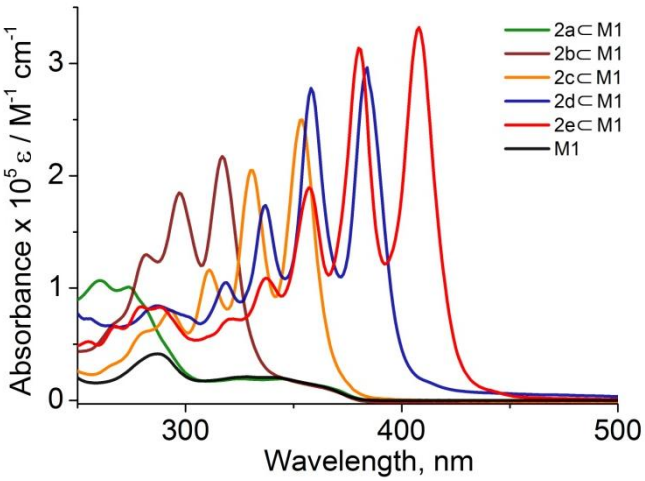

Figure 2.4 The UV-Vis absorption spectra of macrocycle **M1** (black line) and rotaxanes **2a-e⊂M1** in CH_2Cl_2.

The absorption spectra of rotaxanes represent the sum of macrocycle and polyyne absorptions. In the absorption spectra of tetrayne **2a⊂M1** and hexayne **2b⊂M1** rotaxanes (green and orange lines in Figure 2.4, respectably), the absorption of the dumbbell does not obscure the macrocycle which absorbs at up to 390 nm, while in longer rotaxanes the polyyne chain strong absorption overlays with the macrocycle. Another feature is the maintained vibronic progression of the polyyne absorption bands in rotaxanes comparable with bare polyynes[4] with some bathocromic shift of the peak positions (~ 4 nm). In general,

the lowest energy absorption of rotaxanes **2a-e⊂1** is red-shifted and the extinction coefficient increases with the increase of the polyyne chain length due to the extended π-system.

Investigation of ^{1}H-NMR spectra of rotaxanes **2a–e⊂M1** revealed interesting trends. Upon threading, the protons of the macrocycle's resorcinol moiety clearly experience a different environment, as their signals shift in different directions (Figure 2.5). The proton H_h experiences a downfield shift while protons H_f and H_g were up-shifted. In parallel to the increase of the polyyne length, these shifts are decreasing so that in **2e⊂M1** rotaxane, the chemical shift became almost identical to those from free macrocycle **M1**.

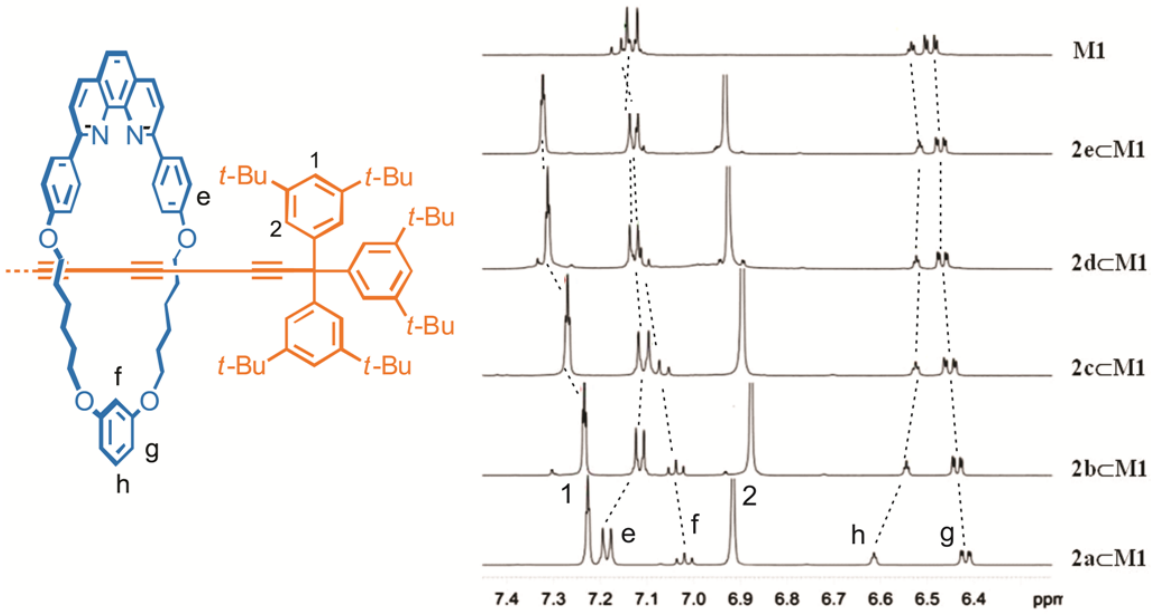

Figure 2.5 The proton shifts in series of rotaxanes **2a-e⊂M1** in ^{1}H NMR (CD_2Cl_2, 500 MHz, 298 K). Top spectrum is the **M1** macrocycle.

This behavior can be explained by interaction of the bulky end-groups.[41] For a short polyyne chain, this effect is the most distinctive, since the endgroups are in very close proximity to the macrocycle. With increasing chain length however, the shifts vanish, a fact suggesting that the macrocycle does not 'feel' the presence of the end-groups anymore. In the ^{1}H NMR, there is another obvious proton shift: the aromatic distal proton of 'supertrityl' end-group gradually downshifts (red cycle, Figure 2.5) while the shift of other two equivalent aromatic protons does not fit any particular trend.

2.9 X-ray crystallographic characterization of rotaxanes

Over decades there has been a strong interest in the crystal structures of polyynes,[42,43] regarding the reduced bond length alternation (BLA) and the deviation from linearity in the crystal lattice.[44] The BLA is

defined as the difference of CC equilibrium bond length between adjacent single and triple bonds: BLA = $d_{(C-C)} - d_{(C\equiv C)}$. For long polyynes, the question of interest is will the triple and single bond lengths converge to one value, or approach two different values? The former (bond length equalization) means a vanishing HOMO/LUMO energy gap. The latter (bond length alternation) implies a persistent energy gap. From the electronic absorption spectra of the series of Tr* polyynes Tykwinski showed that infinitely long polyynes (carbyne) have finite bandgap with λ_{max} = 485 nm (2.56 eV).[4] Another experimental evidence was published from the same group, demonstrating the saturation of BLA through crystallographic analysis of the series of *t*-butyl capped polyynes.[45] This implies that carbyne must be composed of alternating single and triple bonds. Another question is to what degree a carbon chain can easily bend. And, it is in polyyne rotaxanes that the curvature of the carbon chain gains special interest as the molecular encapsulation can impose additional bending in the same place with lattice packing effects.

Here we present four crystal structures of polyyne rotaxanes, and compare them with the structures of similar known polyynes. Crystals were grown by solvent vapor diffusion specified for each molecule below. Diffraction data for **2b⊂M1**, **2b⊂M3** and **2c⊂M1** were collected at 100 K using synchrotron radiation at the Diamond Light Source, beam line I19. The structures were solved using charge flipping[49] with SuperFlip[50] and refined using least-squares within CRYSTALS[51] by Dr. Amber L. Thompson (Oxford Crystallography). The diffraction data for **2b⊂M4** and macrocycle **M4** was collected at 173 K using SuperNova (Cu) X-ray Source. The structure was solved by ShelXS program[52] using Direct Methods and refined with the ShelXL program using Least Squares minimization by Dr. Frank Hampel (Friedrich-Alexander-Universität, Department of Chemistry).

2b⊂M1: Crystals of **2b⊂M1**were grown by diffusion of methanol vapor into a solution of the compound in THF. The asymmetric unit contains one molecule of the **2b⊂M1** and four molecules of methanol, space group is P-1. The molecules of **2b⊂M1** form pairs with π-π interactions (stacking) between vicinal phenanthroline moieties (Figure 2.6). The planes of phenanthroline moieties in the pairs are parallel to each other. The distance between phenanthroline planes is 3.50(2) Å. The planes were fitted through 12 carbon atoms and 2 nitrogen atom of the phenanthroline core. Similar pairing behavior has been reported for the porphyrin dimer rotaxane featuring the same macrocycle **M1**.[11] In the latter case,

however, phenanthroline moieties are shifted over towards the oxyphenyl moieties. The distance between phenanthroline planes in the porphyrin dimer rotaxane [3.47(2) Å] is slightly shorter compared to **2b⊂M1**.

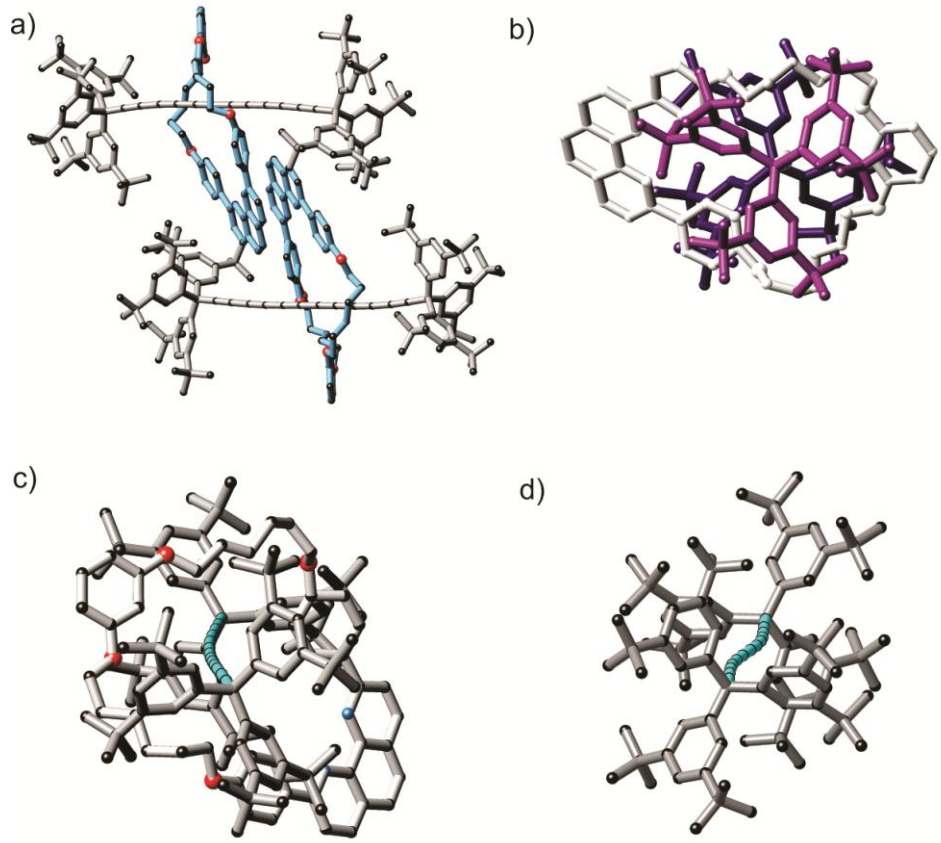

Figure 2.6 (a) The pairs of **2b⊂M1**, (b) the staggered conformation of tris(3,5-di-*tert*-butylphenyl)methyl groups and (c) the bow-like shape of hexayne axle compared to the (d) S-like axle in the free dumbbell[4]. Solvent molecules and hydrogen atoms are omitted for clarity.

The bulky 3,5-di-*tert*-butyl phenyl moieties of the capping groups are in staggered position with respect to each other (Figure 2.6 b). The mean dihedral angle between the C_{Ar} atoms of the 3,5-di-*tert*-butyl phenyl moieties in *anti*-positions, C1 and C14, is 168.3±5.2 °. The axle of **2b⊂M1** in the crystal is slightly bent. The angle C≡C-C(sp) averaged over the axel (177.8±1.1 °) is close to ideal value (180°) and to that in the free dumbbell (177.0±1.4 °).[4] However, in the case of the **2b⊂M1** the bending is non-centro symmetric; the bending of the axle in free dumbbell is centrosymmetric.[4] The polyyne chain of **2b⊂M1** has higher cumulenic character compared to free hexayne, as evidenced by the corresponding bond length alternation values (BLA) (Table 2.3). The average BLA value over the axle in **2b⊂M1** (0.142 ± 0.009 Å) is very close to that in free hexayne (0.143 ± 0.008 Å).

2b⊂M3: Crystals of **2b⊂M3** were obtained by vapor diffusion of methanol into a solution of the compound in CH_2Cl_2. The space group is P1, the asymmetric unit contains one molecule of **2b⊂M3**, one

methanol and two dichloromethane molecules. Interestingly, two adjacent **2b⊂M3** molecules form pairs not through π-π interaction between vicinal phenanthrolines, but through weak interactions between supertrityl groups (Figure 2.7).

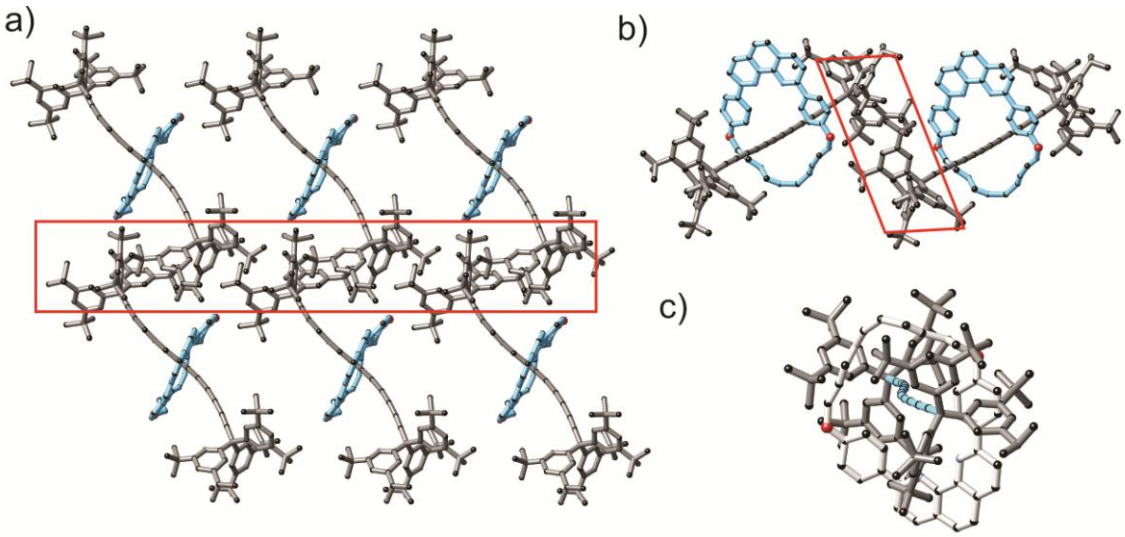

Figure 2.7 The crystal packing of **2b⊂M3** from (a) top and (b) front view. (c) The S-like shape of the polyyne chain in **2b⊂M3** single molecule (solvent molecules and hydrogen atoms are omitted for clarity).

The 3,5-di-*tert*-butyl phenyl moieties of the supertrityl groups are in staggered position with respect to each other. The mean dihedral angle between the C_{Ar} atoms of the 3,5-di-*tert*-butyl phenyl groups in *anti* position is 160.8±2.6°. The axle of **2b⊂M3** in the crystal is S-like bent, similar to the free hexayne, however, the axle loss its centre of symmetry. The angle C≡C-C(sp) averaged over the axel (174.4±2.4°) is different from the mean value in the **2b⊂M1** (177.8±1.1°). The polyyne chain of **2b⊂M1** has higher cumulenic character compared to free hexayne, as evidenced by the corresponding bond length alternation values (BLA) (Table 2.3). The average BLA value over the axle in **2b⊂M3** (0.122 ± 0.008 Å) is noticeably less than that in **2b⊂M1** (0.142 ± 0.009 Å) (Table 2.3).

Table 2.3 Summary of crystallographic data of **2b⊂M1**, **2b⊂M3**, **2b⊂M4** and **2c⊂M1** rotaxanes and free hexayne.

Rotaxane	∠C–C≡C_{avg} (°)	∠phen. $tors_{avg}$ (°)	BLA (Å)	C–C_{avg} (Å)	C≡C_{avg} (Å)	Ref.
2b⊂M1	177.8±1.1	168.3±5.2	0.142 ± 0.009	1.357 ± 0.005	1.214 ± 0.005	48
2b⊂M3	174.4±2.4	160.8±2.6	0.122 ± 0.008	1.343 ± 0.015	1.219 ± 0.016	here
2b⊂M4	175.8 ± 2.0	173.8±4.5	0.143 ± 0.01	1.355 ± 0.006	1.211 ± 0.007	here
2c⊂M1	177.0 ± 1.9	179.7±0.2	0.144 ± 0.01	1.356 ± 0.007	1.211 ± 0.005	here
2b	177.0±1.4	180	0.143 ± 0.008	1.359 ± 0.005	1.208 ± 0.007	4

2b⊂M4: Crystals of **2b⊂M4** were obtained by vapor diffusion of methanol into a solution of the compound in CH_2Cl_2. The space group is $P2_1/c$, asymmetric unit contains one molecule of **2b⊂M4**. In the

solid state, rotaxane molecules form linear strands through two different π-π interactions: one between two adjacent phenanthrolines and the second between two phenyl rings from p-tolyl moieties (Figure 2.8, red squares). The distance between two phenanthrolines planes is 3.75 Å and between two phenyl rings is 3.52 Å. Due to π-π interactions molecules are packed very densely. The shortest interatomic distance between polyynes in adjacent rotaxane molecules is approximately 9.2 Å, which is close to the distance between two **2b⊂M1** molecules (9.1 Å) in the solid state. Similarly, the shortest distance between adjacent polyyne chains in **2b⊂M3** is 11.6 Å (For comparison, the shortest distance between two neighbor molecules of free hexayne in solid state is ~8.1 Å)[4]. It has been shown previously,[46] that for the 1,4 or 1,6 polymerization of diacetylenes in the reactive structures, the distance between the reacting atoms is always less than 4 Å. In all three rotaxane structures distance between two polyynes is double the distance required for intermolecular crosslinking reactions to occur.

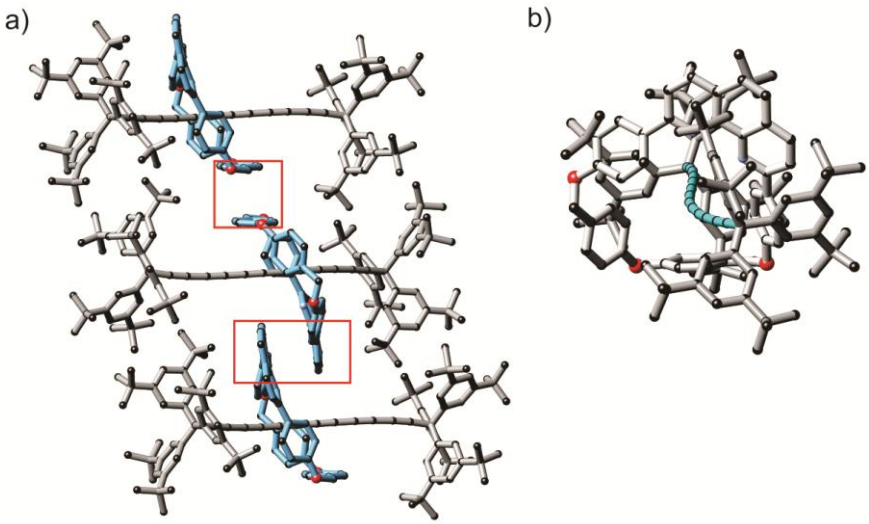

Figure 2.8 (a) The crystal packing of **2b⊂M4** with square lines highlighting the π-π interactions. (b) The semi-helical shape of the polyyne chain in **2b⊂M4** single molecule (solvent molecules and hydrogen atoms are omitted for clarity).

The 3,5-di-*tert*-butyl phenyl moieties of the supertrityl groups are in staggered position with respect to each other. The mean dihedral angle between the C_{Ar} atoms of the 3,5-di-*tert*-butyl phenyl groups in *anti* position is 173.8±4.5 °. The axle of **2b⊂M4** in the crystal is semi-helical. The averaged angle C≡C-C(sp) is 175.8 ± 2 °. The average BLA value of hexayne chain in **2b⊂M4** is 0.143 ± 0.01 Å close to that in **2b⊂M1** (0.142 ± 0.009 Å). All crystallographic data are summarized in Table 2.3.

M4: The crystal of macrocycle **M4** was obtained via slow evaporation of chloroform solution at room temperature. The crystal belongs to P-1 space group, the asymmetric unit contains one molecule M4 and

two chloroform molecules. The maximum inner size of the cavity of macrocycle **M4** is 9.6(2) Å × 10.6(4) Å (internuclear distance, Figure 2.9). The dimension is taken from the distance between two oxygen atoms (a) of oxybenzyl groups and another from the distance between oxygen atom of p-tolyl moiety and carbon atom of phenanthroline, which is vicinal to the nitrogen (b). The plane of the phenanthroline moiety is flat, however, the phenoxy moieties of phenanthroline are twisted (the angle between planes of phenanthroline and oxobenzyl moieties, ϕ_1 = 30.37 ° and ϕ_2 = 45.84 °) and the same for the phenyl rings of the p-tolyl ether moiety. The small size should impose considerable strain within the macrocycle, however the flexible oxygen bridges reduce the overall tension. In the solid state, the two planes of phenanthroline moieties of adjacent macrocycles are parallel, but the phenanthroline units are aligned in opposite direction. The distance between the two macrocycle planes is 3.7(4) Å. (Figure 2.9).

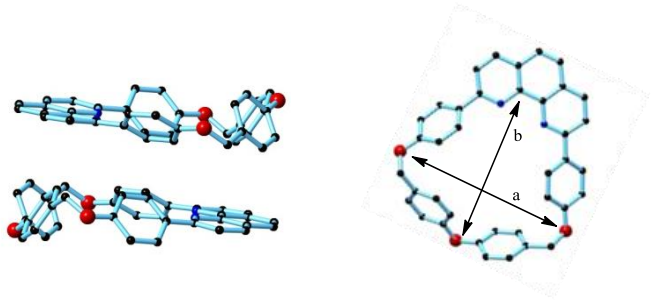

Figure 2.9 The crystal structure of macrocycle **M4** (solvent molecules and hydrogen atoms are omitted for clarity).

2c⊂M1: There are few reports of crystal structures of polyynes with 8 or more triple bonds in literature.[29b,42,45,47] The scarcity of documented crystal structures of extended polyynes is due to the instability of the molecules in solid state. We managed to grow a single crystal of **2c⊂M1** by slow diffusion of methanol into THF solution of the rotaxane at 4 °C.

The asymmetric unit contains one molecule of **2c⊂M1**, space group is P -1. The rotaxane molecules in solid state are aligned next to each other without forming phenanthroline pairs and it seems there is not a noticeable interaction between supertrityl end-groups (Figure 2.10). The distance between two octayne chains from neighboring rotaxanes is ~12.9 Å, longer than in other rotaxanes.

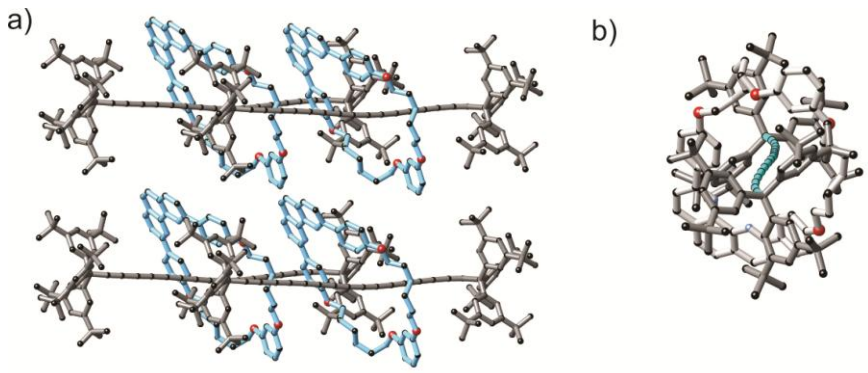

Figure 2.10 (a) The packing of **2c⊂M1** molecules in solid state and (b) the semi-helical shape of the octayne axle.

In the single molecule, the octayne chain gains semi-helical curvature with average C≡C-C(sp) angle equal to 177 ± 1.9 °.The BLA in rotaxane **2c⊂M1** is 0.144 ± 0.01 Å. It is expected to have reduced BLA values when the polyyne chain gets longer,[45] however, this is not a case for rotaxanes when hexayne **2b⊂M1** and octayne **2c⊂M1** rotaxanes are compared. The similar BLA values are probably the result of additional packing effects due to mechanical insulation by the macrocyclic phenanthroline. It is worth mentioning that similar to hexayne rotaxanes, the two supertrityl groups at the ends of the octayne chain are in staggered conformation, and the torsion angle between C_{Ar} groups of supertrityl moiety in *anti* conformation is 179.7 ± 0.2 ° (Table 2.3).

2.10 Conclusion

In conclusion, we have demonstrated that polyyne rotaxanes, up to C24, can be prepared by active-metal templating using phenanthroline- and bipyridine-based macrocycles. The utilization of small macrocycles in polyyne rotaxane synthesis opens doors for polyynes with smaller caps and different functional end-groups to be mechanically insulated. These organic molecules with mechanical bonds can be potentially useful as organic semiconductors. For supramolecular chemistry, polyynes are linear, rigid interconnectors while polyyne rotaxanes contain a mobile macrocycle. This combination of a rigid axle and a mobile macrocycle might be interesting for the molecular design of topologically more complex molecules.

It seems that C24 rotaxane is the upper limit for long polyynes to be threaded with macrocycle under active-metal template Glaser homocoupling conditions. The Glaser homocoupling is one example from the arsenal of the preparative methods in the synthesis of polyynes and we were naturally interested to test

different synthetic strategies for polyyne rotaxanes. This part of the research will be presented in the next chapter.

2.11 Experimental Part: General Experimental Procedures

Unless stated otherwise, all reagents and solvents were used as commercially supplied, without further purification. Dry THF was obtained by passing through alumina under N_2 pressure. Column chromatography was carried out using Silica 60A (particle size 35–70 μm, Fisher, UK) as the stationary phase. Size-exclusion chromatography was carried out using polystyrene beads (Bio-Beads-S-X3, operating range up to 2000 Da and Bio-Beads-S-X1, operating range 10 kDa). Where mixtures of solvents were used, ratios reported are by volume. TLC was performed on precoated silica gel plates (0.25 mm thick, 60 F254, Merck, Germany) and visualized under UV light (254 nm). NMR spectra were recorded at 500 MHz using Bruker AVII 500 or at 400 MHz using Bruker DPX 400 instruments at 298 K, unless stated otherwise. Chemical shifts are reported in parts per million (ppm) from low to high frequency and referenced to the residual solvents resonances.[1] Coupling constants (*J*) are reported in hertz (to an accuracy of ±0.1 Hz). Standard abbreviations indicating multiplicity were used as follows: s = singlet, d = doublet, dd = double doublets, t = triplet, q = quartet, m = multiplet. Melting points (m.p.) were determined by placing the sample between a pair of microscope cover glasses on an electrically heated metal block. MALDI-TOF mass spectrometry was carried out in positive reflectron mode using, in the majority cases, a Micromass MALDI micro MX spectrometer with dithranol (1,8-dihydroxyanthrone) as a matrix. Low resolution ESI-MS was carried out on a Micromass LCT platform and high resolution spectra were measured on Bruker micro TOF II Focus intrument. IR spectra were measured by Brucker Tensor 27 spectrometer with ATR accessory. UV-vis spectra were recorded at ambient temperature on a Perkin-Elmer Lambda 20 or Parkin-Elmer Lambda 25 spectrometers with 1 nm resolution; λ in nm (ε in $L \cdot mol^{-1} \cdot cm^{-1}$).

2.12 Synthesis

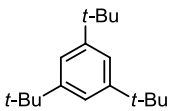

2.6

1,3,5-Tri-*tert*-butylbenzene 2.6:[14] To a mixture of *tert*-butylchloride (517.6 g, 610 mL, 5.6 mol) and benzene (43.8 g, 50.0 mL, 0.56 mol) cooled to –40 °C, $AlCl_3$ (37.12 g, 0.28 mol) was added in small

portions and the reaction mixture was slowly warmed to –20 °C and stirred for 2 h while keeping the temperature below –10 °C. The reaction was quenched via slow addition of a water/ice-mixture (200 mL) at –20 °C. The reaction mixture was warmed to 20 °C and the layers were separated, the organic phase washed with $NaHCO_3$(aq) (3 x 100 mL), brine (3 x 100 mL), dried over $MgSO_4$ and filtered. The solvent was removed *in vacuo* and the reaction crude was precipitated from cold CH_3OH to yield the product **2.6** as a white solid (98.0 g, 71 %). R_f = 0.8 (hexanes). ^{1}H NMR (400 MHz, $CDCl_3$) δ 7.35 (s, 3H), 1.42 (s, 27H). ^{13}C NMR (100 MHz, $CDCl_3$) δ 149.8, 119.5, 35.0, 31.6.; m.p. 69 °C (lit. 72.5-73 °C). As in lit.[14]

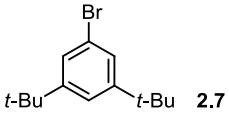

2.7

1-Bromo-3,5-di-*tert*-butylbenzene 2.7:[15] To a solution of 1,3,5-tri-*tert*-butylbenzene **2.6** (95.0 g, 0.386 mol) in dry $CHCl_3$ (420 mL) Fe powder (26.13 g, 0.467 mol) was added at 0 °C. A solution of Br_2 (129.7 g, 41.7 mL, 0.811 mol in 20 mL $CHCl_3$) was added over 30 min through a dropping funnel, and the mixture was stirred for 4 h at 0 °C. The reaction was quenched via the addition of NaOH(aq) (10 %, 100 mL). The mixture was warmed to 20 °C, filtered through a filter paper, and the layers were separated. The organic phase was washed with saturated Na_2SO_3(aq) (150 mL), saturated $NaHCO_3$(aq) (150 mL), brine (150 mL) and dried over $MgSO_4$. The solvent was removed *in vacuo* and the crude product purified by fractional distillation (75−85 °C at $P \approx 3.0 \cdot 10^{-2}$ mbar) to yield the product **2.27** as a white solid (87.7 g, 85%). R_f = 0.85 (hexanes). ^{1}H NMR (400 MHz, $CDCl_3$) δ 7.31 (s, 3H), 1.29 (s, 18H). ^{13}C NMR (100 MHz, $CDCl_3$) δ 153.0, 125.7, 122.2, 121.1, 35.0, 31.3. As in lit.[15]

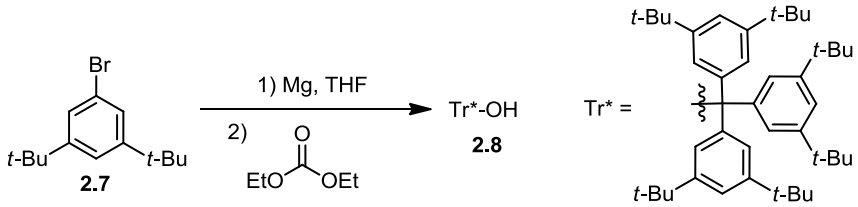

Tris(3,5-di-*tert*-butylphenyl)methanol 2.8:[4] To a mixture of activated (stirring overnight *in vacuo*) Mg turnings (2.57 g, 107 mmol) in dry THF (30 mL) a solution of 1-bromo-3,5-di-*tert*-butylbenzene **2.7** (25 g, 93 mmol) in THF (30 mL) was slowly added under N_2. A small crystal of I_2 was added to promote Grignard reagent formation at reflux. The reaction was maintained at a gentle reflux 30 min. The reaction mixture was cooled to 20 °C, a solution of freshly distilled diethyl carbonate (3.15 g, 3.23 mL, 25.1 mmol) in THF (60 mL) was slowly added, and the resulting mixture was stirred at 20 °C for 2 d under N_2. Then

the reaction mixture was cooled to 0 °C, quenched via the addition of saturated NH_4Cl(aq) (100 mL) and Et_2O (150 mL) was added. The layers were separated, and the organic phase was washed with H_2O (100 mL), brine (100 mL), and dried ($MgSO_4$). The solvent was removed *in vacuo* and the crude product was purified by column chromatography (silica, pentane → pentane/EtOAc 20:1) yielding the product **2.8** (14.1 g, 94%) as a pale yellow solid. ^{1}H NMR (400 MHz, $CDCl_3$) δ 7.28 (t, J = 1.8 Hz, 3H), 7.04 (d, J = 1.8 Hz, 6H), 2.80 (bs, 1H), 1.23 (s, 54H). ^{13}C NMR (100 MHz, $CDCl_3$) δ 149.6, 146.7, 122.6, 120.4, 83.4, 34.9, 31.5. As in lit.[4]

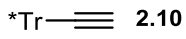

2.10

Tris(3,5-di-*tert*-butylphenyl)methyl-acetylene 2.10:[16] To a solution of tris(3,5-di-*tert*-butylphenyl)methanol **2.8** (19.6 g, 32.89 mmol) in dry THF (60 mL) at 20 °C was slowly added oxalyl chloride (20.69 g, 14.24 mL, 164.4 mmol). The mixture was left under vigorous stirring for 4 h before the solvent was removed *in vacuo* overnight. The light yellow crude product **2.9** was redissolved in minimum amount of THF (40 mL). To this solution ethynylmagnesium bromide (0.5 M in THF, 328 mL, 164 mmol) was added and the mixture stirred at 20 °C for 3 days under N_2. The reaction was cooled to 0 °C, quenched via the addition of saturated NH_4Cl(aq) (100 mL), and Et_2O was added (100 mL). The layers were separated, the organic phase was washed with saturated NaCl(aq) (3 x 100 mL), dried ($MgSO_4$), and filtered. The solvent was removed *in vacuo* and the crude product was purified by column chromatography (silica, hexanes/CH_2Cl_2 10:1) to yield the product **2.10** (17.5 g, 88%) as a colourless solid. ^{1}H NMR (400 MHz, $CDCl_3$) δ 7.29 (t, J = 1.8 Hz, 3H), 7.05 (d, J = 1.8 Hz, 6H), 2.65 (s, 1H), 1.25 (s, 54). ^{13}C NMR (100 MHz, $CDCl_3$) δ 149.7, 144.8, 123.8, 119.8, 90.7, 72.0, 56.1, 34.8, 31.4. FTIR: 3306, 3072 (w), 2960, 2902, 2864, 2124, (w), 2096 (w), 1591 cm^{-1}.As in lit.[16]

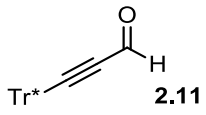

2.11

2.11:[4]A solution of monoyne **2.10** (3.00 g, 4.95 mmol) in THF (150 mL) was degassed, cooled to –78 °C under a N_2 atmosphere, n-BuLi (1.98 mL, 2.5 M in hexanes, 4.95 mmol) was added, and the mixture stirred at –78 °C for 10 min. Anhydrous DMF (0.495 mL, 6.44 mmol) was added slowly over 10 min, the mixture stirred for 40 min on warming to 20 °C The reaction was quenched by pouring into a mixture of ice (200 g) and conc. HCl (1 mL, 10.0 mmol). The pH of the mixture was adjusted to ~7 with saturated

$NaHCO_3$(aq) extracted with hexanes (200 mL) and the resulting layers separated. The organic phase was washed with H_2O (50 mL), brine (50 mL) and dried over $MgSO_4$. The solvent was removed *in vacuo* and the crude product purified by column chromatography (silica gel, CH_2Cl_2/hexanes 1:20) to remove unreacted **2.10** then with CH_2Cl_2/hexanes (1:2) to yield **2.11** (2.74 g, 87.5%) as a white solid. ^{1}H NMR (400 MHz, $CDCl_3$) δ 9.36 (s, 1H), 7.28 (t, J = 2 Hz, 3H), 6.93 (d, J = 2Hz, 6H), 1.19 (s, 54H); ^{13}C NMR (100 MHz, $CDCl_3$) δ 177.0, 150.2, 143.1, 123.7, 120.5, 104.2, 84.2, 56.8, 34.9, 31.3. As in lit.[4]

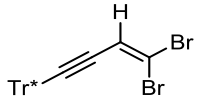

2.12

2.12:[17] A solution of CBr_4 (0.515 g, 1.58 mmol) in CH_2Cl_2 (10 mL) was transferred through canula to a solution of PPh_3 (0.827 g, 3.16 mmol) in CH_2Cl_2 (5 mL) and the resulting mixture stirred at 20 °C under a N_2 atmosphere for 1 h. A solution of **2.11** (0.50 g, 0.79 mmol) in CH_2Cl_2 (10 mL) was added and the reaction stirred for 30 min. The reaction progress was monitored by TLC (CH_2Cl_2/hexanes 1:2).The mixture was concentrated to a minimum and hexanes were added to precipitate the Ph_3PO salt as a white solid along with an oily residue. The supernatant was decanted and filtered through a pad of silica plug. The oily residue left in the flask was dissolved in minimal CH_2Cl_2 and hexanes were added. The heterogeneous mixture was then decanted and the supernatant filtered through silica plug (this procedure was repeated three times). The solvent was removed *in vacuo* and the product was purified by column chromatography (silica, hexanes) to yield **2.12** (535 mg, 87%) as a white solid: R_f = 0.75 (CH_2Cl_2/hexanes 1 : 2). ^{1}H NMR (400 MHz, $CDCl_3$) δ 7.25 (t, J = 2 Hz, 3H), 6.98 (d, J = 2 Hz, 6H), 6.71 (s, 1H), 1.20 (s, 54H). ^{13}C NMR (100 MHz, $CDCl_3$) δ 149.9, 144.4, 123.9, 120.4, 120.0, 105.2, 100.2, 81.0, 57.3, 34.9, 31.4. As in lit.[4]

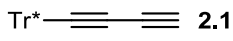

2.1

2.1:[4] A solution of **2.12** (0.20 g, 0.26 mmol) in THF (20 mL) cooled to –78 °C under a N_2 atmosphere *n*-BuLi (0.28 mL, 1.0 M in hexanes, 0.28 mmol) was added. The mixture was stirred at –78 °C for 10 min and the reaction was warmed to 20 °C, stirred for 10 min, cooled to 0 °C, and quenched with saturated NH_4Cl(aq) (50 mL). The mixture was extracted with hexanes (100 mL) and the layers separated. The organic phase was washed with H_2O (50 mL), brine (50 mL), and dried over $MgSO_4$. The solvent was

removed *in vacuo* and the crude product was purified by column chromatography (silica, CH_2Cl_2/hexanes 1:10) to yield **2a** (145 m g, 90%) as a white solid. ^{1}H NMR (400 MHz, $CDCl_3$) δ 7.25 (t, J = 2 Hz, 3H), 6.93 (d, J = 2 Hz, 6H), 2.10 (s, 1H), 1.20 (s, 54H). ^{13}C NMR (100 MHz, $CDCl_3$) δ 149.9, 143.9, 123.8, 120.1, 83.5, 68.8, 68.0, 66.6, 56.7, 34.8, 31.4.; FTIR 3315, 3067 (w), 2952, 2903, 2866, 2224, 1589 cm^{-1}. As in lit.[4]

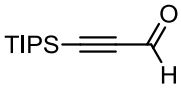

2.13

1-(Triisopropylsilyl)-1-propynal 2.13:[18] To a stirred solution of TIPS-acetylene (2.0 g, 2.45 ml, 11.0 mmol) in ether (15 mL) at 0 ºC was added *n*-BuLi (4.8 mL, 2.5 M in hexane, 12.1 mmol) dropwise over 5 minutes. Then distilled DMF (2.0 mL, 0.032 mmol) was added at –78 ºC. The reaction mixture was allowed to warm up slowly to 0 ºC over a period of 2 h. The reaction was quenched at 0 ºC by pouring it into a solution of water/ice, HCl (10 %, 15 mL). After stirring one hour, the organic phase was separated and the aqueous phase was extracted with ether. The organic layers were combined, dried over $MgSO_4$, filtered and concentrated under reduced pressure. The residual oil was purified by column chromatography (silica, pentane/Et_2O 10:1→5:1) to afford product **2.13** (2.32 g, 98%) as a light yellow oil. R_f = 0.51 (hexanes/CH_2Cl_2 2:1). ^{1}H NMR (400 MHz, $CDCl_3$) δ 9.2 (s, 1H), 1.13–1.07 (m, 21H). ^{13}C NMR (100 MHz, $CDCl_3$) δ 176.6, 104.4, 100.8, 18.4, 10.9. As in lit.[18]

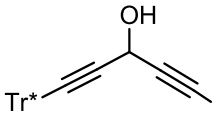

2.14

2.14:[4]A solution of supertrityl acetylene **2.10** (1.85 g, 3.06 mmol) in THF (100 mL) was cooled to –78 °C under a N_2 atmosphere and *n*-BuLi (1.24 mL, 2.5 M in hexanes, 3.08 mmol) was added and the reaction mixture was stirred 15 min. A solution of 3-TIPS-propargylic aldehyde **2.13** (642 mg, 3.06 mmol) in THF (10 mL) was added over 5 min, the resulting mixture warmed to 20 °C and stirred for 1 h. The reaction was cooled to 0 °C, quenched with saturated NH_4Cl(aq) (50 mL), and the mixture was extracted with Et_2O (200 mL). The organic phase was washed with saturated NH_4Cl(aq) (100 mL), H_2O (100 mL), brine (100 mL), and dried over Mg_2SO_4. The solvent was removed *in vacuo* and the crude product purified by column chromatography (silica, pentane/EtOAc 100:1) to yield product **2.14** (2.23 g, 90%) as a pale yellow oil that solidified upon standing: ^{1}H NMR (400 MHz, $CDCl_3$) δ 7.25 (t, J = 2 Hz, 3H), 6.97 (d, J = 2 Hz, 6H), 5.32

(d, J = 8 Hz), 2.14 (d, J = 8 Hz), 1.2 (s, 54H), 1.05 (s, 21H). ^{13}C NMR (100 MHz, $CDCl_3$) δ 149.8, 144.8, 123.9, 120.0, 104.6, 91.9, 85.4, 80.9, 56.3, 53.8, 34.9, 31.5, 18.7, 11.2. EIMS *m/z* 812.5 (M^+), 756.4 ([M – *t*-Bu + H]$^+$), 603.5 ([M – *i*Pr$_3$SiC≡CCO]$^+$). FTIR 3075 (w), 2962, 2900, 2869, 2205, 1749, 1530 cm^{-1}. As in lit.[4]

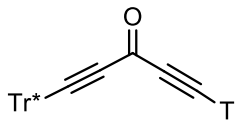

2.15

2.15:[4] To a solution of **2.14** (2.13 g, 2.62 mmol) in CH_2Cl_2 (100 mL) celite (2.25 g), molecular sieves (2.25 g) and pyridinium chlorochromate (PCC) (1.13 g, 5.24 mmol) were added in this order and the reaction mixture was stirred at 20 °C under N_2 atmosphere for 20 h. The mixture was passed through a silica plug (CH_2Cl_2) and the solvents were removed *in vacuo* to yield product **2.15** (2.04 g, 96%) as a yellow solid: ^{1}H NMR (400 MHz, $CDCl_3$) δ 7.29 (t, J = 2 Hz, 3H), 6.96 (d, J = 2 Hz, 6H), 1.2 (s, 54H), 1.11-1.06 (m, 21H). ^{13}C NMR (100 MHz, $CDCl_3$) δ 160.8, 150.3, 143.3, 123.9, 120.5, 105.4, 100.1, 95.6, 85.2, 56.9, 35.0, 31.5, 18.6, 11.2. FTIR 3077, 2960, 2904, 2868, 2205, 2152, 1622, 1592 cm^{-1}. As in lit.[4]

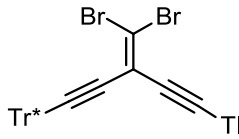

2.16

2.16:[4] A solution of CBr_4 (3.15 g, 9.66 mmol) in CH_2Cl_2 (15 mL) was transferred to the flask of PPh_3 (5.062 g, 19.32 mmol) under N_2 atmosphere and the resulting mixture stirred at 20 °C for 1 h. A solution of **2.15** (3.92 g, 4.82 mmol) in CH_2Cl_2 (25 mL) was cannulated to the solution of ylide and the reaction mixture was stirred for 20 h. The reaction mixture was concentrated to ca. 10 mL and hexanes were added to precipitate the Ph_3PO as a white solid along with an oily residue. The supernatant was decanted and filtered through a silica plug. The oily residue left in the flask was dissolved in minimal CH_2Cl_2 and hexanes were added. the heterogeneous mixture was then decanted and the supernatant filtered through silica plug (this procedure was repeated three times). The solvent was removed *in vacuo* and the crude product was purified by passing through silica plug (EtOAc/hexanes 1:20) to yield **2.16** (4.49 g, 96%) as a white solid: R_f = 0.9 (EtOAc/hexanes 1:25). ^{1}H NMR (400 MHz, $CDCl_3$) δ 7.23 (t, J = 2 Hz, 3H), 6.99 (d, J = 2 Hz, 6H), 1.19 (s, 54H), 1.09–1.05 (m, 21H). ^{13}C NMR (100 MHz, $CDCl_3$) δ 149.8, 144.4, 124.0, 120.0, 115.1, 108.2, 103.6, 102.4, 98.4, 81.1, 57.4, 34.9, 31.6, 18.8, 11.3. As in lit.[4]

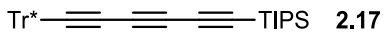

2.17

2.17:[4] To a solution of **2.16** (1.5 g, 0.206 mmol) in hexanes (70 mL) at –78 °C *n*-BuLi was added (0.99 mL, 2.5M in hexanes, 0.247 mmol) dropwise under a N_2 atmosphere. The reaction mixture was warmed to 20 °C over 30 min and the reaction was quenched by the addition of saturated NH_4Cl(aq) (50 mL). The layers were separated and the organic layer dried over $MgSO_4$. The solvent was removed *in vacuo* and the crude product was purified by column chromatography (silica, hexanes) to yield **2.17** (1.5 g, 88%) as a white solid: R_f = 0.6 (CH_2Cl_2/hexanes 1:20). ^{1}H NMR (400 MHz, $CDCl_3$) δ 7.25 (t, J = 2 Hz, 3H), 6.91 (d, J = 2 Hz, 6H), 1.19 (s, 54H), 1.09-1.06 (m, 21H). ^{13}C NMR (100 MHz, $CDCl_3$) δ 150.0, 143.8, 123.7, 120.2, 90.2, 85.0, 83.6, 69.0, 62.5, 61.6, 57.1, 34.8, 31.4, 18.5, 11.3. FTIR 3070 (w), 2963, 2905, 2868, 2211, 2173, 2075, 1594 cm^{-1}. As in lit.[4]

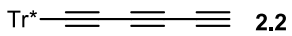

2.2

2.2:[4] To a solution of **2.17** (1.5 g, 1.86 mmol) in wet THF (40 mL THF and 5 μL H_2O) was added TBAF (2.04 mL, 1.0 M in THF, 2.04 mmol). The solution was stirred at 20 °C for 15 min. The reaction was quenched with saturated NH_4Cl(aq) (50 mL) and extracted with hexanes (100 mL). The organic phase was washed with H_2O (50 mL), brine (50 mL), and dried over $MgSO_4$. The solvent was removed *in vacuo* and the crude product purified by slurry washing with Et_2O (x2) to yield **2.2** (1.03 g, 86%) as a white solid: R_f = 0.46 (CH_2Cl_2/hexanes 1:10). ^{1}H NMR (400 MHz, $CDCl_3$) δ 7.26 (t, J = 2 Hz, 3H), 6.90 (d, J = 2 Hz, 6H), 2.07 (s, 1H), 1.19 (s, 54H). ^{13}C NMR (100 MHz, $CDCl_3$) δ 150.1, 143.6, 123.7, 120.3, 84.8, 68.9, 68.5, 66.6, 61.6, 61.3, 57.0, 34.8, 31.4. As in lit.[4]

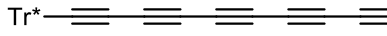

2.19

2.19:[5] To a solution of supertrityl diyne **2.1** (187 mg, 0.297 mmol) and 1-TIPS-6-TMS-hexa-1,3,5-triyne **2.18** (450 mg, 1.49 mmol) in CH_2Cl_2 (10 mL), MeOH (10 mL) and 2,6-lutidine (10 mL) was added K_2CO_3 (225 mg, 1.59 mmol) and the mixture stirred for 10 min at 20 °C. To the mixture was added $Cu(OAc)_2 \cdot H_2O$ (593 mg, 2.97 mmol) and the reaction stirred at 20 °C until it was deemed complete by TLC (about2 h). The reaction was quenched with saturated NH_4Cl (25 mL) and the resulting mixture extracted with hexanes (100 mL). The organic phase was washed with saturated NH_4Cl(aq) (25 mL), H_2O

(2 x 25 mL), brine (25 mL), and dried over $MgSO_4$. The solution was filtered through a plug of silica, the solvent removed *in vacuo* and the crude product purified by column chromatography (silica, hexanes) to yield TIPS-pentayne (180 mg, 71%) as a yellow solid. ^{1}H NMR (400 MHz, $CDCl_3$) δ 7.26 (t, J = 2 Hz, 3H), 6.89 (d, J = 2 Hz, 6H), 1.19 (s, 54H), 1.09–1.05 (m, 21H). ^{13}C NMR (125 MHz, $CDCl_3$) δ 150.1, 143.4, 123.7, 120.4, 89.6, 86.1, 86.0, 68.7, 62.86, 62.84, 62.68, 62.22, 62.21, 61.6, 57.3, 34.8, 31.4, 18.5, 11.3. As in lit.[4]

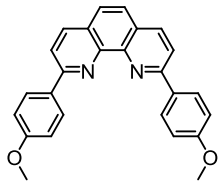

2.22

2,9-bis(4-methoxyphenyl)-1,10-phenanthroline 2.22:[11] The solution of bromoanisole (2.40 mL, 5.55 g, 29.7 mmol) in dry Et_2O (80 mL) was freeze-pump-thaw degassed, then was cooled to -30 °C and *t*-BuLi (1.7 M in pentane, 42 mL, 71.4 mmol) was added by cannula. The reaction was allowed to warm to 20 °C and stirred for 1.5 h. The solution was transferred by cannula to a suspension of 1,10-phenanthroline (1.50 g, 7.57 mmol, dried overnight *in vacuo*) in dry toluene which had been freeze-pump-thaw degassed. The reaction mixture was stirred at 20 °C for 48 h. The reaction was quenched by the addition of of *i*-PrOH (1 mL), then MeOH (1 mL) and finally water(10 mL). The organic layer was decanted and the aqueous layer extracted with CH_2Cl_2. To the combined organic layers was added MnO_2 (30.0 g, 345 mmol) and the resulting suspension stirred for 36 hrs. The suspension was filtered and the filtrate concentrated. Recrystallisation of the crude from toluene gave the product **2.22** as a yellow solid (1.64 g, 55 %). ^{1}H NMR (400 MHz, $CDCl_3$) δ 8.45 (m, 4H), 8.27 (d, J = 8.5 Hz, 2H), 8.09 (d, J = 8.5 Hz, 2H), 7.75 (s, 2H), 7.13 (m, 4H), 3.93 (s, 6H). As in lit.[11]

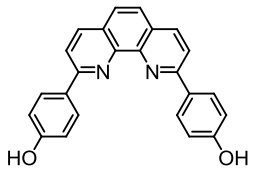

2.20

2,9-bis(4-hydroxyphenyl)-1,10-phenanthroline 2.20:[11] Hydrochloric acid (33%, 16.5 mL) and pyridine (15 mL) were added to a flask equipped for distillation. Water was distilled from the mixture until the internal temperature reached 200 °C. The reaction mixture temperature was lowered to 140 °C and 2,9-bis(4-methoxyphenyl)-1,10-phenanthroline **2.22** (1.5 g, 3.88 mmol) was added. After 3 hrs refluxing under

N_2 at 190 °C the reaction mixture was cooled to room temperature and water (15 mL) was added. The bright yellow precipitate was filtered and the crude product was suspended in an ethanol/water mixture (4:1, 100 mL), neutralised with $NaHCO_3$(aq) and the yellow-orange precipitate was filtered and dried *in vacuo* to yield the product **2.20** (1.4 g, 99 %) as dark yellow powder. ^{1}H NMR (400 MHz, DMSO-d^6) δ 10.30 (s, 2H), 8.78 (d, J = 8.7 Hz, 2H), 8.46 (d, J = 8.5 Hz, 2H), 8.35 (d, J= 8.7 Hz, 4H), 8.12 (s, 2H), 7.08 (d, J = 8.5 Hz, 4H). As in lit.[11]

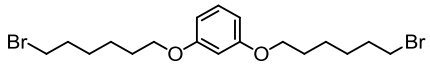

2.21

m-Bis[(4-bromobutyl)oxy]benzene 2.21:[11] Resorcinol (845 mg, 7.68 mmol), 1,6-dibromohexane (7.15 mL, 44.5 mmol) and K_2CO_3 (5.20 g, 37.7 mmol) were dissolved in acetone (300 mL). The reaction mixture was refluxed for 72 h and the solvent removed. The crude was passed over a silica gel column ($PE_{40/60}$/CH_2Cl_2 3:2) affording the product **2.21** (1.6 g, 49%) as a white solid. ^{1}H NMR (400 MHz, $CDCl_3$) δ 7.16 (t, J = 8.1 Hz, 1H), 6.45-6.5 (m, 3H), 4.12 (t, J = 6.5 Hz, 4H), 3.43 (t, J = 6.4 Hz, 4H), 1.75-1.95 (m, 8H), 1.49-1.54 (m, 8H). As in lit.[11]

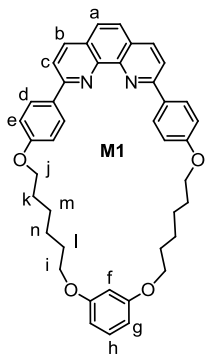

Macrocycle M1:[11] The mixture of 2,9-bis(4-hydroxyphenyl)-1,10-phenanthroline **2.20** (400 mg, 1.1 mmol), m-Bis[(6-bromohexyl)oxy]benzene **2.21** (479 mg, 1.10 mmol) and potassium carbonate (2.00 g, 14.5 mmol) were dissolved in DMSO (200 mL) and heated at 60 °C for 4 hrs. The solvent was removed *in vacuo* and the crude product was purified by column chromatography (silica, CH_2Cl_2/hexanes 3:2) followed by recrystallization from MeOH/CH_2Cl_2 to yield macrocycle (370 mg, 49%) as a white solid. ^{1}H NMR (400 MHz, $CDCl_3$) δ 8.46 (d, J = 8.7 Hz, 4H, H_d), 8.27 (d, J = 8.5 Hz, 2H, H_c), 8.09 (d, J = 8.5 Hz, 2H, H_b), 7.75 (s, 2H H_a), 7.18 (t, 1H, J = 7.1 Hz, H_h), 7.12 (d, J = 8.7 Hz, 4H, H_e), 6.57 (t, J = 2.2 Hz, 1H, H_f), 6.53 (m, 2H, H_g), 4.12 (t, J = 7.0 Hz, 4H, H_j), 4.02 (t, J = 6.04 Hz, 4H, H_i), 1.84-1.97 (m, 8H, $H_{k,n}$), 1.49-1.54 (m, 8H, $H_{l,m}$). ^{13}C NMR (100 MHz, $CDCl_3$) δ 160.43, 156.26, 145.98, 136.68, 131.97, 129.82, 128.92, 127.43, 125.51, 119.11, 114.76, 106.87, 101.08, 68.06, 67.75, 29.49, 29.22, 29.07, 25.97, 25.91. *m/z* (MALDI TOF MS$^+$) 638.10, ($C_{42}H_{42}N_2O_4$); $[M]^+$, requires 638.32. As in lit.[11]

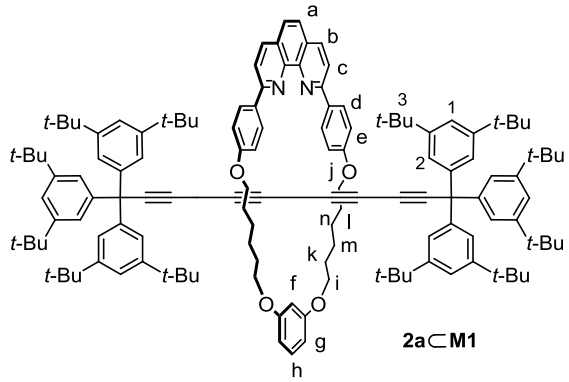

2a⊂M1: To a solution of macrocycle **M1** (10.2 mg, 0.016 mmol) in CH_2Cl_2 (1.0 mL) a solution of CuI (3.1 mg, 0.016 mmol) in CH_3CN (1.0 mL) was added and the mixture was stirred at 20 °C for 1.5 h. The mixture was then dried under vacuum and re-dissolved in dry THF (1.0 mL) (macrocycle-Cu complex solution). **2.1** (25.0 mg, 0.040 mmol) was dissolved in THF (1.0 mL) in a dry Schlenk tube and iodine (4.1 mg, 0.016 mmol), potassium carbonate (9.0 mg, 0.15 mmol) and the THF solution of macrocycle-Cu complex were added. The reaction mixture was flushed with nitrogen and stirred in dark at 60 °C for 24 h. The progress of reaction was monitored by TLC (PE 40/60 : EtOAc = 6 : 1). After stirring for 24 h. iodine (2.0 mg, 8 μmol) and potassium carbonate (9.0 mg, 65 μmol) of were added and the mixture stirred additionally for 24 h. Then the reaction mixture was cooled to 20 °C; CH_3CN (1.5 mL), CH_2Cl_2 (2.0 mL) and the aqueous solution of potassium cyanide (10.0 mg, 0.15 mmol in 1.0 mL of water) were added and the mixture stirred at 20 °C for 6 h. The mixture was diluted with CH_2Cl_2 (4.0 mL), the organic fraction was separated and washed with water (3×5.0 mL) after which solvents were removed. The column chromatography of the crude mixture (silica, $PE_{40/60}$/EtOAc 30 : 1) followed by recrystallization from CH_2Cl_2/MeOH afforded the product **2a⊂M1** as a white solid (10.1 mg, 34%). ^{1}H NMR (500 MHz, CD_2Cl_2) δ 8.51 (d, J = 8.8 Hz, 4H, H_d), 8.31 (d, J = 8.4 Hz, 2H, H_c), 8.14 (d, J = 8.4 Hz, 2H, H_b), 7.79 (s, 2H, H_a), 7.23 (t, J = 1.6 Hz, 6H, H_1), 7.19 (d, J = 8.8 Hz, 4H, H_e), 7.0 (t, J = 8.2 Hz, 1H, H_h), 6.92 (d, J = 1.8 Hz, 12H, H_2), 6.61 (t, J = 2.2 Hz, 1H, H_f), 6.43 (dd, J_1 = 8.2 Hz, J_2 = 2.2 Hz, 2H, H_g), 4.14 (t, J = 7.5 Hz, 4H, H_i), 4.11 (t, J = 6.9 Hz, 4H, H_j), 1.90 (m, 8H, $H_{k,l}$), 1.81 (m, 4H, $H_{m/n}$) 1.59 (m, 4H, $H_{m/n}$), 1.10 (s, 108H, H_3). ^{13}C NMR (125 MHz, CD_2Cl_2) δ 161.0, 160.9, 156.2, 150.6, 146.5, 143.8, 136.7, 132.0, 129.7, 129.2, 127.7, 125.7, 123.9, 120.8, 119.0, 115.2, 108.2, 99.5, 85.6, 69.6, 68.4, 68.0, 63.3, 62.9, 57.7, 35.0, 31.4, 30.0, 29.6, 26.2, 26.1. *m/z* (MALDI TOF MS+) 1891.94, ($C_{136}H_{168}N_2O_4$); $[M]^+$ requires 1893.25. UV-vis (CH_2Cl_2) λ / nm (ε / M^{-1} cm^{-1}), 273 (152000), 295 (4.41), 260 (164000); UV-vis (THF) λ / nm (ε / M^{-1} cm^{-1}) 274 (153000), 259 (162000); m.p. 222–225 °C.

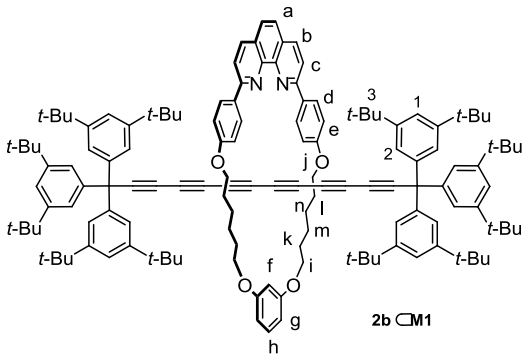

2b⊂M1: To a solution of macrocycle **M1** (19.4 mg, 30 μmol) in CH_2Cl_2 (2.0 mL) a solution of CuI (5.8 mg, 30 μmol) in CH_3CN (1.0 mL) was added and the mixture stirred at 20 °C for 1.5 h. The mixture was then dried under vacuum and re-dissolved in dry THF (1.0 mL) (macrocycle-Cu complex solution). **2.2** (50.0 mg, 0.077 mmol) was dissolved in THF (2.0 mL) in a dry Schlenk tube and iodine (9.8 mg, 38 μmol), potassium carbonate (21.2 mg, 0.15 mmol) and the THF solution of macrocycle-Cu complex were added. The mixture was flushed with nitrogen gas and stirred in dark at 60 ^{o}C for 24 h. The progress of reaction was monitored by TLC ($PE_{40/60}$/EtOAc 6 : 1). Then the reaction mixture was cooled to 20 °C; CH_3CN (3.0 mL), CH_2Cl_2 (3.0 mL) and an aqueous solution of potassium cyanide (20.0 mg, 0.256 mmol in 1.0 mL water) were added and the mixture stirred at 20 °C for 6 h. The mixture was then diluted with CH_2Cl_2 (4.0 mL), the organic fraction separated and washed with water (3×5.0 mL) followed by removal of the solvents. The column chromatography of the crude (silica, $PE_{40/60}$/EtOAc 30 : 1) followed by recrystallization from CH_2Cl_2/MeOH afforded a product **2b⊂M1** as a bright yellow solid (19.0 mg, 32%). ^{1}H NMR (500 MHz, CD_2Cl_2) δ 8.43 (d, J = 8.9 Hz, 4H, H_d), 8.28 (d, J = 8.5 Hz, 2H, H_b), 8.10 (d, J = 8.5 Hz, 2H, H_c), 7.76 (s, 2H, H_a), 7.25 (t, J = 1.6 Hz, 6H, H_1), 7.13 (d, J = 8.8 Hz, 4H, H_e), 7.05 (t, J = 8.1 Hz, 1H, H_h), 6.89 (d, J = 1.6 Hz, 12 H, H_2), 6.55 (t, J = 2.2 Hz, 1H, H_f), 6.45 (dd, J_1 = 8.2 Hz, J_2 = 2.2 Hz, 2H, H_g), 4.12 (t, J = 7.2 Hz, 4H, H_j), 4.00 (t, J = 6.3 Hz, 4H, H_i), 1.90–1.83 (m, 8H, $H_{k,l}$), 1.60 (m, 8H, $H_{m,n}$) 1.13 (s, 108 H, H_3). ^{13}C NMR (125 MHz, CD_2Cl_2) δ 161.0, 160.0, 156.4, 150.7, 146.5, 143.6, 136.9, 132.1, 129.9, 129.2, 127.8, 125.8, 123.9, 121.0, 119.3, 115.2, 107.7, 100.4, 86.5, 69.4, 68.5, 68.0, 63.5, 63.4, 63.0, 62.9, 57.7, 35.1, 31.4, 29.9, 29.5, 26.3, 26.2. *m/z* (MALDI TOF MS+) 1946.3, ($C_{140}H_{168}N_2O_4$); $[M]^+$ requires 1941.3; UV-vis (CH_2Cl_2) λ / nm (ε / M^{-1} cm^{-1}) 317 (255000), 297 (218000), 280 (154000); UV-vis (THF) λ / nm (ε / M^{-1} cm^{-1}) 317 (246000), 297 (206000), 282 (154000); m.p. 217–219 °C.

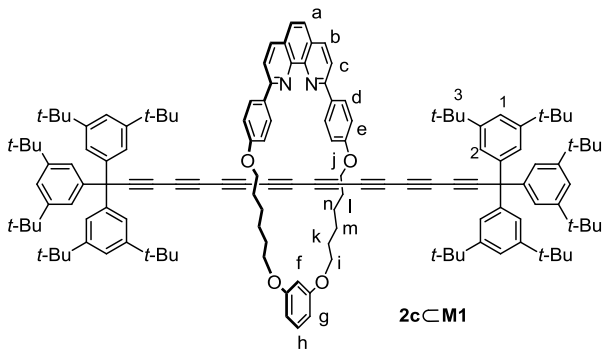

2c⊂M1: A solution of CuI (5.72 mg, 0.0295 mmol) in MeCN (dry, 2 mL) was added to a solution of the macrocycle M**1** (18.8 mg, 0.0295 mmol) in CH_2Cl_2 (dry, 5 mL) and the mixture was stirred at room temperature for 1 h. The solvent was removed *in vacuo* and the formed Cu complex dissolved in dry THF (5 mL). Tetrayne **2.3** (50 mg, 0.074 mmol) was dissolved in THF (4 mL) in a Schlenk tube, iodine (7.6 mg, 0.030 mmol), potassium carbonate (16.6 mg, 0.120 mmol) and the solution of the Cu-complex in THF were added. The mixture was stirred at 60 °C in the dark for 40 h. The reaction mixture was cooled to room temperature. MeCN (3 mL), CH_2Cl_2 (4 mL) and an aqueous KCN solution (30.0 mg, 0.450 mmol, in 3 mL H_2O) were added and the mixture was stirred at room temperature for 6 h. CH_2Cl_2 (25 mL) was added, the organic layer was separated and washed with water (3 × 10 mL). The organic phase was dried ($MgSO_4$) and the solvent removed *in vacuo*. The crude product was purified by column chromatography (silica, hexanes/EtOAc 30:1 → 20:1) to yield **2c⊂M1** as a beige solid (14 mg, 19%). R_f = 0.29 (hexanes/EtOAc 6:1). ^{1}H NMR (400 MHz, CD_2Cl_2) δ 8.44 (d, J = 8.8 Hz, 4H, H_d), 8.27 (d, J = 8.5 Hz, 2H, H_b), 8.09 (d, J = 8.5 Hz, 2H, H_c), 7.75 (s, 2H, H_a), 7.29 (t, J = 1.7 Hz, 6H, H_1), 7.19–7.01 (m, 5H, $H_{e,h}$), 6.53 (t, J = 2.2 Hz, 1H, H_f), 6.46 (dd, J_1 = 8.2 Hz, J_2 = 2.3 Hz, 2H, H_g), 4.13 (t, J = 7.0 Hz, 4H, H_j), 4.00 (t, J = 6.4 Hz, 4H, H_i), 1.99–1.78 (m, 8H, $H_{k,l}$), 1.69–1.56 (m, 8H, $H_{m,n}$), 1.18 (s, 108H, H_3). ^{13}C NMR (100 MHz, CD_2Cl_2) δ 161.18, 161.16, 156.5, 151.0, 146.7, 143.7, 137.1, 132.4, 130.2, 129.4, 128.0, 126.0, 124.1, 121.3, 119.4, 115.4, 107.7, 101.0, 87.2, 69.5, 68.7, 68.4, 64.2, 63.9, 63.7, 63.2, 63.0, 62.7, 58.0, 35.3, 31.6, 30.2, 29.7, 26.5, 26.5. ESI HRMS (MeCN/$CHCl_3$) calcd. for $C_{144}H_{169}N_2O_4$ ($[M+H]^+$) 1990.30769, found 1990.30557.

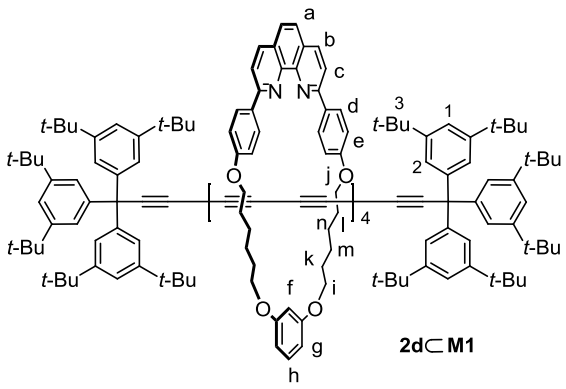

2d⊂M1: To a solution of macrocycle M**1** (9.1 mg, 14 μmol) in CH_2Cl_2 (2.0 mL) a solution of CuI (2.7 mg, 14 μmol) in CH_3CN (1.0 mL) was added and the mixture stirred at 20 °C for 1.5 h. The mixture was then dried under vacuum and re-dissolved in dry THF (2.0 mL) (macrocycle-Cu complex solution). A fresh sample of **2d** was prepared by deprotection by TBAF in THF and by passing it through short column (silica, hexanes/CH_2Cl_2 5 :1). Freshly purified pentayne **2.4** (25.3 mg, 35 μmol) was dissolved in dry THF (4.0 mL) in a dry Schlenk tube, iodine (5.3 mg, 20 μmol), potassium carbonate (19.9 mg, 140 μmol) and THF solution of macrocycle-Cu complex were added. The reaction mixture was flushed with nitrogen gas and stirred in dark at 60 °C for 36 h. The progress of reaction was monitored by TLC ($PE_{40/60}$/EtOAc 6 : 1). The reaction was stirred for 36 h and then cooled to 20 °C, after which CH_3CN (1.0 mL), CH_2Cl_2 (2.0 mL) and an aqueous solution of potassium cyanide (10.0 mg, 0.15 mmol in 1.0 mL water) were added and the mixture stirred at 20 °C for additional 5 h. The mixture was diluted with CH_2Cl_2 (4.0 mL), the organic fraction separated and washed with water (3×5.0 mL) after which solvents were removed. The residue was purified by column chromatography (silica, $PE_{40/60}$/EtOAc 30:1) and further purified using size-exclusion column (on Biobeads-S-X3) in THF to afford a product **2d⊂M1** as a yellow solid (4.5 mg, 15 %). ^{1}H NMR (500 MHz, CD_2Cl_2) δ 8.45 (d, J = 8.7 Hz, 4H, H_d), 8.29 (d, J = 8.5 Hz, 2H, H_b), 8.11 (d, J = 8.5 Hz, 2H, H_c), 7.76 (s, 2H, H_a), 7.29 (t, J = 1.7, 6H, H_1), 7.13–7.08 (m, 5H, $H_{e,h}$), 6.92 (d, J = 1.7, 12 H, H_2), 6.52 (t, J = 2.2, 1H, H_f), 6.47 (dd, J_1 = 8.2 Hz, J_2 = 2.3 Hz, 2H, H_g), 4.12 (t, J = 7.0 Hz, 4H, H_i), 3.99 (t, J = 6.49, 4H, H_j), 1.92–1.85 (m, 8H, $H_{k,l}$), 1.61 (m, 8H, $H_{m,n}$) 1.18 (s, 108 H, H_3). ^{13}C NMR (125 MHz, CD_2Cl_2) δ161.0, 156.2, 150.9, 146.6, 143.7, 137.1, 132.4, 130.2, 129.4, 128.0, 126.1, 124.1, 121.3, 119.4, 115.3, 107.6, 101.1, 87.3, 69.4, 68.7, 68.3, 64.4, 64.1, 64.0, 63.7, 63.3, 62.9, 62.8, 62.4, 58.0, 35.3, 31.6, 30.3, 29.7, 26.5; *m/z* (MALDI TOF MS+) 2041.91, ($C_{148}H_{168}N_2O_4$); $[M]^+$ requires 2039.31; UV-vis (CH_2Cl_2) λ / nm (ε / M^{-1} cm^{-1}) 384 (245000) 358 (229000), 337 (143000), 319 (108000), 287 (86000); UV-vis (THF) λ / nm (ε / M^{-1} cm^{-1}) 383 (268000) 358 (249000), 336 (154000), 318 (119000), 287 (101000). M.p. 214–216 °C.

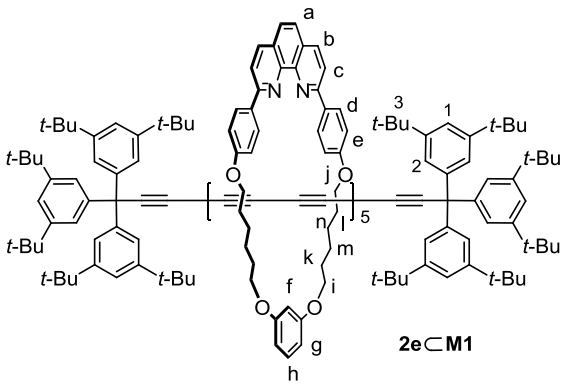

2e⊂M1

2e⊂M1: To a solution of CuI (5.1 mg, 27 µmol) in MeCN (1 mL) was added a solution of the macrocycle M**1** (17 mg, 27 µmol) in CH_2Cl_2 (1 mL). The mixture was stirred for 1.5 h at 20 °C and the solvent was removed *in vacuo* to give the macrocycle-Cu complex. The complex was redissolved in THF (2 mL) and added to a mixture of the freshly prepared hexayne **2.5** (49 mg, 67 µmol), K_2CO_3 (14 mg, 0.10 mmol) and I_2 (6.8 mg, 27 µmol) in THF (2 mL). The reaction mixture was then flushed with N_2 and stirred at 60 °C in the dark for 2 d. CH_2Cl_2 (2 mL), MeCN (2 mL), and KCN (20 mg, 30 mmol in 1 mL H_2O) were added, and the mixture was stirred at 20 °C for 3 h. CH_2Cl_2 (10 mL) was added, the organic phase separated, washed with H_2O (3 x 10 mL), and the solvent removed *in vacuo*. Column chromatography (silica, hexanes/EtOAc 20:1) followed by size exclusion chromatography (Bio Beads SX-3, $CHCl_3$) afforded the product as a yellow-orange solid (6.2 mg, 11%). ^{1}H NMR (500 MHz, CD_2Cl_2) δ 8.44 (d, J = 8.8, Hz, 4H, H_d), 8.28 (d, J = 8.4 Hz, 2H, H_b), 8.10 (d, J = 8.4 Hz, 2H, H_c), 7.76 (s, 2H, H_a), 7.30 (t, J = 1.6 Hz, 6H, H_1), 7.12-7.09 (m, 5H, $H_{e,h}$), 6.92 (d, J = 1.6 Hz, 12H, H_2), 6.51 (t, J = 2.2 Hz, 1H, H_f), 6.46 (dd, J_1 = 8.1 Hz, J_2 = 2.3 Hz, 2H, H_g), 4.12 (t, J = 6.9 Hz, 4H, H_j), 3.99 (t, J = 6.3 Hz, 4H, H_i), 1.93-1.83 (m, 8H, $H_{k,l}$), 1.61 (m, 8H, $H_{m,n}$), 1.19 (s, 108H, H_3): ^{13}C NMR (125 MHz, CD_2Cl_2) δ160.9, 156.2, 150.9, 146.5, 143.5, 136.9, 132.2, 130.0, 129.2, 127.9, 125.9, 123.9, 121.1, 119.2, 115.1, 107.4, 100.9, 87.4, 69.2, 68.5, 68.1, 64.3, 64.0 (two signal is overlapped), 63.8, 63.5, 63.2, 62.9, 62.7, 62.5, 62.2, 57.8, 35.1, 31.5, 29.9, 29.5, 26.3, 26.3; *m/z* (MALDI TOF MS+) 2087.03, ($C_{152}H_{168}N_2O_4$); $[M + H]^+$ requires 2087.30; UV-vis (CH_2Cl_2) λ_{max} / nm (ε / M^{-1} cm^{-1}) 407 (296500), 380 (285000), 359 (212000), 337 (127000) 320 (84300) 289 (96600) 279 (75700) 267 (59800) 254 (47600); UV-vis (THF) λ_{max} / nm (ε / M^{-1} cm^{-1}) 407 (291700), 380 (273000), 356 (205000), 336 (119000) 319 (80100) 288 (94800) 279 (79400) 267 (61200) 255 (48000); M.p. > 370 °C.

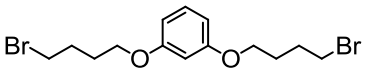

2.23

m-Bis[(6-bromohexyl)oxy]benzene 2.23: The compound was synthesized similarly to **2.21**. Resorcinol (300 mg, 2.72 mmol), 1,4-dibromobutane (2.60 mL, 4.68 g, 21.6 mmol) and K_2CO_3 (19 g, 13.7 mmol) were dissolved in acetone (100 mL). The reaction mixture was refluxed for 3 d and the solvent was

removed. The crude was passed over a silica column ($PE_{40/60}/CH_2Cl_2$ 2:3) affording the product **2.23** (710 mg, 68%) as a white solid. ^{1}H NMR (400 MHz, $CDCl_3$) δ 7.16 (t, J = 8.2, 1H), 6.49 (dd, J_1 = 2.4 Hz, J_2 = 5.8 Hz, 2H), 6.44 (t, J = 2.4 Hz), 3.97 (t, J = 6.1 Hz, 4H), 3.49 (t, J = 6.6, 4H,), 2.10– 2.02 (m, 4H), 1.97–1.90 (m, 4H).

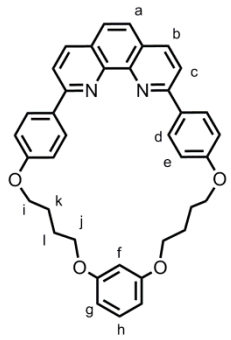

Macrocycle M2: This compound is synthesized similarly to the **M1** macrocycle. To a solution of 2,9-bis(hydroxyphenyl)-1,10 phenanthroline **2.20** (200mg, 0.549 mmol) and 1,3-bis(bromobutyloxy)benzene **2.23** (208 mg, 0.549 mmol) in anhydrous DMSO (100 mL), potassium carbonate (1.50 g, 10.86 mmol) was added and the reaction mixture was stirred 5 h at 60 °C, under nitrogen. The reaction mixture was cooled and solvent was removed under vacuo. The crude mixture was washed with a large excess of water and filtered, then the product was purified by column chromatography (silica gel, THF/CH_2Cl_2 10:1), then by using size-exclusion column (on Biobeads-S-X3) in THF to remove larger macrocyclic molecules. The final recrytsallization from CH_2Cl_2/hexane afforded the product **M2** as a white solid (110 mg, 34.4 %).^{1}H NMR (400 MHz, CD_2Cl_2) δ 8.34 (d, J = 8.9 Hz, 4H, H_d), 8.29 (d, J = 8.4 Hz, 2H, H_b), 8.07 (d, J = 8.4 Hz, 2H, H_c), 7.77 (s, 2H, H_a), 7.18-7.13 (m, 5H, $H_{h,e}$), 6.58 (t, J = 2.4 Hz, 1H, H_f), 6.52 (dd, J_1 = 8.2 Hz, J_2 = 2.4 Hz, 2H, H_g) 4.28 (t, J = 7.2 Hz, 4H, H_i), 4.06 (t, J = 5.9 Hz, 4H, H_j), 2.08 (m, 4H, H_l), 1.98 (m, 4H, H_k): ^{13}C NMR (100 MHz, CD_2Cl_2) δ 160.8, 160.5, 156.5, 146.4, 137.0, 132.7, 130.2, 129.3, 127.8, 125.9, 119.6, 115.6, 106.8, 102.3, 68.6, 68.4, 27.0, 26.3. (MALDI TOF MS+) 583.33, ($C_{38}H_{34}N_2O_4$); $[M]^+$ requires 583.26.

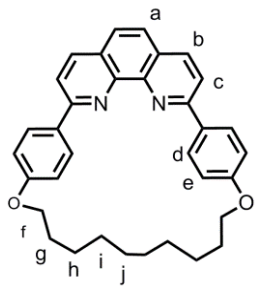

Macrocycle M3. This compound is synthesized similarly to the **M1** macrocycle. To a solution of 2,9-bis(hydroxyphenyl)-1,10-phenanthroline **2.20** (300 mg, 0.82 mmol) and 1,10-dibromodecane (245 mg, 0.82 mmol) in anhydrous DMF (300 mL), potassium carbonate (3.0 g, 21.7 mmol) was added and the reaction mixture was stirred 2 d at 75 °C, under nitrogen. The reaction mixture was cooled and solvent was removed. The crude mixture was washed with a large excess of water and filtered, then column chromatography (silica gel, CH_2Cl_2, gradually EtOAc 0–15%) and recrystallized from CH_2Cl_2/methanol to afford the product **M3** as a white solid (119 mg, 28.8%). ^{1}H NMR (500 MHz, CD_2Cl_2)

δ 8.36 (d, J = 8.8, Hz, 4H, H_d), 8.29 (d, J = 8.2 Hz, 2H, H_b), 8.07 (d, J = 8.5 Hz, 2H, H_c), 7.77 (s, 2H, H_a), 7.11 (d, J = 8.8 Hz, 4H, H_e), 4.25 (t, J = 8.2 Hz, 4H, H_f), 1.81 (m, 4H, H_g), 1.42-1.40 (m, 12H, $H_{h,j,k}$): ^{13}C NMR (125 MHz, CD_2Cl_2) δ 159.9, 156.5, 146.4, 137.0, 132.5, 129.4, 127.8, 125.9, 119.5, 115.9, 68.3, 29.7, 29.4, 28.1, 25.6. (MALDI TOF MS+) (calc. for M+H$^+$) 504.76, ($C_{34}H_{35}N_2O_2^+$); [M+H$^+$] requires 503.26.

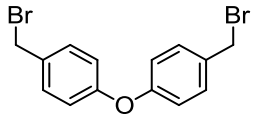

2.24

2.24:[53] A mixture of p-tolyl ether (1.50 g, 7.65 mmol), NBS (2.79 g, 15.6 mmol) and AIBN (120 mg) in CCl_4 (50 mL) stirred under reflux overnight. The reaction mixture was cooled to 0 °C, filtered and washed with water. The organic layer was collected and solvent was removed. Recrystallization from hexane afforded the product **2.24** (1.2 g, 44 %) as a white solid. ^{1}H NMR (400 MHz, $CDCl_3$) δ 7.37 (d, J = 8.53 Hz, 4H), 6.97 (d, J = 8.53 Hz, 4H), 4.50 (s, 4H). As in lit.[50]

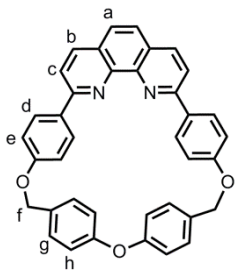

M4: This compound is synthesized similarly to the **M1** macrocycle. A mixture of di(*p*-benzylbromide) ether **2.24** (61 mg, 0.17 mmol) and 2,9-bis(hydroxyphenyl)-1,10-phenanthroline **2.20** (63 mg, 0.17 mmol) were dissolved in dry DMF (70 mL), potassium carbonate (0.80 g, 5.8 mmol) was added and the reaction mixture was stirred at 75 °C under nitrogen. After 2 d stirring, the reaction mixture was cooled and solvent was removed. The crude mixture was suspended in excess water and filtered. Column chromatography (silica, CH_2Cl_2/EtOAc 30:1) afforded product **M4** as a slightly yellow solid (48 mg, 50%). ^{1}H NMR (400 MHz, CD_2Cl_2) δ 8.29 (d, J = 8.3 Hz, 2H, H_c), 7.94 (d, J = 8.3 Hz, 2H, H_b), 7.89 (d, J = 8.8 Hz, 4H, H_d), 7.79 (s, 2H, H_a), 7.28 (d, J = 8.6 Hz, 4H, H_g), 7.10 (d, J = 8.6 Hz, 4H, H_h), 6.97 (d, J = 8.8 Hz, 4H, H_e), 5.34 (s, 4H, H_f). ^{13}C NMR (100 MHz, CD_2Cl_2) δ 159.6, 158.2, 146.7, 136.9, 134.5, 133.2, 129.7, 128.2, 127.8, 126.1, 121.1, 121.0, 117.2, 70.8, 50.6. ESI HRMS (toluene/MeCN) calc. for $C_{38}H_{27}N_2O_3$)(M + H$^+$) 559.20162, found 559.2019.

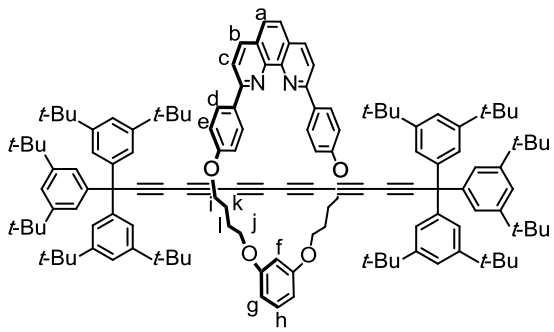

2b⊂M2: To a solution of CuI (6.7 mg, 35 μmol) in MeCN (1 mL) was added a solution of the macrocycle **M2** (20.5 mg, 35 μmol) in CH_2Cl_2 (1 mL). The mixture was stirred for 1.5 h at 20 °C and the solvent was removed *in vacuo* to give the macrocycle-Cu complex. The complex was redissolved in THF (2 mL) and added to a mixture of the triyne **2.2** (57 mg, 88 μmol), K_2CO_3 (13 mg, 0.17 mmol) and I_2 (9 mg, 35 μmol) in THF (2 mL). The reaction mixture was then flushed with N_2 and stirred at 60 °C for 2 d. CH_2Cl_2 (2 mL), MeCN (2 mL), and KCN (20 mg, 30 mmol in 1 mL H_2O) were added, and the mixture was stirred at 20 °C for 3 h. CH_2Cl_2 (10 mL) was added, the organic phase separated, washed with H_2O (3 x 10 mL), and the solvent removed *in vacuo*. Column chromatography (silica, $PE_{40/60}$/EtOAc 30:1 to 20:1) followed afforded the product **2b⊂M2** as a yellow solid (19.6 mg, 28%). ^{1}H NMR (400 MHz, CD_2Cl_2) δ 8.44 (d, J = 8.8, Hz, 4H, H_d), 8.28 (d, J = 8.4 Hz, 2H, H_b), 8.10 (d, J = 8.4 Hz, 2H, H_c), 7.76 (s, 2H, H_a), 7.30 (t, J = 1.6 Hz, 6H, H_1), 7.12-7.09 (m, 5H, $H_{e,h}$), 6.92 (d, J = 1.6 Hz, 12H, H_2), 6.51 (t, J = 2.2 Hz, 1H, H_f), 6.46 (dd, J_1 = 8.1 Hz, J_2 = 2.3 Hz, 2H, H_g), 4.12 (t, J = 6.9 Hz, 4H, H_j), 3.99 (t, J = 6.3 Hz, 4H, H_i), 1.93-1.83 (m, 8H, $H_{k,l}$), 1.61 (m, 8H, $H_{m,n}$), 1.19 (s, 108H, H_3): ^{13}C NMR (500 MHz, CD_2Cl_2) δ 160.5, 160.3, 156.1, 150.4, 146.2, 143.2, 136.5, 132.3,129.7, 128.9, 127.4, 125.5, 123.5, 120.7, 119.0, 115.2, 107.4, 102.0, 86.3, 69.0, 68.3, 67.8, 63.6, 63.4, 62.9, 62.7, 57.4, 34.7, 31.1, 26.4, 26.0; *m/z* (MALDI TOF MS+) 1887.07, ($C_{152}H_{168}N_2O_4$); $[M]^+$ requires 1886.24; UV-vis (CH_2Cl_2) λ_{max} / nm (ε / M^{-1} cm^{-1}) 318 (234000), 298 (195000), 282 (144000); UV-vis (THF) λ_{max} / nm (ε / M^{-1} cm^{-1}) 317 (267900), 297 (220000), 281 (163000);

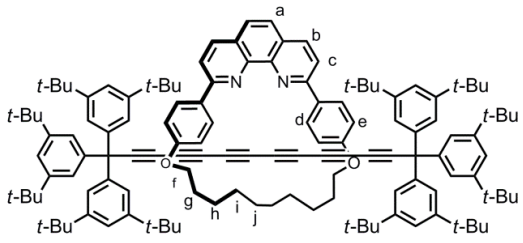

2b⊂M3: To a solution of macrocycle **M3** (18.5 mg, 37 μmol) in CH_2Cl_2 (1.5 mL) a solution of CuI (7 mg, 37 μmol) in CH_3CN (1.0 mL) was added and the mixture stirred at 20 °C for 1.5 h. The mixture was then dried *in vacuo* and redissolved in dry THF (5.0 mL) (macrocycle-Cu complex solution). Triyne **2.2** (60.0 mg, 0.092 mmol) was dissolved in THF (2.0 mL) in a dry Schlenk tube and iodine (11.8 mg, 115 μmol), K_2CO_3 (21.0 mg, 0.15 mmol) and the THF solution of macrocycle·Cu(I) complex were added. The reaction mixture was

flushed with nitrogen gas and stirred in dark at 60 °C for 24 h. The progress of reaction was monitored by TLC ($PE_{40/60}$/DCM 1 : 1). After stirring for 24 h, iodine (2.5 mg, 10 μmol) and K_2CO_3 (6.0 mg, 43 μmol) were added and the mixture stirred additionally for 24 h. Then the reaction mixture was cooled to 20 °C; CH_3CN (1.5 mL), CH_2Cl_2 (1.5 mL) and KCN (13.0 mg, 0.2 mmol in 1.0 mL H_2O) were added and the mixture stirred at 20 °C for 6 h. Mixture was diluted with CH_2Cl_2 (5.0 mL), the organic fraction was separated, washed with water and solvents were removed. The column chromatography of the crude mixture (silica, $PE_{40/60}$/DCM 1 : 1, gradually adding EtOAc 0 – 15%) afforded a product **2b⊂M3** as a yellow solid (11.7 mg, 17%).^{1}H NMR (500 MHz, CD_2Cl_2) δ 8.36 (d, J = 8.9, 4H, H_d), 8.26 (d, J = 8.4, 2H, H_c), 8.03 (d, J = 8.36, 2H, H_b), 7.76 (s, 2H, H_a), 7.25 (t, J = 1.7, 6H, H_1), 7.13 (d, J = 8.9, 4H, H_e), 6.87 (d, J = 1.7, 12H, H_2), 4.20 (t, J = 1.0, 4H, H_f), 1.85 (m, 8H, $H_{k,l}$), 1.81 (m, 4H, H_g) 1.44-1.1.3(m, 12H, $H_{i/h}$), 1.14 (s, 108H, H_3). ^{1}H NMR (500 MHz, CD_2Cl_2) δ 159.7, 156.9, 146.8, 143.6, 136.7, 132.9, 129.6, 127.8, 125.8, 123.9, 121.0, 119.5, 86.7, 69.3, 68.7, 64.3, 63.8, 63.8, 63.4, 57.7, 35.1, 31.4, 30.1, 29.6, 29.4, 28.8, 26.1: (MALDI TOF MS+) 1808.60, ($C_{132}H_{160}N_2O_2$); [M]+ requires 1807.28. UV-vis (CH_2Cl_2) λ / nm (ε / M^{-1} cm^{-1}), 317 (234500), 298(164000), 282 (118000), 267 (66500), UV-vis (THF) λ / nm (ε / $M^{-1}cm^{-1}$) 316 (180000), 297 (139000); 280 (81000), 248 (30000).

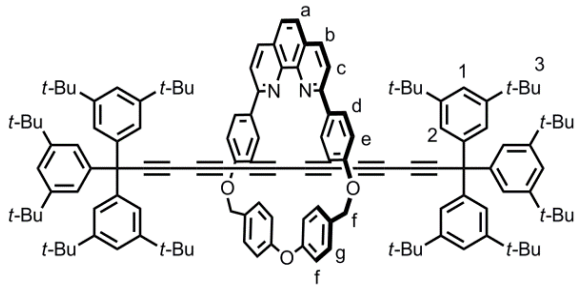

2b⊂M4: To a solution of CuI (5.9 mg, 30 μmol) in MeCN (1 mL) was added a solution of the macrocycle **M4** (17.1 mg, 30 μmol) in CH_2Cl_2. The mixture was stirred for 2.5 h at 20 °C and the solvent was removed *in vacuo* to give the macrocycle·Cu(I) complex. The complex was redissolved in THF (2 mL) and added to a mixture of the triyne **2.2** (50 mg, 76 μmol), K_2CO_3 (17 mg, 123 μmol) and I_2 (8.6 mg, 33 μmol) in THF (2 mL). The reaction mixture was then flushed with N_2 and stirred at 60 °C in the dark. After 3 d, the mixture was cooled to 20 °C, CH_2Cl_2 (2 mL), MeCN (2 mL), and KCN (20 mg in 1 mL H_2O) were added and the solution was stirred for 6 h at 20 °C. CH_2Cl_2 (3 mL) was added, the organic phase was separated and washed with H_2O (3 × 5 mL). After the solvent was removed *in vacuo*, the crude mixture was purified by column chromatography (silica gel, hexanes/EtOAC = 20 : 1) followed by recrystallization (CH_2Cl_2/MeOH) afforded the product **2b⊂M4** as a

yellow-greenish solid (16.2 mg, 23%). ^{1}H NMR (400 MHz, CD_2Cl_2) δ 8.23 (d, J = 8.3 Hz, 2H, H_c), 7.89-7.85 (m, 6H, $H_{b,d}$), 7.75 (s, 2H, H_a), 7.29-77.27 (m, 10H, H1,$_g$), 7.19 (d, J = 8.6 Hz, 4H, H_h), 6.92 (d, J = 1.8 Hz, 12H, H_2), 6.89 (J = 8.8 Hz, 4H, H_e), 5.27 (s, 4H, H_f), 1.17 (s, 108H, H_3): ^{13}C NMR (100 MHz, CD_2Cl_2) δ159.5, 158.4, 158.2, 150.7, 146.9, 143.8, 136.4, 134.4, 134.3, 130.0, 127.7, 127.6, 125.9, 123.9, 122.2, 121.0, 120.8, 116.3, 85.8, 70.4, 69.4, 63.9, 63.6, 63.6, 62.6, 56.6, 35.1, 31.5. (MALDI TOF MS+) 1863.50, ($C_{136}H_{152}N_2O_3$); $[M]^+$ requires 1862.18. UV-vis (CH_2Cl_2) λ_{max} / nm (ε / M^{-1} cm^{-1}), 317 (211000), 297(161000), 281 (115000), 267 (61000), 241 (43000); UV-vis (THF) λ_{max} / nm (ε / $M^{-1}cm^{-1}$) 316 (233800), 297 (179000); 281 (120000), 267 (70000); m.p. 143-145 °C.

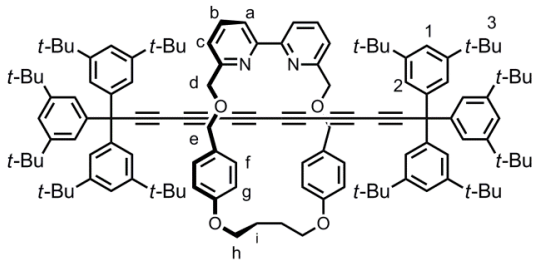

2b⊂M5: To a solution of macrocycle **M5** (10.3 mg, 21 μmol) in CH_2Cl_2 (1.0 mL) a solution of CuI (4.1 mg, 21 μmol) in CH_3CN (1.0 mL) was added and the mixture was stirred at 20 °C for 1.5 h. The mixture was then dried under vacuum and re-dissolved in dry THF (2.0 mL) (macrocycle-Cu complex solution). The triyne **2b** (34.9 mg, 54 μmol) was dissolved in THF (2.0 mL) in a dry Schlenk tube and iodine (5.5 mg, 21 μmol), potassium carbonate (12.0 mg, 86 μmol) and the THF solution of macrocycle·Cu(I) complex were added. The reaction mixture was flushed with nitrogen gas and stirred in dark at 60 °C for 24 h. The progress of reaction was monitored by TLC ($PE_{40/60}$ /EtOAc 6 : 1). After stirring for 24 h. iodine (5.0 mg, 19 μmol) and K_2CO_3 (12.0 mg, 86 μmol) were added and the mixture stirred additionally for 24 h. Then the reaction mixture was cooled to 20 °C; CH_3CN (1.5 mL), CH_2Cl_2 (2.0 mL) and the aqueous solution of potassium cyanide (20.0 mg, 0.31 mmol in 1.0 mL H_2O) were added and the mixture stirred at 20 °C for 6 h. Mixture was diluted with CH_2Cl_2 (2.0 mL), the organic fraction was separated and washed with water (3 × 5.0 mL) and solvents were removed *in vacuo*. The column chromatography of the crude (silica, $PE_{40/}$60/DCM 1:1, gradually adding EtOAc 0 –10%) afforded a product **2b⊂M5** as a yellow solid (9 mg, 23.5%). ^{1}H NMR (500 MHz, CD_2Cl_2) δ 7.87 (d, J = 7.57, 2H, Ha), 7,56 (t, J = 7.88, 2H, Hb), 7.37-7.35 (m, 8H, Hc,1), 7.07 (d, J = 8.51, 2H, Hf), 7.03 (d, J = 1.89, 12H, H2), 6.67 (d, J = 8.51, 2H, Hg), 4.62 (s, 4H, He), 4.53 (s, 4H, Hd), 3.87 (t, J = 6.62, 4H, Hh), 1.83 (m, 4H, Hi), 1.26 (s, 108H, H3): ^{13}C NMR (125 MHz, CD_2Cl_2) δ 159.2, 158.9, 155.7, 150.8, 143.9, 136.9, 130.4, 129.9, 124.0, 121.1, 120.9, 119.8, 115.1, 85.6, 77.9, 72.6,

71.6, 69.9, 67.1, 63.6, 62.7, 62.3, 62.3, 57.8, 35.2, 31.5, 25.2: (MALDI TOF MS+) 1784.78, ($C_{128}H_{156}N_2O_4$); $[M]^+$ requires 1785.2. UV-vis ($CHCl_3$) λ_{max} / nm (ε / M^{-1} cm^{-1}), 317 (211000), 297(161000), 281 (115000), 267 (61000), 241 (43000); UV-vis (THF) λ_{max} / nm (ε / $M^{-1}cm^{-1}$) 316 (180000), 297 (139000); 280 (81000), 248 (30000).

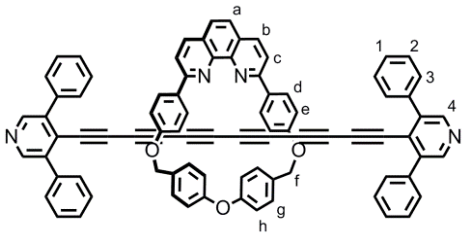

Py2⊂M4: To a solution of Py(Ph)$_2$-TIPS-triyne **Py1** (50 mg, 0.11 mmol) TBAF (1.0 M in THF, 0.12 mL, 0.12 mmol) was added dropwise in wet THF (10 mL + 10 μL H_2O). After 10 min stirring at 20 °C the reaction was quenched via addition of saturated NH_4Cl(aq) (10 mL). The organic phase was separated, the aqueous phase extracted with CH_2Cl_2 (2 × 10 mL), and the combined organic phases were washed with H_2O (10 mL) and saturated NaCl(aq) (10 mL). The solvents were reduced *in vacuo* and the mixture filtered through a plug of Al_2O_3 (EtOAc). The solvent volume was reduced *in vacuo*, THF was added and the volume of solvents was reduce *in vacuo*. This procedure repeated until EtOAc was removed completely. The residue dissolved in THF (2 mL) was then added to a mixture of the CuI·**M4** complex (prepared as a 1:1 complex: CuI(9.5 mg, 0.050 mmol) and macrocycle **M4** (28 mg, 0.050 mmol) in CH_2Cl_2 (2 mL) and CH_3CN (2 mL)), K_2CO_3 (27 mg, 0.20 mmol), and I_2 (13 mg, 0.050 mmol) in THF (3 mL). The mixture was stirred at 60 °C for 24 h, cooled to 20 °C and quenched via addition of KCN (20 mg in 1 mL H_2O), deluted with CH_2Cl_2 (1 mL) and CH_3CN (1 mL). After 2 h stirring the organic phase was separated, the aqueous phase extracted with CH_2Cl_2 (2 × 10 mL) and the combined organic phases were washed with H_2O (10 mL) and saturated NaCl(aq) (10 mL). The solvent was removed *in vacuo* and column chromatography (Al_2O_3, hexane/EtOAc 4:1) afforded the product **Py2⊂M4** as a yellow solid (1.1 mg, 2%). ^{1}H NMR (500 MHz, CD_2Cl_2) δ 8.58 (s, 4H), 8.27 (d, *J*=8.3 Hz, 2H), 7.89 (d, *J*=8.3 Hz, 2H), 7.79 (s, 2H), 7.75 (d, *J*=8.7 Hz, 4H), 7.55–7.51 (m, 8H), 7.45–7.36 (m, 12H), 7.05 (d, *J*=8.6 Hz, 4H), 7.00 (d, *J*=8.6 Hz, 4H), 6.77 (d, *J*=8.7 Hz, 4H), 5.20 (s, 4H). ^{13}C NMR (125 MHz, CD_2Cl_2) δ 159.4, 158.3, 158.0, 149.2, 146.8, 140.6, 136.8, 136.5, 134.3, 134.2, 129.9, 129.6, 129.0, 128.9, 127.7, 127.4, 126.0, 125.2, 122.1, 120.8, 116.2, 83.2, 73.7, 70.2, 70.1, 66.5, 64.3, 61.8. *m/z* (MALDI TOF MS+) ($C_{88}H_{66}N_4O_4$); $[M+ H^+]^+$ requires 1163.39 found 1163.80.

2.12 References

1. Chalifoux, W. A.; Tykwinski, R. R. *C. R. Chimie* **2009**, *12*, 341–358.
2. Gibtner, T.; Hampel, F.; Gisselbrecht, J.-P.; Hirsch, A. *Chem. Eur. J.* **2002**, *8*, 408– 432.
3. Zheng, Q.; Gladysz, J. A. *J. Am. Chem. Soc.* **2005**, *127*, 10508–10509.
4. (a) Chalifoux, W. A.; Tykwinski, R. R. *Nat. Chem.* **2010**, *2*, 967–971. (b) Chalifoux, W. A. *'Towards Carbyne: Synthesis and Study of Extremely Long Polyynes*' PhD thesis, University of Alberta, Alberta.
5. (a) Diederich, F. *Nature* **1994**, *369*, 199–207. (b) Huuskonen, J.; Buston, J. E. H.; Scotchmer, N. D.; Anderson, H. L. *New J. Chem.* **1999**, *23*, 1245–1252. (c) Simpkins, S. M. E.; Kariuki, B. M.; Cox, L. R. *J. Organomet. C.* **2006**, *691*, 5517–5523. (d) Sugiyama, J.; Tomita, I. *Eur. J. Org. Chem.* **2007**, 4651–4653. (e) Shir, I. B.; Sasmal, S.; Mejuch, T.; Sinha, M. K.; Kapon, M.; Keinan, E. *J. Org. Chem.* **2008**, *73*, 8772–8779.
6. (a) Mróz, M. M.; Lanzani, G.; Virgili, T.; McDonnell, S. O.; Frampton, M. J.; Anderson, H. L. *Phys. Rev. B.* **2009**, *80*, 45111–45118. (b). Oddy, F. E.; Brovelli, S.; Stone, M. T.; Klotz, E. J. F.; Cacialli, F.; Anderson, H. L. *J. Mater. Chem.* **2009**, *19*, 2846–2852. (c) Frampton, M. J.; Claridge, T. D. W.; Latini, G.; Brovelli, S.; Cacialli, F.; Anderson, H. L. *Chem. Commun.* **2008**, 2797–2799. (d) Frampton, M. J.; Anderson, H. L. *Angew. Chem. Int. Ed.* **2007**, *46*, 1028–1064.
7. (a) Stahl, J.; Bohling, J. C.; Bauer, E. B.; Peters, T. B.; Mohr, W.; Martín-Alvarez, J. M.; Hempel, F.; Gladysz, J. A. *Angew. Chem. Int. Ed.* **2002**, *41*, 1871–1876.
8. de Quadras, L.; Bauer, E. B.; Mohr, W.; Bohling, J. C.; Peters, T. B.; Martín-Alvarez, J. M.; Hampel, F.; Gladysz, J. A. *J. Am. Chem. Soc.* **2007**, *129*, 8296–8309.
9. Taylor, T. J.; Gabbaï, F. P. *Organometallics* **2006**, *25*, 2143–2147.
10. Zhao, C.; Kitaura, R.; Irle, S.; Shinohara, H. *Phys. Chem. C* **2011**, *115*, 13166–13170.
11. Langton, M. J.; Matichak, J. D.; Thompson, A. L.; Anderson, H. L. *Chem. Sci.* **2011**, *2*, 1897–1901.
12. Later, Gladysz and coworkers reported the synthesis of Pt-capped octayne rotaxane threaded with phenanthroline macrocycle M1: Weisbach, N.; Baranová, Z.; Gauthier, S.; Reibenspies, J. H.; Gladysz, J. A. *Chem. Comm.* **2012**, *48*, 7562–7564.
13. (a) Saito, S.; Takahashi E.; Nakazono, K. *Org. Lett.* **2006**, *8*, 5133–5136. (b) Berná, J.; Crowley, J. D.; Goldup, S. M.; Hänni, K. D.; Lee, A.-L.; Leigh, D. A. *Angew. Chem. Int. Ed*. **2007**, *46*, 5709–5713. (c) Crowley, J. D.; Goldup, S. M.; Gowans, N. G.; Leigh, D. A.; Ronaldson, V. E.; Slawin, A. M. Z. *J. Am. Chem. Soc.* **2010**, *132*, 6243–6248.
14. Ditto, S. R.; Card, R. J.; Davis, P. D.; Neckers, D. C. *J. Org. Chem.* **1979**, *44*, 894–896.
15. Bartlett, P. D.; Roha, M.; Stiles, R. M. *J. Am. Chem. Soc.* **1954**, *76*, 2349–2353.
16. Khuong, T.-A. V.; Zepeda, G.; Ruiz, R.; Khan, S. I.; Garcia-Garibay, M. A. *Cryst. Growth Des.* **2004**, *4*, 15–16.
17. Ramirez, F.; Desai, N. B.; McKelvie, N. *J. Am. Chem. Soc.* **1962**, *84*, 1745–1747.
18. Robles, O.; McDonald, F. E. *Org. Lett.* **2008**, *10*, 1811–1814.
19. Hay, A. S. *J. Org. Chem.* **1962**, *27*, 3320–3321.
20. Glaser, C. *Ann. Chem.* **1870**, *154*, 137–171.
21. Eglinton, G.; Galbraith, A. R. *Chem. Ind. (London)* **1956**, 737–738.
22. Siemsen, P.; Livingston, R. C.; Diederich, F. *Angew. Chem. Int. Ed.* **2000**, *39*, 2632–2657.
23. (a) V. Aucagne, K. D. Hänni, D. A. Leigh, P. J. Lusby and D. B. Walker, *J. Am. Chem. Soc.* **2006**, *128*, 2186–2187. (b) Crowley, J. D.; Goldup, S. M.; Lee, A.; Leigh, D. A.; McBurney, R. T. *Chem. Soc. Rev.* **2009**, ***38***, 1530–1541.
24. (a) Saito, S.; Nakazono, K.; Takahashi, E. *J. Org. Chem.* **2006**, *71*, 7477–7480. (b) Chambron, J. C.; Heitz, V.; Sauvage, J.P. *J. Am. Chem. Soc*. **1993**, *115*, 12378–12384. (c) Hubin, T. J.; Busch, D. H. *Coord. Chem. Rev*. **2000**, *200*, 5–52.
25. Wada, Y.; Wakabayashi, T.; Kato T. *J. Phys. Chem. B*, **2011**, *115*, 8439–8445.
26. Leigh, D. A.; Crowley J. D.; Lusby, P. J. *J. Am. Chem. Soc.* 2007, **129**, 11950–11963.
27. For more references on mechanistic studies of Glaser coupling see: (a) Wendlandt, A. E.; Suess, A. M.; Stahl, S. S. *Angew. Chem. Int. Ed.* **2011**, *50*, 11062–11087.. (b) He, C.; Ke, J.; Xu, H.; Lei, A. *Angew. Chem. Int. Ed.* **2013**, *52*, 1527–1530. (c) Zhang, G.; Yi, H.; Zhang, G.; Dang, Y.; Bai, R.; Zhang, H.; Miller, J. T.; Kropf, A. J.; Bunel, E. E. Lei, A. *J. Am. Chem. Soc.* **2014** , *136* , 924–926.
28. Wardman, P. *J. Phys. Chem. Ref. Data* **1989**, *18*, 1637–1755.
29. (a) Gibtner, T.; Hampel, F.; Gisselbrecht, J.-P.; Hirsch, A. *Chem. Eur. J.* **2002**, *8*, 408–432. (b) Eisler, S.; Slepkov, A. D.; Elliott, E.; Luu, T.; McDonald, R.; Hegmann, F. A.; Tykwinski, R. R. *J. Am. Chem. Soc.* **2005**, *127*, 2666–2676. (c) Chalifoux, W. A.; McDonald, R.; Ferguson, M. J.; Tykwinski, R. R. *Angew. Chem. Int. Ed.* **2009**, *48*, 7915–7919.
30. a) Cheetham, A. G.; Hutchings, M. G.; Claridge, T. D. W.; Anderson, H. L. *Angew. Chem. Int. Ed.* **2006**, *45*, 1596–1599. b) Fernandes, A.; Viterisi, A.; Coutrot, F.; Potok, S.; D Leigh, . A.; Aucagne, V.; Papot, S. *Angew. Chem. Int. Ed*. **2009**, *48*, 6443–6447. (c) Schneider, H.-J.; Agrawal, P.; Yatsimirsky, A. K. *Chem. Soc. Rev.* **2013**, ***42***, 6777–6800.
31. a) Yau, C. M. S.; Pascu, S. I.; Odom, S. A.; Warren, J. E.; Klotz, E. J. F.; Frampton, M.; J. Williams, C. C.; Coropceanu, V.; Kuimova, M. K.; Phillips, D.; Barlow, S.; Bredas, J.-L.; Marder, S. R.; Millar, V.; Anderson, H. L.

Chem. Commun. **2008**, 2897–2899. b) Gassensmith, J. J.; Baumes, J. M.; Smith, B. D. *Chem. Commun*. **2009**, 6329–6338. c) Baumes, J. M.; Gassensmith, J. J.; Giblin, J.; Lee, J.-J.; White, A. G.; Culligan, W. J.; Leevy, W. M.; Kuno, M.; Smith, B. D. *Nat. Chem*. **2010**, *2*, 1025–1030.

32. a) Cacialli, F.; Wilson, J. S.; Michels, J. J.; Daniel, C.; Silva, C.; Friend, R. H.; Severin, N.; Samori, P.; Rabe, J. P.; O Connell, M. J.; Taylor, P. N.; Anderson, H. L. *Nat. Mater*. 2**002**, *1*, 160–164. b) Frampton, M. J.; Anderson, H. L. *Angew. Chem. Int. Ed*. **2007**, *46*, 1028–1064. c) Terao, J.; Tanaka, Y.; Tsuda, S.; Kambe, N.; Taniguchi, M.; Kawai, T.; Saeki, A.; Seki, S. *J. Am. Chem. Soc*. **2009**, *131*, 18046–18047.

33. Blanco-Rodriguez, A. M.; Towrie, M.; Collin, J. P.; Záliš, S.; Vlćek, A. Jr. *Dalton Trans.* **2009**, 3941–3949.

34. (a) Lahlali, H.; Jobe, K.; Watkinson, M.; Goldup, S. M. *Angew. Chem. Int. Ed.* **2011**, *50*, 4151–4155. (b) Winn, J.; Pinczewska, A.; Goldup, S. M. *J. Am. Chem. Soc.* **2013**, *135*, 13318–13321.

35. (a) Wang, C.; Batsanov, A. S.; Bryce, M. R.; Martín, S.; Nichols, R. J.; Higgins, S. J.; García-Suárez, V. M.; Lambert, C. J. *J. Am. Chem. Soc.* **2009**, *131*, 15647–15654. (b) Moreno-García, P.; Gulcur, M.; Manrique, D. Z.; Pope, T.; Hong, W.; Kaliginedi, V.; Huang, C.; Batsanov, A. S.; Bryce, M. R.; Lambert, C.; Wandlowski, T. *J. Am. Chem. Soc.* **2013**, *135*, 12228–12240.

36. Cretu, O.; Botello-Mendez, A. R.; Janowska, I.; Pham-Huu, C.; Charlier, J-C.; Banhart, F. *Nano Lett*. **2013**, *13*, 3487–3493.

37. (a) Crljen, Z.; Baranovic, G. *Phys. Rev. Lett*. **2007**, 98, 116801–116804. (b) Garcia-Suarez, V. M.; Lambert, C. J. *Nanotechnology*, **2008**, *19*, 455203.

38. Gulcur, M.; Moreno-García, P.; Zhao, X.; Baghernejad, M.; Batsanov, A. S.; Hong, W.; Bryce, M. R.; Wandlowski, T. *Chem. Eur. J.* **2014**, *20*, 4653–4660.

39. Standley, B.; Bao, W.; Zhang, H.; Bruck, J.; Lau, C. N.; Bockrath, M. *Nano Lett*. **2008**, *8*, 3345–3349.

40. Slepkov, A. D.; Hegmann, F. A.; Eisler, S.; Elliott, E.; Tykwinski, R. R. *J. Chem.Phys.* **2004**, *120*, 6807-6810.

41. Wannere, S. C.; von Rague Schleyer, P. *Org. Lett*., **2003**, *5*, 605-608.

42. (a) Szafert, S.; Gladysz, J. A. *Chem. Rev.* **2003**, *103*, 4175. (b) Szafert, S.; Gladysz, J. A. *Chem. Rev*. **2006**, *106*, PR1–PR33.

43. Owen, G. R.; Gauthier, S.; Weisbach, N.; Hampel, F.; Bhuvanesh, N.; Gladysz, J. A. *Dalton Trans.*, **2010**, 39, 5260–5271.

44. Hoffmann, R. *Angew. Chem. Int. Ed.* **1987**, *26*, 846–878.

45. Chalifoux, W. A.; MacDonald, R.; Ferguson, M. J.; Tykwinski, R. R. *Angew. Chem. Int. Ed.* **2009**, *48*, 7915–7919.

46. (a) Baughman, R. H.; Yee, K. C. *J. Polym. Sci. Macromol. Rev.* **1978**, *13*, 219–239. (b) Enkelmann, V. *Chem. Mater*. **1994**, *6*, 1337–1340.

47. Mohr, W.; Stahl, J.; Hampel, F.; Gladysz, J. A. *Inorg. Chem.* **2001**, *40*, 3263–3264.

48. Movsisyan, L. D.; Kondratuk, D. V.; Franz, M.; Thompson, A. L.; Tykwinski, R. R.; Anderson, H. L. *Org. Lett.* **2012**, *14*, 3424–3426.

49. (a) Palatinus, L.; van der Lee, A. *J. Appl. Cryst*. **2008**, *41*, 975. (b) Palatinus, L. *Acta Cryst.* **2013**, *B69*, 1.

50. Palatinus L.; Chapuis, G. *J. Appl. Cryst*. **2007**, *40*, 786.

51. (a) Betteridge, P. W.; Carruthers, J. R.; Cooper, R. I.; Prout, K.; Watkin, D. J. *J. Appl. Cryst.* **2003**, *36*, 1487. (b) Cooper, R. I.; Thompson, A. L.; Watkin, D. J. *J. Appl. Cryst*. **2010**, *43*, 1100.

52. Sheldrick, G. M. *Acta Cryst.* **2008**, *A64*, 112–122.

53. Golden, J.H**.** *Chem. Soc.* **1961**, 1604–1610.

Chapter 3

Molecular shuttles can be fabricated, Where every little helps, Bent or cross-like

Chapter 3. Synthesis of polyyne rotaxanes via active-metal template heterocoupling reaction

3.1 Introduction

While, the previous chapter was dedicated to the synthesis of polyyne rotaxanes through homocoupling of alkynes, in this chapter the synthesis of polyyne rotaxanes via heterocoupling reaction of terminal alkyne and alkynyl halide is described.

The Glaser homocoupling reaction of acetylenes usually gives satisfactory results for symmetric acetylenes. However, homocoupling becomes inapplicable for the formation of unsymmetrical polyynes, due to the lack of reaction selectivity. The problematic synthesis of asymmetric polyynes was solved through utilization of the cross-coupling protocols, developed by Cadiot and Chodkiewicz[1] and Negishi[2]. For example, in the Cadiot-Chodkiewicz heterocoupling reaction the oxidative addition of a 1-hallo-acetylene (usually bromoacetylene) to a Cu-acetylide produces a Cu(III) intermediate which undergoes reductive elimination affording the cross-coupled product, as the only product in many cases (Scheme 3.1).[3] Iodo- and bromoalkynes are the most commonly employed partners in the reaction, whereas chloroalkynes are rarely used due to their low reactivity.[3] Most preparative methods for iodoalkynes involve iodination of metal acetylides generated from terminal alkynes,[4] or reactions of activated terminal alkynes with iodine and other iodinating reagents.[5] Bromacetylenes are relatively easy to prepare by the treatment of terminal acetylene with triphenylphosphine/tetrabromomethane,[6] or by reacting alkynes with *N*-bromosuccinimide (NBS) in the presence of silver nitrate catalyst.[7] Both methods use mild reaction conditions and give products in excellent yields (>90%).

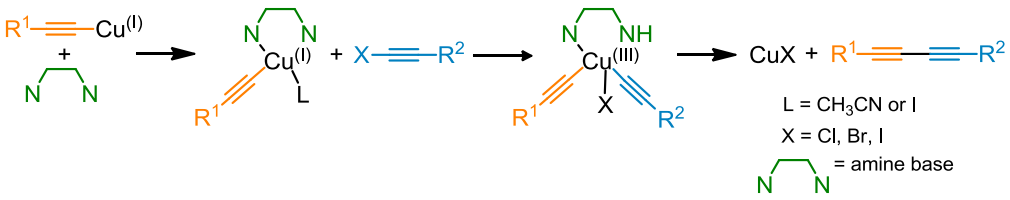

Scheme 3.1 Proposed mechanism for the Cadiot-Chodkiewicz cross-coupling.

This method has been successfully applied to the synthesis of biologically active molecules,[8] long polyynes and acetylene scaffoldings.[9] The cross-coupling of polyynes in the presence of a catalytic macrocycle could potentially produce rotaxanes with asymmetric axles, which could be exploited to make, for example, molecular shuttles.[10] In molecular shuttles, there are two or more discrete binding sites or stations on the rotaxane axle and the macrocycle can move (shuttle) between these sites, sometimes

without a significant energy barrier. Weak interactions between the axle and the thread are desirable, as this will provide high macrocycle mobility between two stations. From this perspective, a polyyne axle is an excellent choice for the construction of molecular shuttles due to its linear, rigid structure and minimum axle-macrocycle interactions. Additionally, an asymmetric polyyne axle can be exploited to prepare rotaxanes with planar chirality[11] which arises when there is a dissymmetry in both the macrocycle and the axle. The capability of Cadiot-Chodkiewicz cross-coupling of tethered acetylenes to synthesize molecular shuttles[3b] and catenanes[12] was demonstrated for the first time by Leigh and co-workers, however, the use of the cross-coupling of polyynes to construct multiple triple bonds (i.e. more than two triple bonds) in the rotaxane axle has been missing. Consequently, we were interested in the utilization of the Cadiot-Chodkiewicz heterocoupling reaction in the synthesis of polyyne rotaxanes. Our search for new synthetic strategies for the polyyne rotaxanes resulted in the synthesis of [3]rotaxanes with different topological order.

3.2 Improving the reaction yield of hexayne rotaxanes

Our first aim was to choose a model reaction to test the cross-coupling strategy in the rotaxane synthesis. We decided to start from the reaction of Tr*-triyne **2.2** and 1-bromotriyne **3.1** in the presence of macrocycle **M1**, which was expected to give the hexayne rotaxane **2b⊂M1** (Chapter 2). This rotaxane has previously used for the optimisation of the reaction condition in the active-template synthesis of rotaxanes through the Glaser homocoupling strategy.

The supertrityl triyne **2.2** was brominated by NBS and the product **3.1** was isolated in 95% yield (Scheme 3.2).[13] The fresh bromotriyne **3.1** is a light yellowish solid and it is stable in the dark at 4 °C, but it decomposes slowly under light.

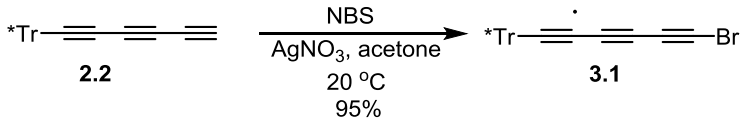

Scheme 3.2 The synthesis of bromotriyne **3.1**.

In the next step, stoichiometric amounts of triyne **2.2** and bromotriyne **3.1** were added to a THF solution of the CuI·**M1** complex, and the reaction was stirred under a nitrogen atmosphere in the dark, at 60 °C (Scheme 3.3). The reaction was over after 4 h stirring, with complete consumption of the starting

polyynes (monitored by TLC), and the corresponding rotaxane **2b⊂M1** was isolated in 38% yield (Table 3.1, entry 1). The rotaxane yield is slightly higher than the yield from homocoupling (32%). In the latter case, we used a slight excess of the **2.2** (2.5 eq.), thus, in the next test reaction, we added excess amounts of **2.2** (1.2 eq) and **3.1** (1.2 eq). The reaction was complete after 4 h and the product rotaxane was isolated in 43% yield (Table 3.1, entry 2).

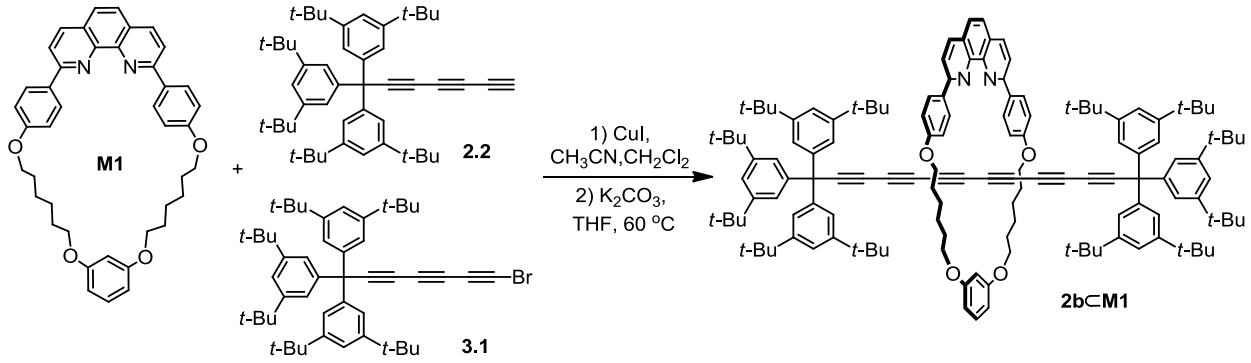

Scheme 3.3 Synthesis of rotaxane **2b⊂M1** via Cadiot-Chodkiewicz cross-coupling.

We continued to increase the amount of **3.1** up to 1.7 eq. and isolated the product rotaxane in 53% yield (Table 3.1, entry 3). Later, we repeated this reaction keeping the amount of **2.2** constant (1.2 eq.) while varying the amount of the **3.1** (1.5–1.7 eq.) and always obtained the rotaxane in good yields (47–53%). In these series of test experiments, we kept the concentrations of starting materials roughly the same. Finally, we carried out the reaction at 20 °C using stoichiometric amounts of **2.2** and **3.1**. The reaction went to completion after 3 days and gave the rotaxane **2b⊂M1** in 18% yield (Table 3.1, entry 4), while at 40 °C the reaction was complete after 24 h and the rotaxane yield was 26% yield (Table 3.1, entry 5). Compared to the homocoupling reaction, which failed at 40 °C, the rotaxination of polyynes via cross-coupling is more effective and proceeds at lower temperatures, which opens new possibilities to utilize other, unstable polyynes in the synthesis of rotaxanes.

Table 3.1 Optimization of the synthesis of hexayne rotaxanes under Cadiot-Chodkiewicz heterocoupling conditions. (Yields are calculated based on the CuI·macrocycle complexes. Reactions were carried out in deoxygenated THF. The concentration of reagents was about 0.01mmol/mL calculated for the CuI·macrocycle complexes)

Entry	Macrocycle, *eq*	**2.2**, *eq*	**3.1**, *eq*	T, °C	Time	Product yield
1	**M1**, 1	1	1	60	4 h	**2b⊂M1**, 38%
2	**M1**, 1	1.2	1.2	60	4 h	**2b⊂M1**, 43%
3	**M1**, 1	1.2	1.7	60	4 h	**2b⊂M1**, 53%
4	**M1**, 1	1	1	40	1 d	**2b⊂M1**, 26%
5	**M1**, 1	1	1	20	3 d	**2b⊂M1**, 18%
6	**M4**, 1	1.2	1.5	60	5 h	**2b⊂M4**, 54%

The differences in the mechanism between homo- and heterocoupling of alkynes could impose different sensitivity towards the geometry of the macrocycle.[3b,c] To be sure in the applicability of the heterocoupling reaction for the synthesis of polyyne rotaxanes with small macrocycles, the macrocycle **M4** was tested under optimized reaction conditions (Scheme 3.4). To our surprise, the reaction worked better than the corresponding homocoupling, yielding the rotaxane **2b⊂M4** in 54% (Table 3.1, entry 6). This result indicated that size of the macrocycle is not a limiting factor for rotaxanation of polyynes by Cadiot-Chodkiewicz cross-coupling reaction.

To further increase the rotaxane yield, we tested modified versions of the heterocoupling of alkynes. A report by Ferri and co-workers demonstrated that the yields of copper-catalyzed cross-coupling of bromoalkynes with terminal alkynes was improved in the presence of a catalytic amount of $PdCl_2(PPh_3)_2$.[14] Based on this reported, we attempted the synthesis of hexayne rotaxane **2b⊂M1** using 5% $PdCl_2(PPh_3)_2$ as a co-catalyst. To the mixture of CuI·**M1** in THF, **2.2** (1.1 eq) and **3.1** (1.5 eq) were added K_2CO_3 (4 eq.) and the Pd-catalyst. The reaction mixture was deoxygenated and stirred at 40 °C in the dark for 24 h. The reaction gave complex mixture which was difficult to separate and after elaborate workup the rotaxane **2b⊂M1** was obtained in 18.5% yield. The yield was low compared to the result from the Pd-free cross-coupling at the same temperature (26%, Table 3.1, entry 4) and the purification of final compound was tedious. Thus, the use of a Pd co-catalyst was determined to be less effective and we abandoned this route.

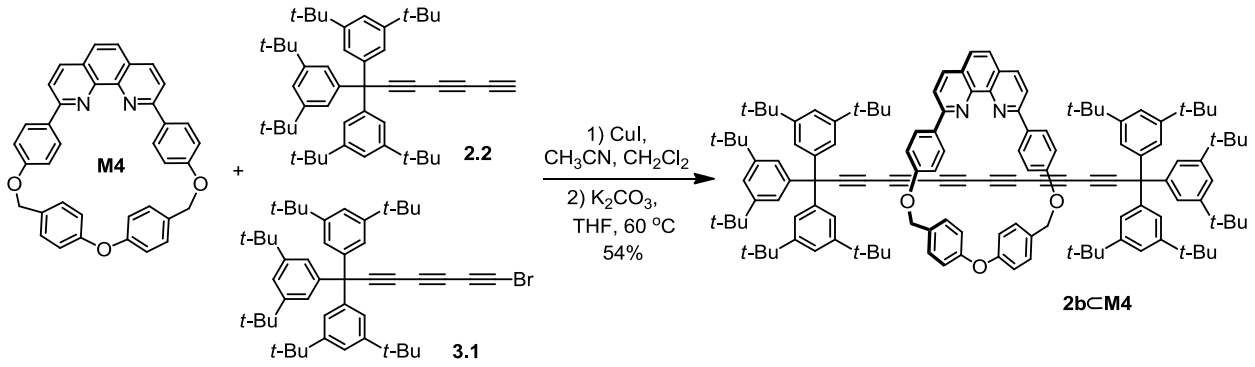

Scheme 3.4 Synthesis of rotaxane **2b⊂M4** via Cadiot-Chodkiewicz cross-coupling.

Leigh and co-workers reported the synthesis of rotaxanes using a non-traditional Cadiot–Chodkiewicz coupling procedure of mixing the alkyne and alkyne halide with neutral amine bases, creating the copper acetylide by treatment of terminal alkyne with *n*-BuLi, followed by transmetalation with CuI.[3b] To veryfy the usefulness of this strategy for polyyne rotaxane wynthesis we carried out the preparation of rotaxane **2b⊂M1** following the published procedure. The reaction components were mixed in order **2.2**, CuI and *n*-

BuLi in THF, at –78 °C, the reaction mixture was allowed to warm to 0 °C over 30 min. The mixture of free macrocycle **M1** and bromide **3.1** in a THF then was added at –78 °C and the resulting solution was warmed to room temperature and stirred overnight. The reaction was quenched by addition of aqueous cyanide and the product **2b⊂M1** was isolated in 15% yield (Scheme 3.5).

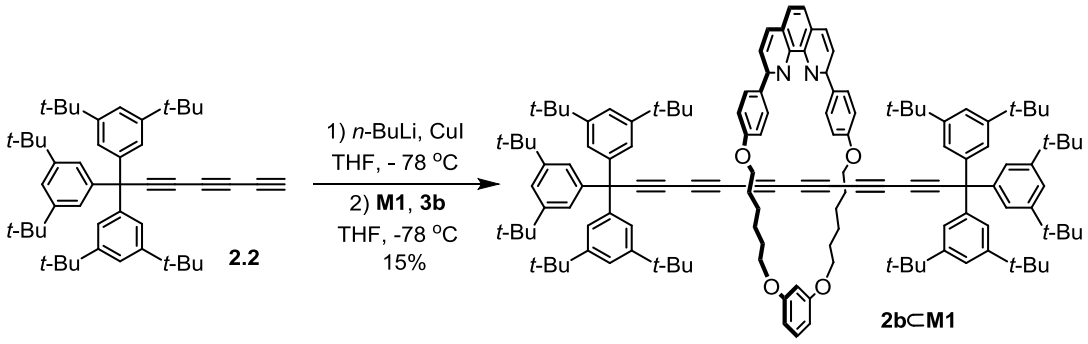

Scheme 3.5 Synthesis of rotaxane **2b⊂M1** by treatment of terminal alkyne **2.2** with *n*-BuLi, followed by transmetalation with CuI.

Alternatively, when the reaction components were mixed in the order **2b**, *n*-BuLi, then transferred to a THF solution of preformed CuI·**M1** complex, followed by the addition of solution of bromide **3.1** at –78 °C, the product was not formed. While the first route worked, it did not give satisfactory results.

Thus, our newly adopted synthetic strategy for the synthesis of polyyne rotaxanes via Cadiot-Chodkiewicz heterocoupling allows the reaction to be carried out under mild conditions, proceeds faster, gives higher product yields and can be applied for the formation of rotaxanes with small macrocycles.

3.3 Selectivity of the cross-coupling reaction and the synthesis of porphyrin-based polyyne rotaxanes.

The selectivity of the cross-coupling reactions for preparing polyyne has been challenging, due to the competing self-coupling reaction of the alkynyl halide. This 'secondary' reaction is thought to proceed via halogen-metal exchange and results in a mixture of products which is sometimes difficult to separate.[1] In some cases, high selectivity for the cross-coupled product can be achieved by careful choice of the amine base and reagent concentrations,[15] or by applying a polymer-supporting technique.[16] In the cross-coupling protocol for the synthesis of rotaxanes, reported by Leigh and co-workers, some combination of coupling partners proved to be highly selective (>98%), but this selectivity was not general.[3b]

The cross-coupling of two different polyynes in the presence of a catalytic Cu(I)-macrocycle could potentially afford three different rotaxanes - two symmetric and one asymmetric - providing that there is little selectivity (Figure 3.1).

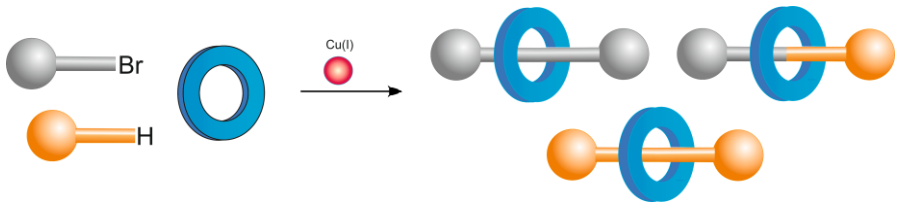

Figure 3.1 Schematic presentation of the three possible rotaxanes from Cadiot-Chodkiewicz coupling.

To test the selectivity of the cross-coupling reaction, the supertrityl diyne **2.1** (1.0 eq.) and triyne bromide **3.1** (1.1 eq.) were mixed with CuI·**M1** (1.0 eq.) in THF and K_2CO_3 (4 eq.) was added. The reaction mixture was stirred overnight at 60 °C. After aqueous cyanide workup, a rotaxane-containing fraction was separated on silica column, dried and the yield calculated (20%). However, the ^{1}H NMR showed that the product contains a mixture of two rotaxanes (Scheme 3.6).

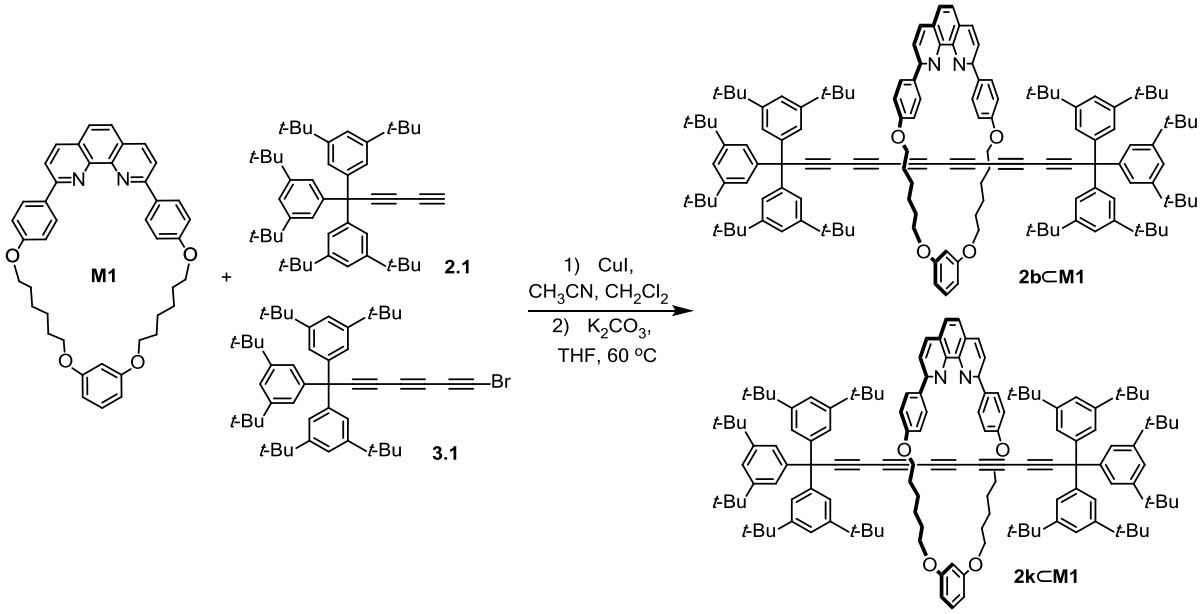

Scheme 3.6 Synthesis of polyyne rotaxanes under cross-coupling conditions results in the mixture of rotaxanes **2b⊂M1** and **2k⊂M1**.

The composition of the product mixture was confirmed by MALDI spectrometry. Interestingly, only two of the three possible rotaxanes were formed. The ratio of hexayne and pentayne rotaxanes (4:1) was estimated from distinguishable protons in the ^{1}H NMR spectrum (Figure 3.2), while the tetrayne rotaxane was missing. We did not pursue the further separation of the rotaxanes as they had similar polarity on silica. This example suggested that under the used reaction conditions there was a significant proton-

halogen exchange (scrambling) between the coupling partners, while the lack of formation of short tetrayne rotaxane was not understood.

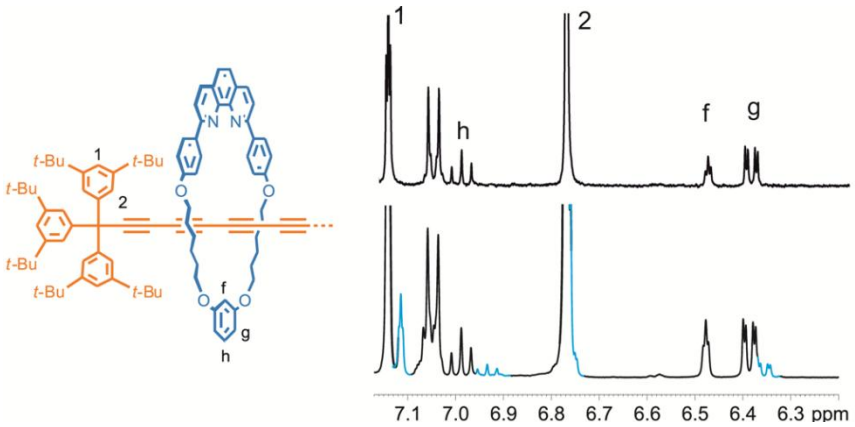

Figure 3.2 The ^{1}H NMR (400 MHz, 298 K, $CDCl_3$) spectra of hexayne rotaxane **2b⊂M1** (top) compared to the product mixture from the cross-coupling reaction (bottom). The blue colored peaks belong to the pentayne rotaxane **2k⊂M1**.

This result suggest that asymmetric rotaxanes still could be synthesized through the Cadiot-Chodkiewicz protocol, but the lack of the selectivity may be severe problem. The next logical step was to explore changing the nature of the coupling partners. A decision was made to test the cross-coupling reaction for porphyrin-polyyne mixed rotaxanes. Porphyrin rotaxanes have been a focus of research for decades.[17] Many of them represent important class of molecular machines,[18] assemblies able to undergo photoinduced electron and energy transfer processes[19] and switchable receptors.[20] From the molecular topology point of view, in rotaxanes, porphyrins can act either as stoppering groups or as a part of the macrocycle. For example, the Anderson group recently reported the synthesis of butadiyne linked [2]rotaxanes where porphyrins served as capping groups.[21] In this work, the TIPS monoprotected, acetylene-terminated porphyrin **3.6** was used under active metal template homocoupling conditions in the presence of the macrocycle **M1** affording the rotaxane product, which in its turn, after the removal of the TIPS group, was used to prepare catenanes. The presence of two acetylenes in *meso* positions of the porphyrin makes it a good candidate for the synthesis of polyyne-porphyrin [2] and [3]rotaxanes under cross-coupling conditions and, if successful, could help test the selectivity of the reaction.

The porphyrin **3.7** was synthesized as described in literature.[22] The porphyrin free-base core was synthesized by the condensation of dipyromethane (generously provided by Dr. Dmitry Kondratuk) with 3,5-di(*t*-butyl)benzaldehyde using Lindsey's conditions to afford the product **3.2** in 49% yield (Scheme 3.7).[23] Free base porphyrin **3.2** was metalated by treatment with $Zn(OAc)_2 \cdot 2H_2O$ which gave the porphyrin

3.3 in 72% yield. The bromination of **3.3** by treatment with NBS resulted in the *meso*- substituted dibromoporphyrin **3.4** in 78% yield. Sonogashira coupling of the dibromoporphyrin **3.4** with TIPS-acetylene afforded TIPS-protected porphyrin **3.5** in quantitative yield (98%).

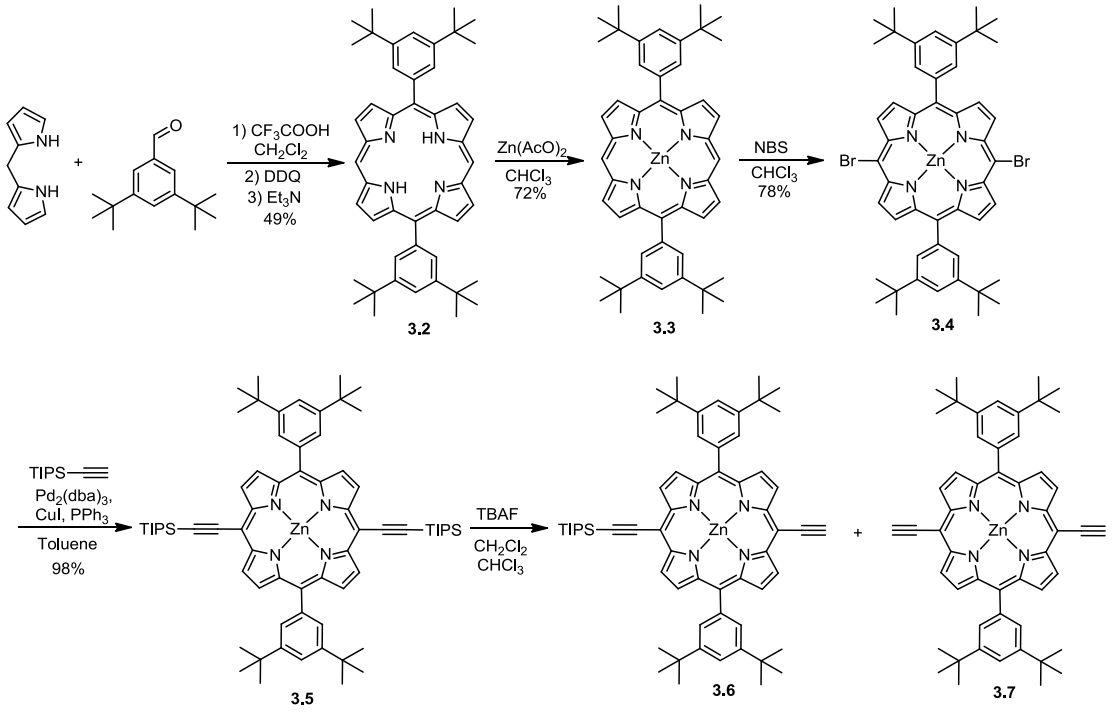

Scheme 3.7 Synthesis of porphyrin **3.6**.

Statistical deprotection of **3.5** with TBAF gave a mixture of the unreacted starting material (46%), half-protected **3.6** (26%) and fully deprotected **3.7** (6%) which are easily separated on silica. For the rotaxane synthesis, the porphyrin **3.6** (1.0 eq.), supertrityl bromotriyne **3.1** (1.5 eq.) and CuI·**M1** complex (1.0 eq.) were dissolved in toluene/THF (2:1) mixture, then K_2CO_3 was added, the reaction mixture was degassed and stirred for 3 days at 60 °C. After aqueous cyanide workup followed by silica column and recrystallization, the product **3a⊂M1** was isolated in 19% yield (Scheme 3.8).

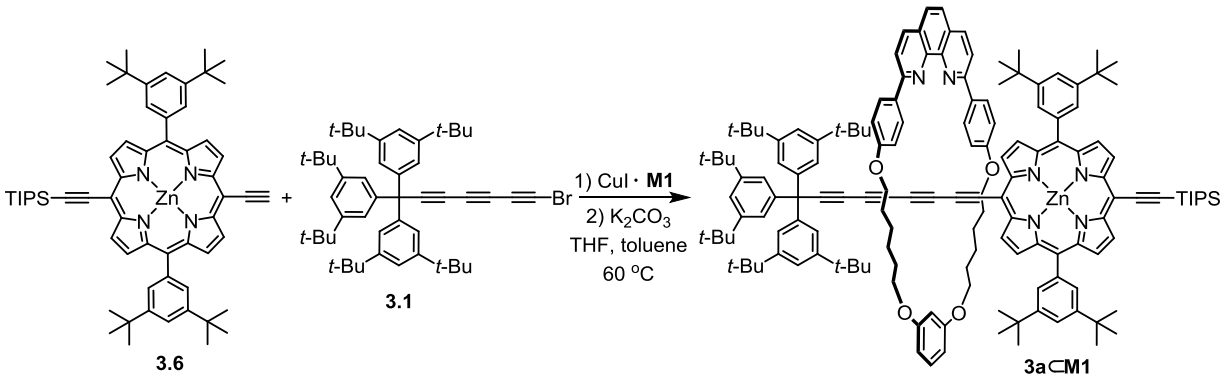

Scheme 3.8 The synthesis of porphyrin [2]rotaxane **3a⊂M1**.

To our surprise, the formation of hexayne or two-porphyrin-capped rotaxanes was not observed, i.e. no homocoupling product was formed. This was confirmed by TLC and NMR analysis and MALDI spectrum of crude reaction mixture before quenching. While yield of the rotaxane is only 20%, the cross-coupling of the polyyne and porphyrin was highly selective. The reason of this high degree of selectivity is not clear: It could be different reactivity of terminal acetylene, compared to the supertrityl diyne, or steric factors could be involved too.

In the rotaxane **3a⊂M1** the second *meso* position of the porphyrin can serve as a coupling partner after the removal of the TIPS group, thus, allowing us to thread the axle a second time. The synthesis of the [3]rotaxane could once again to demonstrate the selectivity of the heterocoupling reaction on this system. In the literature, there are few examples of porphyrinic axles threaded with multiple macrocycles leading to poly[n]rotaxanes,[17d,24] porphyrinic arrays[25] and a spectacular star-shaped [5]rotaxane.[26]

The rotaxane **3a⊂M1** (1.03 eq.) was deprotected using TBAF (97% yield) and added to a solution of supertrityl bromotriyne **3.1** (1.4 eq.) and CuI·**M1** (1.0 eq) complex in toluene/THF (2:1). K_2CO_3 was added, the reaction mixture was deoxygenated and stirred for 2 days at 70 °C. After aqueous cyanide workup, the crude reaction mixture was purified by silica column and size-exclusion chromatography to remove the traces of unreacted rotaxane **3a⊂M1**. The final product **3b⊂2M1** was obtained after the recrystallisation in 23% yield (Scheme 3.9). Once again, the reaction was highly selective, affording the product without formation of hexayne or porphyrin rotaxanes by-products formed from alkynyl halide or porphyrin homocoupling, respectively.

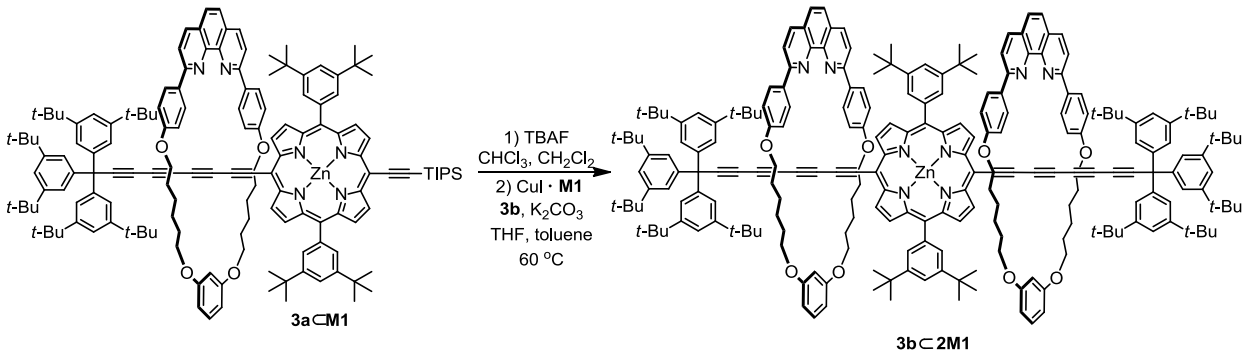

Scheme 3.9 The synthesis of porphyrin [3]rotaxane **3b⊂2M1**.

Porphyrin-polyyne rotaxanes combine the electronic properties of porphyrins and polyynes with the high flexibility and mobility of the mechanically locked phenanthroline macrocycle. This unique combination of molecular motifs and their properties in [3]rotaxane may allow the control of the

photochemical behaviour of the compounds by dictating the shape and mobility of the rotaxanes to perform photoinduced electron or energy transfer. These new dynamic systems could be useful for testing of theories of electron and energy transfer between non-covalently bonded rotaxane components due to possibility to excite them selectively.

3.4 Characterization of 3a⊂M1 and 3b⊂2M1 rotaxanes.

Both the porphyrin-polyyne mixed [2] and [3]rotaxanes were characterized by MALDI spectrometry, NMR and UV-Vis spectroscopy and X-ray crystallography (discussed at the end of this chapter). The UV-Vis absorption spectra of **3a⊂M1** and **3b⊂2M1** present the sum of the absorptions of the rotaxane components, i.e. macrocycle **M1**, porphyrin core and tetrayne chain. For rotaxane **3a⊂M1**, the absorptions of the tetrayne chain, porphyrin moiety and macrocycle are overlapped in the high energy region of the spectrum (250–380 nm), then the porphyrin intense Soret (455 nm) and Q (650 nm) bands follow (Figure 3.3). In rotaxane **3a⊂M1**, both the Soret and the Q bands are red-shifted compared to parent **3.5** porphyrin by 19 and 25 nm, respectively. In rotaxane **3b⊂2M1**, compared to the **3a⊂M1** both Soret and Q bands are red-shifted by 13 and 24 nm, respectively. The red-shift is due to the extended conjugation between the porphyrin and polyyne π-systems. Interestingly, the Soret and the Q bands in **3b⊂2M1** and **3a⊂M1** are more intense than in **3.5**, again as a result of extended electronic delocalization.[27]

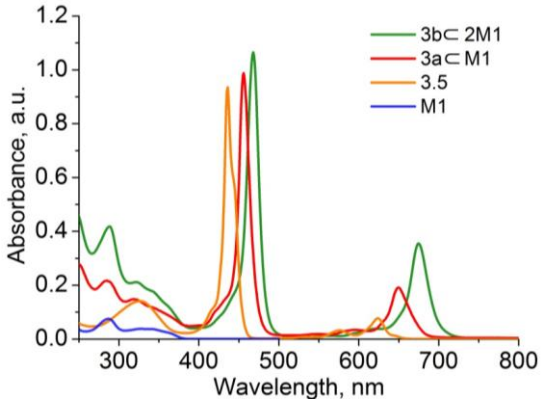

Figure 3.3 UV-Vis absorption spectra of porphyrin **3.5**, macrocycle **M1**, rotaxanes **3b⊂2M1** and **3a⊂M1**, measured in CH_2Cl_2. Concentrations of the solutions were similar.

The ^{1}H NMR spectra of rotaxanes **3b⊂2M1** and **3a⊂M1** show that in the **3a⊂M1** rotaxane the H_j and H_i protons of the macrocycle are unresolved, while in the rotaxane **3b⊂2M1** each geminal H_j/H_j' and H_i/H_i' proton signals is split (diastereotopic). The assignment of the these peaks was confirmed by NOEs observed in the NOESY spectrum. The signal of each diastereotopic pair was not possible to assign,

whereas NOE's observed for each Hi, Hj and between the adjacent protons (Figure 3.4 b) The splitting is a consequence of the asymmetric axle, where two "faces" of the ring experience different chemical environments - one looking to the porphyrin and the other to the supertrityl group (Figure 3.4).

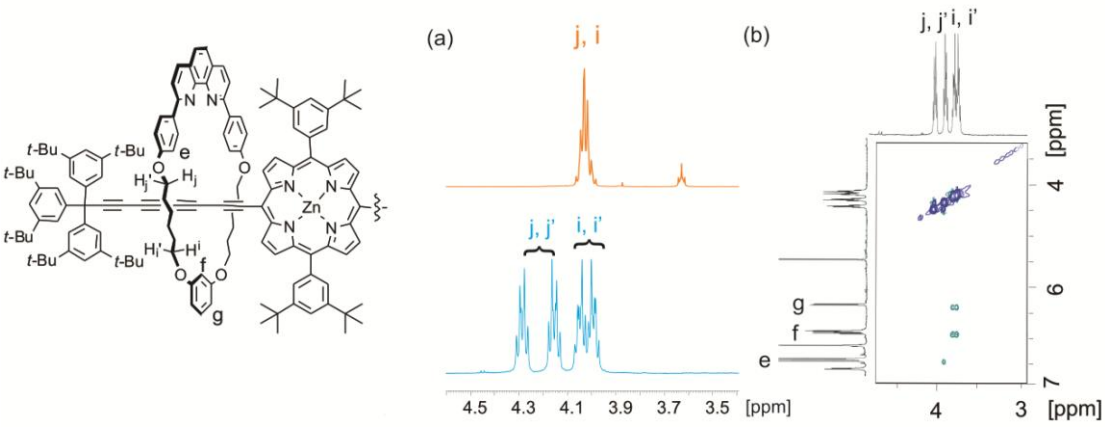

Figure 3.4 (a) A portion of the ^{1}H NMR (500 MHz, CD_2Cl_2, 298K) spectra of **3b⊂2M1** (blue) and **3a⊂M1** (orange) rotaxanes, showing the resonances of H_j and H_i protons. (b) A part of NOESY spectrum of rotaxane **3b⊂2M1** shows NOEs of H_i, H_j and the adjacent protons.

3.5 Synthesis and characterization of a [3]rotaxane with two identical hexayne axles threaded with one macrocycle

Examples of rotaxanes with multiple axles passing through a single ring are rare.[28] The challenge in preparing this type of rotaxanes is to satisfy the relative structural demands on the cyclic ring and thread(s). The ring may require more than one template site to assemble multiple threads (using traditional template methods), and the cavity of the macrocycle must be large enough to accommodate two axles, yet still small enough to prevent dethreading. Additionally, the macrocycle-thread interactions that direct the assembly of the rotaxane, must overcome sometimes severe steric hindrance between crowded thread units. So far, single-ring threaded [3]rotaxanes have been synthesized utilizing hydrophobic interactions in aqueous solution,[28a] octahedral metal centres as templates[28b,c] hydrogen-bond formation between a thread and axles[28d] and an active-metal templated homocoupling reaction.[28e] The axles can be identical[28b,c,d,e] or have different structures[28a] and can be assembled using the same or different type of reactions for each step of the threading. Another interesting example of active-metal templated [3]rotaxane synthesis was reported by the Leigh group, using a bicyclic macrocycle.[29] In this case, the substituted pyridine, which is part of the macrocycle, coordinates the metal and catalyzes the threading of one side of the bicyclic macrocycle. Next, the pyridine turns to the other side of the macrocycle and catalyzes another covalent bond formation capturing the second axle into the interlocked architecture. This system was exploited to

make a [3]rotaxane with identical and different axles, and it was shown that molecular architecture could be assembled in a stepwise manner by using the same or different reactions (Figure 3.5).

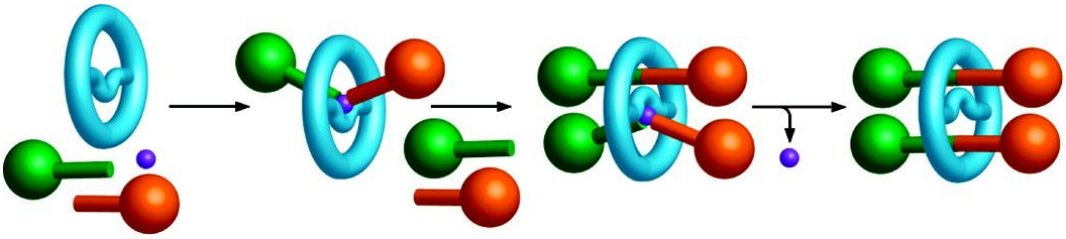

Scheme 3.5 Active template synthesis of macrobicyclic [3]rotaxanes. The metal (purple) coordinates to the binding site. The metal can then promote formation of a covalent bond through each cavity of the macrocycle in turn, generating a doubly threaded [3]rotaxane. If the second thread forms significantly more slowly than the first (negative allostery), then the reaction can effectively be stopped at the intermediate [2]rotaxane stage and a different set of building blocks or even a different metal employed in a different active template reaction to form the second thread of the macrobicyclic [3]rotaxane. If the threads being formed are not symmetrical through the mirror plane formed by the macrocycle, two different diastereoisomers (syn and anti arrangements of the threads) can be formed even though the threads themselves may be constitutionally identical.[29]

The idea of extending these approaches to polyyne-based polyrotaxanes was unprecedented, but highly desirable, owing to the growing interest in the construction of new carbon rich materials.[30] Simple CPK modelling showed that, for example, the **M1** macrocycle cavity is large enough to accommodate two polyyne chains, but the gap between them is narrow, which could create favourable conditions for cross-linking reactions,[31] while the **M5** macrocycle is too small to accommodate two polyyne chains. The supertrityl groups are another 'obstacle': their bulky nature creates huge steric strain when two polyynes are captured inside the macrocycle. As a result, the polyyne chains must be significantly bent or must have a cross-like alignment (Figure 3.6).

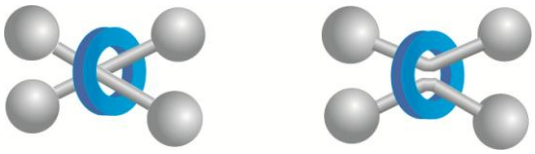

Figure 3.6 Possible alignment of two polyyne axles within the macrocycle cavity.

Despite the modelling indicating that the threading of two polyyne axles may be strongly unfavourable, we decided to test the synthesis of this interesting molecule. For this task, we decided to use rotaxane **2b⊂M1** as a template to prepare the stoichiometric CuI complex, which would later react with supertrityl triyne **2.2** to construct the [3]rotaxane (**2b)$_2$⊂M1** under alkyne homocoupling reaction conditions (Scheme 3.10). To the solution of the CuI·**2b⊂M1** complex in THF, triyne **2.2** (2.5 eq.), I_2 (1 eq.) and K_2CO_3 (4 eq.) were added and the reaction mixture was stirred at 60 °C for 2 days.

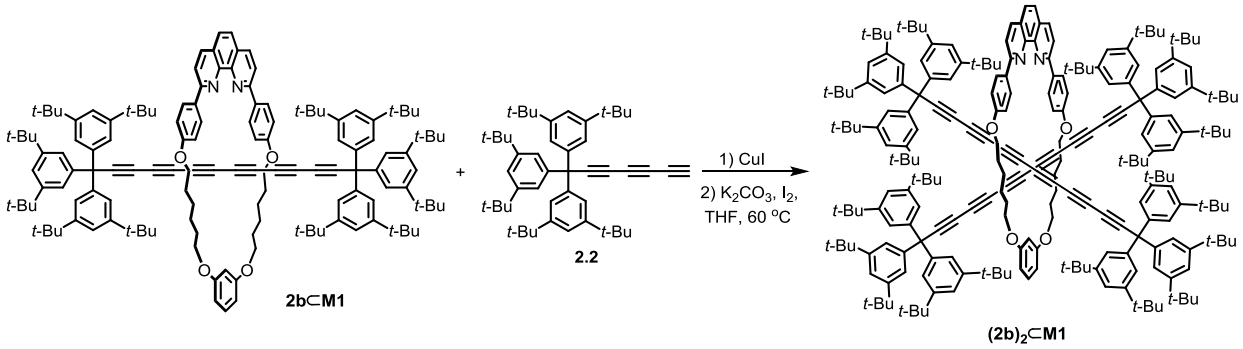

Scheme 3.10 Attempted synthesis of hexayne [3]rotaxane **$(2b)_2$⊂M1** via alkyne homocoupling.

After complete consumption of **2.2**, confirmed by TLC, the MALDI spectrum of the crude reaction mixture showed an intense peak corresponding to the starting rotaxane **2b⊂M1** coordinated to a K^+ ion (*m/z* $(C_{140}H_{168}N_2O_4K)^+$ = 1981.94). To our delight, the spectrum contained two tiny bumps corresponding to the [3]rotaxane **$(2b)_2$⊂M1** (*m/z* $(C_{238}H_{394}N_2O_4)$ = 3244.8) and its Cu(I) complex (*m/z* $(C_{238}H_{394}N_2O_4Cu)^+$ = 3308.7) (Figure 3.7).

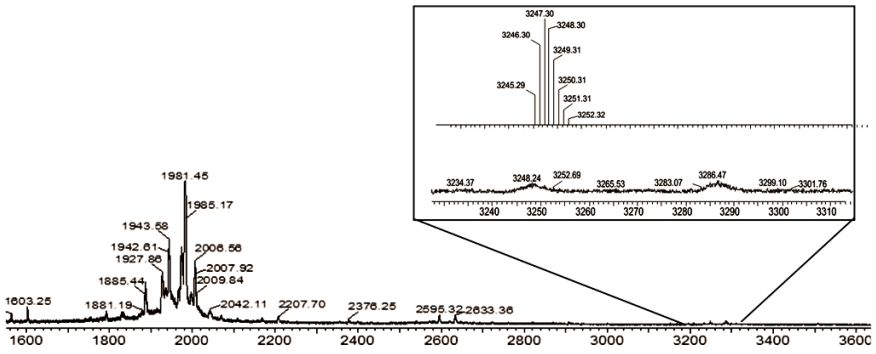

Figure 3.7 The MALDI TOF spectrum of the crude reaction mixture from the attempted synthesis of **$(2b)_2$⊂M1** rotaxane via homocoupling of triyne **2.2**. The magnified part of the spectrum shows the traces of the [3]rotaxanes and its Cu^+ complex that match with the calculated mass of the molecule.

Thus, it became clear that threading the hexayne axle within the single macrocycle is possible: The question was how to increase the product yield. The Cadiot-Chodkiewicz cross-coupling in our previous experiments always resulted in higher yields of rotaxanes and we chose this route to improve the yield of [3]rotaxane.

In the cross-coupling reaction the CuI·**2b⊂M1** complex (1.0 eq.) mixed with **2.2** (1.2 eq.) and **3.1** (1.6 eq.) in THF. The oxygen-free reaction mixture stirred for 36 hours at 60 °C (Scheme 3.11). After aqueous cyanide workup followed by silica column and size-exclusion chromatography, the [3]rotaxane **$(2b)_2$⊂M1** was obtained in 6% yield.

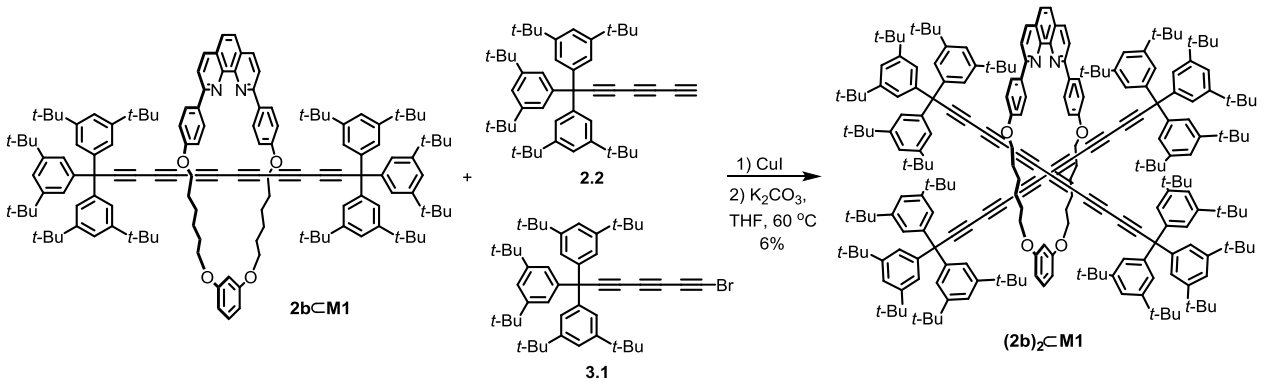

Scheme 3.11 The synthesis of hexayne [3]rotaxane **$(2b)_2$⊂M1** via alkyne heterocoupling.

The product yield was low compared to the reported yields of other two-axle threaded [3]rotaxanes, however, in reported cases, to achieve moderate or good yields for the [3]rotaxanes, 5- or 10-fold excess of the second axle components were used.[28e,29] The isolated rotaxane **$(2b)_2$⊂M1** was stable at 4 °C, while at room temperature the solid decomposed slowly over weeks.

The **$(2b)_2$⊂M1** rotaxane was characterized by mass spectrometry (Figure 3.8), NMR and UV-Vis absorption spectroscopy.

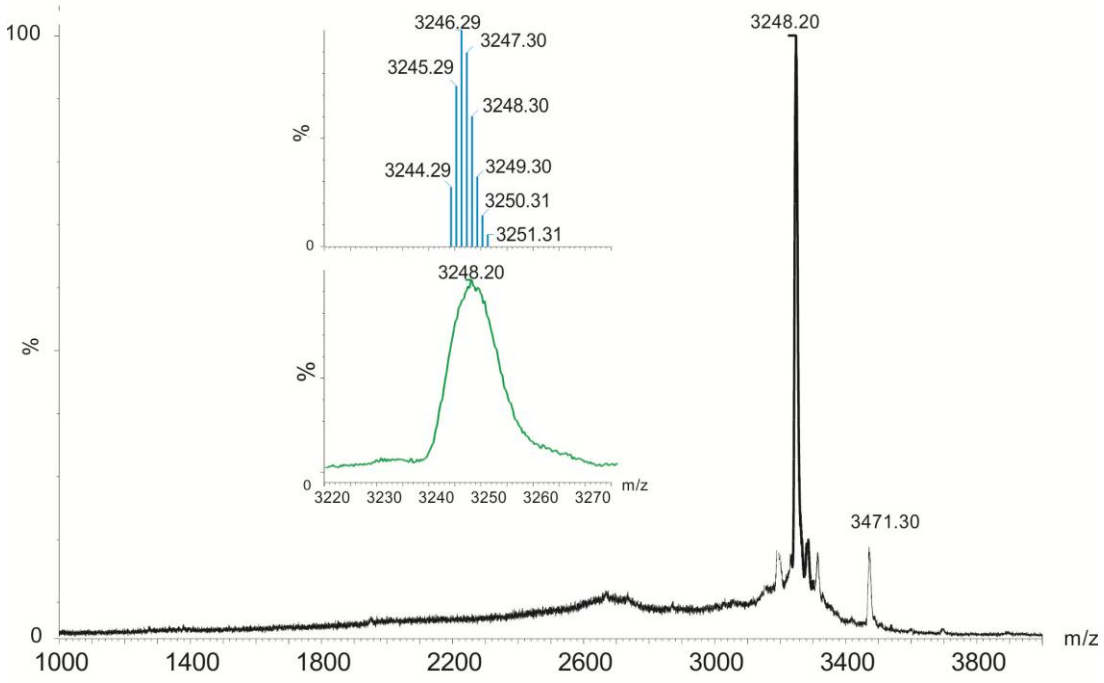

Figure 3.8 The MALDI TOF spectrum of the **$(2b)_2$⊂M1** rotaxane. The inset shows the match between the calculated (m/z $[M+H^+]^+$ = 3247.28) and experimentally found molecular weight (m/z $[C_{238}H_{295}O_4N_2]^+$ = 3248.20). The small peak at m/z = 3471.3 corresponds to the mass of complex of the rotaxane with 1 molecule of dithranol.

The polyyne absorption extinction coefficient is double that of the parent **2b⊂M1** [2]rotaxane, as was expected. When the spectra of the [2] and [3]rotaxanes were normalized according the polyyne lowest energy absorption band (at 317 nm, arising from the lowest (υ = 0) to the higher energy vibrational state (υ = 1, 2, etc) transition) interesting features were noticed (Figure 3.3). The second vibronic band at ~297 nm was red-shifted by 1 nm and increased in intensity. This increase in intensity can be explained by larger deformations along the nuclear coordinate of symmetry resulting in a higher probability of transitions to the higher energy vibronic states.[32] This phenomenon was described previously for long polyynes,[13] where it was explained by the increased flexibility in the molecules, and studied thoroughly by Raman spectroscopy.[33] Considering the supercrowded nature of the [3]rotaxane, the deformation of the polyyne chains from linearity is highly expected.

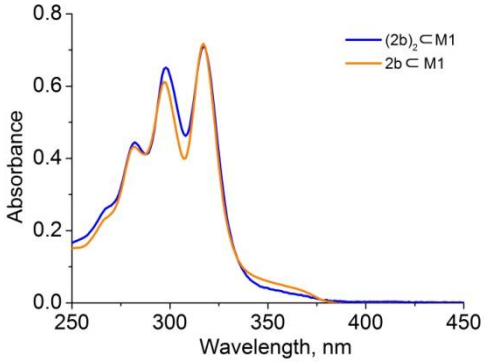

Figure 3.9 The comparison of absorption spectra of **2b⊂M1** and **(2b)$_2$⊂M1** rotaxanes (recorded in CH_2Cl_2) normalized according the lowest energy vibronic transition band at 317 nm.

Thus, the UV-Vis spectrum indicates the enhanced polyyne chain deformation in [3]rotaxane compared to parent [2]rotaxane, however, the exact conformation of the hexayne chains in solution is not clear and both bent and cross-like structures are possible (Figure 3.6). To investigate the alignment of the carbon chains in the [3]rotaxane, NMR spectroscopy was employed, and the compound was studied by ^{1}H, ^{13}C, variable-temperature (VT), HSQC and ROESY NMR techniques.

The comparison of ^{1}H NMR signals of parent **2b⊂M1** [2]- and **(2b)$_2$⊂M1** [3]rotaxanes revealed that the macrocycle proton resonances differ between these two strctures (Figure 3.10). The H_d, H_b, H_e, H_h, H_g, H_j and H_i protons are upfield shifted, while the H_c proton is downfield shifted. Resonances of the dumbbell protons, H_1 and H_2, are unaffected.

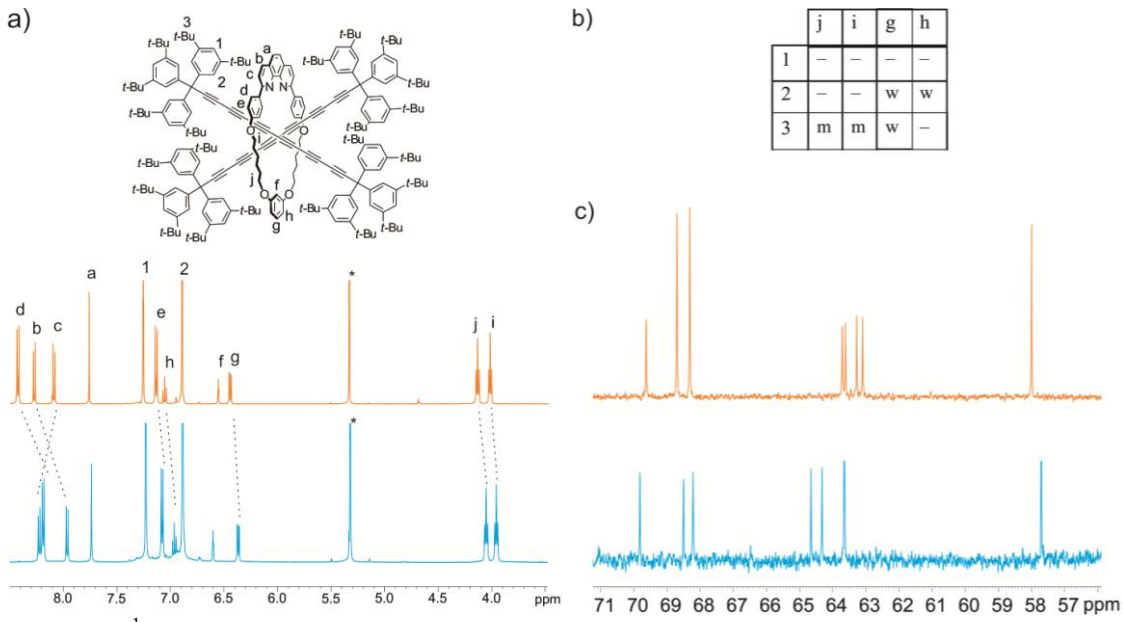

Figure 3.10 (a) ^{1}H NMR spectra of **2b⊂M1** (orange) and **(2b)$_2$⊂M1** (blue) rotaxanes (500 MHz, CD_2Cl_2, 298 K). Asterisk denotes the solvent peak. (b) NOE correlations between the dumbbell and macrocycle from the ROESY spectrum of **(2b)$_2$⊂M1** (500 MHz, CD_2Cl_2, 298 K, 200 μs mixing time, m = medium, w = weak). (c) ^{13}C NMR spectra of **2b⊂M1** (orange) and **(2bg)$_2$⊂M1** (blue) rotaxanes (125 MHz, CD_2Cl_2, 298 K), showing the region containing resonances of the polyyne *sp* carbons.

The ^{13}C NMR spectrum of the **(2b)$_2$⊂M1** rotaxane shows four resonances (two peaks are overlapped) around 64 ppm, where resonances of *sp* carbon atoms from the middle of the polyyne chain are located (Figure 3.10, c). Compared to the **2b⊂M1** rotaxane, these resonances are slightly shifted downfield. The ^{13}C NMR indicates that the two polyyne chains in the **(2b)$_2$⊂M1** [3]rotaxane are undistinguishable, at least by the NMR spectroscopy at room temperature, and experience an identical influence from the macrocycle. Furthermore, the observed NOEs show a weak interaction between protons of dumbbell end groups and the macrocycle (Figure 3.10, b).

The VT ^{1}H NMR spectra of the [3]rotaxane could reveal more structural information. In particular, the restricted (hindered) rotation of the macrocycle around the axle at low temperatures would lead to the different rotamers, distinguishable in NMR time scale. In this case, protons of axle (H2, H3), which interact through space with the macrocycle protons, would be expected to split, as their would experience different magnetic environments in each rotamer. So, when the rotation is slow (no interconvention between rotamers within the NMR timescale), the NMR shift separation (split) of the signals is given by Eq. 5.1:

$$k = \frac{1}{\tau} \ll \pi \frac{\Delta \upsilon}{\sqrt{2}} \quad (5.1)$$

where k is rotamers interconversion rate constant (s^{-1}), τ is interconversion time (s) and $\Delta\nu$ is the NMR shift separation of the signals (Hz) at low temperatures. This equation indicates that different positions of the same nucleus can have distinct signals when the chemical shift different ($\Delta\nu$) corresponds to a time spent by the nuclei in different positions longer than the interconversion time τ ($k << \tau$). Alternatively, when $k >> \tau$, the signals collapse to a single one.

A series of ^{1}H NMR spectra in CD_2Cl_2 were recorded at different temperatures (Figure 3.11). At temperatures as low as 193 K, line-broadening of the macrocycle protons and dumbbell protons were observed, but there was not splitting of the peaks, indicating that the macrocycle rotation rate is still fast on the NMR timescale at this temperature. Thus, it appears that despite the steric crowding of the rotaxane the macrocycle mobility is not severely impeded.

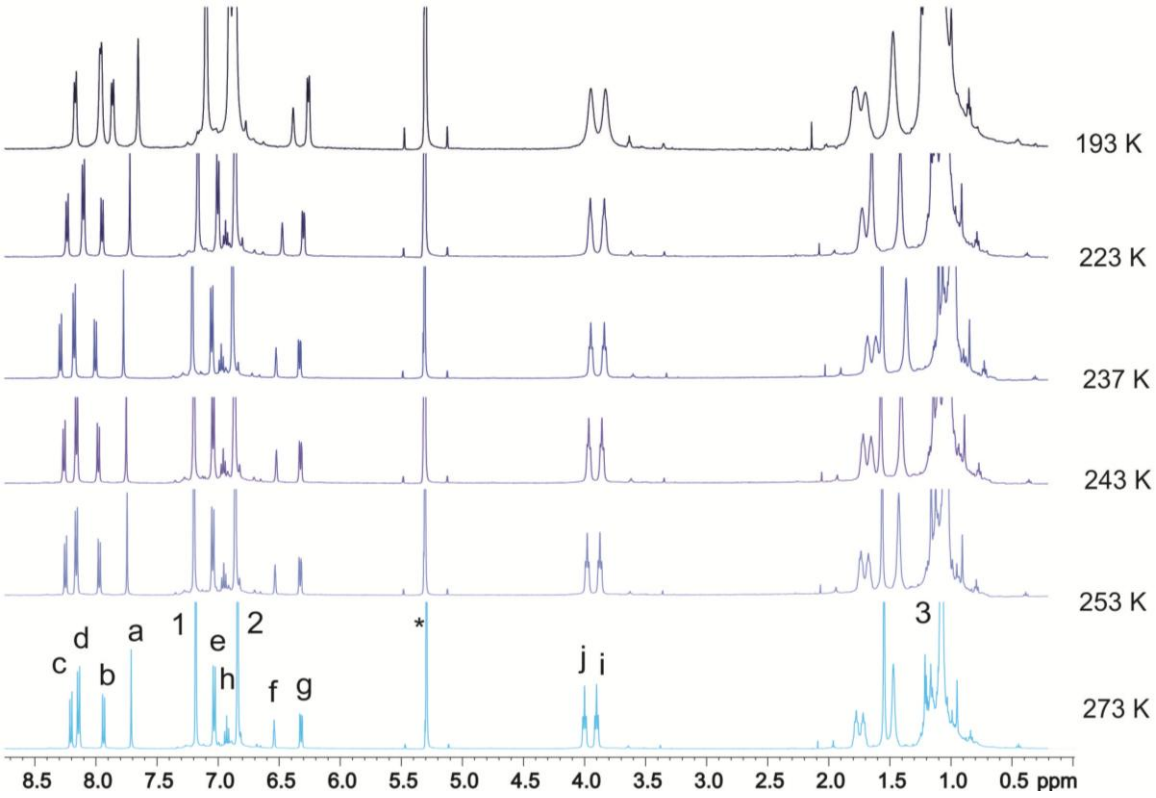

Figure 3.11 VT ^{1}H NMR spectra of **(2b)$_2$⊂M1** [3]rotaxane (500 MHz, CD_2Cl_2). The assignments correspond to the labelling shown in figure 3.7. The asterisk denotes the solvent peak.

The final structure was ultimately demonstrated only after the determination of the X-ray crystal structure of the compound, discussed in the next part of this chapter.

3.6 X-ray structure of 3a⊂M1, 3b⊂2M1 and $(2b)_2$⊂M1 rotaxanes.

Diffraction data were collected at 100 K using synchrotron radiation at the Diamond Light Source, beam line I19, the structures were solved and refined by Dr. Amber L. Thompson (Chemistry Research Laboratory, University of Oxford).

3a⊂M1: Dark green crystals of **3a⊂M1** were grown by vapour diffusion of CH_3OH into a solution of the compound in CH_2Cl_2 at room temperature. The crystals are assigned to the P $2_1/c$ space group, and the asymmetric unit contains one molecule of **3a⊂M1** and one CH_3OH coordinated to the Zn centre of the porphyrin (Figure 3.12). The distance (*r*) between the Zn and O atom of the CH_3OH is 2.119 Å. The Cambridge Structural Database (CSD) revealed numerous Zn porphyrin structures with five-coordinated methanol with similar *r* (Zn-O) distances. Due to the coordination, the Zn atom is slightly out of the porphyrin plane (0.308 Å). The 3,5-di(*t*-butyl)phenyl (Ar') substituents of the porphyrin moiety are almost perpendicular to the porphyrin plane (about 68°). The torsion angle (ϕ) between two Ar' plains is 47.5°. The tetrayne chain is slightly bent in an arc-shaped fashion. The average C≡C and C–C bond lengths are 1.215 ± 0.014 Å and 1.358 ± 0.024 Å, respectively, and the average ∠C–C≡C angle is 176.3 ± 1.3°. The Tr* and TIPS groups are in staggered conformation with respect to each other. The TIPS-acetylene chain is deviated from linearity and the ∠Si–C≡C angle is 173.4°.

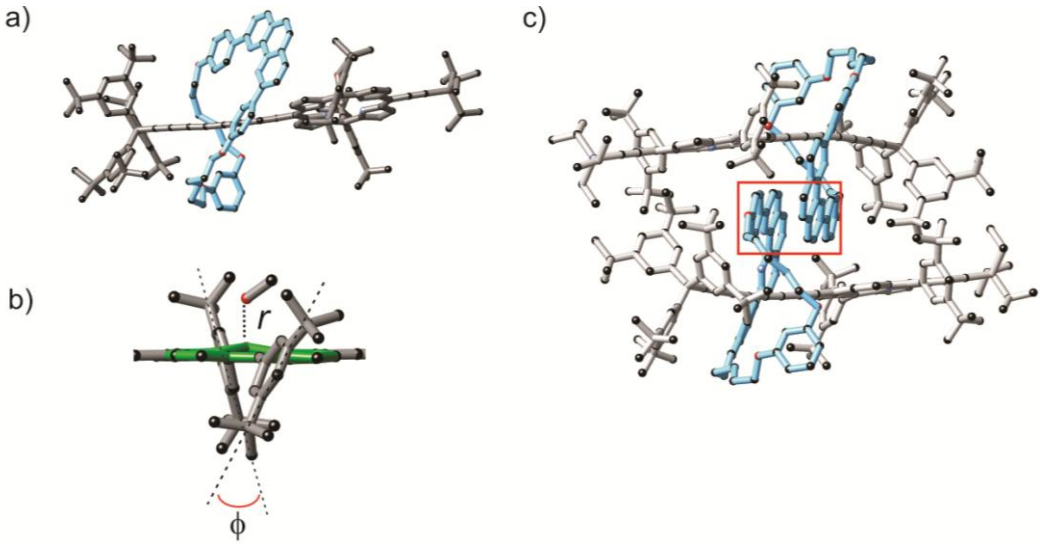

Figure 3.12 (a) X-ray crystal structure of rotaxane **3a⊂M1** viewed down the crystallographic *c*-axis. (b) The part of the crystal structure with green-coloured porphyrin moiety. (c) The pairs of the **3a⊂M1** molecules with highlighted π-π stacking of adjacent phenanthrolines. Hydrogen atoms are omitted for clarity.

The macrocycle is bent into a U-shape in such way that the phenanthroline and resorcinol moieties look towards the porphyrin plane. In the crystal the molecules of **3a⊂M1** form pairs through π-π interactions

between vicinal phenanthroline moieties (Figure 3.12c) The distance between phenanthroline planes is 3.52(3) Å. In the **3a⊂M1** molecular pairs, two dumbbells are aligned opposite each other in a way that the TIPS group of one dumbbell is in close contact with the Tr* group of the second dumbbell.

3b⊂2M1: Dark green crystals of **3b⊂2M1** was grown by diffusion of CH_3OH into a solution of the compound in CH_2Cl_2 at room temperature. The crystals are assigned to the P -1 space group, asymmetric unit contains one molecule of **3b⊂2M1** and one CH_3OH coordinated to the Zn centre of the porphyrin (Figure 3.13). The distance (*r*) between the Zn and O atom of the CH_3OH is 2.123 Å, and the Zn atom is slightly out of the porphyrin plane (0.397 Å), similar to the **3a⊂M1**. The tetrayne chains are slightly bent in a arc-shaped fashion, similar to the **3a⊂M1**. The average C≡C and C–C bond lengths are identical (within error) for both tetrayne chains and are 1.221 ± 0.030 Å (triple bond) and 1.367 ± 0.027 Å (single bond). The 3,5-di(*t*-butyl)phenyl (Ar') substituents of the porphyrin moiety are almost perpendicular to the porphyrin plane (~62°). The torsion angle (ϕ) between two Ar' planes is 50.7°. Two Tr* end-groups are in staggered position in respect to each other.

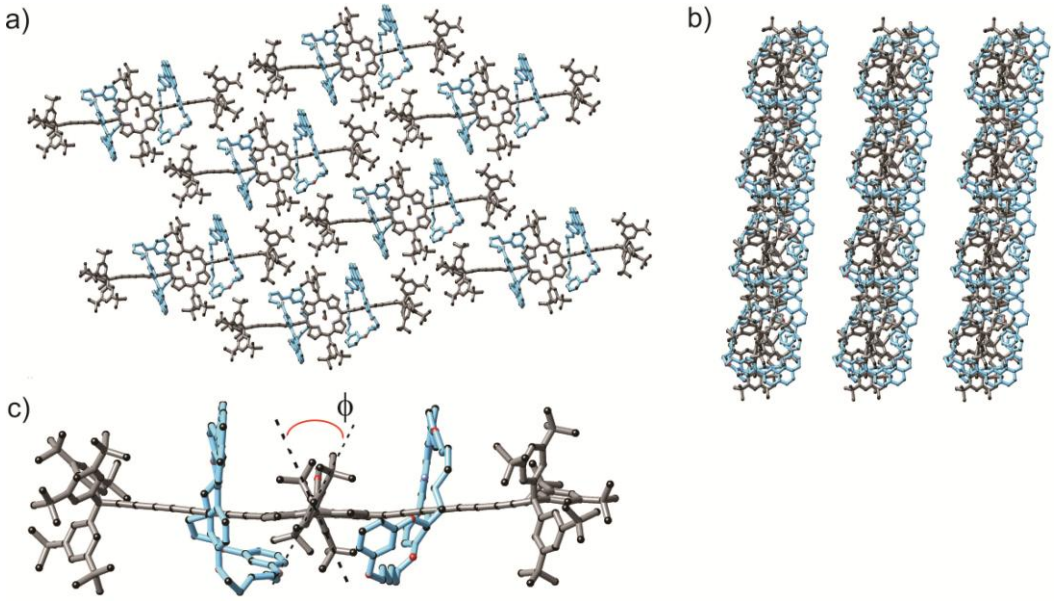

Figure 3.13 The crystal packing diagram of the rotaxane **3b⊂2M1** viewed down to (a) crystallographic *a* axis and (b) side view. (c) The crystal structure the **3b⊂2M1** molecule. Hydrogen atoms are omitted for clarity.

The two macrocycles are bent into a U-shape and enclose the porphyrin plane from the top and the bottom. In the crystal, **3b⊂2M1** molecules do not form pairs, while are equally separated from each other (Figure 3.13, a) within the same layer. Molecular layers are also separated from each other forming a multilayer 3D structure (Figure 3.13 b). It seems, two opposite Tr* groups and the bulky Ar' groups shield

the molecule in such way, that the formation of molecular pairs through π-π interactions between vicinal phenanthrolines becomes unfavourable.

(2b)$_2$⊂M1: The crystals of **(2b)$_2$⊂M1**were grown by slow diffusion of CH_3OH into a solution of the compound in THF at room temperature. The asymmetric unit contains one molecule of **(2b)$_2$⊂M1**, and the crystal belongs to the P -1 space group. Two hexayne chains are aligned in cross-like fashion. Every chain is slightly arch-bent and two hexaynes form a helix inside the cavity of the macrocycle (Figure 3.14). The two hexayne chains have same curvature within error: For one axle the average ∠C–C≡C angle is 176.2 ± 2.4° and for the second one the average ∠C–C≡C angle is 175.6 ± 2.9°. In one dumbbell the average C≡C and C–C bond length values are 1.221 ± 0.022 Å and 1.390 ± 0.015 Å, respectively. In the second dumbbell the average C≡C and C–C bond length values are 1.197 ± 0.013 Å and 1.410 ± 0.043 Å, respectively. For polyyne [2]rotaxanes and extended free polyynes (see chapter two) the C≡C triple bonds get shorter near the end groups and longer in the middle of the chain, whereas the single C–C bonds are longest near the end groups and shortest in the middle of the chain. For **(2b)$_2$⊂M1**rotaxane this trend is not observed. The macrocycle sits in the middle of two hexayne chains and supertrityl groups of each chain are in close contact with each other. The closest distance between the two hexayne chains 3.345 Å, which is less than the sum of van der Waals radii of two *sp* carbon atoms (3.4 Å).[34] Despite the close proximity of the polyyne chains, one might have expected rapid cross-linking, but this is not observed and the compound is stable, which might reflect the crossed alignment which prevents significant orbital overlap. In the crystal the **(2b)$_2$⊂M1**molecules form a pair but no vicinal phenanthroline interactions were noticed (Figure 3.14, c, d).

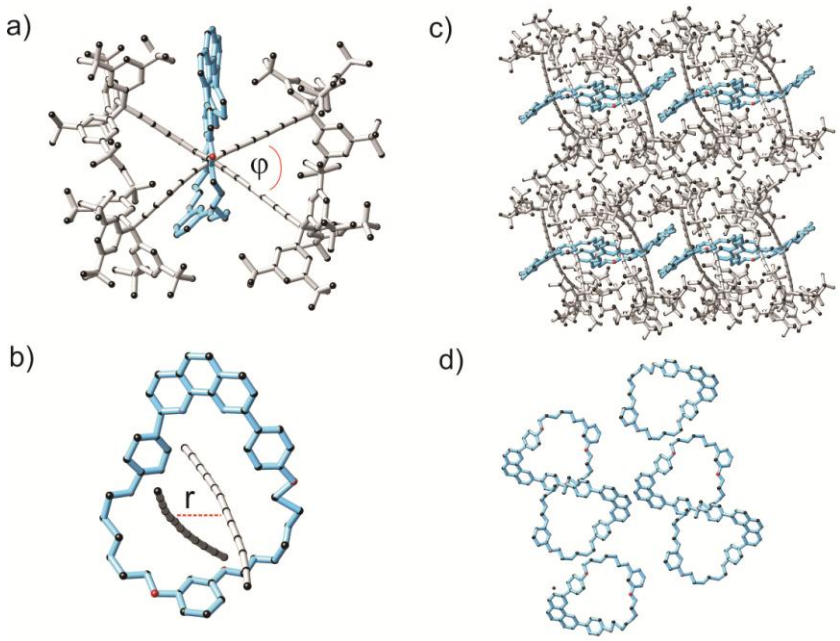

Figure 3.14 (a) The X-ray structure of the **(2b)$_2$⊂M1**molecule. (b) Helix-type conformation of two hexayne chains inside the macrocycle cavity. (c) The crystal packing viewed down to the crystallographic *a* axis. (d) The crystal packing viewed down to the crystallographic *c* axis. The polyyne chains are omitted in this case for clear presentation of the macrocycles orientation. Hydrogen atoms are omitted for clarity.

3.7 Conclusion

We have demonstrated that Cadiot-Chodkiewicz cross-coupling of polyynes is a suitable strategy for the preparation of polyyne rotaxanes. While the cross-coupling is not always selective for alkyne and haloalkyne partners, it is possible to achieve high selectivity for alkyne halide and porphyrin combination, which successively made available the synthesis of polyyne-porphyrin mixed [2] and [3]rotaxanes. This adopted strategy could be exploited later to make porphyrin-polyyne based molecular shuttles or chiral rotaxanes. Threading of two identical hexayne chains through the cavity of a macrocycle was achieved through the heterocoupling reaction. The isolated [3]rotaxane is one of the few examples of double-axle threaded [3]rotaxanes and is a potentially significant addition to the class of carbon-rich supramolecular structures.

3.8 Experimental Part: General Experimental Procedures

2,2'-Dipyrromethane was prepared by Dr. Dmitry Kondratuk, and all other reagents and solvents were used as commercially supplied, without further purification. Dry THF was obtained by passing through alumina under N_2 pressure. When required, solutions were deoxygenated by freeze-pump-thaw degassing three cycles followed by backfilling with N_2. Column chromatography was carried out using silica 60A (particle size 35–70 μm, Fisher, UK) as the stationary phase. Size-exclusion chromatography was carried

out using polystyrene beads (Bio-Beads-S-X3, operating range up to 2000 Da and Bio-Beads-S-X1, operating range 10 kDa). Where mixtures of solvents were used, ratios are reported by volume. TLC was performed on precoated silica gel plates (0.25 mm thick, 60 F254, Merck, Germany) and visualized under UV light (254 nm). NMR spectra were recorded on Bruker instruments, DPX 400 or AVII 500 with cryobrobe. Chemical shifts are reported in parts per million (ppm) and referenced to the residual solvents resonances.[35] Coupling constants (*J*) are reported in hertz (Hz, to an accuracy of ±0.1 Hz). Standard abbreviations indicating multiplicity were used as follows: *s* = singlet, *d* = doublet, *dd* = double doublets, *t* = triplet, *q* = quartet, *m* = multiplet. Melting points (m.p.) were determined by placing the sample between a pair of microscope glasses on an electrically heated metal block. MALDI-TOF mass spectrometry was carried out in positive reflectron mode using a Micromass MALDI micro MX spectrometer with dithranol (1,8-dihydroxyanthrone) as a matrix. UV-vis spectra were recorded at ambient temperature on a Perkin-Elmer Lambda 20 or Parkin-Elmer Lambda 25 spectrometers with 1 nm resolution; λ in nm (ε in $L \cdot mol^{-1} \cdot cm^{-1}$). Diffraction data were collected and the structure solved and refined by Dr. Amber L. Thompson (Chemistry Research Laboratory, University of Oxford). The data were collected at 100 K using synchrotron X-ray radiation at the Diamond Light Source, Beamline I19. The structure was solved using SuperFlip[36] and refined using full-matrix least-squares within the CRYSTALS software suite.[37]

3.9 Synthesis of known and novel compounds.

*The synthesis of supertrityl triyne **2.2**, macrocycles **M1** and **M4** is described in Chapter 2.*

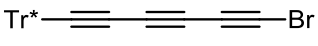

3.1

1-Bromo-triyne 3.1:[13] To a mixture of **2.2** (300 mg, 0.46 mmol) in acetone (30 mL) was added *N*-bromosuccinimide (98.2 mg, 0.55 mmol) and $AgNO_3$ (15.6 mg, 0.092 mmol). The reaction was stirred at 20 ºC for 10 h and monitored by TLC (hexanes). The reaction mixture was quenched by adding water (10 mL) and then extracted with a CH_2Cl_2 (3 × 50 mL). The organic layers were combined, washed with brine (20 mL), and dried over $MgSO_4$. The solvent was removed *in vacuo* and the crude product purified by passing through a plug of silica (CH_2Cl_2/hexanes 1:5) to yield **3.1** (330 mg, 95%) as a slightly yellow solid. R_f = 0.4 (hexanes). ^{1}NMR (400 MHz, $CDCl_3$) 7.26 (t, *J* = 2 Hz, 3H), 6.91 (d, *J* = 2 Hz, 6H), 1.19 (s, 54H). ^{13}C NMR (100 MHz, $CDCl_3$) 150.1, 143.6, 123.7, 120.3, 84.5, 68.5, 66.4, 62.4, 60.0, 57.1, 40.0, 34.8, 31.4. As in lit.[13]

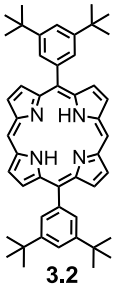

3.2

Free Base 5,15-bis-(3,5-bis-*tert*-butyl-phenyl)-porphyrin 3.2: [23] 3,5-Bis(*tert*-butyl)benzaldehyde[3] (0.90 g, 4.1 mmol) and dipyrromethane (0.6 g, 4.1 mmol) were placed in a dry flask under N_2 and dissolved in CH_2Cl_2 (800 mL). The solution was degassed three times by repeated evacuation and purging with nitrogen. Trifluoroacetic acid (0.20 mL, 2.5 mmol) was added and the reaction mixture stirred in the dark for 3 h. DDQ (1.21 g, 5.33 mmol) was added and stirring continued for 0.5 h. After quenching of the acid by addition of triethylamine (4.0 mL) the mixture was passed through a short silica cplug (CH_2Cl_2). Recrystallization from CH_2Cl_2/MeOH gave **3.2** as a red powder (0.69 g, 49%). ^{1}H NMR (400 MHz, $CDCl_3$) -3.10 (br. s, 2H, N*H*), 1.58 (s, 36H), 7.85 (t, 2H, *J* = 2.0 Hz), 8.16 (d, 4H, *J* = 2.0 Hz), 9.15 (d, 4H, *J* = 4.5 Hz), 9.42 (d, 4H, *J* = 4.5 Hz), 10.33 (s, 2H). As in lit.[22]

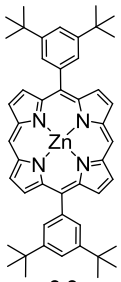

3.3

Zinc 5,15-bis-(3,5-bis-*tert*-butyl-phenyl)-porphyrin 3.3:[22] $Zn(OAc)_2 \cdot 2H_2O$ (1.43 g, 6.6 mmol) was dissolved in methanol (13 mL) and added to a solution of free-base porphyrin **3.2** (0.86 g, 1.25 mmol) in $CHCl_3$ (130 mL). The reaction was stirred at room temperature for 1 h. The mixture was passed through a short silica plug (CH_2Cl_2). The crude product was recrystallized by layer addition (CH_2Cl_2/MeOH) to give **3.3** as a purple powder (0.68 g, 72%). ^{1}H NMR (400 MHz, $CDCl_3$) 1.59 (s, 36H), 7.86 (t, 2H, *J* = 2.0 Hz,), 8.17 (d, 4H, *J* = 2.0 Hz), 9.23 (d, 4H, *J* = 4.5 Hz), 9.45 (d, 4H, *J* = 4.5 Hz), 10.36 (s, 2H). As in lit.[22]

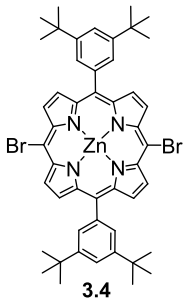

3.4

Zinc 5,15-bis-(3,5-bis-*tert*-butyl-phenyl)-10,20-dibromo-porphyrin 3.4:[22] To a solution of zinc porphyrin **3.3** (0.10 g, 0.13 mmol) in $CHCl_3$ (10 mL) and pyridine (0.1 mL) was added dropwise solution of *N*-bromosuccinimide (0.05 g, 0.26 mmol) in $CHCl_3$ (10 mL). After stirring in the dark for 1 h, the reaction was quenched with acetone (0.5 mL). The solvent was removed and the crude product recrystallized by layer addition from CH_2Cl_2/MeOH to give a purple solid **3.4** (94 mg, 78%). ^{1}H NMR (400 MHz, $CDCl_3$): δ 1.50 (s, 36H), 7.80 (t, J = 2.0 Hz), 7.99 (d, J = 2.0 Hz, 4H), 8.91 (d, J = 4.5 Hz, 4H), 9.66 (d, J = 4.5 Hz). As lit.[22]

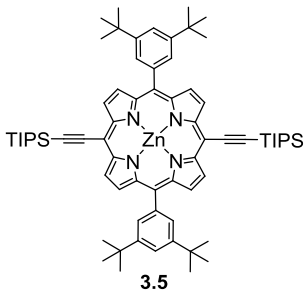

3.5

Zinc 5,15-bis-(3,5-bis-*tert*-butyl-phenyl)-10,20-bis-triisopropylsilanylethynyl-porphyrin 3.5:[22] *tris*-(Dibenzylideneacetone)-di-palladium(0) (52.5 mg, 57.5 µmol), CuI (22 mg, 0.115 mmol), triphenylphosphine (30.2 mg, 0.115 mmol) and dibromoporphyrin 3.4 (0.524 g, 5.77 mmol) were placed in a dried Schlenk tube under argon. Toluene (50 mL), *i*-Pr_2NH (20 mL) and pyridine (1.1 mL) were added and the reaction mixture deoxygenated. Triisopropyl acetylene (0.39 mL, 8.65 mmol) was added by syringe. The reaction mixture was stirred at 80 °C for 2 h., solvents removed and the residue passed through a short silica plug (CH_2Cl_2). Recrystallization by layer addition (CH_2Cl_2/MeOH) gave the 3.5 product as a green solid (0.75 g, 98 %). ^{1}H NMR (400 MHz, $CDCl_3$) 0.90 (t, 18H, J = 7.0 Hz), 1.02 (m, 12H), 1.39 (m, 24H, -CH_2), 1.58–1.51 (m, 48H), 1.77 (m, 12H), 7.83 (t, 2H, J = 1.5 Hz,), 8.06 (d, 4H, J = 1.5 Hz), 8.98 (d, 4H, J = 4.5 Hz), 9.74 (d, 4H, J = 4.5 Hz). As lit.[22]

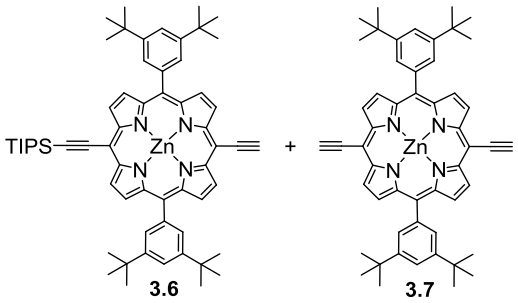

Zinc 5,15-bis-(3,5-bis-*tert*-butyl-phenyl)-10-ethynyl-20-trihexylsilanylethynyl-porphyrin 3.6 and Zinc 5,15-bis-(3,5-bis-*tert*-butyl-phenyl)-10,20-bis-ethynyl-porphyrin 3.7:[22] Protected porphyrin 3.5 (0.40 g, 0.36 mmol) was dissolved in CH_2Cl_2 (70 mL) and $CHCl_3$ (70 mL). Tetra-*n*-butylammonium fluoride (0.54 mL, 1 M in THF, 1.54 mmol) was added to the stirred solution. The progress of the reaction was monitored by TLC until an optimal product mixture was reached and the reaction then quenched with CH_3COOH (0.4 mL, 0.7 mmol). The volume was reduced and the mixture passed through a short silica plug (CH_2Cl_2). Column chromatography (50:1:1, 40-60 petroleum ether : EtOAc : py) gave 3.6 (94 mg, 26 %) and 3.7 (6 mg, 6 %) as green solids. (Recovered starting material = 190 mg, 46%). 3.6 ^{1}H NMR (400 MHz, $CDCl_3$) 0.91 (t, 9H, *J* = 7.0 Hz), 1.01–1.05 (m, 6H), 1.37–1.44 (m, 12H), 1.52–1.57 (m, 42H), 1.76–1.81 (m, 6H), 4.15 (s, 1H), 7.81 (t, 2H, *J* = 2.0 Hz), 8.03 (d, 4H, *J* = 2.0 Hz,), 8.92 (m, 4H), 9.68 (m, 4H,). As in lit.[22]

3.7 ^{1}H NMR (400 MHz, $CDCl_3$) 1.55 (s, 36H), 4.15 (s, 2H), 7.79 (t, 2H, *J* = 1.5 Hz), 8.01 (d, 4H, *J* = 1.5 Hz), 8.91 (d, 4H, *J* = 4.5 Hz), 9.67 (d, 4H, *J* = 4.5 Hz). As in lit.[22]

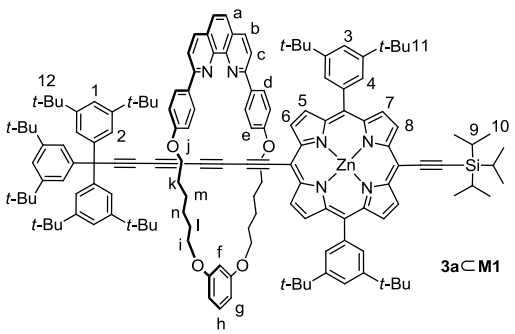

3a⊂M1: To a solution of macrocycle **M1** (14.7 mg, 23.0 µmol) in CH_2Cl_2 (1.5 mL) a solution of CuI (4.4 mg, 23 µmol) in MeCN (1.5 mL) was added and the mixture was stirred for 1 h at 20 °C. The solvent was removed *in vacuo* and the residue redissolved in a 1:1 mixture of THF and toluene (2 mL). This solution was then added to a mixture of porphyrin **3.6** (22 mg, 23 µmol), bromotriyne **3.1** (25 mg, 35 µmol), and K_2CO_3 (13 mg, 92 µmol) in toluene (2 mL). The mixture was degassed through pump-freeze-thaw cycles, flushed with nitrogen, and stirred at 60 °C for 3 d. After cooling to 20 ºC, the reaction was quenched by the addition of KCN (20 mg, 0.3 mmol, in 1 mL H_2O), deluted with CH_2Cl_2 (1 mL), MeCN (1 mL), and and stirred at 20 ºC for 2 h.

CH_2Cl_2 (10 mL) was added, the organic phase separated, washed with H_2O (10 mL), brine (10 mL), and the solvents were removed. Column chromatography (silica, hexane/EtOAc/pyridine 100:1:1 → 10:1:1) followed by recrystallization from CH_2Cl_2/MeOH afforded the product **3a⊂M1** as a green solid (10 mg, 19.4%). ^{1}H NMR (500 MHz, CD_2Cl_2) δ 9.63 (d, *J* = 4.5 Hz, 2H, H_6), 9.35 (d, *J* = 4.6 Hz, 2H, H_8), 8.79 (d, *J* = 4.5 Hz, 2H, H_5), 8.60 (d, *J* = 4.6 Hz, 2H, H_7), 8.53 (d, *J* = 8.8 Hz, 4H, H_d), 8.09 (d, *J* = 8.4 Hz, 2H, H_b), 7.98 (d, *J* = 8.4 Hz, 2H, H_c), 7.91 (d, *J* = 1.8 Hz, 4H, H_4), 7.80 (t, *J* = 1.8 Hz, 2H, H_3), 7.53 (s, 2H, H_a), 7.29 (t, *J* = 1.7 Hz, 3H, H_1), 7.25 (d, *J* = 8.7 Hz, 4H, H_e), 6.99 (d, *J* = 1.7 Hz, 6H, H_2), 6.95 (t, *J* = 8.2 Hz, 1H, H_h), 6.91 (t, *J* = 2.3 Hz, 1H, H_f), 6.38 (dd, *J* = 8.2 Hz, 2.3 Hz, 2H, H_g), 4.14–4.02 (m, 8H, $H_{j,i}$), 1.87–1.52 (m, 16H, $H_{k,l,m,n}$), 1.49 (s, 36H, H_{11}), 1.43–1.39 (m, 21H, $H_{9,10}$), 1.17 (s, 54H, H_{12}). ^{13}C NMR (125 MHz, CD_2Cl_2) δ_C 161.03, 160.96, 156.0, 153.9, 152.1, 151.2, 150.6, 150.4, 149.0, 146.2, 143.9, 141.6, 136.6, 133.8, 133.0, 132.1, 131.2, 130.6, 129.9, 129.8, 129.2, 127.5, 125.5, 124.9, 123.9, 121.4, 120.9, 119.0, 115.3, 110.2, 107.6, 102.8, 100.6, 98.7, 96.2, 87.8, 82.5, 81.7, 71.1, 70.0, 68.3, 68.2, 66.9, 64.0, 63.7, 57.8, 35.2, 35.1, 31.8, 31.4, 29.9, 29.4, 26.20, 26.19, 19.2, 12.2. *m/z* (MALDI TOF MS+) ($C_{152}H_{176}N_6O_4SiZn$); [M+H$^+$] requires 2244.3 found 2244.32. UV-vis (THF) λ_{max} / nm (ε / M^{-1} cm^{-1}) 285 (94000), 320 (57000), 456 (542000), 607 (14000), 661 (129000). UV-vis (CH_2Cl_2) λ_{max} / nm (ε / M^{-1} cm^{-1}) 285 (95500), 319 (64500), 456 (435000), 661 (84100). M.p. 130–131 °C.

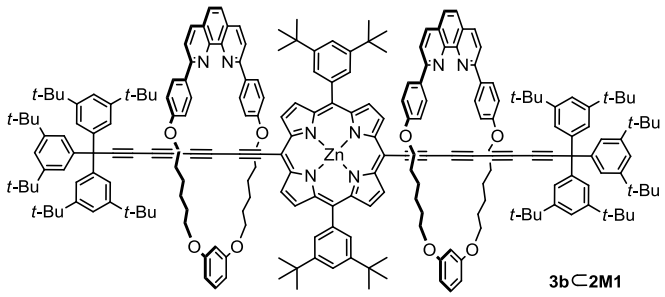

3b⊂2M1. TIPS-protected porphyrin rotaxane **3a⊂M1** (41 mg, 18.3 μmol) was dissolved in the mixture of CH_2Cl_2 (20 mL) and $CHCl_3$ (5 mL) and TBAF (36.6 mL, 26.6 1.0 M solution in THF) was added at 20 ºC. The reaction stirred 3 h. at 40 °C. The reaction progress was monitored by TLC (Py/EtOAc/$PE_{40/60}$ 1:1:10). After complete consumption of starting materials the reaction mixture was passed through a short silica plug (CH_2Cl_2 + 5% Py) and solvents were removed *in vacuo* resulting *d*-**3a⊂M1** deprotected rotaxane (37 mg, 17.8 μmol). To a solution of macrocycle **M1** (11.3 mg, 17.8 μmol) in CH_2Cl_2 (1.5 mL) a solution of CuI (3.4 mg, 17.8 μmol) in MeCN (1.5 mL) was added and the mixture was stirred for 1 h at 20 °C. The solvent was removed *in vacuo* and the residue re-dissolved in a 1:1 mixture of THF and toluene (9 mL). This solution

was then added to a mixture of *d*-**3a⊂M1** deprotected rotaxanes, bromotriyne **3.1** (18 mg, 24.8 μmol), and K_2CO_3 (9.8 mg, 71 μmol). The reaction mixture was degassed through pump-freeze-thaw cycles, flushed with nitrogen, and stirred at 70 °C for 2 d. After cooling to 20 ºC, the reaction was quenched by the addition of ETDA (20.8 mg, 0.71 mmol, in 1 mL H_2O), deluted with CH_2Cl_2 (2 mL), MeCN (1 mL) and stirred at 20 ºC for 2 h. Additional CH_2Cl_2 (10 mL) was added, the organic phase separated, washed with H_2O (10 mL), brine (10 mL), and solvents were removed. Column chromatography (silica, hexane/EtOAc/pyridine 100:1:1 → 5:1:1) followed by SEC column (Bio-Beads-S-X, $CHCl_3$ + 1% Py, to remove traces of unreacted rotaxane) and recrystallization from CH_2Cl_2/MeOH afforded the product **3b⊂2M1** as a green solid (11 mg, 23%). ^{1}H NMR (500 MHz, CD_2Cl_2) 9.15 (d, *J* = 6.1 Hz, 4H), 8.40 (d, *J* = 8.7 Hz, 8H), 8.37 (d, *J* = 4.6 Hz, 4H), 7.79–7.77 (m, 6H), 7.63 (d, *J* = 8.4 Hz, 4H), 7.45 (d, *J* = 8.4 Hz, 4H), 7.30 (t, *J* = 1.7 Hz, 6H), 7.26 (d, *J* = 8.8 Hz, 8H), 7.0 (d, *J* = 1.7 Hz, 8H), 6.77–6.71 (m, 8H), 6.20 (dd, J_1 = 8.12 Hz, J_2 = 2.3 Hz, 4H), 4.28 (m, 4H), 4.16 (m, 4H), 4.07–3.97 (m, 8H), 1.90 (m, 8H), 1.83–1.60 (m, 32H), 1.51 (s, 36H), 1.43–1.39 (m, 12H), 1.19 (s, 108H). ^{13}C NMR (125 MHz, CD_2Cl_2) δ 160.9, 160.9, 155.2, 153.0, 150.8, 150.7, 150.4, 149.2, 145.2, 143.9, 141.0, 135.8, 133.3, 132.0, 130.9, 129.8, 129.7, 129.2, 128.3, 126.5, 124.8, 124.5, 124.0, 121.6, 121.0, 120.9, 118.2, 115.3, 107.5, 100.6, 98.4, 88.2, 82.8, 81.5, 71.7, 69.9, 68.4, 68.3, 67.5, 63.7, 63.6, 59.9, 57.9, 35.3, 35.1, 31.9, 31.5, 29.9, 29.4, 26.3, 26.3, 25.4. *m/z* (MALDI TOF MS+) ($C_{234}H_{260}N_8O_8Zn$); [M+] requires 3378.96 found 3378.48. UV-vis (THF) λ_{max} / nm (ε / M^{-1} cm^{-1}) 288 (129000), 320 (57000), 466 (452000), 651 (155000), 661 (129000). UV-vis (CH_2Cl_2) λ_{max} / nm (ε / M^{-1} cm^{-1}) 288 (126000), 467 (361000), 689 (115000). M.p. 150–152 °C.

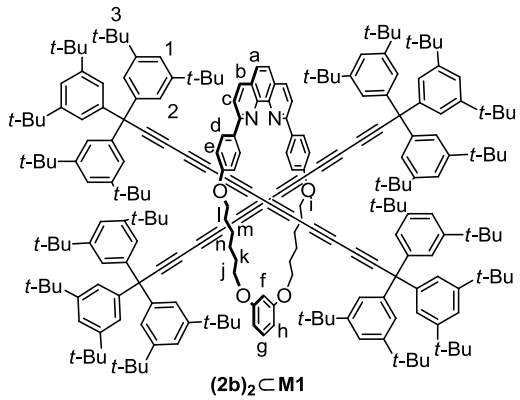

To a solution of rotaxane **2b⊂M1** (60 mg, 30.49 mmol) in CH_2Cl_2 (4.0 mL) a solution of CuI (5.9 mg, 30.49 mmol) in CH_3CN (1.0 mL) was added and the mixture stirred at 20 °C for 1.5 h. The mixture was then dried under vacuum and re-dissolved in dry THF (5.0 mL) (macrocycle-Cu complex solution). A fresh sample of **3.1** (35.6 mg, 48.8 mmol) was added to the solution with **2b** (23.8 mg, 36.6 mmol) with potassium carbonate (19.9 mg, 0.14 mmol). The reaction mixture was degassed through three time freeze-pump-thaw

and flushed with nitrogen gas and stirred in dark at 60 °C for 36 h. The progress of reaction was monitored by TLC ($PE_{40/60}$/EtOAc 6 : 1). The reaction was stirred for 36 h, cooled to 20 ºC, then CH_3CN (1.0 mL), CH_2Cl_2 (2.0 mL) and KCN (10.0 mg, 0.15 mmol in 1.0 mL water) were added and the mixture stirred at 20 ºC for additional 5 h. The mixture was diluted with CH_2Cl_2 (4.0 mL), the organic fraction separated and washed with water (3×5.0 mL) after which solvents were removed. The residue was purified by column chromatography (silica, PE $_{40/60}$/EtOAc = 30 : 1) and further purified using size-exclusion column (on Biobeads-S-X1) in CH_2Cl_2 to afford a product as a yellow solid (5 mg, 5 %). ^{1}H NMR (500 MHz, CD_2Cl_2, 298 K) 8.23 (d, J = 4.4, 2H, H_c), 8.19 (d, J = 4.1, 4H, $H4_d$), 7.95 (d, J = 4.0, 2H, H_b), 7.74 (s, 2H, H_a), 7.23 (t, J = 3.6, 12H, H_1), 7.07 (d, J = 4.1, 4H, $H_{e,}$), 6.98 (t, J = 3.5, 1H, $H_{h,}$), 6.88 (d, J = 3.4, 24 H, H_2), 6.59 (t, J = 3.3, 1H, H_f), 6.36 (dd, J_1 = 6.2 Hz, J_2 = 3.2, 2H, H_g), 4.04 (t, J = 4.0, 4H, H_i), 3.99 (t, J = 3.9, 4H, H_j), 1.82–1.76 (m, 8H, $H_{k,l}$), 1.61 (m, 8H, $H_{m,n}$) 1.12 (s, 108 H, H_3). ^{13}C NMR (125 MHz, CD_2Cl_2, 298 K) 161, 160.6, 157.6, 150.5, 146.9, 143.8, 136.5, 133.0, 129.6, 129.5, 127.7, 125.7, 123.9, 120.9, 120.2, 115.4, 108, 101.2, 86.1, 69.8, 68.5, 68.2, 64.7, 64.3, 63.6, 63.6, 57.7, 35.5, 31.4, 30.4, 30.0, 26.4, 26.4; *m/z* (MALDI TOF MS+) cal. for $C_{238}H_{394}N_2O_4$ $[M]^+$ 3244.8, found 3244.3. Uv-vis(THF) λ_{max} / nm (ε / M^{-1} cm^{-1}) 317 (391000), 298 (366000), 285 (317000), 267 (192000). UV-vis (CH_2Cl_2) λ_{max} / nm (ε / M^{-1} cm^{-1}) 317 (417000), 298 (38300), 282 (262000), 267 (154000).

3.10 References

1.(a) Chodkiewicz, W.; Cadiot, P. *C.R. Hebd. Seances Acad. Sci*. **1955**, *241*, 1055–1057. (b) Cadiot, P.; Chodkiewicz, W. In *Chemistry of Acetylenes*; Viehe, H. G., Ed; Dekker: New York, **1969**, Chapter 9.

2. (a) Negishi, E.; Okukado, N.; Lovich, S. F.; Luo, F. T. *J. Org. Chem.* **1984**, *49*, 2629–2632. (b) Metay, E.; Hu, Q; Negishi, E.-I. *Org. Lett*. **2006**, *8*, 5773–5776. (c) Negishi, E.-I.; Anastasia, L. *Chem. Rev*. **2003**, 1*03*, 1979–2017.

3. For mechanistic studies: (a) Zhang, G.; Yi, H.; Zhang, G.; Dang, Y.; Bai, R.; Zhang, H.; Miller, J. T.; Kropf, A. J.; Bunel, E. E.; Lei, A. *J. Am. Chem. Soc.* **2014**,*136*, 924–926. (b) Berná, J.; Goldup, S. M.; Lee, A.-L.; Leigh, D. A.; Symes, M. D.; Teobaldi, G.; Zerbeto, F. *Angew Chem. Int. Ed.* **2008**, *47*, 4392–4396. (c) Siemsen, P.; Livingston, R. C.; Diederich, F. *Angew. Chem. Int. Ed*. **2000**, *39*, 2632–2657.

4. (a) Cohen, M. J.; McNelis, E. *J. Org. Chem.* **1984**, *49*, 515–518. (b) Rao, M. L. N.; Periasamy, M. *Synth. Commun.* **1995**, *25*, 2295–2299. (c) Kabalka, G. W.; Mereddy, A. R.; *Tetrahedron Lett.* **2004**, *45*, 1417–1419.

5. (a) Nishikawa, T.; Shibaya, S.; Hosokowa, S.; Isobe, M. *Synlett* **1994**, 485–486. (b) Brunel, Y.; Rousseau, G. *Tetrahedron Lett*. **1995**, *36*, 2619–2622. (c) Nasker, D.; Roy, S. *J. Org. Chem*. **1999**, *64*, 6896–6897. (d) Yan, J.; Li, J.; Cheng, D. *Synlett*. **2007**, *15*, 2442–2444.

6. Wagner, A.; Heitz, M. P.; Mioskowkski, C. *Tetrahedron Lett.* **1990**, *31*, 3141–3144.

7. (a) Nishikawa, T.; Shibuya, S.; Hosokawa, S.; Isobe, M. *Synlett* **1994**, 485–486. (b) Hofmeister, H.; Annen, K.; Laurent, H.; Wiechert, R. *Angew. Chem. Int. Ed.* **1984**, *23*, 727–729.

8. Marino, J. P.; Nguyen H. N. *J. Org. Chem*. **2002**, *67*, 6841–6844.

9. Utesch, N. F.; Diederich, F. *Org. Biomol. Chem*. **2003**, *1*, 237–239.

10. (a) Anelli, P. L.; Spencer, N.; Stoddart, J. F. *J. Am. Chem. Soc*. **1991**, *113*, 5131–5133. b) Bissell, R. A.; Cordova, E.; Kaifer, A. E.; Stoddart, J. F. *Nature* **1994**, *369*, 133–136. (c) Hernández, J. V.; Kay, E. R. Leigh, D. A. *Science*, **2004**, *306*, 1532–1537. (d) Steuerman, D. W.; Tseng, H. R.; Peters, A. J.; Flood, A. H.; Jeppesen, J. O.;

Nielsen, K. A.; Stoddart J. F.; Heath, J. R. *Angew. Chem., Int. Ed.* **2004**, *43*, 6486–6491. (e) Tian, H.; Wang, Q.-C. *Chem. Soc. Rev.* **2006**, *35*, 361–374. (f) Berna, J.; Alajarin, M.; Orenes, R.-A. *J. Am. Chem. Soc.* **2010**, *132*, 10741–10747.

11. (a) Reuter, C.; Schmieder, R.; Vögtle, F. *Pure Appl. Chem.* **2000**, *7*2, 2233–2241. (b) Kameta, N.; Nagawa, Y.; Karikomi, M.; Hiratani, K. *Chem. Commun*. **2006**, 3714–3716. (c) Bordolli, R.; Goldup, S. M. *J. Am. Chem. Soc.* **2014**, *136*, 4817–4820.

12. S. M. Goldup, D. A. Leigh, T. Long, P. R. McGonigal, M. D. Symes, J. Wu, *J. Am. Chem. Soc.* **2009**, *131*, 15924–15927.

13. Chalifoux, W. A. *'Towards Carbyne: Synthesis and Study of Extremely Long Polyynes*' PhD thesis, University of Alberta, Alberta, **2009**.

14. Alami, M.; Ferri, F. *Tetrahedron Lett.* **1996**, *37*, 2763–2766.

15. Brandsma, L. *Preparative acetylene chemistry*, Elsevier, Amsterdam, **1988**, chap. 10, 219–227.

16. Montierth, J. M.; DeMario, D. R.; Kurth, M. J.; Schore, N. E. *Tetrahedron* **1998**, *54*, 11741–11748.

17. For the porphyrin rotaxane recent reviews see: (a) Durola, F.; Heitz, V.; Reviriego, F.; Roche, C.; Sauvage, J.-P.; Sour, A.; Trolez, Y. *Acc. Chem. Res.* **2014**, *47*, 633–645. (b) Coumans, R. G. E.; Elemans, J. A. A. W.; Rowan, A. E.; Nolte, R. J. M. *Chem. Eur. J.* **2013**, *19*, 7758–7770. (c) Beletskaya, I.; Tyurin, V. S.; Tsivadze, A. Y.; Guilard, R.; Stern, C. *Chem. Rev*. **2009**, *109*, 1659–1713. (d) Faiz, J. A.; Heitz, V.; Sauvage, J.-P. *Chem. Soc. Rev*. **2009**, *38*, 422–442.

18. a) Harada, A. *Acc. Chem. Res*. **2001**, *34*, 456 –464. b) Dietrich-Buchecker, C.; Jimenez-Molero, M. C.; Sartor, V.; Sauvage, J. P.; *Pure Appl. Chem.* **2003**, *75*, 1383–1393. c) Kinbara, K.; Aida, T.; *Chem. Rev.* **2005**, *105*, 1377–1400; d) Kay, E. R.; Leigh, D. A.; Zerbetto, F. *Angew. Chem. Int. Ed.* **2007**, *46*, 72–191. e) Coskun, A.; Banaszak, M.; Astumian, R. D.; Stoddart, J. F.; Grzybowski, B. A. *Chem. Soc. Rev.* **2012**, *41*, 19–30.

19. (a) Schuster, D. I.; Li, K.; Guldi, D. M. *C. R. Chim.* **2006**, *9*, 892–908. (b) Flamigni, L. *J. Photochem. Photobiol. C* **2007**, *8*, 191–210. (c) Aratani, N.; Kim, D.; Osuka, A. *Acc. Chem. Res.* **2009**, 4*2*, 1922–1934. (d) Ventura, B.; Flamigni, L.; Beyler, M.; Heitz, V.; Sauvage, J. P. *Chem. Eur. J*. **2010**, *16*, 8748–8756.

20. a) Frey, J.; Tock, C.; Collin, J. P.; Heitz, V.; Sauvage, J.-P. *J. Am. Chem.Soc.* **2008**, *130*, 4592 –4593. (b) Collin, J. P.; Frey, J.; Heitz, V.; Sauvage, J.-P.; Tock, C.; Allouche, L. *J. Am. Chem. Soc.* **2009**, *131*, 5609–5620. (c) Collin, J. P.; Durola, F.; Frey, J.; Heitz, V.; Reviriego, F.; Sauvage, J.-P.; Trolez, Y.; Rissanen, K. *J. Am. Chem. Soc*. **2010**, *132*, 6840–6850. (d) Collin, J. P.; Durola, F.; Heitz, V.; Reviriego, F.; Sauvage, J.-P.; Trolez, Y. *Angew. Chem. Int. Ed.* **2010**, *49*, 10172–10175. (e) Roche, C.; Sour, A.; Sauvage, J.-P. *Chem. Eur. J*. **2012**, *18*, 8366–8376.

21. Langton, M. J.; Matichak, J. D.; Thompson, A. L.; Anderson, H. L. *Chem. Sci*. **2011**, *2*, 1897–1901.

22. (a) DiMagno, S. G.; Lin, V. S. Y.; Therien, M. J. *J. Org. Chem.* **1993**, *58*, 5983–5993. (b) J. K. Sprafke, *Supramolecular Control of Synthesis and Electronic Structure of Porphyrin Oligomers*, D.Phil. thesis, University of Oxford, Oxford, **2011**.

23. Lindsey, J. S. *Acc. Chem. Res.* **2010**, *43*, 300–311.

24. (a) Chambron, J.-C.; Heitz V.; Sauvage, J.-P. *J. Am. Chem. Soc*.**1993**, *115*, 12378–12384. (b) Solladié, N.; Chambron, J.-C.; Sauvage, J.-P. *J. Am. Chem. Soc.***1999**, *121*, 3684–3692.

25. (a) Yamada, Y.; Okamoto, M.; Furukawa, K.; Kato T.; Tanaka, K. *Angew. Chem., Int. Ed.* **2012**, *51*, 709–713. (b) Yamada, Y.; Mihara, N.; Shibano, S.; Sugimoto K.; Tanaka, K. *J. Am. Chem. Soc.* **2013**, *135*, 11505–11508.

26. Zhang, H.; Liu, Q.; Li, J.; Qu, D-H. *Org. Lett.* **2013**, *15*, 338–341.

27. (a) Anderson, H. L. *Inorg. Chem.* **1994**, *33*, 972–981. (b) Taylor, P. N.; Huuskonen, J.; Aplin, R. T.; Anderson, H. L.; Huuskonen, J.; Rumbles, G.; Williams, E. *Chem. Comm.* **1998**, 909–910.

28. a) Klotz, E. J. F.; Claridge, T. D. W.; Anderson, H. L. *J. Am. Chem. Soc.* **2006**, *128*, 15374–15375. (b) Prikhod'ko, A. I.; Durola, F.; Sauvage, J.-P. *J. Am. Chem. Soc*. **2008**, *130*, 448–449. (c) Prikhod'ko, A.; Sauvage, J.-P. *J. Am. Chem. Soc.* **2009**, *131*, 6794–6807. (d) Lee, C. F.; Leigh, D. A.; Pritchard, R. G.; Schultz, D.; Teat, S. J.; Timco, G. A.; Winpenny, R. E. P. *Nature* **2009**, *458*, 314–318. (e) Cheng, H. M.; Leigh, D. A.; Maffei, F.; McGonigal, P.R.; Slawin, A. M. Z.; Wu, J. *J. Am. Chem. Soc.* **2011**, *133*, 12298–12303.

29. Goldup, S. M.; Leigh, D. A.; McGonigal, P. R.; Ronaldson, V. E.; Slawin, A. M. Z. *J. Am. Chem. Soc.* **2010**, *132*, 315–320.

30. *Carbon-Rich Compounds: From Molecules to Materials*, Haley,M. M., Tykwinski, R. R., Eds.; Wiley-VCH: Weinheim, **2006**

31. Enkelmann, V. *Chem. Mater.* **1994**, *6*, 1337–1340.

32. Atkins, P. W.; Friedman, R. S. *Molecular Quantum Mechanics*; 3 ed.; Oxford University Press: New York, **1997.**

33. Lucotti, A.; Tommasini, M.; Fazzi, D.; Del Zoppo, M.; Chalifoux, W. A.; Ferguson, M. J.; Zerbi, G.; Tykwinski, R. R. *J. Am. Chem. Soc.* **2009**, *131*, 4239–4244.

34. Rowland, R. S.; Taylor, R. *J. Phys. Chem.* **1996**, *100*, 7384–7391.

35. Fulmer, G. R.; Miller, A. J. M.; Sherden, N. H.; Gottlieb, H. E.; Nudelman, A.; Stoltz, B. M. Bercaw, J. E.; Goldberg, K. I. *Organometallics* **2010**, *29*, 2176–2179.

36. Palatinus, L.; Chapuis, G. J. *Appl. Cryst.* **2007**, *40*, 786–790.

37. Betteridge, P. W.; Carruthers, J. R.; Cooper, R. I.; Prout, K.; Watkin, D. J. *J. Appl. Cryst.* **2003**, *36*, 1487.

Chapter 4

Too close to each other, Forbidden transition, A sink for excited states energies

Chapter 4. Photophysics of Threaded sp^1-Carbon Chains and Rhenium Tricarbonyl Complexes

4.1 Introduction

In this chapter the excited state behavior of supertrityl-capped hexayne and its rotaxanes is described using time-resolved UV-vis, NIR and IR absorption spectroscopy.

Polyynes, and materials based on chains of linear sp^1 carbon atoms, have long been a focus of research, as models for carbyne, the elusive 1D allotrope of carbon,[1] and this field has been stimulated by the extraordinary mechanical,[2,3] charge-transport[4-7] and nonlinear optical[8] properties of these materials. Additionally, the acetylene unit has been extensively employed to transfer excitation energy in optoelectronic gates and metaloporphyrin arrays,[9] or in photonic wires, where the butadiyne link mediates efficient triplet energy transfer between two fluorescent dyes.[9c,d] By contrast, in the rotaxinated polyynes the macrocyclic chromophore is threaded around the polyyne chain through a mechanical bond and the investigation of the polyyne-macrocycle through-space interactions upon optical excitation presents attractive scientific interest , considering the rich photophysics and intriguing excited state behaviour of polyynes.[33-43]

The presence of the phenanthroline unit in these rotaxanes allows different metals to be coordinated within the macrocycle cavity.[10] For example, rhenium carbonyl complexes of phenanthroline and bipyridine derivatives are well-known phosphorescent labels for biomolecules,[11] materials in organic light-emitting devices,[12] and they are promising sensitizers of electron-transfer (ET) and energy-transfer processes (EET).[13,14] The close proximity of the coordinated metal and polyyne, when they are both locked inside the macrocycle, serves as an unique model to examine the polyyne-metal remote interactions.[15] For this reason, the $Re(CO)_3Cl$ rotaxane and $Re(CO)_3Cl$ macrocycle complexes were prepared[16] and UV-Vis, FTIR, time-resolved IR (TRIR), transient absorption (TA) spectroscopy were applied in combination with X-ray crystallography to study hexayne dumbbell **2.2**,[17] macrocycle **M1**,[18] hexayne rotaxane **2b⊂M1**, $Re(CO)_3$·**M1** and $Re(CO)_3$·rotaxane $Re(CO)_3Cl$·**2b⊂M1** in the ground and excited states. (Additionally, another $Re(CO)_3Cl$ hexayne rotaxane with smaller macrocycle **M2** has been prepared, the synthesis and photophysical studies of which are given in *Appendix A*). For convenience we will use the following designation for the compounds (Chart 4.1): Hexayne-**H**, macrocycle-**M**, rotaxane-**H⊂M**, $Re(CO)_3Cl$·macrocycle-**M(Re)** and $Re(CO)_3Cl$·rotaxane-**H⊂M(Re)**.

The represented material describes the intriguing photophysical properties of a new class of polyyne rotaxanes demonstrating the ability of the polyyne chain to harvest effectively singlet and triplet excited energy from rotaxinated chromophore. Our experiments uncover the potential to use polyyne rotaxanes as supramolecular photonic wires and shed a light on the properties of insulated carbon-rich materials.

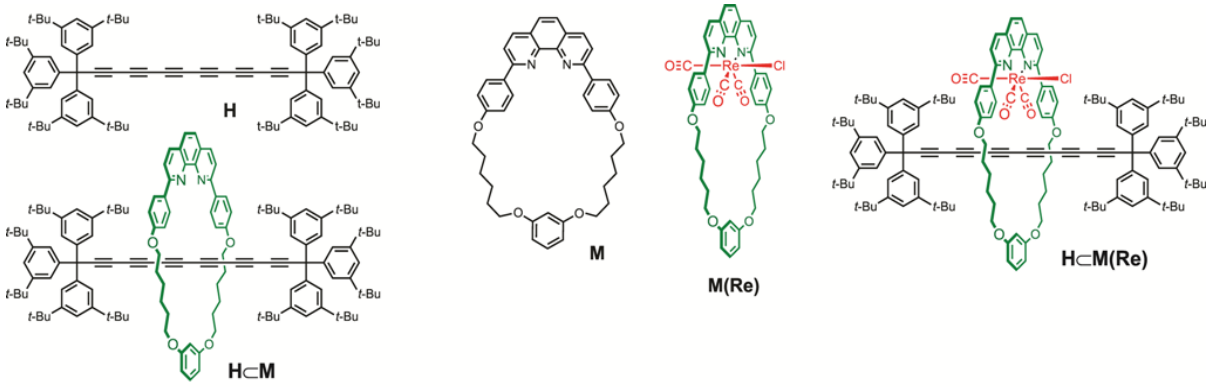

Chart 4.1 Structure of **H** hexayne, **M** macrocycle, **H⊂M** hexayne rotaxane, **H⊂M(Re)** $Re(CO)_3Cl$·rotaxane and **M(Re)** $Re(CO)_3Cl$·macrocycle.

4.2. Synthesis of $Re(CO)_3Cl$ complexes H⊂M(Re) and M(Re)

$Re(CO)_3Cl$·macrocycle complex **M(Re)** was prepared according to the published procedure (Scheme 4.1).[16] To the solution of the macrocycle **M1** in toluene $Re(CO)_5Cl$ was added and the suspension was stirred at reflux. After simple workup, the product was isolated in 63% yield as a yellow solid.

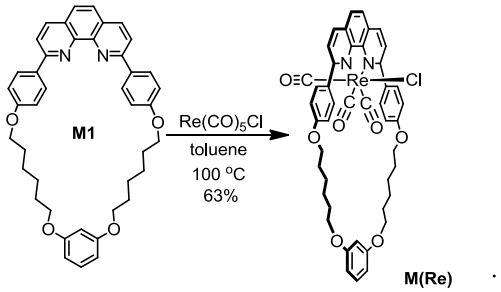

Scheme 4.1 Synthesis of the $Re(CO)_3Cl$·**M1** rhenium tricarbonyl complex of the macrocycle **M1**.

The **H⊂M(Re)** complex was prepared in a similar way: **2b⊂M1** was reacted with $Re(CO)_5Cl$ in toluene at 100 °C. This reaction was found to give the rhenium(I) carbonyl rotaxane complex **H⊂M(Re)** in 70% yield (Scheme 4.2).

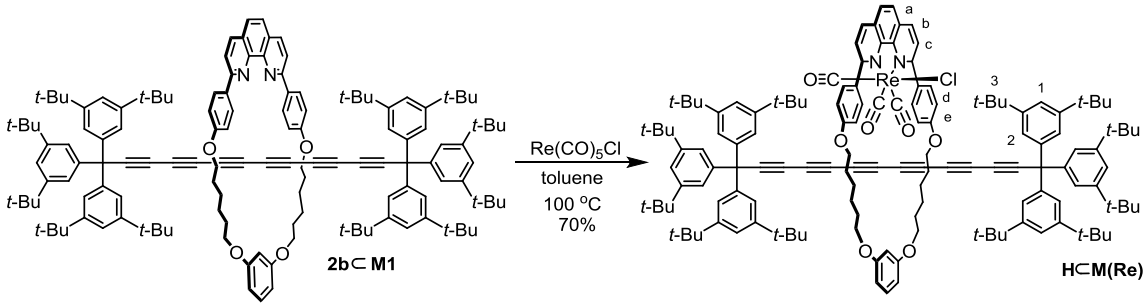

Scheme 4.2 Synthesis of the **H⊂M(Re)** rhenium tricarbonyl complex of the rotaxane **2b⊂M1.**

4.3 NMR characterization of $Re(CO)_3Cl$ complexes

Both rhenium(I)tricarbonyl complexes **M(Re)** and **H⊂M(Re)** were characterized by NMR, FTIR, UV-Vis absorption spectroscopy and MALDI spectrometry. The ^{1}H NMR spectrum of the **M(Re)** shows that proton signals of the phenanthroline moiety are split due to desymmetrization of the molecule. This happens because the Re centre preserves octahedral geometry, discussed in the crystallography section below, and as a result, one face of the macrocycle 'looks' to the axial carbonyl group while the other face to the axial chlorine atom. Interestingly, in the **H⊂M(Re)** complex the symmetry of the rhenium center is imposed on the polyyne, splitting the resonances of the dumbbell component (proton signals from supertrityl group, H1, H2 and H3, Figure 1a, for the peak assignment see Scheme 4.2): **H⊂M(Re)** shows twice as many *sp* ^{13}C resonances as **2b⊂M1** (Figure 1b).

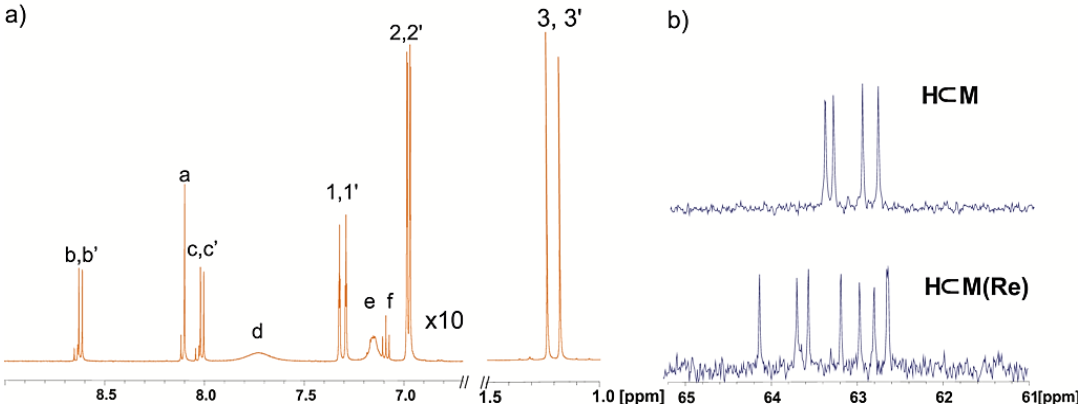

Figure 4.1 (a) 1H NMR of the **H⊂M(Re)** showing the splitting of the macrocycle protons as well as dumbbell protons signals (500 MHz, 298 K, CD_2Cl_2). (b) The ^{13}C NMR spectrum of **H⊂M(Re)**, showing only the resonances of the 8 central carbons of the C12 polyyne chain compared with that of rotaxane **H⊂M** (4 resonances, 125 MHz, 298 K, CD_2Cl_2).

4.4 Steady-state fluorescence spectra of $Re(CO)_3Cl$ complexes

The **M(Re)** complex shows normal luminescence behavior (emission λ_{max} = 550 nm, quantum yield ϕ = 0.030 in toluene under air). Surprisingly, no luminescence is detected from **H⊂M(Re)** under these conditions. Evidently the proximity of the C12 polyyne chain quenches the emission from the rhenium center (Figure 4.2). This result was surprising because the HOMO-LUMO gap of the hexayne (absorption λ_{max} 315 nm) appears to be too large to accept excitation from the $Re(CO)_3Cl$ unit (emission λ_{max} 605 nm), while the electron-affinity of the polyyne is insufficient for it to quench the rhenium luminescence by photoinduced electron transfer.[19,20] Moreover, addition of the hexayne dumbbell **H**[17] to the **M(Re)** solution in toluene did not alter the luminescence of the rhenium complex, demonstrating that the polyyne needs to be in close proximity to quench the luminescence, although, the mechanism of this quenching process was not known.

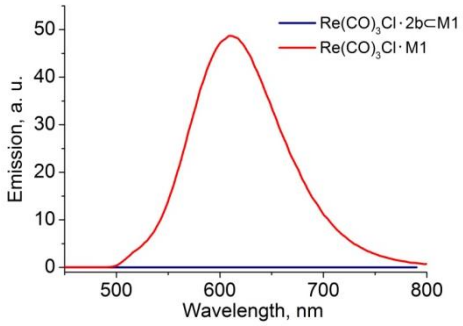

Figure 4.2 Spectra of the **M(Re)** (red) and the **H⊂M(Re)** (blue) measured in air-saturated toluene. Both solutions had the same concentration (ca. 1 μM) and both were excited at 350 nm under identical conditions. The luminescence quantum yield of **M(Re)** (ϕ = 0.033) was measured using zinc tetraphenylporphyrin as a standard (ϕ = 0.11).[21]

4.5 Ground state UV-Vis absorption and IR spectroscopy

The UV absorption spectrum of hexayne **H** in dichloromethane (Figure 2a) shows an intense band at 275–325 nm, with a well-defined vibronic progression of ~2060 cm^{-1}, corresponding to the vibrational mode of the S_n state.[17,33-43] The vibrational progression matches well with the ground state C≡C stretch frequency (2175–2195 cm^{-1}) seen in the IR spectrum (Figure 4.3b). Hexayne **H** also displays a weak absorption band at 350–450 nm, dominated by a vibronic progression of 2040–2169 cm^{-1} (insert in Figure 4.3a). We assign this band to the forbidden $S_0 \rightarrow S_1$ transition, as reported in the absorption spectra of many other long polyynes[33-42] (although we cannot exclude the possibility that it is a transition to another low-lying singlet excited state, other than S_1). This $S_0 \rightarrow S_1$ transition at 350–450 nm is about 500 times weaker

than the $S_0 \rightarrow S_n$ absorption at 275–325 nm. For the **H⊂M** rotaxane, the third vibrational band of the $S_0 \rightarrow S_1$ transition is obscured by the intense absorption of macrocycle at ~390 nm, but the first two bands are clearly visible and do not change their position, while in the **H⊂M(Re)** rotaxane, all the $S_0 \rightarrow S_1$ transitions are hidden by the intense **M(Re)** absorption.

The absorption spectrum of the macrocycle **M** (Figure 4.3a) consists of a broad, lower energy π-π* band, extending to 390 nm, and a n-π* band at around 275 nm.[44] The absorption spectrum of the rotaxane **H⊂M** is essentially the sum of its two components, thread and dumbbell, with a slight (~4 nm) bathochromic shift of the hexayne peaks (Figure 4.3a); the presence of the threaded macrocycle slightly changes the environment of the polyyne chain. Similar results were obtained for $Re(CO)_3Cl$ complexes: The **M(Re)** absorption spectrum consists of two transitions; a low-energy MLCT, extending to about 490 nm, and a higher energy intraligand (IL) π-π* transition.[45] The spectrum of the **H⊂M(Re)** is the sum of its components with a slight (~2 nm) red-shift in the hexayne peaks (Figure 4.3a).

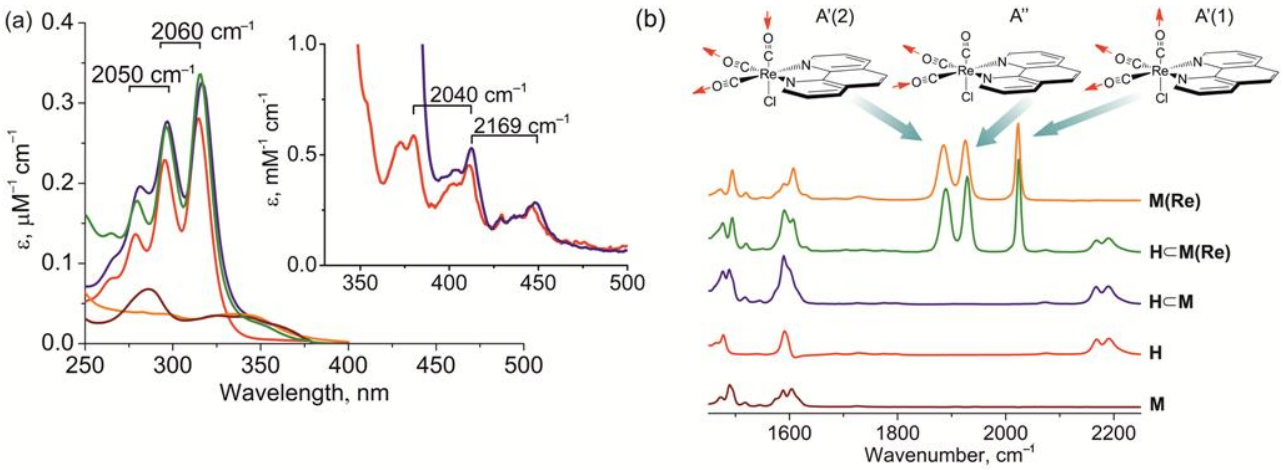

Figure 4.3 (a) UV-vis absorption and (b) IR spectra of the hexayne **H** (red), the rotaxane **H⊂M** (blue), **H⊂M(Re)** (green), **M(Re)** (orange), and **M** (brown), all recorded in CH_2Cl_2. Concentrations of the compounds for IR measurements are 1.5 mM; path length 0.5 mm. (a) Insert depicts the weak $S_0 \rightarrow S_1$ absorption. (b) The top picture depicts the three stretching modes of carbonyl groups.[46] The same color code is used for spectra in (a) and (b).

IR spectra were measured in dichloromethane (Figure 4.3b). The hexayne **H** has a broad collective band with two overlapping stretches (2175 and 2195 cm^{-1}) which are characteristic of long polyyne chains,[47] assigned to the symmetric σ_g C≡C stretch mode and the β-IR mode, respectively. In the rotaxanes **H⊂M** and **H⊂M(Re)**, the C≡C stretch is unshifted, at around 2200 cm^{-1}, indicating that threading does not perturb the ground state vibrational structure of hexayne. The three carbonyl groups of the $Re(CO)_3Cl$ moiety give rise to three sharp, intense bands at 1894 (A'(2)), 1932 (A'') and 2025 (A'(1)) cm^{-1} for

H⊂M(Re) and 1885 (A''), 1924 (A'(2)) and 2022 (A'(1)) cm^{-1} for **M(Re)**, which are characteristic of *fac*-rhenium tricarbonyl polypyridyl complexes.[46] The positions of the IR bands indicate the C_s (or pseudo C_3) symmetry of the Re center: two normal ν(CO) modes are symmetric (A'(1) and A'(2)) involving all three CO ligands, while one mode (A'') is anti-symmetric involving only in the plane stretching of two CO groups (Figure 4.3b). On threading, the A'' and A'(2) bands of $Re(CO)_3Cl$·macrocycle **M(Re)** shift to higher wavenumber, by 8 cm^{-1} and 9 cm^{-1}, respectively. The relative intensities of all CO bands are similar in both $Re(CO)_3Cl$-complexes.

4.6 X-ray crystallography

To gain more insights into this family of compounds, we have also compared the X-ray crystal structures of **H**, **H⊂M**, **H⊂M(Re)** and **M(Re)**. The crystal structures of hexayne dumbbell **H** was reported previously.[17] The crystal structure of rotaxane **H⊂M** is discussed in Chapter 2. Crystals of $Re(CO)_3Cl$·macrocycle **M(Re)** were grown by slow evaporation of a solution in toluene at 4 °C; single crystal X-ray diffraction data were collected at 150 K using an Oxford Diffraction (Agilent) SuperNova A diffractometer by Dr. Amber Thompson (Oxford Crystallography). Crystals of the $Re(CO)_3Cl$·rotaxane complex **H⊂M(Re)** were grown from dichloromethane solution by slow diffusion of methanol vapor at room temperature; single crystal X-ray diffraction data were collected at 100 K using synchrotron radiation at the Diamond Light Source, beamline I19.[22] In both cases, data were reduced using CrysAlisPro. **M(Re)** was found to crystallize in P-1 with one molecule of **M(Re)** and two molecules of toluene in the asymmetric unit, while **H⊂M(Re)** crystallized in P 2_1/n with one molecule of **H⊂M(Re)** in the asymmetric unit. The structures were solved using charge flipping[23] with SuperFlip[24] and refined using least-squares within CRYSTALS.[25] The difference map for **H⊂M(Re)** indicated the presence of diffuse electron density believed to be disordered solvent. SQUEEZE[26] was used leaving a void from which the electron density was removed. The structures of the hexayne dumbbell **H**,[17] rotaxane **H⊂M**, rhenium rotaxane **H⊂M(Re)** and rhenium-macrocycle complex **M(Re)** are compared in Figure 4.4. The two rotaxanes, **H⊂M** and **H⊂M(Re)**, show similar bond length alternation within experimental error: 0.143 ± 0.008 Å in **H⊂M** and 0.155 ± 0.010 Å in **H⊂M(Re)**, compared with 0.158 ± 0.008 Å for **H**.[9] The closest distance between carbonyl group oxygen and polyyne chain carbon in **H⊂M(Re)** is 3.085(5) Å (CO–

C(5)), which is less than the sum of the van der Waals radii (3.35 Å);[27] the three shortest CO···C≡C contacts are shown in Figure 4.4e.

The hexayne chain in **H⊂M(Re)** is severely bent, with a single-arc conformation, unlike the double-arc of **H**.[20] The angle between the two terminal C1 and C12 atoms and the centroid of the middle C6-C7 bond of **H⊂M(Re)** is 155.6(1) ° (compared with 171.8(1) ° in **H⊂M** and 180 ° in **H**); the average value for this parameter for the 22 hexaynes in the Cambridge Structural Database[28] is 175.3 ° (s.d. 7.1 °),[8a,17,29,30.31,32] and only one other hexayne has been reported with a comparable angle (155.3(2) °).[30] The angles between the three carbonyl groups lie in the range 85.20(17)–92.55(17) ° (with an average of 88.7 °) in **H⊂M(Re)** and 85.47(16)–90.53(16) ° (with an average of 87.9 °) in **M(Re)**, and the local C_s symmetry of the rhenium center is preserved in both $Re(CO)_3Cl$ complexes (Figure 4.4).

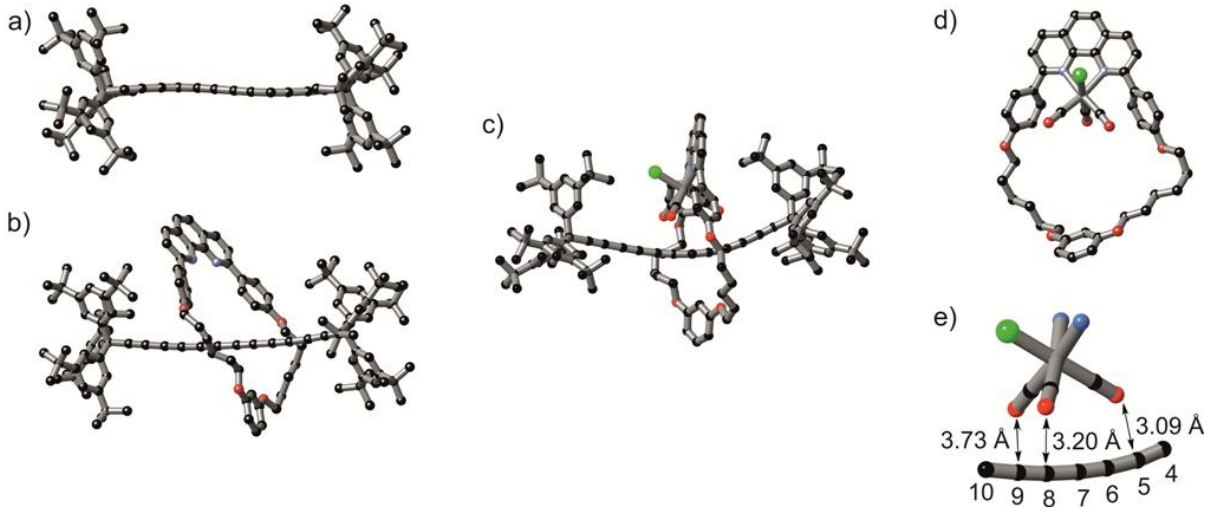

Figure 4.4 The solid state structures of (a) hexayne **H**, (b) rotaxane **H⊂M**, (c) $Re(CO)_3Cl$·rotaxane **H⊂M(Re)** and (d) $Re(CO)_3Cl$·macrocycle **M(Re)**. The closest distances between CO groups and C≡C chain in the $Re(CO)_3Cl$·rotaxane **H⊂M(Re)** are also shown (e). Hydrogen atoms and solvent molecules are omitted for clarity.

4.7 Time-resolved absorption and IR spectroscopy

We carried out a systematic study of the dynamic processes in the excited states of this family of compounds, using TRIR and TA spectroscopy. The time-resolved experiments were carried out in the Research Complex at Harwell, with the collaboration with Professor Anthony Parker (Central Laser Facility, CLF). All experiments were performed within of 2-week visit to the CLF, with the great help of Professor Anthony Parker, Professor Michael Towrie and Dr. Gregory Greetham.

Initially, we examined the excited state behavior of the hexayne **H** and the macrocycle **M** separately, and then we moved to the topologically more complex rotaxane **H⊂M**, the rhenium tricarbonyl complex

of macrocycle **M(Re)** and rhenium tricarbonyl rotaxane complex **H⊂M(Re)**. Two regions of the TRIR spectra are particularly informative: the high frequency region at 1900–2300 cm^{-1} and the "fingerprint" region at 1400–1900 cm^{-1}. The kinetic data for **H**, **H⊂M** and **H⊂M(Re)** are summarized in Tables 4.1–4.4.

4.7.1 Photophysics of Hexayne H

TRIR is an excellent technique for examining the kinetics of transient species, with a time-resolution of < 200 fs.[48] When investigating the photophysics of polyynes, strong signals are observed for the C≡C triple-bond stretch (2100–2200 cm^{-1}), providing information on ground-state depletion and recovery (through the negative ΔA "bleach" signal), and probing the evolution of singlet and triplet excited states, which can be distinguished by their different C≡C stretch frequencies (reflecting their different extents of bond length alternation). Despite these attractive features, there have been no previous ultrafast TRIR studies of polyynes,[49] which is surprising because, despite extensive investigation, the excited states of polyynes remain poorly understood. Theoretical and experimental studies agree that the first singlet excited states (S_1) are generally "dark states" — which means that S_0–S_1 transitions are dipole forbidden.[33–42] Consequently, the absorption spectra are dominated by transitions to higher singlet excited states ($S_0 \rightarrow S_n$) while the $S_0 \rightarrow S_1$ absorption band is weak or unobservable. Internal conversion (IC, $S_n \rightarrow S_1$), is very rapid, but fluorescence from S_1 is normally too slow to compete with intersystem crossing (ISC, $S_1 \rightarrow T_1$) and nonradiative decay (IC, $S_1 \rightarrow S_0$). Unsubstituted polyynes, H-(C≡C)$_n$-H, exhibit an intense allowed absorption band to a high-energy singlet state ($^1\Sigma^+_g \rightarrow {}^1\Sigma^+_u$), as well as weak absorption bands at longer wavelengths, which are about 1000-times less intense and involve low-lying singlet states ($^1\Sigma^+_g \rightarrow {}^1\Sigma^-_u$ and $^1\Sigma^+_g \rightarrow {}^1\Delta_u$).[33-36] Other polyynes, R-(C≡C)$_n$-R, show similar behavior,[37-42] although their electronic structures can be complicated by involvement of the end groups (particularly if R = aryl), and it can be difficult to identify the dark states. Knowledge of the energy of the dark S_1 state is essential for estimating the optical HOMO-LUMO gap, and for understanding charge transport.[4-7]

Computational studies have shown that the excited states of polyynes generally have reduced bond length alternation, *i.e.* the C≡C triple bonds become longer and the C-C single bonds become shorter.[41,50,51] This prediction is supported by analysis of vibrational structure in electronic transitions[34]and by time-

resolved resonance Raman studies on the T_1 state of diphenyl butadiyne (Ph-C≡C-C≡C-Ph),[52] and an intriguing metastable photoexcited polyyne has been identified at low temperatures which appears to have a cumulenic structure (=C=C= rather than -C≡C-).[53] Here we present the first TRIR study of an extended polyyne. We show that optical excitation generates a short-lived higher singlet state (S_n) which has a lifetime of 0.9 ps in the free hexayne **H**. TRIR also enables the S_1 and T_1 states of the polyyne to be directly observed and their C≡C stretch frequencies (S_0: 2175, 2195 cm^{-1}; S_1: 2177 cm^{-1}; T_1: 2047 cm^{-1}) provide clear evidence for a slight increase in cumulenic character in the excited states (more in T_1 than S_1).

Excitation of hexayne **H** at 310 nm, results in an immediate bleach of the ground state C≡C stretch at 2175–2195 cm^{-1} (within the time-resolution of our instrument, <200 fs) and a new absorption band appears at 2063 cm^{-1} (Figure 4.5a). This band, which corresponds to the C≡C stretch in the singlet excited state, shifts to 2077 cm^{-1} over ~5 ps (Figure 4.5a) in parallel with a ~15% band narrowing (measured at the half maximum). These two spectral changes are typical indications of intramolecular vibrational relaxation (IVR) and cooling of 'hot' state(s);[54] the time-dependent vibrational shift may also contain contributions from solvent reorganization around the nascent excited state.[54] Previously, the formation of a vibrationally hot polyyne upon vertical excitation was postulated from the broadness of the TA spectra at short time delays.[38] To our knowledge, this is the first time that the vibrational relaxation of a 'hot' excited long polyyne has been characterized via vibrational spectroscopy. $S_n \rightarrow S_1$ internal conversion occurs on a faster time-scale than this IVR, as discussed below.

The S_1 band at 2077 cm^{-1} decays to a new band at 2047 cm^{-1} corresponding to the T_1 triplet excited state C≡C stretch (Figure 4.5b); the rates of this decay (τ_1 = 0.44 ± 0.02 ns) and of the growth of the band at 2047 cm^{-1} (τ_2 = 0.48 ± 0.05 ns, Figure 4.5c) give the rate of ISC, as summarized in Table 4.1. The lower frequency of the C≡C stretch in the excited states (2077 cm^{-1} in S_1 and 2047 cm^{-1} in T_1 *vs.* 2175 and 2195 cm^{-1} in S_0) reflect a reduced bond-length-alternation in the excited states.[34,36,50-52,29i] The intensity of the C≡C ground state bleach band at 2175–2195 cm^{-1} does not change during ISC, indicating that the triplet yield is near unity.

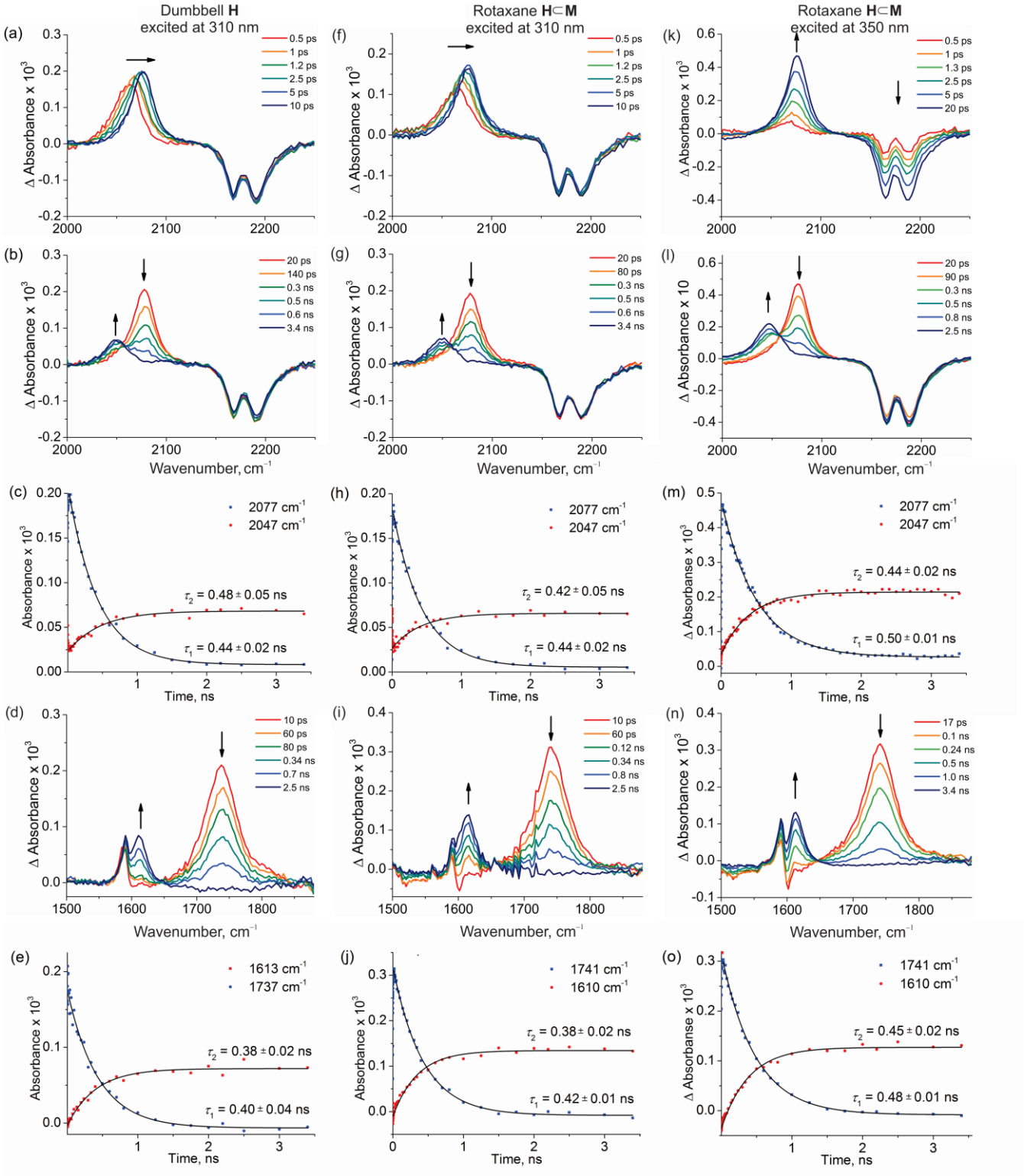

Figure 4.5 TRIR spectra and excited state kinetics of hexayne dumbbell **H** excited at 310 nm (a–e), rotaxane **H⊂M** excited at 310 nm (f–j) and 350 nm (l–o). Laser energy: 80–100 nJ, solvent: CH_2Cl_2.

Spectacular changes are also observed in the fingerprint region (Figure 4.5d), and these are useful for confirming the species assignments and associated kinetics. Immediately after excitation, a band appears at ~1740 cm^{-1}, which decays gradually, giving a new band at 1610 cm^{-1}. These two bands display similar kinetics (1740 cm^{-1} decay time: $\tau_1 = 0.40 \pm 0.04$ ns; 1610 cm^{-1} rise time: $\tau_2 = 0.38 \pm 0.02$ ns, Figure 4.5e)

to the bands at 2040–2080 cm^{-1} and are attributed to the same excited species, $S_1 \rightarrow T_1$. The lifetime of the T_1 state of **H** in deoxygenated dichloromethane is 16.0 ± 3.6 μs (estimated from the 1610 cm^{-1} band; excitation with a 1 ns pulse at 266 nm; Figure 4.6).

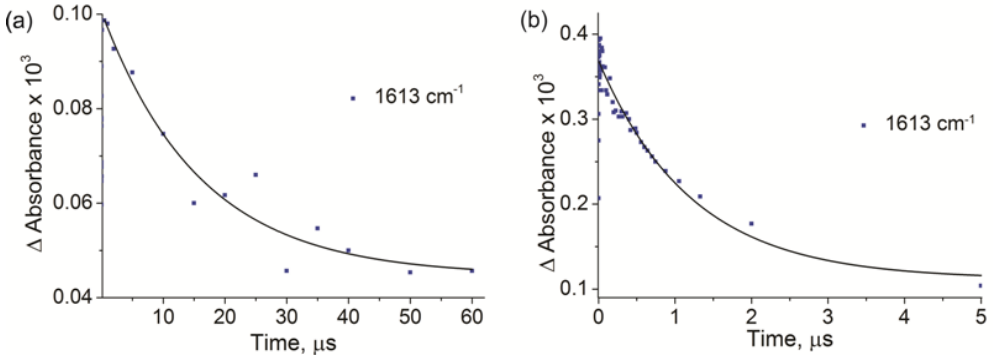

Figure 4.6 Excited state dynamic changes in dumbbell **H** on excitation at 266 nm in TRIR spectra. (a) Single exponential decay of 1613 cm^{-1} band in deoxygenated (τ_2 = 16.0 ± 3.6 μs) and (b) air-saturated (τ_1 = 1.2 ± 0.1 μs) CH_2Cl_2 (laser energy = 200 nJ). This enhanced decay in the presence of oxygen supports assignment of the 1613 cm^{-1} band to the triplet excited state of the hexayne.

At early times, the fingerprint band of the singlet excited state at 1741 cm^{-1} shifts to 1737 cm^{-1}, while decreasing in intensity, over 3 ps (Figure 4.7). The direction of this spectral shift is opposite to that expected for IVR and solvation processes and we tentatively assign it to $S_n \rightarrow S_1$ internal conversion.

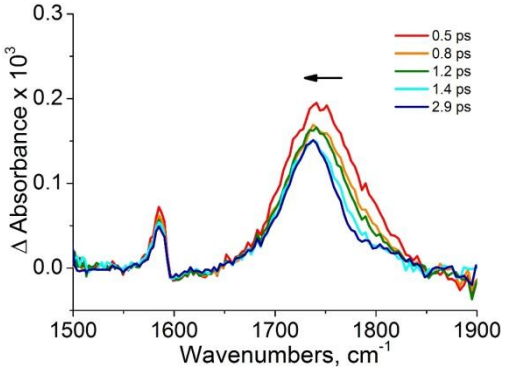

Figure 4.7 TRIR spectra of hexayne dumbbell **H** in fingerprint region at early time delays (0–3 ps). Excitation λ = 310 nm; laser energy = 200 nJ; solvent: CH_2Cl_2.

TA spectra show a similar fast process: Excitation at 310 nm generates a band at 421 nm, which grows with a rise time of τ_1 = 0.93 ± 0.08 ps (Figure 4.8). This rise is too slow for direct vertical excitation (in TRIR spectra the bleach of ground state C≡C stretching appears within the 200 fs instrument time-resolution). Thus, the most reasonable explanation is the formation of the S_1 state via the symmetry-allowed S_0-S_n transition.

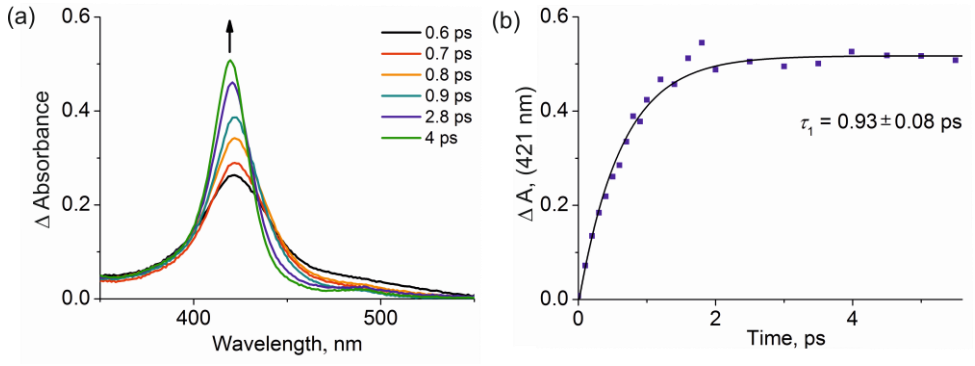

Figure 4.8 Growth of the S_1 state of hexayne **H** following excitation at 310 nm in CH_2Cl_2: (a) TA spectra and (b) signal at 421 nm (τ_1 = 0.93 ± 0.08 ps).

At longer times, TA confirms that the S_1 state undergoes an intersystem crossing, resulting in a band at 343 nm, corresponding to the T_1 state (Figure 4.9a). The kinetics of T_1 band growth at 343 nm (τ_2 = 0.45 ± 0.09 ns) and S_1 decay (τ_1 = 0.44 ± 0.02 ns) (Figure 4.9b) are similar to those extracted from TRIR spectra.

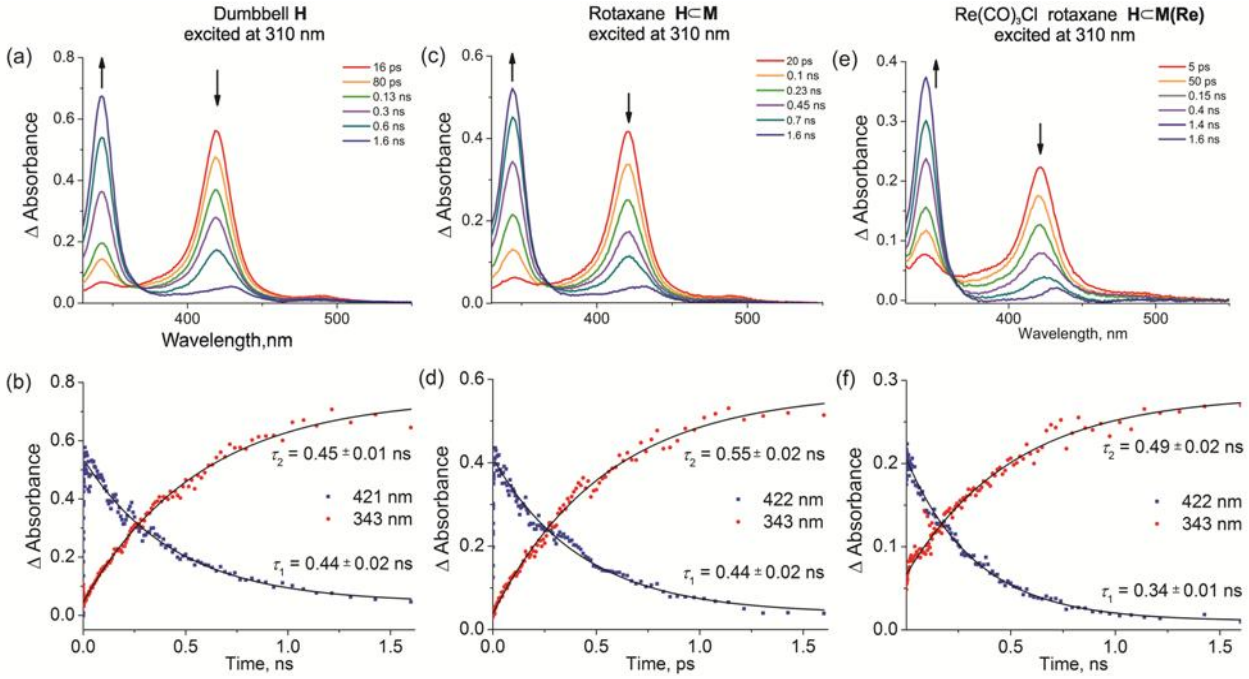

Figure 4.9 TA spectra and excited state kinetics of hexayne dumbbell **H** (a,b, laser energy = 50 nJ), rotaxane **H⊂M** (c,d, laser energy = 70 nJ) and **H⊂M(Re)** (e,f, laser energy = 70 nJ); excited at 310 nm; solvent: CH_2Cl_2.

Examination of the NIR TA showed a short-lived broad band at 1185 nm which appears immediately following the excitation pulse (Figure 4.10). The decay time of this band (τ_1 = 0.82 ± 0.13 ps; Figure 4.10b) matches the growth of the S_1 state in the visible region of TA spectrum (τ_1 = 0.93 ± 0.08 ps) and we therefore assign it to the S_n state of the hexayne. To our knowledge, this is first time that a $S_n \rightarrow S_1$ transition of any polyynes has been characterized by TRIR and NIR TA spectroscopy, although the S_1 and S_n states of the diphenylacetylene were studied by emission spectroscopy.[49,55] π-Conjugated terminal aryl groups may play an important role in the excited state dynamics of diphenylacetylene, while the

'supertrityl' capped hexayne **H** presents a 'pure' case of a polyyne chain, so its behavior can be regarded as intrinsic to the *sp*-hybridized carbyne chain.

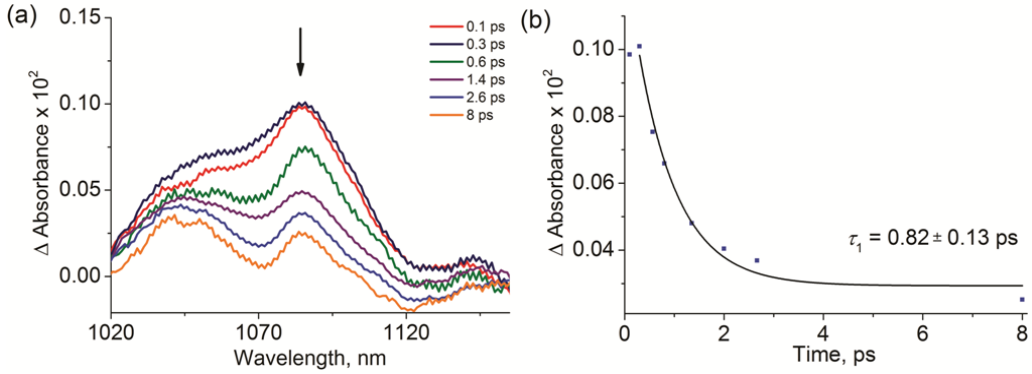

Figure 4.10 Transient absorption spectra of hexayne **H** in NIR region following excitation at 310 nm. (a) The decay of S_n state and (b) its single exponential kinetics (1085 nm, τ_1 = 0.82 ± 0.13 ps). Excitation λ = 310 nm; laser energy = 60 nJ, solvent: CH_2Cl_2.

Table 4.1 Excited state bands, transitions and lifetimes for hexayne **H** in CH_2Cl_2 excited at 310 nm.

TRIR band	Lifetime (τ)	Assignment	TA band	Lifetime (τ)	Assignment
2077 cm^{-1}	0.44 ± 0.02 ns	$S_1 \rightarrow T_1$ decay	421 nm	0.44 ± 0.02 ns	$S_1 \rightarrow T_1$ decay
2047 cm^{-1}	0.48 ± 0.05 ns	$S_1 \rightarrow T_1$ growth	343 nm	0.45 ± 0.01 ns	$S_1 \rightarrow T_1$ growth
1737 cm^{-1}	0.40 ± 0.04 ns	$S_1 \rightarrow T_1$ decay	421 nm	0.93 ± 0.08 ps	$S_n \rightarrow S_1$ growth
1610 cm^{-1}	0.38 ± 0.02 ns	$S_1 \rightarrow T_1$ growth	1085 nm	0.82 ± 0.13 ps	$S_n \rightarrow S_1$ decay
1610 cm^{-1} [a]	16.0 ± 3.6 μs	$T_1 \rightarrow S_0$ decay			

[a] Excited at 266 nm and measured in O_2-free CH_2Cl_2.

4.7.2 Photophysics of Macrocycle M.

The excited states of 2,9-diaryl phenanthrolines have been studied before,[44a] and the $^1\pi\pi^*$ singlet state lifetime is estimated to be a few ns in dichloromethane, while the triplet $^3\pi\pi^*$ state lives for about a second at 77 K. As expected, the TRIR spectrum of macrocycle **M** does not exhibit any features in the high frequency region (on excitation at 350 or 310 nm). In the fingerprint region, transient features appear at 1470 cm^{-1}, 1510 cm^{-1} and 1520–1600 cm^{-1} (Figure 4.13a). The transients have similar decay rates, indicating that they arise from the same excited species. The sharpest peak at 1504 cm^{-1} was chosen for kinetic analysis and fitted to a single-exponential decay yielding a singlet lifetime of 2.1 ± 0.2 ns (Figure 4.11).

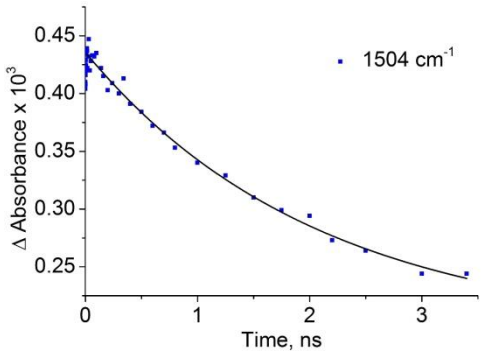

Figure 4.11 Single exponential decay of 1504 cm^{-1} TRIR band (τ_1 = 2.07 ± 0.24 ns) of the macrocycle **M** on excitation at 350 nm. Laser energy = 100 nJ; solvent: CH_2Cl_2.

The TA spectra show a very broad band between 350 and 700 nm (Figure 4.12) with distinguishable peaks at 365 and 652 nm. Within a few ns, the peak at 365 nm decays and a new peak grows at 436 nm, but the total intensity of broad envelope does not change dramatically over time. The decay constant of the 365 nm band is τ_1 = 1.8 ± 0.2 ns, matching with the lifetime of the 1504 cm^{-1} TRIR band. We ascribed the band at 365 nm to the singlet and the band at 436 nm to triplet excited state macrocycle.

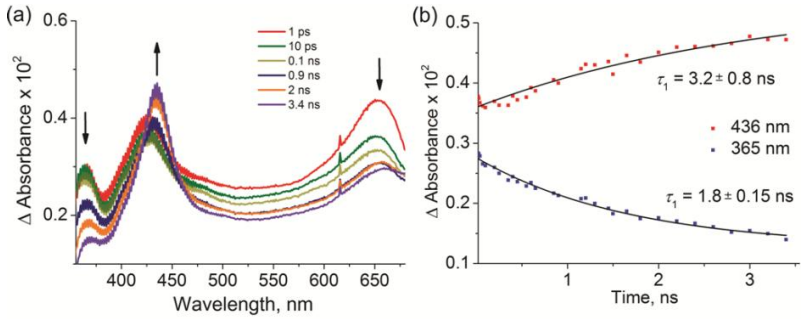

Figure 4.12 (a) Excited state TA spectra of macrocycle **M** on excitation at 350 nm; laser energy = 100 nJ; solvent: CH_2Cl_2. (b) The kinetics of the 365 nm band assigned to the decay of the singlet state (τ_1 = 1.8 ± 0.15 ns), while the growth of the band at 436 nm is assigned to the triplet state formation and has similar kinetics (τ_1 = 3.2 ± 0.8 ns).

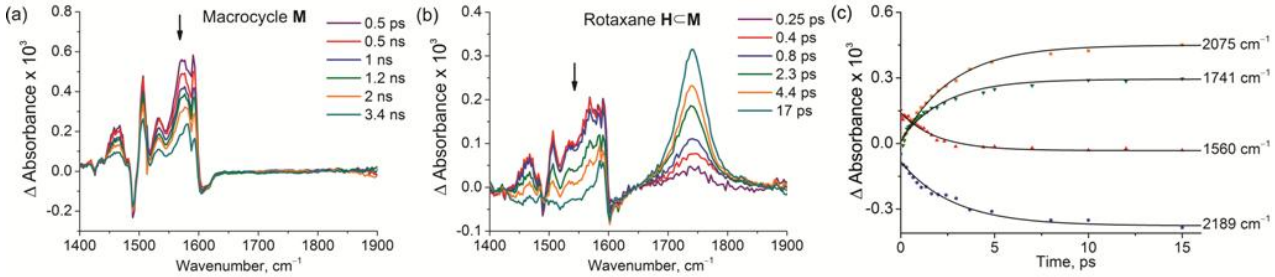

Figure 4.13 TRIR spectra of (a) macrocycle **M** and (b) rotaxane **H⊂M** excited at 350 nm. (c) Kinetics of the singlet EET from M to the dumbbell estimated from the different spectral regions and bands, excited at 350 nm. Laser energy: 45 nJ; solvent: CH_2Cl_2.

4.7.3 EET in rotaxane H⊂M

It is possible to excite the different components of the rotaxane separately: At 350 nm, where only the macrocycle absorbs, or at 310 nm, where absorption by the hexayne predominates (both components absorb at 310 nm, but the molar absorption coefficient of the hexayne is higher by a factor of 12).

The TRIR spectra of **H⊂M**, when excited at 310 nm, are almost identical to those of hexayne **H** (compare Figure 4.5f,g with Figure 4.5a,b). The initially formed 'hot' S_1 state undergoes IVR and the observed frequency shift resembles that of the **H** (Figure 4.5f). The bleach of the C≡C stretch around 2190 cm^{-1} does not change intensity during ISC, indicating again that the triplet yield is near unity, as in the hexayne **H**. The kinetics are summarized in Table 4.2. The data from the fingerprint region at late time delays (>15 ps) match with those from the high frequency region: the dumbbell S_1 band at 1741 cm^{-1} decays giving rise to a T_1 band at 1610 cm^{-1} (Figure 4.5j). At early time delays, the growth of the singlet S_1 hexayne at 1741 cm^{-1} is biexponential (Figure 4.14), in contrast to the single-exponential growth of the same band in free dumbbell **H** (Figure 4.5j). This behavior results from two processes operating in parallel: (a) excitation of the macrocycle and energy transfer to the polyyne (τ_1), and (b) direct excitation of the hexayne (τ_2 < 200 fs; instrument response limited). Partial direct excitation of the macrocycle is confirmed by the band at 1500–1600 cm^{-1} (Figure 4.14), which decays over 4 ps due to energy transfer to the hexayne dumbbell.

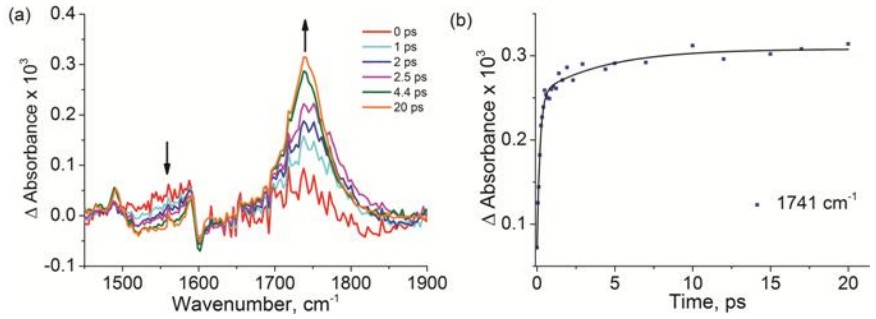

Figure 4.14 Excited state dynamics in rotaxane **H⊂M** on excitation at 310 nm from TRIR spectra. (a) Early-time spectral changes in the fingerprint region. (b) Biexponential growth of 1741 cm^{-1} singlet hexayne band (τ_1 = 4.3 ± 1.6 ps, A_1 = 0.43; τ_2 = 0.19 ± 0.02 ps, A_2 = 0.57).

Excitation of the rotaxane **H⊂M** at 350 nm, where only the macrocyclic component absorbs, was investigated to test for energy transfer between the two components. (Irradiation of free hexayne **H** at this wavelength does not produce detectable TA and TRIR signals, because **H** has negligible absorption at 350 nm.) On excitation of **H⊂M** at 350 nm, the ground state C≡C stretch band gradually bleaches, at around

2190 cm^{-1}, and the S_1 polyyne band gradually grows at 2077 cm^{-1} (Figure 4.4k), indicating transfer of singlet excitation from the macrocycle to the dumbbell. After 20 ps, the TRIR spectra from excitation at 350 nm become identical to those for excitation at 310 nm (compare Figure 4.5k,l with Figure 4.5f,g), and the decay kinetics are the same (Figure 4.5m and Table 4.3). The IVR observed upon excitation of **H⊂M** at 310 nm does not occur when the system is excited at 350 nm (compare Figure 4.5k with Figure 4.5f), which shows that EET does not generate vibrationally 'hot' excited states, in contrast to direct excitation.

Examination of the fingerprint region of the TRIR spectra of **H⊂M** after excitation at 350 nm showed a fast (< 10 ps) decay of a band at 1500–1600 cm^{-1} corresponding to the singlet macrocycle and the parallel rise of the S_1 excited hexayne (1741 cm^{-1}) (Figure 4.13b). This is direct evidence of singlet-singlet energy transfer from the excited state macrocycle to the ground state hexayne. The decay of the macrocycle band at 1560 cm^{-1} (τ_1 = 3.2 ± 0.2 ps) and the growth of the singlet S_1 hexayne at 1741 cm^{-1} (τ_1 = 2.7 ± 0.2 ps) are single-exponential (Figure 4.13c). The growth of the 2077 cm^{-1} band of the singlet hexayne (τ_1 = 2.6 ± 0.1 ps) and the bleach of the ground state stretching mode at 2189 cm^{-1} (τ_1 = 2.9 ± 0.3 ps) are also single-exponential. The very weak $S_0 \rightarrow S_1$ oscillation strength of the polyyne implies that this fast EET occurs by a Dexter mechanism. The triplet lifetime of the hexayne component in **H⊂M** (τ_1 = 14.0 ± 2.2 μs in deoxygenated solution, Table 4.1, Figure 4.15) is similar to that of the hexayne **H**.

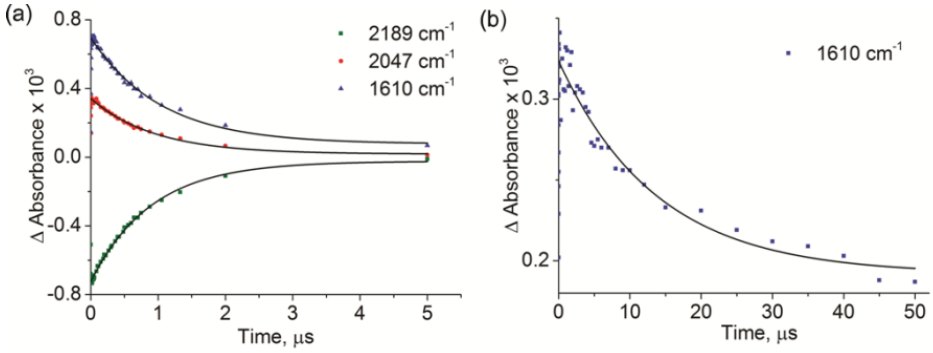

Figure 4.15 (a) Excited state dynamic changes in rotaxane **H⊂M** on excitation with ns laser at 266 nm in TRIR spectra. Single exponential decay of 2047 cm^{-1} band of triplet dumbbell (τ_1 = 0.95 ± 0.04 μs), single exponential recovery of 2189 cm^{-1} ν(C≡C) bleach (τ_1 = 0.90 ± 0.03 μs) and single exponential decay of the 1610 cm^{-1} band (τ_1 = 1.04 ± 0.05 μs) in air-saturated CH_2Cl_2. (b) The kinetics of decay of the dumbbell triplet state in rotaxane **H⊂M** in deoxygenated CH_2Cl_2 (τ_1 = 14.0 ± 2.2 μs).

TA spectra of rotaxane **H⊂M**, with excitation at 350 nm, showed formation of a transient S_1 absorption band at 421 nm (Figure 4.16), similar to that of free dumbbell **H**. The rise-time of this band (τ_1 = 3.2 ± 0.4 ps, Figure 4.16a), due to S_1(macrocycle)→S_1(hexayne), agrees with the TRIR data. On a longer timescale,

this band decays (τ_2 = 0.42 ± 0.04 ns) due to intersystem crossing. The growing T_1 state was observed as a shoulder at 360 nm, but overlap with the excitation wavelength made it difficult to observe the triplet (Figure 4.16b).

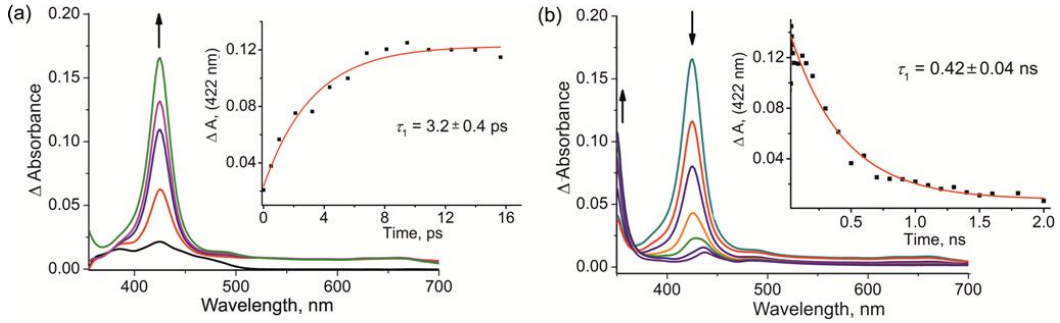

Figure 4.16 Transient absorption spectra of **H⊂M** following excitation at 350 nm. (a) The formation of singlet excited state. (b) Decrease of singlet and increase of triplet (as a shoulder) TA bands. Inserts show the corresponding kinetics, excited at 350 nm. Laser energy: 200 nJ; solvent: CH_2Cl_2.

TA spectral changes of **H⊂M** excited at 310 nm are similar those in dumbbell **H**. The singlet S_1 band at 422 nm grows at early time delays (τ_1 = 1.8 ± 0.2 ps, Figure 4.17) due to $S_n \rightarrow S_1$ relaxation. Later, this band decays and the triplet band at 343 nm grows (Figure 4.9d, Table 4.2).

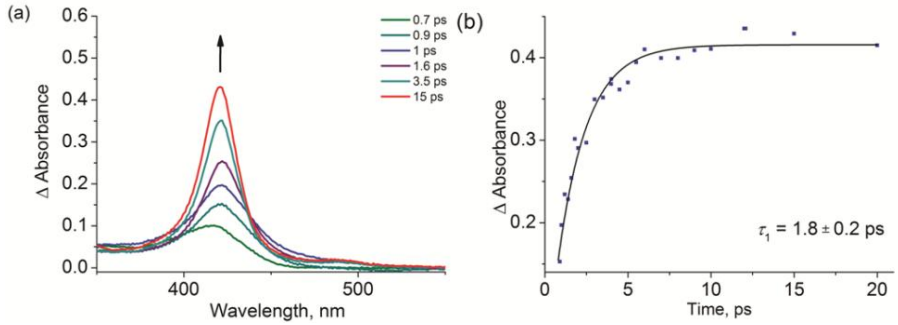

Figure 4.17 Excited state dynamic changes of rotaxane **H⊂M** on excitation at 310 nm in TA spectra. (a) Single exponential growth of the band at 422 nm and (b) its kinetics (τ_1 = 1.8 ± 0.2 ps).

The eventual formation of the polyyne triplet state was confirmed by carrying out TA experiments of the rotaxane **H⊂M** in presence of β-carotene.[56] Excitation of the **H⊂M** at 355 nm resulted in triplet-triplet sensitization of the β-carotene (Figure 4.18). The processes observed by TA and TRIR are summarized in Figure 4.19.

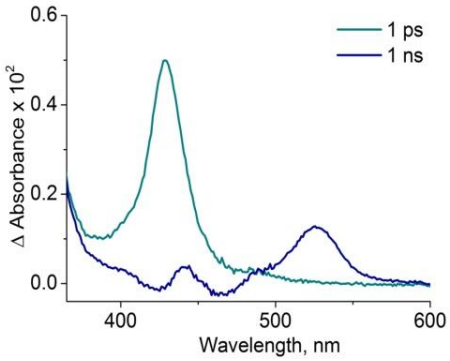

Figure 4.18 TA spectra measured in deoxygenated CH_2Cl_2 upon the excitation of rotaxane **H⊂M** with 355 nm laser in presence of *β*-carotene (~150 mM). After 1 ps the singlet polyyne band at 422 nm is visible, later, 1 ns after excitation, the singlet polyyne band disappears and new band appear at 526 nm corresponding to the triplet excited state β-carotene.[56] The triplet β-carotene formation is the result of the energy transfer from triplet excited polyyne. Unfortunately, the triplet polyyne band at 343 nm is obscured by excitation laser and is not visible.

Table 4.2 Excited state bands, transitions and lifetimes for rotaxane **H⊂M** excited at 310 nm in CH_2Cl_2.

TRIR band	Lifetime (τ)	Assignment	TA band	Lifetime (τ)	Assignment
2077 cm^{-1}	0.44 ± 0.02 ns	$S_1 \rightarrow T_1$ decay	422 nm	1.8 ± 0.2 ps	$S_n \rightarrow S_1$ growth
2047 cm^{-1}	0.42 ± 0.05 ns	$S_1 \rightarrow T_1$ growth	422 nm	0.44 ± 0.02 ns	$S_1 \rightarrow T_1$ decay
1741 cm^{-1}	0.42 ± 0.01 ns	$S_1 \rightarrow T_1$ decay	343 nm	0.55 ± 0.02 ns	$S_1 \rightarrow T_1$ growth
1610 cm^{-1}	0.38 ± 0.02 ns	$S_1 \rightarrow T_1$ growth			
2047 cm^{-1} [a]	0.88 ± 0.04 μs	$T_1 \rightarrow S_0$ decay			
1610 cm^{-1} [a]	1.04 ± 0.05 μs	$T_1 \rightarrow S_0$ decay			
1610 cm^{-1} [ab]	14.0 ± 2.2 μs	$T_1 \rightarrow S_0$ decay			

[a] Excited at 266 nm; [b]in O_2-free CH_2Cl_2.

Table 4.3 Excited state bands, transitions and lifetimes for rotaxane **H⊂M** excited at 350 nm in CH_2Cl_2.

TRIR band	Lifetime (τ)	Assignment	TA band	Lifetime (τ)	Assignment
2077 cm^{-1}	0.50 ± 0.01 ns	$S_1 \rightarrow T_1$ decay	422 nm	3.2 ± 0.4 ps	*EET*, S_1 growth of hexayne
2047 cm^{-1}	0.44 ± 0.02 ns	$S_1 \rightarrow T_1$ growth	422 nm	0.42 ± 0.04 ns	$S_1 \rightarrow T_1$ decay
1741 cm^{-1}	0.48 ± 0.01 ns	$S_1 \rightarrow T_1$ decay			
1610 cm^{-1}	0.45 ± 0.02 ns	$S_1 \rightarrow T_1$ growth			
1506 cm^{-1}	3.2 ± 0.2 ps	*EET*, S_1 decay of macrocycle			
1741 cm^{-1}	2.7 ± 0.2 ps	*EET*, S_1 growth of hexayne			

4.7.4 Excited state dynamics of $Re(CO)_3Cl$-macrocycle complex M(Re)

The excited state dynamics of 1,10-phenanthroline-based $Re(CO)_3Cl$ complexes have been thoroughly described in the literature,[44,57] and will only be outlined briefly here for discussion of changes when part of the rotaxane. Optical excitation creates both ^{1}IL and ^{1}MLCT states that undergo intersystem crossing to at least two thermally equilibrating, 'hot', triplet ^{3}IL and ^{3}MLCT states, over ~150 fs. The IL state arises from phenanthroline π-π* transition, and the MLCT state involves the d orbitals of Re atom. Internal

conversion between the ^{3}IL and ^{3}MLCT states takes place on a timescale of ps to ns, depending on the solvent and ligand structure. Later, the ^{3}MLCT state relaxes to the vibrationally cooled lowest excited state, which decays on the ns time-scale via radiative and non-radiative pathways.[58]

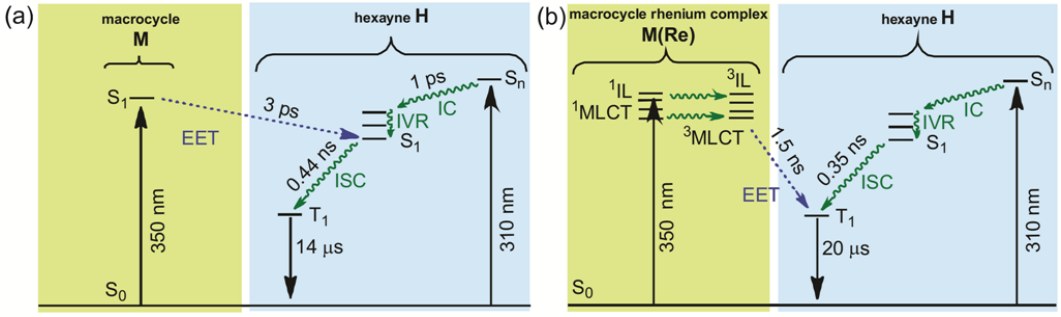

Figure 4.19 Energy diagram summarizing excited-state processes in (a) dumbbell **H** and rotaxane **H⊂M**, and (b) **M(Re)** and $Re(CO)_3Cl$·rotaxane complex **H⊂M(Re)**.

On excitation of **M(Re)** at 350 nm, TRIR spectra show several positive red-shifted bands, as well as negative bands originating from the depleted ground state (Figure 4.20a). The broad positive band at 1935–2005 cm^{-1} represents the overlap of two A" and A'(2) excited state bands.[58d,e,59a] The time-dependent shift of these two bands is complex, as it incorporates the instantaneous shift, as a result of Frank-Condon excitation and formation of hot singlet states, the ISC, the establishment of the equilibrium between ^{3}IL and lower ^{3}MLCT states; probably, the initial IVR of the hot ^{3}MLCT state and all these processes are accompanied with solvent reorganization.[58,59]

Over 10 ps, the low energy shoulder of the excited state A" band decreases. The higher energy weak shoulder next to the excited state A'(2) band also decreases over 10 ps. The A"and A'(2) collective band undergoes a ~17 cm^{-1} shift to higher frequency with a 26% intensity increase, while the ground state A" band bleach increases by 22%. The bleach intensity changes can be attributed to an overlapping absorption decrease, (lower absorption cross section) which originates from the ^{3}IL state and which decays over a short time by the conversion of the ^{3}IL to the ^{3}MLCT state.[61a] The second excited band (A'(1)) at 2054 cm^{-1} shows a more pronounce intensity increase (62%), hypsochromic shift (12 cm^{-1}) and band narrowing (64%) (Figure 4.20a). Whereas the shift to higher frequency is due to an increasing contribution of the ^{3}MLCT state,[69a] the band-narrowing, apparently involves vibrational relaxation steps, stemming from local-solvent reorganization. These spectral changes resemble the exited state dynamics of the $Re(CO)_3$(4-Et-pyridine) 2,2'-bipyridine complex.[60] We ascribe the final TRIR spectral pattern, seen at longer time

delays, to the relaxed lowest excited-state ^{3}MLCT (see Figure 4.19 for a summary of the excited states and kinetics).

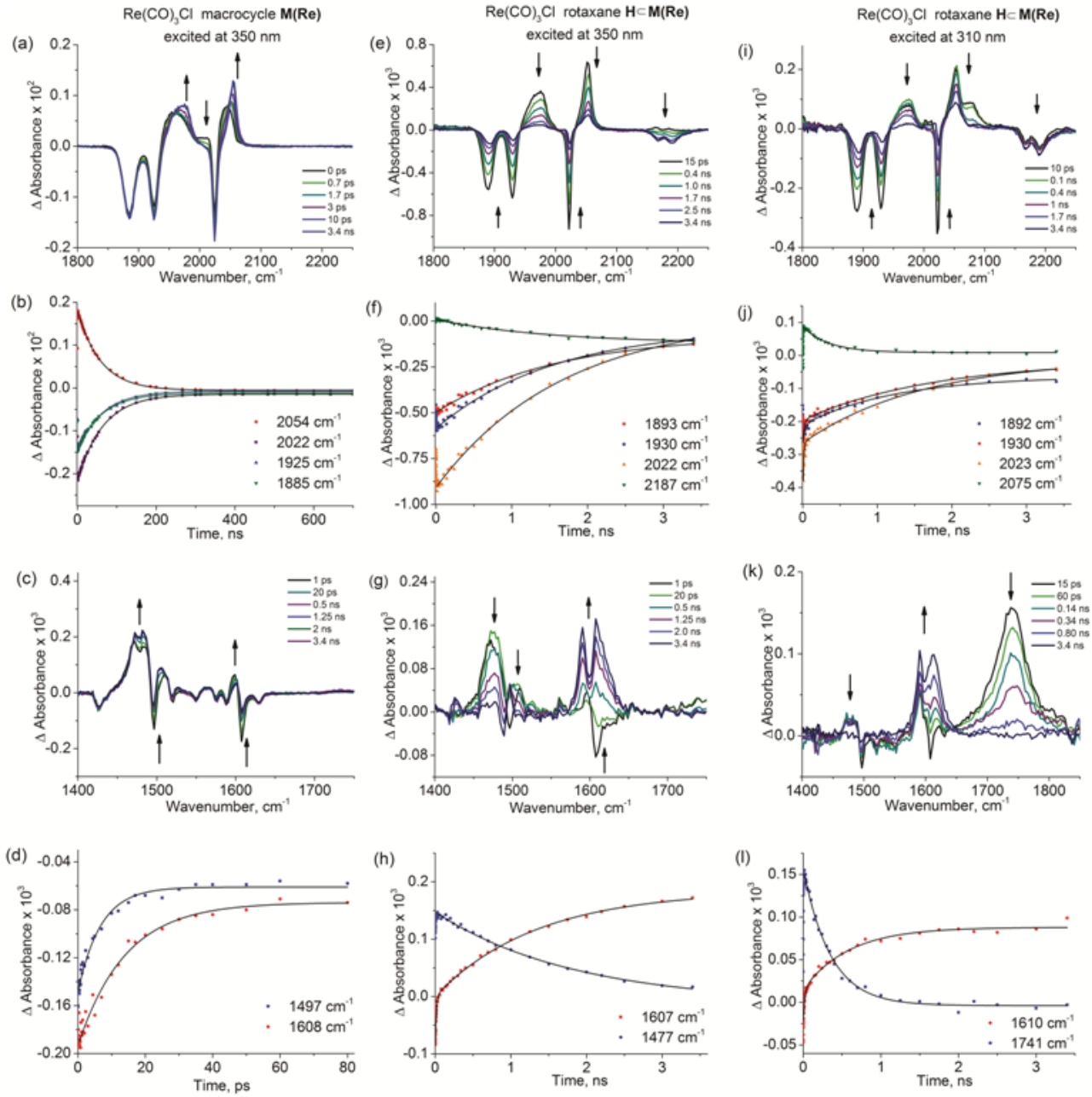

Figure 4.20 TRIR spectra and excited state kinetics of the **M(Re)** (a–c) excited at 350 nm, **H⊂M(Re)** excited at 350 nm (d–f) and 310 nm (g–i). Laser energy: 100–200 nJ; solvent: CH_2Cl_2.

We were interested to estimate the lifetime of the ^{3}MLCT triplet excited state of the $Re(CO)_3Cl$·macrocycle **M(Re)**. Kinetic data were extracted from TRIR spectra, exciting the molecule at 266 nm. All negative and positive bands show similar single-exponential kinetics. The triplet lifetime is 93 ns under oxygen-free conditions (Figure 4.20) and 63 ns in the presence of air (Figure 4.19b, Table 4.4).

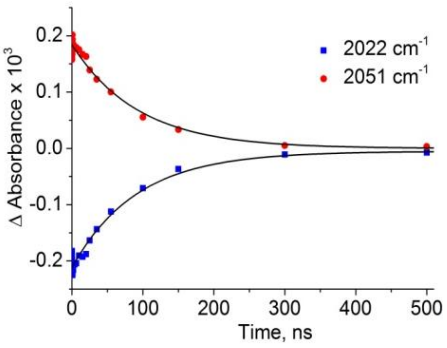

Figure 4.21 The kinetics of the decay of triplet excited M(Re) in deoxygenated CH_2Cl_2, extracted from the bleach recovery of A" ground state band (2022 cm^{-1}, τ_1 = 92.3 ± 6.4 ns) and the decay of excited state A" band (2051 cm^{-1}, τ_1 = 93.6 ± 7.2 ns).

In the fingerprint region of the TRIR spectrum of **M(Re)**, two bleaches of ground-state bands at 1497 cm^{-1} and 1608 cm^{-1} appear immediately after excitation, and recover within ~30–40 ps while the transient bands 1480 cm^{-1} and 1595 cm^{-1} grow slightly (Figure 4.20c). The positions of the bleach-bands in **M(Re)** and **M** are similar, suggesting that they originate from the phenanthroline framework, and are not strongly perturbed by the presence of the Re-localized triplet state. Furthermore, in **M(Re)**, these bands show single-exponential recovery kinetics (1497 cm^{-1}: τ_1 = 6.8 ± 0.6 ps; 1608 cm^{-1}: τ_1 = 14.0 ± 1.2 ps; Figure 4.19d), on a timescale similar to the ν(CO) shifts observed in the transients in the carbonyl stretching region. Thus we tentatively assign the bleach recovery at 1497 cm^{-1} and 1608 cm^{-1} to the cooling and IVR of the initially formed hot states.

4.7.5 The EET in the $Re(CO)_3Cl$·rotaxane complex H⊂M(Re).

The ground state CO and C≡C stretch vibrations of **H⊂M(Re)** occur at different frequencies, allowing each component to be observed separately. TRIR spectra of **H⊂M(Re)** following excitation of the macrocycle component at 350 nm show immediate bleaching of ground state carbonyl stretching bands (Figure 4.22). The excited state CO bands at 2051 cm^{-1} and 1975 cm^{-1} shift to high frequencies within 20 ps, due to the $^3IL \rightarrow {}^3MLCT$ conversion and vibration relaxation, as in **M(Re)**. However, in contrast to **M(Re)**, the CO bleaches of **H⊂M(Re)** undergo rapid recovery (Figure 4.20e.g). The recovery of the CO bleach is accompanied by bleaching of the C≡C band at ~2190 cm^{-1}, indicating energy transfer from $Re(CO)_3Cl$·macrocycle to the hexayne chain. The rate of C≡C bleaching matches that of the recovery of all three CO bands (Figure 4.19f). Kinetic data are summarized Table 4.4.

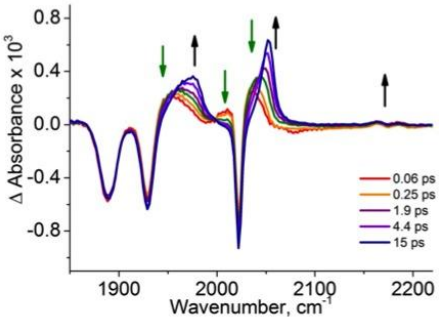

Figure 4.22 TRIR spectra of $Re(CO)_3Cl$·rotaxane complex **H⊂M(Re)** in polyyne stretching region at early time delays (0–15 ps). Excitation λ = 350 nm; laser energy = 200 nJ, solvent: CH_2Cl_2.

The TRIR spectra of **H⊂M(Re)** in the high frequency region do not reveal the nature of energy transfer, as the triplet and singlet state bands of the hexayne at 2040–2080 cm^{-1} overlap with excited state A'(1) band. The necessary information was obtained from the fingerprint region: The initial bleach of the excited $Re(CO)_3Cl$·macrocycle at 1607 cm^{-1} band recovers and then the band corresponding to the triplet state hexayne at *ca.* 1610 cm^{-1} grows over 2 ns (Figure 4.20h). At the same time the triplet $Re(CO)_3Cl$·macrocycle band around 1470 cm^{-1} decays (τ_1 = 1.86 ± 0.15 ns). These spectral changes clearly demonstrate triplet-triplet energy transfer from the $Re(CO)_3Cl$·macrocycle moiety to the threaded hexayne.

The growth kinetics of the 1607 cm^{-1} band (Figure 4.20h) are biexponential (τ_1 = 14.0 ± 0.6 ps, A_1 = 0.35; τ_2 = 1.13 ± 0.05 ns, A_2 = 0.65) with the fast component matching that of decay of the bleach at 1607 cm^{-1} in $Re(CO)_3Cl$·macrocycle **M(Re)**. This implies that in excited **H⊂M(Re)** initially the $^3IL \rightarrow {}^3MLCT$ conversion with vibrational cooling and solvent reorganization take place prior to triplet energy transfer to the hexayne from a relaxed ^3MLCT state. Indeed, the hexayne ground state C≡C band at ~2200 cm^{-1} does not show any bleach over the first 20–30 ps, while the $^3IL \rightarrow {}^3MLCT$ and other relaxations take place (Figures 4.20g).

The TRIR spectra of **H⊂M(Re)** using excitation at 350 nm did not show any singlet excited state polyyne band, before or after energy transfer, excluding the possibility of singlet energy transfer from the $Re(CO)_3Cl$·macrocycle. Singlet energy transfer does not occur because intersystem crossing in the $Re(CO)_3Cl$·macrocycle complexe is ultrafast, and all spectral changes originate from triplet excited $Re(CO)_3Cl$·macrocycle. Thus, triplet sensitization of the hexayne in **H⊂M(Re)** upon excitation of the molecule at 350 nm explains the quenching of emission of $Re(CO)_3Cl$·macrocycle **M(Re)** at room

temperature by the threaded dumbbell. To estimate the triplet energy transfer efficiency, we compared the relative intensities of the C≡C at ~2200 cm^{-1} and A'(1) C=O bands at 2054 cm^{-1} in the ground state IR spectrum ($A/B = GS_r = 6.71$; top) with that of the same bands when maximally bleached (15 ps and 45 ns after excitation, respectively, under air) in the TRIR spectra ($C/D = ES_r = 6.81$) (Figure 4.23). The triplet energy transfer efficiency (^3EET) was estimated using the equation:

$$\phi\,{}^{3}{}_{EET} = \frac{GS_r}{ES_r}$$

This calculation gave $\Phi_{EET} = 6.71/6.81 = 0.99$. The same calculation was also carried out using TRIR spectra from an oxygen-free solution of **H⊂M(Re)**; under these conditions, the bleach of the C≡C and A'(1) C=O bands were most intense 15 ps and 5.50 μs after excitation, respectively; $C/D = ES_r = 6.72$ (Figure 4.23); $\Phi_{EET} = 6.71/6.72 = 1.00$.

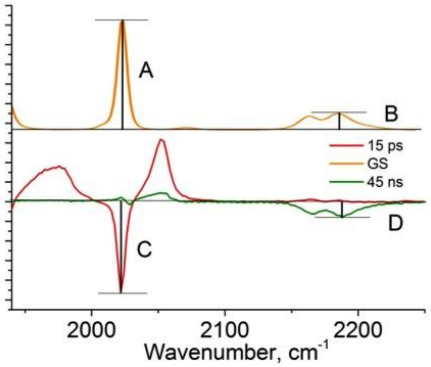

Figure 4.23 Comparison of IR and TRIR spectral intensities for **H⊂M(Re)**.

Another noteworthy feature of the **H⊂M(Re)** rotaxane is the perturbation of the ground state hexayne by excited **M(Re)** (after excitation, before energy transfer) which appears as a slightly enhanced absorption at ~2200 cm^{-1} (Figures 4.12e and 4.24). Later, when **M(Re)** is in its relaxed state, after EET, the carbonyl bleaches do not reach to the asymptotic level, although all positive transient bands disappear (Figure 4.24) as a result of electronic perturbation by the nearby triplet hexayne. In both cases, this effect serves to report the presence of a nearby excited state constituent. The triplet state polyyne lifetimes in deoxygenated and oxygen-containing solutions (Figure 4.24) are similar to those of the rotaxane **H⊂M** (Table 4.2). These processes are summarized in Figure 4.19b.

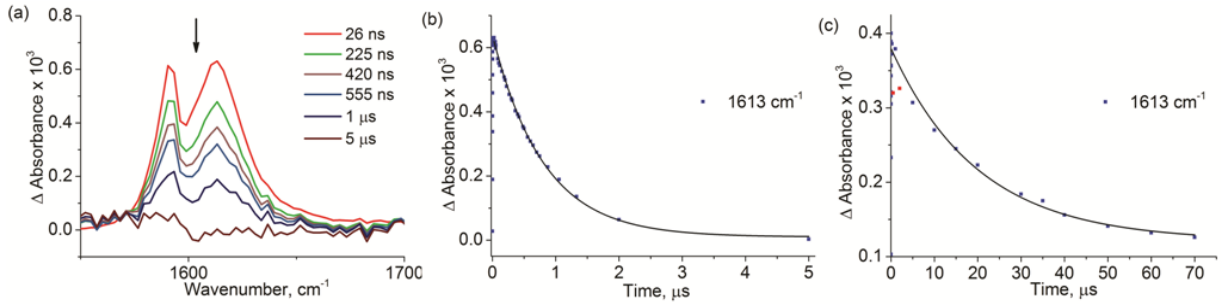

Figure 4.24 (a) TRIR spectra of $Re(CO)_3Cl$·rotaxane **H⊂M(Re)** complex in fingerprint region. (b) Kinetics of 1610 cm^{-1} triplet band in oxygen containing ($\tau 1$ = 0.81 ± 0.02 μs) and (c) deoxygenated CH_2Cl_2 (τ_1 = 20.2 ± 1.7 μs). Excitation λ = 266 nm; laser energy = 100 nJ.

Direct excitation of the hexayne component of **H⊂M(Re)** at 310 nm generates the singlet state hexayne via direct excitation, as well as triplet macrocycle (Figure 4.20i) followed by triplet energy transfer to the hexayne. In Figure 4.20i, for example, the band around 2070 cm^{-1}, corresponding to singlet hexayne, decreases gradually (τ_1 = 0.35 ± 0.03 ns) while the C≡C bleach, which appeared immediately upon excitation, increases (~2200 cm^{-1}) due to triplet energy transfer from macrocycle to hexayne. Upon triplet EET the excited macrocycle bands also decrease and the ν(CO) bleach recovers (Figure 4.20, Table 4.5). Comparable changes are observed in fingerprint region (Figure 4.20k) where the singlet hexayne band at 1741 cm^{-1} decreases and triplet band at 1610 cm^{-1} increases. Kinetic analysis of the fingerprint region shows that the singlet hexayne band at 1741 cm^{-1} decays in a single-exponential fashion (Figure 4.20l, τ_1 = 0.35 ± 0.01 ns); the decay constant matches that of the singlet band at 2070 cm^{-1}.

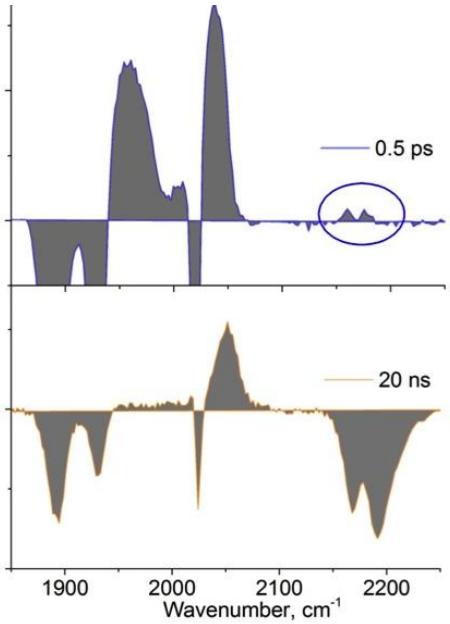

Figure 4.25 TRIR spectra of **H⊂M(Re)** showing the mutual electronic perturbation of components. Top picture shows the enhanced ground state ν(C≡C) band absorption (circled) due to nearby triplet **M(Re)**. Bottom picture shows that despite the transients of **M(Re)** disappeared due to EET, however, the ground state ν(CO) bands (negative bleach) still are visible as an effect of nearby triplet dumbbell.

TA spectra of **H⊂M(Re)** excited at 310 nm show the formation of singlet and triplet excited states similar to rotaxane **H⊂M** and hexayne **H** excited at 310 nm (Figure 4.9a,c). Within 5 ps the band of the singlet hexayne at 422 nm grows over the broad transient envelope band of the macrocycle (Figure 4.26). The singlet state band at 422 nm decays single-exponentially with τ_1 = 0.34 ± 0.01 ps. The broad band of the macrocycle also decreases and the growth of hexayne triplet band at 343 nm is single-exponential (τ_2 = 0.49 ± 0.02 ns, Figure 4.9f). Both τ_1 and τ_2 values agree with the TRIR data. The kinetic data are summarized in Table 4.4 and Table 4.5.

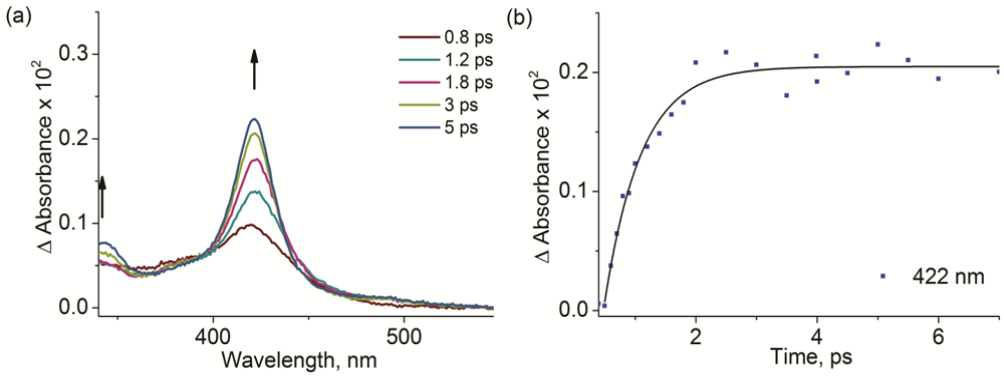

Figure 4.26 TA spectra of $Re(CO)_3Cl$·rotaxane **H⊂M(Re)** in CH_2Cl_2 (excitation λ = 310 nm). (a) The growth of the singlet and triplet polyyne transient bands, and (b) the single exponential growth of singlet S_1 polyyne transient at 422 nm (τ_1 = 0.60 ± 0.6 ps).

Table 4.4 Excited state bands, transitions and lifetimes for **H⊂M(Re)** excited at 350 nm in CH_2Cl_2.

TRIR band	Lifetime (τ)	Assignment
1470 cm^{-1}	1.86 ± 0.15 ns	^{3}EET, T_1 decay of macrocycle
1610 cm^{-1}	14.0 ± 0.6 ps (A_1 = 0.35)	relaxation
	1.10 ± 0.05 ns (A_2 = 0.65)	^{3}EET, growth of T_1 polyyne
1892 cm^{-1}	1.59 ± 0.12 ns	νCO_{gs} bleach (decaying); ^{3}EET
1930 cm^{-1}	1.50 ± 0.11 ns	
2022 cm^{-1}	1.70 ± 0.09 ns	
2185 cm^{-1}	1.44 ± 0.12 ns	νC≡C bleach (growing); ^{3}EET
1610 cm^{-1} [a]	20.2 ± 1.7 μs	polyyne $T_1 \rightarrow S_0$ decay

[a] Excited at 266 nm and measured in O_2-free CH_2Cl_2.

Table 4.5 Excited state bands, transitions and lifetimes of $Re(CO)_3Cl$·rotaxane **H⊂M(Re)** excited at 310 nm in CH_2Cl_2.

TRIR band	Lifetime (τ)	Assignment	TA band	Lifetime (τ)	Assignment
1892 cm^{-1}	10.8 ± 2.0 ps, A_1 = 0.38, 1.14 ± 0.11 ns, A_2 = 0.62	T_1, νCO	422 nm 422 nm	0.60 ± 0.6 ps 0.34 ± 0.01 ns	S_1 growth S_1 decay
1930 cm^{-1}	8.20 ± 0.88 ps, A_1 = 0.5, 1.60 ± 0.17 ns, A_2 =0.5	T_1, νCO			
2023 cm^{-1}	9.60 ± 1.15 ps, A_1 = 0.43, 1.71 ± 0.19 ns, A_2 = 0.57	T_1, νCO			
2075 cm^{-1}	0.36 ± 0.03 ps	S_1 decay of hexayne			
1610 cm^{-1}	12.2 ± 1.6 ps, A_1 = 0.35, 0.54 ± 0.04 ns, A_2 =0.65	T_1 growth of hexayne			
1741 cm^{-1}	0.35 ± 0.01 ns	S_1 decay of hexayne			

4.8 Time-resolved anisotropy

TRIR anisotropy data were obtained for **H**, **M(Re)** and **H⊂M(Re)** by manipulating the polarization between pump light and probe IR beams.

Separately, the anisotropy of **H** was determined from the bleach of ground state and S_1 excited state ν(C≡C) modes. The bleach of the C≡C ground state band and singlet band at 2077 cm^{-1} show intensity dependence on the angle of the probing beam (90°-perpendicular (⊥), 0°-parallel (∥) or 54.7°-magic). The spectra shown below are measured at 20 ps after excitation when the molecule is in its relaxed S_1 state (Figure 4.27).

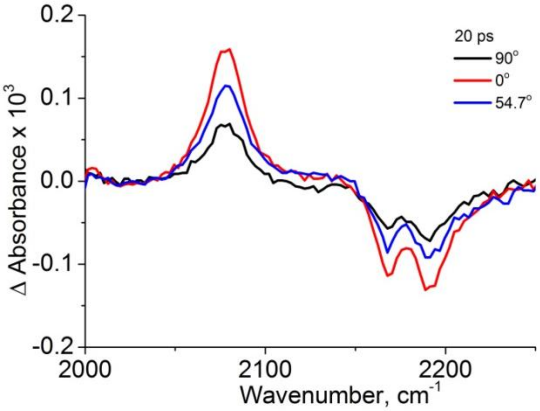

Figure 4.27 TRIR spectra of hexayne **H** measured at 20 ps after excitation. The probing beam was fixed at parallel, perpendicular or magic angle position regarding the pumping beam. Excitation λ = 310 nm; laser energy = 80 nJ, solvent: CH_2Cl_2.

The anisotropy is calculated according to the equation:

$$r = \frac{I_{\parallel} - I_{\perp}}{I_{\parallel} + 2I_{\perp}} \quad (4.1)$$

Calculated anisotropy from the S_1 singlet excited band at 2077 cm^{-1} is 0.29. This value is close to the theoretical one (condition, when transition dipoles in the ground and excited states are collinear, and there are not processes which result in depolarization, the excited state population is preferentially oriented along the *z*-axis and the value of $I_{\perp}$is one-third the value of $I_{||}$ ($I_{||} = 3I_{\perp}$), the anisotropy is 0.4) indicating that orientation of the dipole moments between excitation and S_1 conversion is nearly parallel at t = 20 ps. The anisotropy measured from the ground state 2191 cm^{-1} band is 0.25. The anisotropy values are slightly less than those obtained from fluorescence anisotropy studies of α,ω-diphenylpolyynes which can be the result of significant bending of polyyne chain of **H** in solution.[39b]

To estimate the rate of the depolarization of the molecule the equation (4.2) was used,[61]

$$r(t) = \frac{I_{\parallel}(t) - I_{\perp}(t)}{I_{\parallel}(t) + 2I_{\perp}(t)} \quad (4.2)$$

where $r(t)$, $I_{||}(t)$ and $I_{\perp}(t)$ are the anisotropy, parallel and perpendicular intensity at particular t time delay, respectively. Then the $r(t)$ values were plotted against the time delays (Figure 4.28).

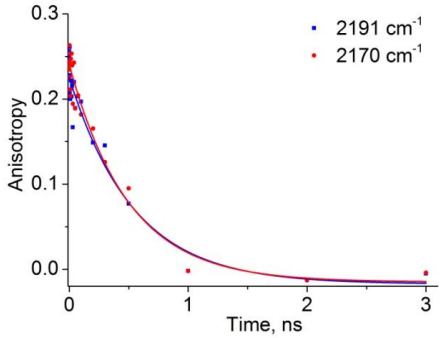

Figure 4.28 Depolarization of the **H** estimated from the bleach band.

We followed the depolarization of the **H** through two ν(C≡C) bands at 2170 cm^{-1} and 2191 cm^{-1} and both showed similar depolarization rates. The measured polarization decay rate of hexayne **H** is single exponential with $\tau \sim 0.50$ ns. To our knowledge, this is the first anisotropy decay report for polyynes. The kinetic data are summarized in the Table 4.6.

Table 4.6 Anisotropy values and decay rates of the **H** estimated from the bleach bands. r_0 is extrapolated to 0 time from the decay curves.

Band	Lifetime (τ)	r	r_0
2170 cm^{-1}	0.50 ± 0.09 ns	0.24	0.26
2191 cm^{-1}	0.54 ± 0.1 ns	0.29	0.29

The anisotropy (*r*) of **M(Re)** is measured 1 ps after excitation (350 nm). For ground state A'(2) band *r* = 0.21 and for A" band *r* = -0.16. The third A'(1) band is not polarized (Figure 4.29). These values are different from the reported anisotropy measurements for $Re(R\text{-}bpy)(CO)_3Cl$ (R = COOH, bpy = 2,2'-bipyridine) complex.[54] The excited state ν(CO) bands show insignificant polarization. Depolarization (tumbling) rate of **M(Re)** is $\tau \sim 80$ ps, almost 6 time faster than **H** which is not a surprise considering the bulky nature of the dumbbell.

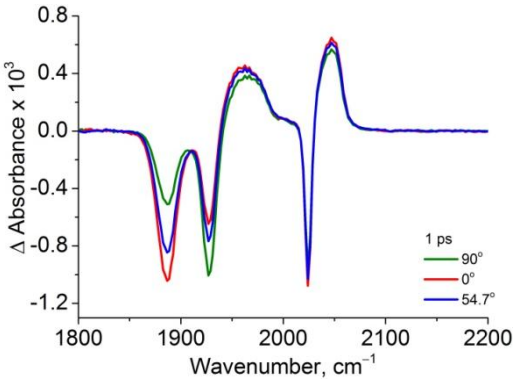

Figure 4.29 Excitation of **M(Re)** complex at 350 nm showed pronounced polarization effect.

The *r* absolute values are close to each other but are opposite by sign which indicates that vibrational transition vectors of two *A'(2)* and *A''* modes align perpendicular to each other. Two excited state bands at 1975 cm^{-1} and 2054 cm^{-1} showed very little (0.04-00.05) anisotropy value which is not taken into consideration. We followed the anisotropy dynamic of **M(Re)** molecule using equation (2) and plotting *r(t)* time evolution (Figure 4.30).

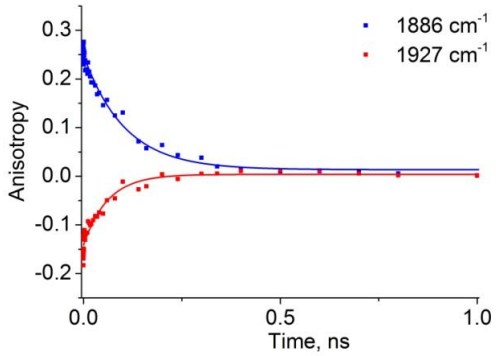

Figure 4.30 The anisotropy decay of **M(Re)** estimated from *A'(2)* and *A''* modes.

The kinetic data are summarized in Table 4.7.

Table 4.7 The anisotropy decay kinetics of **M(Re)** estimated from *A'(2)* and *A''* modes. r_0 is extrapolated to 0 time from the decay curves.

TRIR band	Lifetime (τ)	r	r_0
1886 cm^{-1} (*A'(2)*)	-	0.06	-
2022 cm^{-1} (*A'(1)*)	-	-0.06	-
2077 cm^{-1}	0.23 ± 0.05 ns	0.32	0.35
2191 cm^{-1}	0.40 ± 0.1 ns	0.29	0.39

When excited at 310 nm both ν(CO) and ν(C≡C) bands in the **H⊂M(Re)** show polarization (Figure 4.31). Ground state (bleach) and S_1 excited state ν(C≡C) bands have anisotropy values, similar to the free dumbbell **H** (Table 4.8). In contrast to the **M(Re)**, the ground state A'(2) bleach of $Re(CO)_3Cl$·macrocycle in **H⊂M(Re)** has positive polarization (r = +0.06), the second bleach (A") is not polarized and the third (A'(1)) band anisotropy value is (r = –0.06).

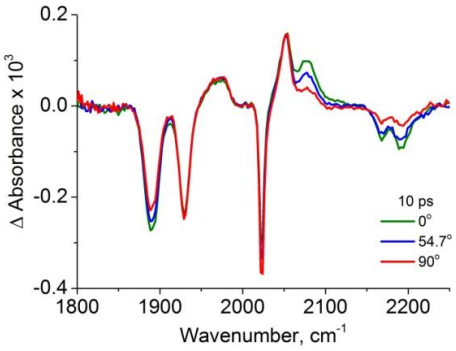

Figure 4.31 Polarization of **H⊂M(Re)** excited at 310 nm.

The orientation of transition vectors of CO vibrations of $Re(CO)_3Cl$·macrocycle in **H⊂M(Re)** is changed in a way that A'(2) mode becomes polarized while (A") mode loses its anisotropy. The excited state ν(CO) bands have almost no anisotropy, similar to the **M(Re)**. All data are summarized in the Table 4.8.

Table 4.8 Calculated anisotropy values and decay kinetics for **H⊂M(Re)** rotaxane excited at 310 nm, after 10 ps delay. r_0 is extrapolated to 0 time from the decay curves.

TRIR band	Lifetime (τ)	r	r_0
1886 cm^{-1} (*A'(2)*)	104 ± 7 ps	0.21	0.27
1927 cm^{-1} (*A''*)	63 ± 3 ps	–0.16	–0.18

The depolarization rate of the dumbbell in **H⊂M(Re)** is τ ~0.4 ns (estimated for 2191 cm^{-1} band, Table 4.8, Figure 4.32), faster than depolarization of **H** (0.4 ns vs 0.5 ns). This is unusual as the increase in the volume of the molecule (from **H** to **H⊂M(Re)**) it is expected to slow down the rotational and translation

motion, therefore, the depolarization rate; the faster depolarization in **H⊂M(Re)** may reflect the mobility and nonlinearity of the threaded hexayne unit.

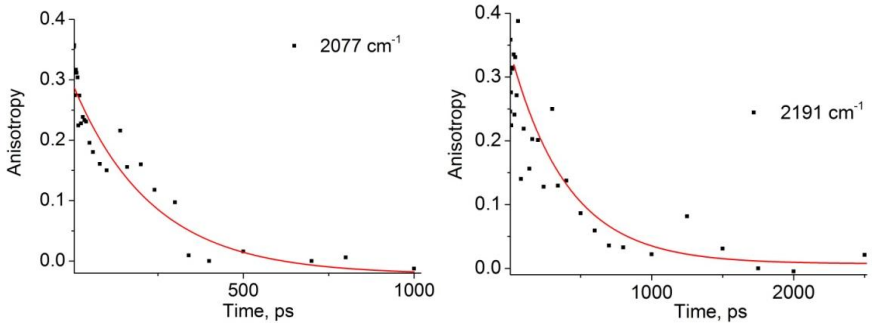

Figure 4.32 Anisotropy decay kinetics of dumbbell in **H⊂M(Re)** estimated for 2077 cm^{-1} singlet band (left) and 2191 cm^{-1} bleach band (right).

The anisotropy of the ν(CO) bands in **H⊂M(Re)** is calculated 1 ps after excitation of the molecule at 350 nm (Figure 4.33). Anisotropy value of ground state A'(2) band from the bleach is –0.17, slightly less than in **M(Re)**. For A" band r = +0.14, similar to anisotropy measured for **M(Re)**. The third A'(1) band and excited state ν(CO) bands are not polarized similar to the **M(Re)**. The anisotropy of ν(CO) modes in **H⊂M(Re)** is different when the molecule is excited at 310 and 350 nm.

Depolarization of $Re(CO)_3Cl$·macrocycle in **H⊂M(Re)** is connected mostly to the non-directional rotation of the macrocycle around polyyne axle. The depolarization rate is $\tau \sim 0.27$ ns (averaged from two A'(2) and A", Table 4.9) more than 3 time slower than the free **M(Re).** The change in dynamics of anisotropy decay of macrocycle in **H⊂M(Re)** must be result of the staggering of macrocycle rotation by bulky end-groups and weak interaction of carbonyl groups with polyyne chain π-system (see crystal structure). However, we would not exclude the influence of decreased degree of Brownian motion on depolarization when macrocycle is threaded with the dumbbell.

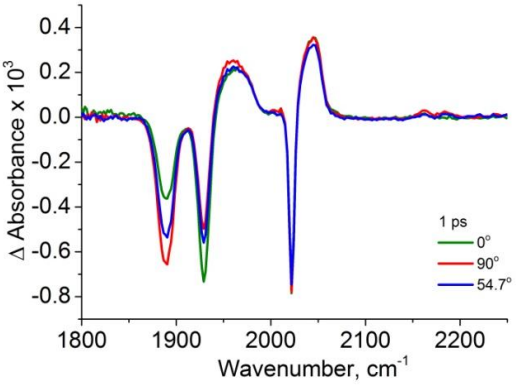

Figure 4.33 The anisotropy of the ν(CO) bleaches are calculated 1 ps after excitation of the **H⊂M(Re)** at 310 nm.

Anisotropy decay dynamics were calculated using equation (2) and plotting the *r(t)* against time (Figure 4.34).

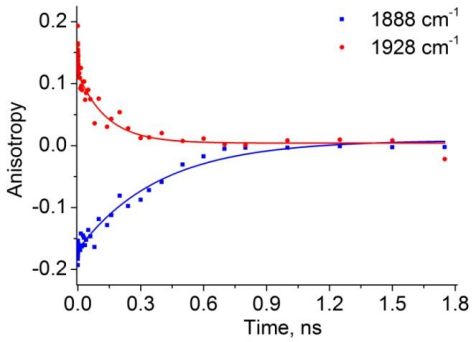

Figure 4.34 The anisotropy decay kinetics for *A′(2)* and *A″* modes in the **H⊂M(Re)** excited at 350 nm.

The anisotropy decay kinetics for *A′(2)* and *A″* modes is summarized in the Table 4.9.

Table 4.9 Summary of anisotropy decay kinetics of the **H⊂M(Re**) excited at 350 nm.

TRIR band	Lifetime (τ)
1888 cm^{-1} (*A′(2)*)	0.39 ± 0.04 ns
1928 cm^{-1}(*A″*)	0.14 ± 0.02 ns

4.9 Conclusion

Despite the alluring elemental simplicity of their molecular structures, polyyne chromophores exhibit remarkably rich and complex photophysical behavior. Here we have shown that TRIR is an excellent technique for probing their excited state dynamics. We have also demonstrated that rotaxane synthesis is a powerful strategy for fixing a photoactive unit near the center of a polyyne chain, for studying singlet and triplet energy transfer through space, between non-bonded components. The X-ray crystallography showed significant bending of the polyyne chain in the **H⊂M(Re)** and close-contacts between CO and polyyne units. The macrocycle and dumbbell in the **H⊂M(Re)** rotaxane did not show spectroscopically significant

interactions in the ground state, while the excited state TRIR spectra revealed mutual electronic perturbation of both components. The mechanism of the quenching of the emission from $Re(CO)_3$·macrocycle in the **H⊂M(Re)** was found to be triplet energy transfer from the lowest metal-to–ligand charge transfer (^{3}MLCT) excited state of the **M(Re)** to the ground state **H** hexayne (time constant: τ = 1.5 ns). Surprisingly, an efficient singlet energy transfer from the excited macrocycle **M** to the threaded hexayne **H** dumbbell in the rotaxane **H⊂M** was observed: The energy transfer takes place within a few ps without creating 'hot' vibrational states in hexayne. Additionally, we carried out comprehensive examination on photophysics of bare hexayne, characterizing the internal conversion (IC) by UV-vis TA, for the first time by NIR-TA, and the vibrational cooling of the singlet excited states by TRIR spectroscopy. The anisotropy data allow us to estimate depolarization rates of **H⊂M(Re)** and its individual components. Time-dependent anisotropy decay kinetics showed that the rate of depolarization of **M(Re)** in **H⊂M(Re)** slowed down three times compared to the free **M(Re)** as a result of hindered rotation of the macrocyclic component upon threading the linear axle.

Previously it was found that butadiyne bridges can mediate quantitative *intramolecular* triplet EET between covalently bonded chromophores.[62] Here we demonstrate the *intermolecular* triplet EET properties of polyynes in a covalently non-bonded rotaxane. The singlet and triplet excitation energy harvesting properties of polyynes resemble those of the carotenes, which harvest both triplet and singlet energy in photosynthetic systems.[63] It is intriguing to consider why nature exclusively preferred conjugated double rather triple bonds for photosynthetic energy transfer. Understanding the excited states of polyyne in supramolecular assemblies, such as the rotaxane studied here, is important for further application of materials based on chains of linear sp^1 carbon atoms in molecular and optoelectronic devices.[1] This study demonstrates how the photochemistry of a system can be controlled through non-bonded interactions, without altering the chromophore or relying on diffusion, through synthesis of rotaxane architectures.

4.10 Experimental Section: Materials

The unthreaded hexayne dumbbell **H**,[17] and macrocycle **M**[18] were prepared as described previously. Synthesis of rotaxane **H⊂M** is described in Chapter 2. **H⊂M(Re)** and $Re(CO)_3Cl$·macrocycle **M(Re)** complexes are synthesized according the published procedure.[16]

M(Re): A solution of the macrocycle **M1** (50.0 mg, 0.08 mol) and rhenium(I) pentacarbonyl chloride (35.4 mg, 0.098 mol) in toluene (6.0 mL) was refluxed under nitrogen for 4 h. The solution was cooled to 20 °C, solvent removed and the residue dried under vacuum. The column chromatography of the residue (silica gel, PE 40/60 : EtOAc : CH_2Cl_2 = 1 : 1 : 4) followed by precipitation from hexanes afforded the product as a yellow solid (47.0 mg, 63.0%). ^{1}H NMR (400 MHz, CD_2Cl_2, 298 K) 8.60 (d, *J* = 8.4, 2H, H_b), 8.06 (s, 2H, H_a), 7.99 (d, *J* = 8.4, 2H, H_c), 7.71 (br. s, 4H, H_d), 7.13–7.08 (m, 5H, $H_{f,e}$), 6.48–6.43 (m, 3H, $H_{g,h}$), 4.19–4.07 (m, 4H, H_j), 3.93 (t, *J* = 6.3, 4H, H_i), 1.91–1.71 (m, 8H, $H_{k,l}$), 1.6–1.4 (m, 8H, $H_{m,n}$). ^{13}C NMR (125 MHz, $CDCl_3$, 298 K) 193.7, 192.5, 164.4, 160.9, 160.4, 148.7, 137.7, 134.3 (br.), 132.0 (br.), 129.7, 129.6, 126.7, 126.2, 116.1 (br.), 113.9 (br.), 107.0, 100.9, 68.0, 68.1, 53.4, 29.6, 28.7, 25.8, 25.7; *m/z* (MALDI TOF MS+) 944.2, ($C_{45}H_{42}ClN_2O_7Re$); $[M]^+$ requires 944.2; UV-vis ($CHCl_3$) λ / nm (ε / M^{-1} cm^{-1}) 334 (19800); m.p. 290 °C.

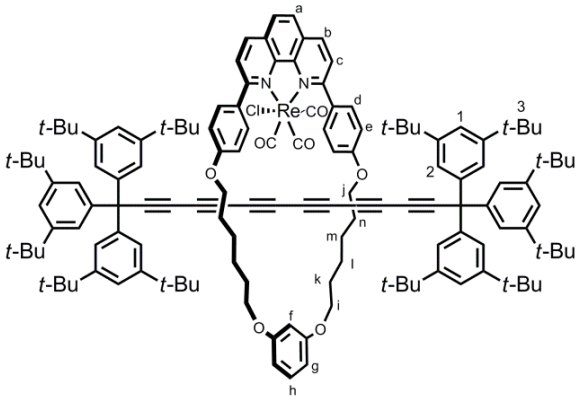

H⊂M(Re): A solution of hexayne rotaxane **2b⊂M1** (25.0 mg, 0.013 mol) and rhenium(I) pentacarbonyl chloride (5.6 mg, 0.015 mol) in toluene (4.0 mL) was refluxed under nitrogen for 6 h. The solution was cooled to 20 °C, solvent removed and the residue dried under vacuum. Recrystallization of the residue from hexanes afforded the product as a yellow solid (20.0 mg, 70%). ^{1}H NMR (400 MHz, CD_2Cl_2, 298 K) 8.59 (d, *J* = 8.2, 2H, H_b), 8.06 (s, 2H, H_a), 7.98 (d, *J* = 8.4, 2H, H_c), 7.68 (br. s, 4H, H_d), 7.28–7.24 (m, 6H, H_1), 7.11 (br. s, 4H, H_e), 7.05 (t, *J* = 8.2, 1H, H_h), 6.94 (d, *J* = 1.7, 6 H, H_2), 6.92 (d, *J* = 1.7, 6 H, H_2), 6.50 (t, *J* = 2.2, 1H, H_f), 6.43–6.41 (dd, J_1 = 8.2 Hz, J_2 = 2.2, 2H, H_g), 4.20–4.01 (m, 4H, H_j), 3.95 (t, *J* = 6.7, 4H, H_i), 1.90–1.76 (m, 8H, $H_{k,n}$), 1.60–1.50 (m, 8H, $H_{m,l}$), 1.21 (s, 54H, H_3), 1.15 (s, 54H, H_3). ^{13}C NMR (125 MHz, CD_2Cl_2, 298 K) 193.9, 19.3, 164.5, 161.4, 161.1, 150.7. 150.7, 149.2, 143.8, 138.5, 138.2, 134,6, 130.0, 129.8, 127.2, 127.2, 126.6, 124.4, 123.9, 123.9, 121.0, 120.9, 107.6, 100.4, 85.8, 70.0, 69.7, 68.6, 68.2, 64.1, 63.7, 63.6, 63.2, 63.0, 62.8, 62.6, 57.7, 57.7, 35.1, 35.1, 31.5, 31.4, 29.9, 28.9, 26.0, 25.9; *m/z* (MALDI TOF MS+) 2248.2, ($C_{143}H_{168}ClN_2O_7Re$); $[M]^+$ requires 2248.2; UV-vis ($CHCl_3$) λ / nm (ε / M^{-1}

cm^{-1}) 326 (301000), 297 (235000), 280 (173000), 267 (112000); UV-vis (THF) λ / nm (ε / M^{-1} cm^{-1}) 315 (311000), 296 (244000), 280 (178000): m.p. 277–278 °C.

4.11 Time-Resolved Spectroscopy

The ULTRA instrument at the STFC Rutherford Appleton Laboratory was used and is described in detail elsewhere.[64] Briefly, an amplified titanium sapphire laser (Thales Optronique) produces ~50 fs pulses at a 10 kHz repetition rate. The laser fundamental output (800 nm) is split into two parts. The first generates UV pump pulses through an optical parametric amplifier (TOPAS OPA) at 310 or 350 nm. The second part of the fundamental is used to generate probe pulses: ~400 cm^{-1} broad mid-IR probe pulses through a second OPA for TRIR experiments or a white light continuum (330−680 nm) through focussing of the fundamental into a 2 mm CaF_2 plate for TA experiments. Typical pump and probe beam diameters in the sample were 130 and 80 μm, respectively, the lower diameter probe being used to ensure only activated sample is interrogated. UV pump pulse energy was kept around 0.1 μJ. All experiments were carried out with the pump and probe set at the magic angle (54.7 °). The probe pulses were split in two, one part subsequently focused into the sample overlapping with the pump beam and the other for use as a reference of laser spectral and intensity variations. The probe and reference pulses were dispersed onto array detectors to measure the spectrum of each laser shot (using 128-element HgCdTe detectors for TRIR experiments and 512-pixel silicon single-diode arrays for TA experiments). By modulating the pump pulses at 5 kHz (the probe measured at 10 kHz) normalized pump on – pump off difference spectra can be collected in real time. The TRIR and TA spectra (see below) are presented as normalized difference spectra (each spectrum averaged over a few seconds), thus, positive bands correspond to photo-generated transient absorption while negative bands indicate ground state bleaching.

The pump–probe time delay was controlled by an optical delay line for femtosecond to nanosecond measurements, while the nanosecond to microsecond measurements were recorded using the same spectrometers but replacing the femtosecond pump laser with a 1 ns duration 5 kHz (for pump on – pump off measurements as above) laser operating at 266 nm.

The sample absorbance was 0.2−0.3 at the pump wavelength (310 or 350 nm) in a 0.1 mm pathlength flow cell with 2 mm CaF_2 windows. The cell was raster-scanned to avoid sample decomposition on window surfaces. Sample integrity was checked by IR and UV-vis spectra measured before and after each

experiment. All spectral fitting procedures and kinetic analysis were performed using OriginPro 8.5.1 software. TA spectra were corrected for group velocity dispersion over the wide spectral range.

Spectroscopic measurements were performed in air-saturated or deoxygenated dichloromethane or toluene solutions of spectroscopic quality (Aldrich). Deoxygenation was done by three freeze-pump-thaw cycles and sample preparation was carried out in glove box under nitrogen atmosphere. Fluorescence spectra were recorded on a J-Y Spex Fluoromax 2 fluorimeter. Ground state UV-vis spectra were recorded at ambient temperature on a Perkin-Elmer Lambda 20 or Parkin-Elmer Lambda 25 spectrometers with 1 nm resolution; λ in nm (ε in $L \cdot mol^{-1} \cdot cm^{-1}$).

4.12 References

1. (a) Diederich, F.; Rubin, Y. *Angew. Chem. Int. Ed. Engl.* **1992**, *31*, 1101–1123. (b) Diederich, F. *Nature* **1994**, *363*, 199–207. (c) *Acetylene Chemistry: Chemistry, Biology, and Material Science*, Editors: Diederich, F.; Stang, P. J.; Tykwinski, R. R. Wiley-VCH, Weinheim, Germany, **2005**. (d) Chalifoux, W. A.; Tykwinski, R. R. *C. R. Chim.* **2009**, *12*, 341–358. (e) Diederich, F.; Kivala, M. *Adv. Mater.* **2010**, *22*, 803–812. (f) Januszewski, J. A.; Tykwinski, R. R. *Chem. Soc. Rev.* **2014**, *43*, 3184–3203. (g) Hoheisel, T. N.; Schrettl, S.; Szilluweit, R.; Frauenrath, H. *Angew. Chem. Int. Ed.* **2010**, *49*, 6496–6515. (h) Chernick, E. T.; Tykwinski, R. R. *J. Phys. Org. Chem.* **2013**, *26*, 742–749.

2. Itzhaki, L.; Altus, E.; Basch, H.; Hoz, S. *Angew. Chem. Int. Ed.* **2005**, *44*, 7432–7435.

3. Liu, M.; Artyukhov, V. I.; Lee, H.; Xu, F.; Yakobson, B. I. *ACS Nano* **2013**, *7*, 10075–10082.

4. (a) Wang, C.; Batsanov, A. S.; Bryce, M. R.; Martín, S.; Nichols, R. J.; Higgins, S. J.; García-Suárez, V. M.; Lambert, C. J. *J. Am. Chem. Soc.* **2009**, *131*, 15647–15654. (b) Moreno-García, P.; Gulcur, M.; Manrique, D. Z.; Pope, T.; Hong, W.; Kaliginedi, V.; Huang, C.; Batsanov, A. S.; Bryce, M. R.; Lambert, C.; Wandlowski, T. *J. Am. Chem. Soc.* **2013**, *135*, 12228–12240.

5. Vail, S. A.; Krawczuk, P. J.; Guldi, D. M.; Palkar, A.; Echegoyen, L.; Tomé, J. P. C.; Fazio, M. A.; Schuster, D. I. *Chem. Eur. J.* **2005**, *11*, 3375–3388.

6. Cretu, O.; Botello-Mendez, A. R.; Janowska, I.; Pham-Huu, C.; Charlier, J.-C.; Banhart, F. *Nano Lett.* **2013**, *13*, 3487–3493.

7. Al-Backri, A.; Zólyomi, V.; Lambert, C. J. *J. Chem. Phys.* **2014**, *140*, 104306.

8. (a) Slepkov, A. D.; Hegmann, F. A.; Eisler, S.; Elliott, E.; Tykwinski, R. R. *J. Chem. Phys*. **2004**, *120*, 6807–6810. (b) Eisler, S.; Slepkov, A. D.; Elliott, E.; Luu, T.; McDonald, R.; Hegmann, F. A.; Tykwinski, R. R. *J. Am. Chem. Soc.* **2005**, *127*, 2666–2676. (c) Samoc, M.; Dalton, G. T.; Gladysz, J. A.; Zheng, Q.; Velkov, Y.; Ågren, H.; Norman, P.; Humphrey, M. G. *Inorg. Chem.* **2008**, *47*, 9946–9957.

9. (a) Ambroise, A.; Wagner, R. W.; Dharma Rao, P.; Riggs, J. A.; Hascoat, P.; Diers, J. R.; Seth, J.; Lammi, R. K.; Bocian, D. F.; Holten, D.; Lindsey, J. S. *Chem. Mater.* **2001**, *13*, 1023-1034. (b)Holten, D.; Bocian, D. F.; Lindsey J. S. *Acc. Chem. Res.* **2002**, *35*, 57-69. (c) Grosshenny, V.; Harriman, A.; Ziessel, R. *Angew. Chem. Int. Ed.* **1995**, *34*, 1100-1102. (d) Wagner, R. W.; Lindsey, J. S. *J. Am. Chem. Soc*. **1994,** *116*, 9759–9760.

10. . (a) Accorsi, G.; Listorti, A.; Yoosaf, K.; Armaroli, N. *Chem. Soc. Rev.* **2009**, *38*, 1690–1700. (b) Bencini, A.; Lippolis, V. *Coord. Chem. Rev.* **2010**, *254*, 2096–2180.

11. Lo, K. K.-W.; Louie, M.-W.; Zhang, K. Y. *Coord. Chem. Rev*. **2010**, *254*, 2603–2622.

12. Cleland, D. M.; Irwin, G.; Wagner, P.; Officer, D. L.; Gordon, K. C. *Chem.-Eur. J.* **2009**, *15*, 3682–3690.

13. Vlček, A. Jr. *Top. Organomet. Chem*. **2010**, *29*, 73–114.

14. Kumar, A.; Sun, S.-S.; Lees, A. J. *Top. Organomet. Chem*. **2010**, *29*, 1–35.

15. (a) Lang, H.; Koehler, K.; Blau, S. *Coord. Chem. Rev*. **1995**, *143*, 113–168. (b) Dias, R. H. V.; Flores, J. A.; Wu, J.; Kroll, P. *J. Am. Chem. Soc*. **2009**, *131*, 11249–11255. (c) Das, A.; Dash, C.; Yousufuddin, M.; Celik, M. A.; Frenking, G.; Dias, R. H. V. *Angew. Chem. Int. Ed.* **2012**, *51*, 3940 –3943.

16. Pu, Y.-J., Harding, R. E.; Stevenson, S. G.; Namdas, E. B.; Tedeschi, C.; Markham, J. P. J.; Rummings, R. J.; Burn, P. L.; Samuel, I. D. W. *J. Mater. Chem.* **2007**, *17*, 4255–4264.

17. Chalifoux, W. A.; Tykwinski, R. R. *Nature Chem*. **2010**, *2*, 967–971.
18. Saito, S.; Nakazono K.; Takahashi, E. *J. Org. Chem.* **2006**, *71*, 7477–7480.
19. Gibtner, T.; Hampel, F.; Gisselbrecht, J.-P.; Hirsch, A. *Chem.-Eur. J.* **2002**, *8*, 408–432.
20. Wright, P. J.; Muzzioli, S.; Werrett, M. V.; Raiteri, P.; Skelton, B. W.; Silvester, D. S.; Stagni, S.; Massi, M. *Organometallics* **2012**, *31*, 7566–7578.
21. Seybold P. G.; Gouterman M. *J. Mol. Spec.* **1969**, *31*, 1–13.
22. Nowell, H.; Barnett, S. A.; Christensen, K. E.; Teat, S. J.; Allan, D. R. *J. Synch. Rad*. **2012**, *19*, 435–441.
23. (a) Palatinus, L.; van der Lee, A. *J. Appl. Cryst*. **2008**, *41*, 975–984. (b) Palatinus, L. *Acta Cryst.* **2013**, *B69*, 1–16.
24. Palatinus L.; Chapuis, G. *J. Appl. Cryst*. **2007**, *40*, 786–790.
25. (a) Betteridge, P. W.; Carruthers, J. R.; Cooper, R. I.; Prout, K.; Watkin, D. J. *J. Appl. Cryst.* **2003**, *36*, 1487. (b) Cooper, R. I.; Thompson, A. L.; Watkin, D. J. *J. Appl. Cryst*. **2010**, *43*, 1100–1107.
26. (a) Spek, A. *J. Appl. Cryst*. **2003**, *36*, 7–13. (b) van der Sluis, P.; Spek, A. L. *Acta Cryst*. **1990**. *A46*, 194–201.
27. Rowland, R. S.; Taylor, R. *J. Phys. Chem.* **1996**, *100*, 7384–7391.
28. (a) Allen, F. H. *Acta Cryst.* **2002**, *B58*, 380–388 .(b) Szafert, S.; Gladysz, J. A. *Chem. Rev*. **2006**, *106*, PR1–PR33.
29. (a) Sakurai, A.; Akita, M.; Moro-oka, Y. *Organometallics* **1999**, *18*, 3241–3244. (b) Peters, T. B.; Bohling, J. C.; Arif, A. M.; Gladysz, J. A. *Organometallics* **1999**, *18*, 3261–3261. (c) Adams, R. D.; Qu, B.; Smith, M. D. *Organometallics* **2002**, *21*, 3867–3872. (d) Classen, J.; Gleiter, R.; Rominger, F. *Eur. J. Inorg. Chem.* **2002**, 2040–2046. (e) Mohr, W.; Stahl, J.; Hampel, F.; Gladysz, J. A. *Chem. Eur. J.* **2003**, 9, 3324–3340. (f) Qi, H.; Gupta, A.; Noll, B. C.; Snider, G. L.; Lu, Y.; Lent, C.; Fehlner, T. P. *J. Am. Chem. Soc.* **2005**, *127*, 15218–15227. (g) Luu, T.; Elliott, E.; Slepkov, A. D.; Eisler, S.; McDonald, R.; Hegmann, F. A.; Tykwinski, R. R. *Org. Lett.* **2005**, *7*, 51–54. (h) Bruce, M. I.; Zaitseva, N. N.; Nicholson, B. K.; Skelton, B. W.; White, A. H. *J. Organomet. Chem.* **2008**, *693*, 2887–2897. (i) Lucotti, A.; Tommasini, M.; Fazzi, D.; Del Zoppo, M.; Chalifoux, W. A.; Ferguson, M. J.; Zerbi, G.; Tykwinski, R. R. *J. Am. Chem. Soc.* **2009**, *131*, 4239–4244. (j) Frank, B. B.; Kivala, M.; Blanco, B. C.; Breiten, B.; Schweizer,W. B.; Laporta, P. R.; Biaggio, I.; Jahnke, E.; Tykwinski, R. R.; Boudon, C.; Gisselbrecht, J.-P.; Diederich, F. *Eur. J. Org. Chem.* **2010**, 2487–2503. (k) Gulia, N.; Osowska, K.; Pigulski, B.; Lis, T.; Galewski, Z.; Szafert, S. *Eur. J. Org. Chem.* **2012**, 4819–4830.
30. Mohr, W.; Stahl, J.; Hampel, F.; Gladysz, J. A. *Inorg. Chem.* **2001**, *40*, 3263–3264.
31. Taylor, T. J.; Gabbaï, F. P. *Organometallics* **2006**, *25*, 2143–2147.
32 (a) Stahl, J.; Bohling, J. C.; Bauer, E. B.; Peters, T. B.; Mohr, W.; Martin-Alvarez, J. M.; Hampel, F.; Gladysz, J. A. *Angew. Chem. Int. Ed.* **2002**, *41*, 1871–1872. (b) de Quadras, L.; Bauer, E. B.; Mohr, W.; Bohling, J. C.; Peters, T. B.; Martín-Alvarez, J. M.; Hampel, F.; Gladysz, J. A. *J. Am. Chem. Soc.* **2007**, *129*, 8296–8296.
33. Kloster-Jensen, E.; Haink, H.-J.; Christen, H. *Helv. Chim. Acta* **1974**, *57*, 1731–1744.
34. Pino, T.; Ding, H.; Güthe, F.; Maier, J. P. *J. Chem. Phys.* **2001**, *114*, 2208–2212.
35. Wakabayashi, T.; Nagayama H.; Daigoku, K.; Kiyooka, Y.; Hashimoto, K. *Chem. Phys. Lett.* **2007**, *446*, 65–70.
36. Wakabayashi, T.; Wada, Y.; Iwahara, N.; Sato, T. *J. Phys.: Conference Series*, **2013**, *428*, 012004.
37. Eastmond, R.; Johnson, T. R.; Walton, D. R. M. *Tetrahedron*, **1972**, *28*, 4601–4616.
38. (a) Hirata, Y.; Okada, T.; Nomoto, T. *Chem. Phys. Lett.* **1998**, *293*, 371–377. (b) Saltiel, J.; Kumar, V. K. R. *J. Phys. Chem. A* **2012**, *116*, 10548−10558
39. (a) Nagano, Y.; Ikoma, T.; Akiyama, K.; Tero-Kubota. S. *J. Chem. Phys*. **2001**, *114*, 1775–1784. (b) Nagano, Y.; Ikoma, T.; Akiyama, K.; Tero-Kubota, S. *J. Am. Chem. Soc*. **2003**, *125*, 14103–14112.
40. Simpkins, S. M. E.; Weller, M. D.; Cox, L. R. *Chem. Commun*. **2007**, 4035–4037.
41. Deperasińska, I.; Szemik-Hojniak, A.; Osowska, K.; Rode, M. F.; Szczepanik, A.; Wiśniewski, Ł.; Lis, T.; Szafert. S. *J. Photochem Photobiol. A* **2011**, *217*, 299–307.
42. Fazzi, D.; Scotognella, F.; Milani, A.; Brida, D.; Manzoni, C.; Cinquanta, E.; Devetta, M.; Ravagnan, L.; Milani, P.; Cataldo, F.; Lüer, L.; Wannemacher, R.; Cabanillas-Gonzalez, J.; Negro, M.; Stagira, S.; Vozzi, C. *Phys. Chem. Chem. Phys*. **2013**, *15*, 9384–9391.
43. Wakabayashi, T.; Tabata, H.; Doi, T.; Nagayama, H.; Okuda, K.; Umeda, R.; Hisaki, I.; Sonoda, M.; Tobe, Y.; Minematsu, T.; Hashimoto, K.; Hayashi, S. *Chem. Phys. Lett.* **2007**, *433*, 296–300.
44. (a) Armaroli, N.; De Cola, L.; Balzani, V.; Sauvage, J.-P.; Dietrich-Buchecker, C. O.; Kern, J.-M. *J. Chem. Soc., Faraday Trans.* **1992**, *88*, 553–556. (b) Bandyopadhyay, B. N.; Harriman, A. *J. Chem. Soc., Faraday Trans. 1* **1977**, *73*, 663–674.

45. (a) Luong, J. C.; Faltynek, R. A.; Wrighton, M. S. *J. Am. Chem. Soc.* **1980**, *102*, 7892–7900. (b) Pomestchenko, I. E.; Polyansky, D. E.; Castellano, F. N. *Inorg. Chem.* **2005**, *44*, 3412–3421.

46. (a) Wagner, J. R.; Hendricker, D. G. *J. Inorg. Nucl. Chem.* **1975**, *37*, 1375–1379. (b) Gamelin, D. R.; George, M. W.; Glyn, P.; Grevels, F.-W.; Johnson, F. P. A.; Klotzbücher, W.; Morrison, S. L.; Russell, G.; Schaffner, K.; Turner, J. J. *Inorg. Chem*. **1994**, *33*, 3246–3250.

47. Tabata, H.; Fujii, M.; Hayashi, S.; Doi, T.; Wakabayashi, T. *Carbon* **2006**, *44*, 3168–3176.

48. (a) George, M. W.; Turner, J. J. *Coord. Chem. Rev.* **1998**, *177*, 201–217. (b) Butler, J. M.; George, M. W.; Schoonover, J. R.; Dattelbaum, D. M.; Meyer, T. J. *Coord. Chem. Rev.* **2007**, *251*, 492–514.

49. TRIR studies of diphenylacetylene have been reported: (a) Ishibashi, T.; Okamoto, H.; Hamaguchi, H. *Chem. Phys. Lett.* **2000**, *325*, 212–218. (b) Nomoto, T.; Ishibashi, T.; Okamoto, H.; Hamaguchi, H. *J. Mol. Str*. **2005**, *735–736*, 197–202.

50. Haque, M.; Yin, L.; Nugraha, A. R. T.; Saito, R. *Carbon* **2011**, *49*, 3340–3345.

51. Karpfen, A.; Liscka, H. *Chem. Phys.* **1986**, *102*, 91–102.

52. Yoneda, H.; Hiura, H.; Takahashi, H. *J. Mol. Struct.* **1993**, *301*, 47–56.

53. Yildizhan, M. M.; Fazzi, D.; Milani, A.; Brambilla, L.; Zoppo, M. D.; Chalifoux, W. A.; Tykwinski, R. R.; Zerbi, G. *J. Chem. Phys.* **2011**, *134*, 124512–124518.

54. (a) Asbury, J. B.; Wang, Y.; Lian, T. *Bull. Chem. Soc. Jpn.* **2002**, *75*, 979–983. (b) Chudoba, C.; Nibbering, E. T. J.; Elsaesser, T. *Phys. Rev. Lett.* **1998**, *81*, 3010–3013.

55. (a) Okuyama, K.; Hasegawa, T.; Ito, M.; Mikami, N. *J. Phys. Chem.* **1984**, *88*, 1711–1716. (b) Gutmann, M.; Gudipati, M.; Schönzart, P.-F.; Hohlneicher, G. *J. Phys. Chem.* **1992**, *96*, 2433–2442.

56. Moore, A. L.; Joy, A.; Tom, R.; Gust, D.; Moore, T. A.; Bensasson, R. V.; Land, E. J. *Science* **1982**, *216*, 982–984. (b) Gust, D.; Moore, T. A.; Moore, A. L.; Devadoss, C.; Liddell, P. A.; Hermant, R.; Nieman, R. A.; Demanche, L. J.; DeGraziano, J. M.; Gouni, I. *J. Am. Chem. Soc*. **1992**, *114*, 3590–3603.

57. (a) Wrighton, M. S.; Morse, D. L. *J. Am. Chem. Soc.* **1974**, *96*, 998–1003. (b) Fredericks, S. M.; Luong, J. C.; Wrighton, M. S. *J. Am. Chem. Soc.* **1979**, *101*, 7415–7417. (c) Wallace, L.; Jackman, D. C.; Rillema, D. P.; Merkert, J. W. *Inorg. Chem*. **1995**, *34*, 5210–5214. (d) Striplin, D. R.; Crosby, G. A. *Coord. Chem. Rev*. **2001**, *211*, 163–175.

58. (a) Nahhas, A. E.; Consani, C.; Blanco-Rodríguez, A. M.; Lancaster, K. M.; Braem, O.; Cannizzo, A.; Towrie, M.; Clark, I. P.; Záliš, S.; Chergui, M.; Vlček, A. Jr. *Inorg. Chem*. **2011**, *50*, 2932–2943. (b) Blanco-Rodríguez, A. M.; Towrie, M.; Collin, J.-P.; Záliš, S.; Vlček, A. Jr. *Dalton Trans*. **2009**, 3941–3949. (c) Blanco-Rodríguez, A. M.; Ronayne, K. L.; Záliš, S.; Sykora, J.; Hof, M.; Vlček, A. Jr. *J. Phys. Chem. A* **2008**, *112*, 3506–3514. (d) Dattelbaum, D. M.; Omberg, K. M.; Hay, P. J.; Gebhart, N. L.; Martin, R. L.; Schoonover, J. R.; Meyer, T. J. *J. Phys. Chem. A* **2004**, *108*, 3527–3536. (e) Bredenbeck, J.; Helbing, J.; Hamm, P. *J. Am. Chem. Soc.* **2004**, *126*, 990–991.

59. (a) Vlček, A. Jr.; Záliš, S. *Coord. Chem. Rev*. **2007**, *251*, 258–287. (b) Dattelbaum, D. M.; Omberg, K. M.; Schoonover, J. R.; Martin, R. L.; Meyer, T. J. *Inorg. Chem.* **2002**, *41*, 6071–6079. (c) Blanco-Rodríguez, A. M.; Busby, M.; Ronayne, K.; Towrie, M.; Grădinaru, C.; Sudhamsu, J.; Sýkora, J.; Hof, M.; Záliš, S.; Di Bilio, A. J.; Crane, B. R.; Gray, H. B.; Vlček, A. Jr. *J. Am. Chem. Soc.* **2009**, *131*, 11788–11800.

60. (a) Liard, D. J.; Busby, M.; Matousek, P.; Towrie, M.; Vlček, A., Jr. *J. Phys. Chem. A* **2004**, *108*, 2363–2369. (b) Cannizzo, A.; Blanco-Rodríguez, A. M.; Nahhas, A. E.; Šebera, J.; Záliš, S.; Vlćek, A. Jr.; Chergui, M. *J. Am. Chem. Soc.* **2008**, *130*, 8967–8974.

61. Chang, C-W.; Lu, Y-C.; Wang, T.-T.; Diau, E. W.-G. *J. Am. Chem. Soc*. **2004**, *126*, 10109–10118.

62. Holten, D.; Bocian, D. F.; Lindsey J. S. *Acc. Chem. Res.* **2002**, *35*, 57–69.

63. Griffiths, M.; Sistrom, W. R.; Cohen-Bazire, G.; Stanier, R. Y. *Nature* **1955**, *176*, 1211–1214. (b) Beddard, G. S.; Davidson, R. S.; Trethewey, K. R. *Nature* **1977**, *267*, 373–374.

64. Greetham, G. M.; Burgos, P.; Cao, Q.; Clark, I. P.; Codd, P. S.; Farrow, R. C.; George, M. W.; Kogimtzis, M.; Matousek, P.; Parker, A. W.; Pollard, M. R.; Robinson, D. A.; Xin, Z.-J.; Towrie, M. *Appl. Spectrosc*. **2010**, *64*, 1311−1319.

Chapter 5

An attack on the protected chain, Size is matter again, Rearrangement needs to be carried out

Chapter 5. Synthesis of masked polyyne rotaxanes

5.1 Introduction

In this chapter the synthesis of insulated polyyne precursors is discussed the farther modification of which would result in the polyyne rotaxanes.

The synthesis of polyynes mostly relies on oxidative coupling reactions of terminal acetylenes.[1] One of the limitation of these methods is the instability of the oligoynes required as intermediates, an obstacle which has encouraged the development of alternative synthetic strategies where the polyyne framework is assembled first in a protected or masked form. In the final step, the linear carbon chain is constructed through either elimination or extrusion of masking functional groups.[2] The details of the 'masked' polyyne synthesis are reviewed in Chapter 1. While these routes have afforded a number of interesting polyyne derivatives,[3] in most cases their generality has yet to be established. In recent years the Fritsch–Buttenberg–Wiechell (FBW) rearrangement of carbene/carbenoid intermediates has evolved into an alternative valuable synthetic methodology for the preparation of polyyne structures from *geminal* dihaloolefin masked acetylene precursors (Scheme 5.1).[4]

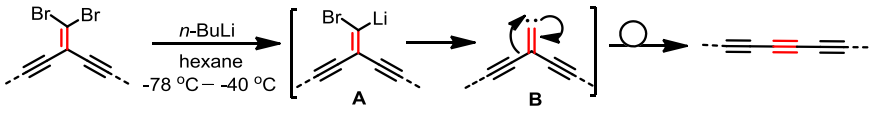

Scheme 5.1 The transformation of 1,1-dibromo-2,2-dialkynylethenes into polyynes. A and B are proposed intermediates.[4]

We are interested in the realization of the idea of masked polyynes in the synthesis of rotaxanes. For this purpose, *geminal* dibromoolefin acetylenes have been chosen to prepare Tr*- and TIPS-ended polyyne rotaxanes. Particularly, TIPS-capped rotaxanes are promising precursors for the further attachment of [2]rotaxanes, which would lead to the formation of polyrotaxanes.

We also tested the Pt-alkyne compound for the synthesis of polyyne rotaxanes, and the result of this approach is presented in *Appendix B*.

5.2 Synthesis of supertrityl-capped dibromoolefin polyyne rotaxanes

Geminal dibromoolefin acetylenes are intermediate molecules in the synthesis of supertrityl polyynes (Chapter 2) and, therefore, they are suitable targets to probe the synthesis of masked polyyne rotaxanes.

The initial rotaxane synthesis design focused on the coupling of a dibromoolefin partner with a linear polyyne under homo- or heterocoupling conditions to give a rotaxane with one dibromoolefin moiety on the axle (Figure 5.1). This choice was rationalized by the reported trend that a single carbenoid rearrangement proceeds more easily than a two-fold one, while the four-fold rearrangement on a single molecular framework has failed.[5]

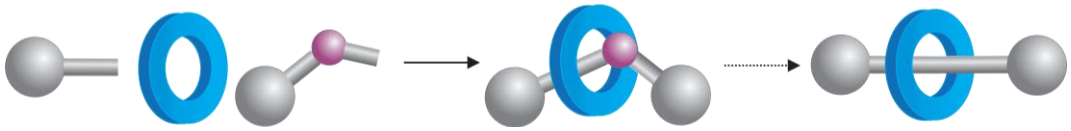

Figure 5.1 Schematic presentation of the masked polyyne rotaxane synthesis. The *gem*-dibromoolefin acetylene moiety (pink sphere) later undergoes FBW rearrangement to give a linear polyyne rotaxane

In the first attempt, the TIPS-protected dibromoolefin **2.16** was deprotected by TBAF and the free acetylene **5.1** was isolated quantitatively (100%, Scheme 5.2). The precursor **5.1** (1.25 eq.), I_2 (1.2 eq.), and K_2CO_3 (4.0 eq) were mixed with linear triyne **2.2** (1.25 eq.) in the presence of CuI·**M1** macrocycle complex (1.0 eq.) in THF, and the reaction mixture was stirred at 60 °C for 24 h. The consumption of the reagents was confirmed by TLC and after aqueous cyanide workup the rotaxane **2b⊂M1** was isolated in 11 % yield but no asymmetric, target rotaxane was formed (Scheme 5.2).

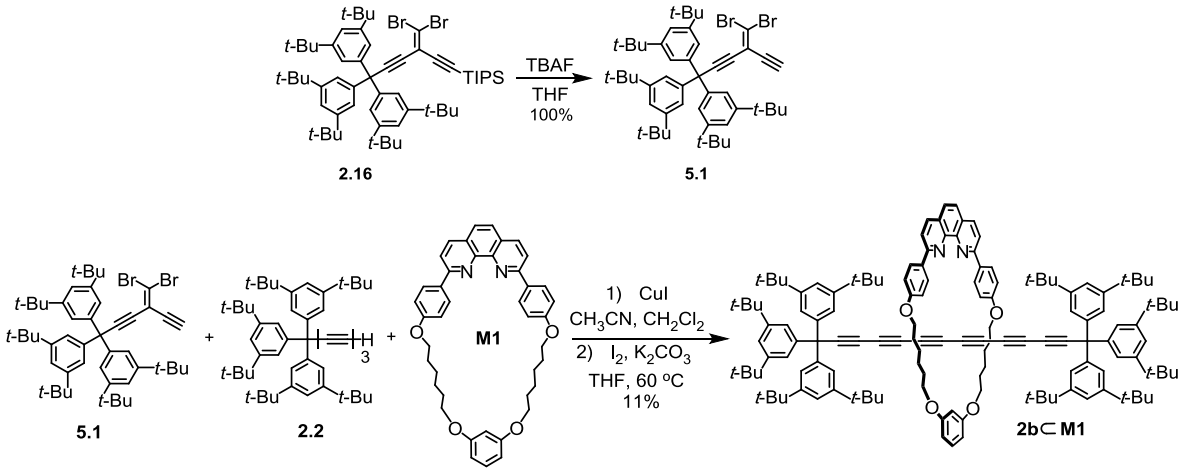

Scheme 5.2 Attempted synthesis of a dibromoolefin rotaxane via alkyne homocoupling .

A plausible explanation for this result is that a single terminal acetylene bond in precursor **5.1** is too short to be threaded, which leads exclusively to the formation of the kinetically more favourable linear hexayne rotaxane **2b⊂M1**. The cross-coupling reaction, on the other hand, always provided higher yields of the polyyne rotaxanes in our experiments, and we decided to apply the same strategy here. The dibromoolefin **5.1** (1.2 eq.) was added to a solution of supertrityl bromide **3.1** (1.7 eq.) and CuI·**M1** (1.0

eq.) in THF (Scheme 5.3). After purification of the reaction crude by column chromatography one promising fraction was isolated. The ^{1}H NMR and MALDI spectra confirmed that it contains the rotaxane **2b⊂M1** and unidentified compound(s).

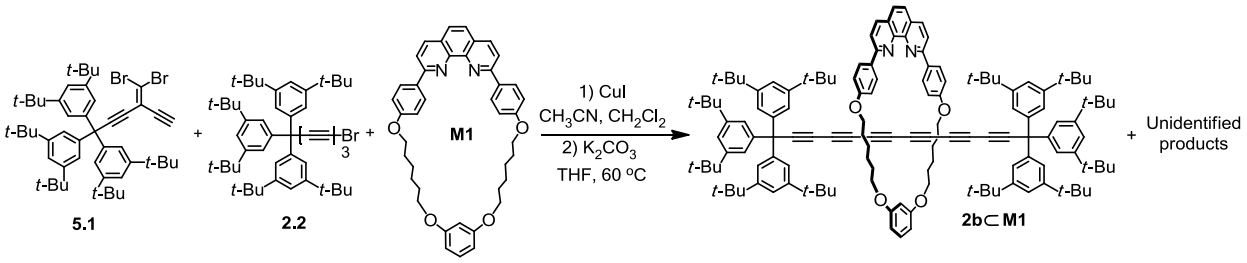

Scheme 5.3 Attempted synthesis of a dibromoolefin rotaxane via alkyne heterocoupling.

The formation of the linear rotaxane **2b⊂M1** is due to a significant proton-bromine exchange, noticed in the Cadiot-Chodkiewicz coupling reactions before, but the by-products could not be identified. Attempts to further separate the reaction products by column chromatography were not successful due to the similar polarity of the by-products, and we abandoned the exploration of this route.

As an alternative option, the coupling partners of the reaction were changed. The 1-bromo-dibromolefin **5.2** (Scheme 5.4) was prepared[6] and coupled with triyne **2.2** in the presence of the CuI·**M1** complex. As in the previous case, the rotaxane **2b⊂M1** was separated from the reaction crude together with unidentified compound(s), the separation and characterization of which again was not successful. It could be that in the transition state the Cu-acetylide cross-couples with the dibromolefin moiety (Castro-Stephens type coupling).[7] To test this hypothesis the TIPS-protected dibromolefin **2.16** was subjected to the reaction conditions with bromotriyne **3.1** under heterocoupling conditions. The Cu-acetylide, formed by the reaction of Cu(I) with bromotriyne might react with TIPS-protected dibromolefin, however, no reaction took place excluding the Castro-Stephens coupling scenario as a competing process.

It became clear from these attempts that the synthesis of rotaxanes with one dibromoolefin moiety on the axle is most probably not accessible under the tested conditions considering, due to difficulties with the purification and identification of the final products. Thereby, we redirect our attention towards the synthesis of the rotaxanes bearing two dibromoolefin moieties on the axle (Figure 5.2).

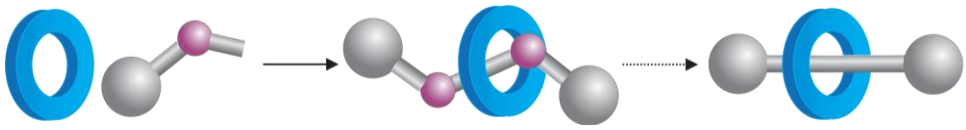

Figure 5.2 Schematic presentation of the rotaxane synthesis with two *gem*-dibromolefin moieties (pink sphere) followed by FBW rearrangement to afford a linear carbon framework.

The homocoupling reaction of **5.1** under active-metal template conditions was carried out in the presence of **M1** macrocycle. After two days of stirring at 60 °C no reaction took place which indicated that one terminal acetylene unit is too short to be threaded. (Similar negative results were obtained for the supertrityl monoyne discussed in Chapter 2.) Despite this failure we wanted to test once more the efficiency of the heterocoupling reaction. 1-Bromoacetylene **5.2** was prepared by treatment of **5.1** with NBS (Scheme 5.4),[6] and used under heterocoupling reaction conditions. After stirring for 2 days the TLC confirmed the complete consumption of starting materials and the rotaxane **5a⊂M1** was isolated in 9.5% yield (Scheme 5.4).

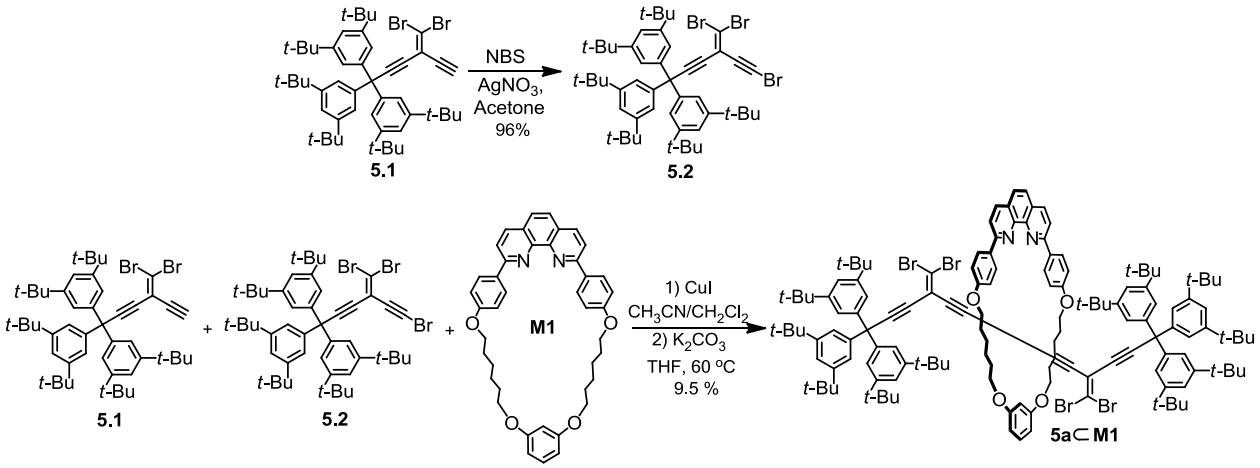

Scheme 5.4 Synthesis of 1-bromoalkyne **5.2** and rotaxane **5a⊂M1**.

Once again, the cross-coupling reaction proved its 'superiority' over the homocoupling in the synthesis of polyyne rotaxanes. However, it is necessary to mention that for an efficient synthesis of rotaxanes, the terminal acetylene must be extended to reduce the steric hindrance. Thus, a dibromoolefin precursor with a butadiyne terminal chain was synthesized following the route described in Scheme 5.5.[6] 1,4-Bis(TMS)butadiyne was lithiated with MeLi at 0 °C in THF, then a solution of aldehyde **2.11** in THF was added. The corresponding alcohol **5.3** was obtained in 67% yield as a brown oil. Compound **5.3** is prone to decomposition at room temperature, therefore we quickly proceeded to the next stage of alcohol oxidiation by PCC to the ketone **5.4** yielding the product as a orange solid (93%). The subsequent dibromoolefination

under Ramirez–Corey–Fuchs reaction conditions[8] led to **5.5** in 61% yield. Deprotection of the TMS group was achieved using K_2CO_3 to yield the polyyne **5.6** in 49%.[6]

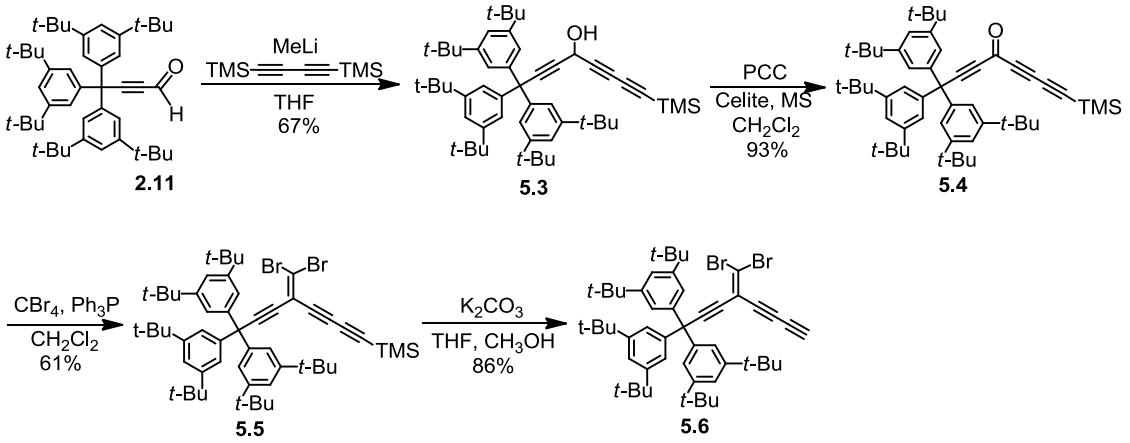

Scheme 5.5 Synthesis of polyyne **5.6**.

The polyyne precursor **5.6** could be used under both hetero- and homocoupling reaction conditions, however, there was a fear that bromine terminated **5.6** would be unstable (the homologous **5.2** decomposed slowly in the solid state). For this reason the homocoupling reaction was used which turned out to be very successful (Scheme 5.6). The reaction of the **5.6** and Cu·**M1** complex in THF was complete after stirring for 2 days and the rotaxane **5b⊂M1** was isolated in 51 % yield.

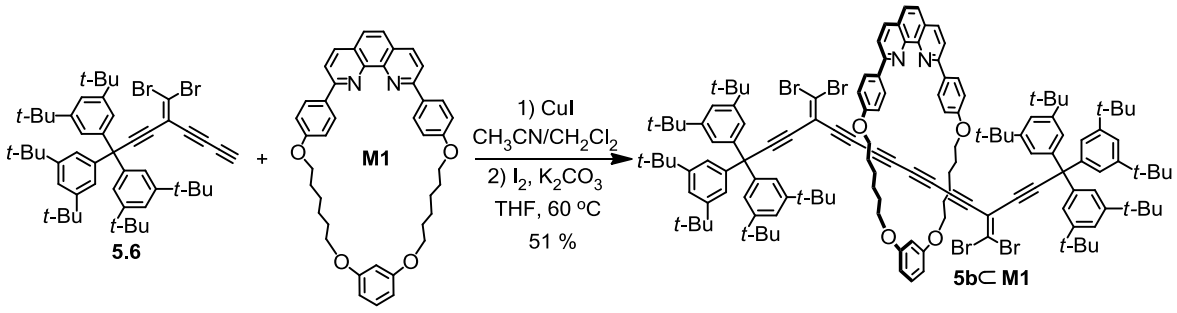

Scheme 5.6 Synthesis of rotaxane **5b⊂M1**.

The 5-fold improvement of the reaction yield does not leave any ambiguity about the important role that steric factors play in the synthesis of these rotaxanes.

Both **5a⊂M1** and **5b⊂M1** rotaxanes were characterized by ^1H and ^{13}C NMR, MALDI, UV-Vis absorption techniques and X-ray crystallography. MALDI TOF spectra were recorded with dithranol (1,8-dihydroxyanthrone) as a matrix. Under positive reflectron mode both rotaxanes showed along the main molecular peak [M^+] as well as other peaks rising from the degradation of the molecule by stepwise loss of bromine atoms.

UV-Vis absorption spectra of **5a⊂M1** and **5b⊂M1** rotaxanes are shown in Figure 5.3. While the spectrum of **5a⊂M1** is dominated by the absorption of the macrocycle in the high energy region (240-350 nm), in the spectrum of rotaxane **5b⊂M1** the absorption of the molecule is about 2.5 times higher compared to the **5a⊂M1** rotaxane, and there are three distinguishable bands at 421 nm, 389 nm and 361 nm. All these spectral differences arise from the extended π-conjugated system in rotaxane **5b⊂M1**.

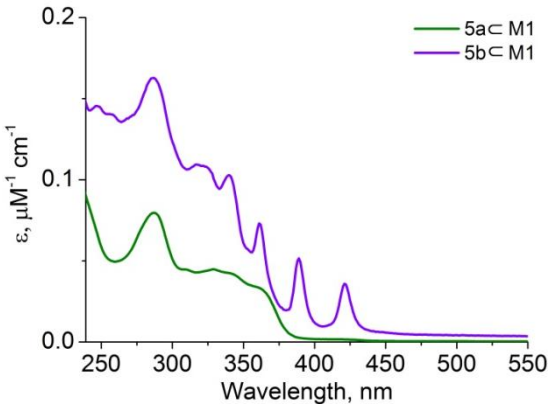

Figure 5.3 Absorption spectra of rotaxanes **5a⊂M1** and **5b⊂M1** recorded in CH_2Cl_2.

Crystals of **5a⊂M1** were grown by slow CH_3OH vapour diffusion into the solution of the compound in CH_2Cl_2 at room temperature, and the crystal structure of the rotaxane was obtained by X-ray diffraction. The asymmetric unit contains one molecule of **5a⊂M1**, one molecule of CH_2Cl_2 and seven molecules of CH_3OH. One of the methanol molecules is coordinated to the bromine atom by week hydrogen bond (*r*(H··Br) = 2.95 Å, Figure 5.4, b). The crystal belongs to the P-1 space group. The solid state packing of the molecules is shown in Figure 5.4 a. Despite many rotaxane solid state structures, described in this thesis, no particular π-π is observed between the phenanthrolines of the molecules. The macrocycle in **5a⊂M1** sits exactly on the top of one of the dibromoolefin moieties, like a shield. Due to this, the dibromoolefins have slightly different structures. For example, in the macrocycle-nested dibromoolefin part, the ∠C(sp)–C(sp^2)–C(sp) angle is 119.0° while the same angle for the macrocycle free part is 116.2°. Similarly, the ∠Br–C(sp^2)–Br angle of the macrocycle-nested dibromoolefin is 114.8°, and for the macrocycle free moiety the ∠Br–C(sp^2)–Br angle is 116.3°. The dibromoolefin moieties are facing opposite directions with a slightly twisted angle: the torsion angle is 141.85°. Both central triple bonds have a similar length (1.202 Å) within error, and the length of the single bond between them is 1.386 Å.

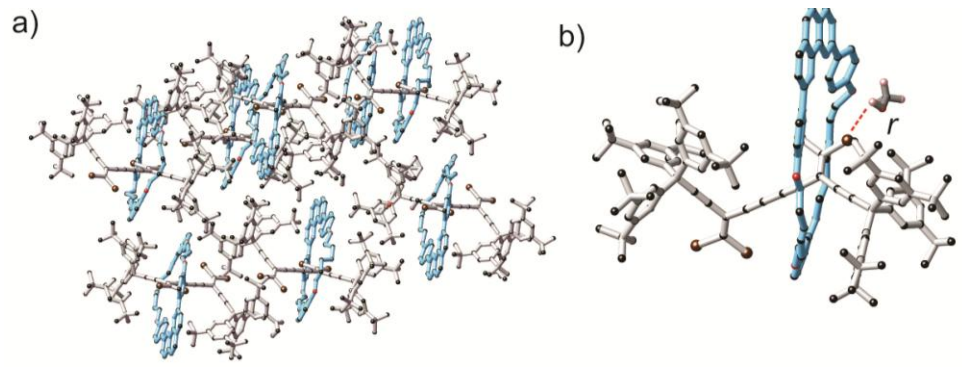

Figure 5.4 (a) Crystal packing of the **5a⊂M1** rotaxane viewed down the crystallographic *c** axis. Solvents and hydrogen atoms are omitted for clarity. (b) Crystal structure of the **5a⊂M1** molecule showing the week hydrogen bond between a bromine atom and one of the seven molecules of methanol.

*The diffraction date for **5b⊂M1** rotaxane have been collected, however the crystal structure has not been solved and refined.*

5.3 Attempted construction of polyyne frameworks in rotaxanes via FBW rearrangement

The Fritch-Buttenberg-Wiechell (FBW) rearrangement,[10] which generally proceeds through a carbenoid intermediate (Figure 5.1), has become a well-established method for alkyne synthesis since the development of successful methods for the migration of alkyne groups, discovered by the Tykwinski research group in the 2000s.[4,9] The basis of this method is the treatment of 1,1-dibromo-2,2-dialkynylethenes with *n*-BuLi which leads to the *in situ* formation of a carbenoid species that readily undergoes 1,2-migration of the pendant alkynyl group to yield the corresponding polyyne.[7] The reaction is usually carried out at low temperatures in hexane (Scheme 5.1).

In the case of rotaxanes **5a⊂M1** and **5b⊂M1**, we found out that the rotaxanes were not soluble in hexane despite the presence of the dumbbell moieties. However, toluene was used which, according to the reports, could serve as an alternative non-coordinating reaction solvent.[4a] Diluted solutions of the compound were prepared in rigorously dried toluene, and *n*-BuLi (in a slight excess, 2.2 eq.) was added at –78 °C.[4,6,9] The reaction mixture was slowly warmed up to –30 °C and quenched by aqueous NH_4Cl. However, after the final workup at room temperature the UV-vis spectrum of the crude reaction mixture showed that the octayne framework was not formed and no trace of the expected rotaxane **2h⊂M1** was detected (Scheme 5.7).

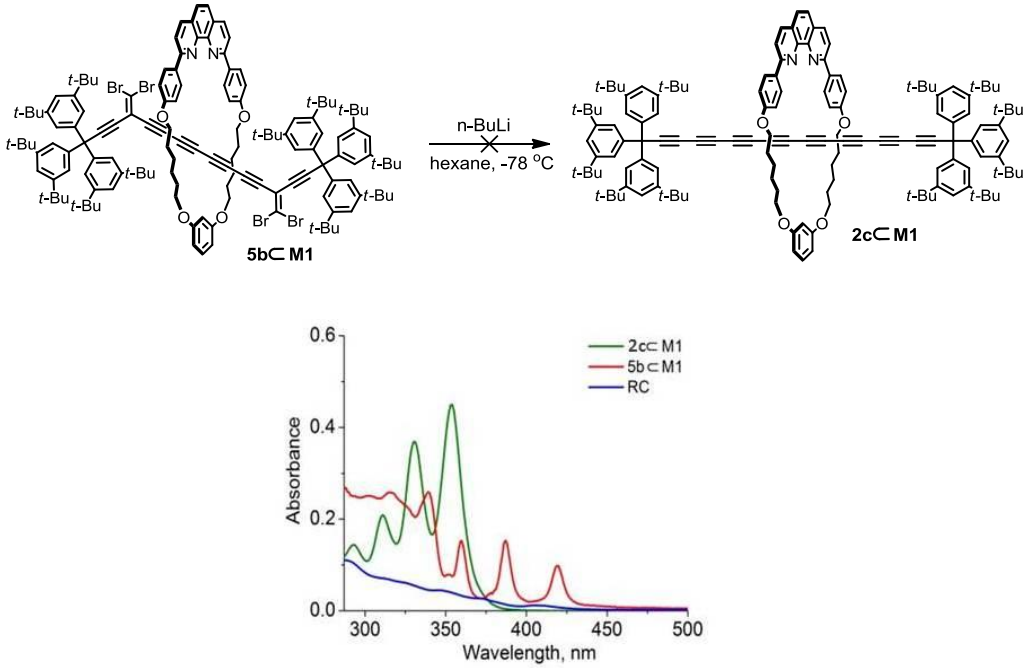

Scheme 5.7 Attempted synthesis of the octayne rotaxane **2c⊂M1** via FBW rearrangement of rotaxane **5b⊂M1**. The inserted UV-Vis spectra compare the absorption spectrum of initial rotaxane **5b⊂M1**, the spectrum of rotaxane **2c⊂M1** and the absorption spectrum of the crude mixture (RC) showing no trace of starting material and expected product. The spectra are recorded in toluene at room temperature with different concentrations.

After column chromatography two fractions were separated but none of them corresponded to the expected rotaxane **2h⊂M1**. It was thought that probably the protonated species could be formed resulting from a *in situ* lithium-proton exchange in intermediate **A** (Scheme 5.8), where traces of water existing in the reaction mixture serve as a sources of protons.[4] To suppress the lithium-proton exchange, the reaction was repeated using an excess of *n*-BuLi (10 eq. instead of 2.2 eq.), however the result was disappointing. Likewise, test reactions conducted in toluene at different temperatures (adding *n*-BuLi at –78 °C to –20 °C) were equally unsuccessful.

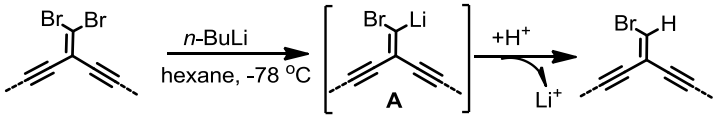

Scheme 5.8 Formation of protonated species by *in situ* lithium-proton exchange

To get more insights into the reaction we investigated the interaction of *n*-BuLi with individual components of the rotaxane, i.e. macrocycle and dibromoolefin polyyne dumbbell, using similar reaction conditions to the previously attempted FBW rearrangements of rotaxane **5b⊂M1**. Macrocycle **M1** did not react with excess *n*-BuLi (4.0 eq.) even at room temperature. The free dumbbell **5b** was synthesized via Hay coupling.[6,11] To a mixture of CuCl in CH_2Cl_2 was added TMEDA, and oxygen was bubbled for 10

min. through the solution. The butadiyne terminated **5.6** was added and the reaction mixture was stirred for 5 min. The crude product was passed through silica plug and the dumbbell **5b** was isolated quantitatively (Scheme 5.9).

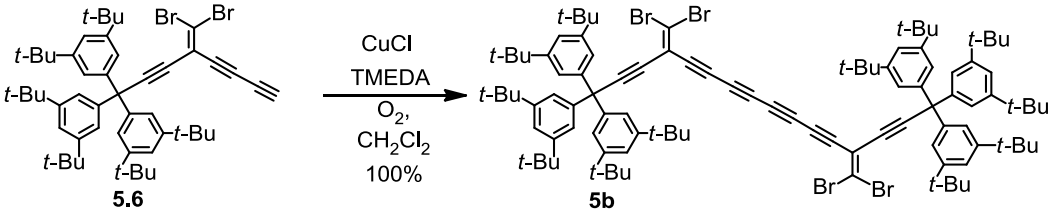

Scheme 5.9 Synthesis of the dumbbell **5b**.

The rearrangement of **5b** was carried out in toluene by adding *n*-BuLi (2.2 eq.) at –90 °C and slowly warming the temperature by 10 °C over 10 min. while the reaction progress was monitored by taking aliquots every 10 min. and recording the UV-Vis spectrum (Figure 5.5). The first recorded spectrum showed that at –90 °C dramatic spectral changes took place: an intense absorption band appeared around 310 nm with characteristic vibronic bands indicative of a hexayne chain and a shoulder at 350 nm which resembles the absorption of an octayne dumbbell.[6a] However, to our disappointment, at –80 °C these bands decreased and at –30 °C the mentioned pattern of absorption was completely lost. This experiment suggested that, the FBW rearrangement of supertrityl-capped dumbbell might be achievable in toluene but the reaction must be quenched at lower temperatures to avoid secondary reactions at relatively higher temperatures.

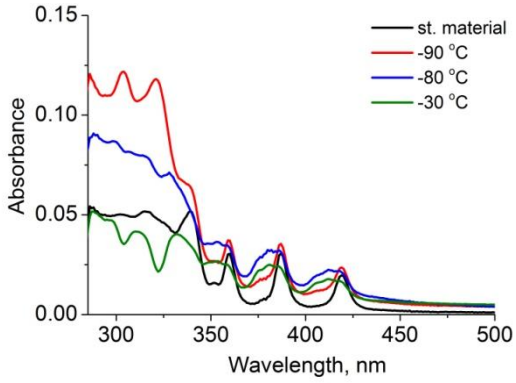

Figure 5.5 Monitoring of the FBW rearrangement reaction of dumbbell **5b** via UV-vis absorption spectra at different temperatures (Solvent: toluene).

We further investigated the interaction of unthreaded and rotaxinated polyyne chains with *n*-BuLi. For these tests we chose supertrityl hexayne **2b**[6a] and hexayne rotaxane **2b⊂M1.** First, to hexayne dumbbell **2b**

(1.0 eq) was added *n*-BuLi (4.0 eq.) in toluene at –78 °C. However, no reaction took place. This is consistent with the observation that triyne chain stays intact towards the *n*-BuLi in the synthesis of **2.17** via FBW rearrangement (Chapter 2). In the next step the **2b⊂M1** rotaxane was tested itself and, to our surprise, the UV-Vis absorption monitoring revealed that the characteristic hexayne chain absorption was altered in the course of the reaction (Figure 5.6, b). After workup a fraction was isolated by silica column chromatography and identified by MALDI and ^{1}H NMR techniques as the product of the addition of a butyl group to the hexayne chain (Scheme 5.10).

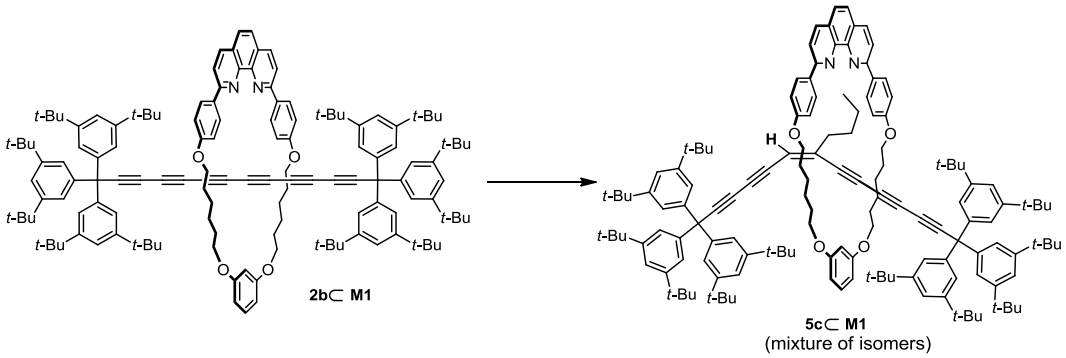

Scheme 5.10 Reaction of *n*-BuLi with rotaxane **2b⊂M1**.

The MALDI spectrum unambiguously showed a molecular peak (*m/z* = 2000.34) corresponding to the peak of M+butane (calc. *m/z* = 2000.38) (Figure 5.6). While the product left a single spot on the TLC plate, the ^{1}H NMR revealed that the separated fraction was a mixture of regioisomers (Figure 5.6c). As expected, the signals corresponding to the protons of the supertrityl groups, marked as 1 and 2 in Figure 5.6c, were split due to desymmetrization of the dumbbell. The proton signals of the macrocycle were not affected while two additional signals appeared at 5.94 and 5.83 ppm. The total integral of these peaks and their distinct chemical shifts confirmed the presence of regioisomers with the ethylenic proton being situated at different positions of the carbon backbone. We did not determine the precise composition of the mixture and the absolute structures of the regioisomers, as the purification of the product mixture was challenging.

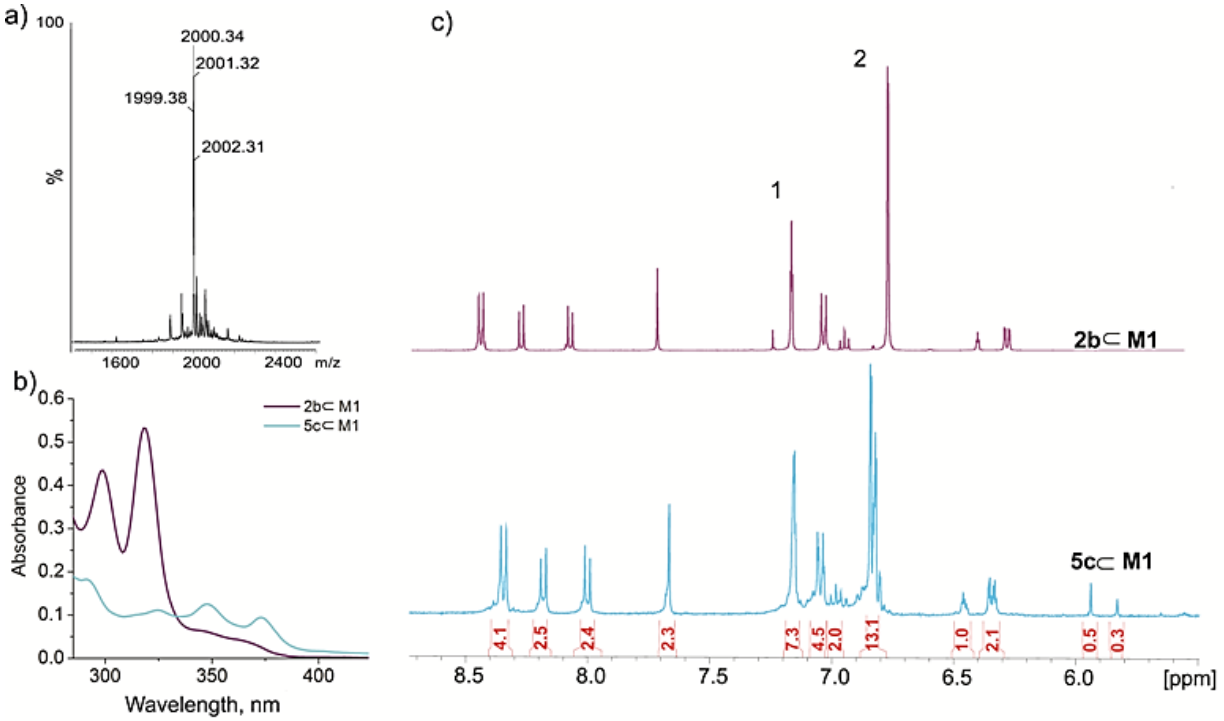

Figure 5.6 Identification and characterization of rotaxane **5c⊂M1** by (a) MALDI TOF spectrometry, (b) UV-Vis (in toluene) and (c) ^{1}H NMR spectroscopy (400 MHz, CD_2Cl_2, 298 K). In (c) the ^{1}H NMR spectrum of the **2b⊂M1** rotaxane is shown for comparison.

The origin of the reactivity change in unthreaded and threaded polyynes was not understood, but we assume that the nitrogen atoms of the phenanthroline may play a pivotal role by facilitating the attack of the butyl group. Thereby, a suggestion was made that blocking the nitrogen atoms through coordination of a metal ion to the phenanthroline could disable this undesirable addition reaction.

As a first choice equimolar amounts of CuI and rotaxane **5b⊂M1** were mixed in a CH_3CN : CH_2Cl_2 1:1 solution, and the complexation of Cu(I) to the rotaxane was confirmed bychanges in the UV-Vis spectrum. The CuI·**5b⊂M1** complex was redissolved in dry toluene and the FBW rearrangement was attempted, but disappointingly no target polyyne rotaxane was formed. It was envisioned that Cu(I) may catalyze the dimerisation of the intermediate carbene/carbenoid species and form a [3]cumulenic structure.[11] We changed the metal to Zn^{2+} ion, using $ZnCl_2$ which is unable to carry out the carbene dimerization. However, experiment showed that this strategy was equally unsuccessful, which may be because Zn^{2+} binds weakly to 1,10-phenanthroline.[12]

One more attempt was done with Re complexes, the synthesis of which is described in Chapter 4. Re-rotaxane complexes are robust, stable and chemically inert towards the polyyne chain, which makes them good candidates for FBW rearrangement. Thus, we synthesized the **$Re(CO)_3Cl$·5b⊂M1** complex with

80% yield using the conditions described in Chapter 4 (Scheme 5.11). Despite the close proximity of the dibromoolefin moieties to the metal centre the molecule is stable in the solid state and solution. The FBW rearrangement has not been tested yet due to time restrictions, but its accomplishment stays under high importance.

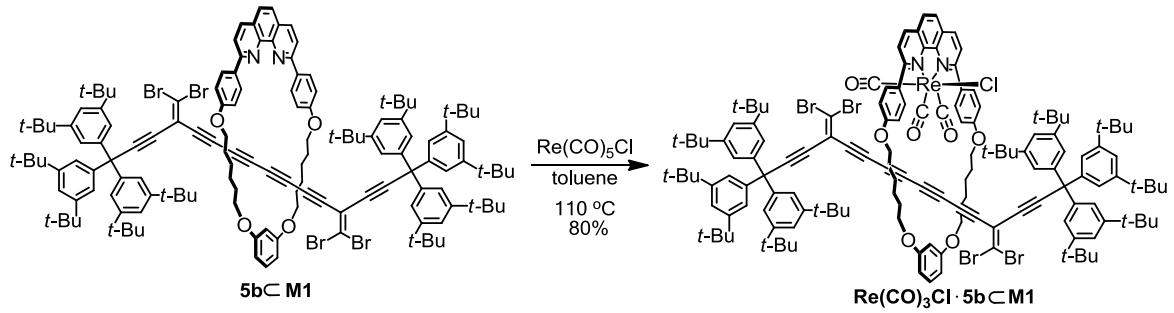

Scheme 5.11 The synthesis of rotaxane **Re(CO)$_3$Cl·5b⊂M1**.

5.4 Synthesis of TIPS-capped rotaxanes

Besides their use as intermediates in the formation of polyynes chains, dibromoolefin groups may also be used as temporary rotaxane stoppers that allow the subsequent extension of the axle to form polyrotaxane for example.

In dibromoolefin rotaxanes, the bromine atoms themselves may obstruct the movement of the small macrocycles along the axle and prevent deslipping. However, the CPK models of rotaxanes indicated that the dibromoolefin moiety itself is not bulky enough even for the smallest macrocycle to reliably disable the dissociation of interlocked components. The same modelling revealed that in the TIPS-capped dibromoolefins,[5] the end-group can disable the sliding out of macrocycle **M4** (Chapter 2) from the dumbbell. Therefore, our curiosity focused on the synthesis of TIPS-capped dibromoolefin-functionalized rotaxanes.

First, the synthesis of the TIPS-capped dibromoolefin rotaxanes with one acetylene terminated precursor was considered, The acetylene precursor **5.10** was synthesized according to a reported procedure.[5,19] The TIPS-acetylene was transformed to the TIPS-propargylic aldehyde **2.13** in 84% yield (Chapter 2). The aldehyde **2.13** was reacted at low temperature with lithiated TMS-acetylene to afford the product **5.7** in 71% yield. Subsequent oxidation with PCC (**5.8**, 84%) and dibromoolefination gave the product **5.9** in 55% yield. The selective deprotection of **5.9** was achieved by K_2CO_3 in CH_3OH/THF mixture affording the product **5.10** quantitatively (Scheme 5.12).

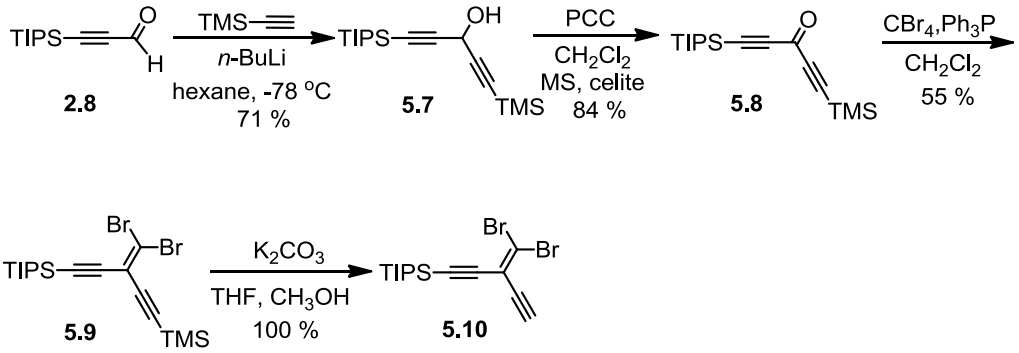

Scheme 5.12 Synthesis of the TIPS-capped dibromoolefin precursor **5.10**.

The acetylene **5.10** was reacted with macrocycle **M4** under homocoupling conditions, however no traces of corresponding rotaxane were identified. It was believed that the problem again arises from the short acetylene terminal end-group, and extended acetylenic chain must overcome the steric requirement. Thus, the synthesis of a new TIPS-capped butadiyne-terminated precursor was carried out according to published procedures.[5] TIPS-acetylene was converted to the TIPS-propargylic acid **5.11** in excellent yield (96%) (Scheme 5.13).[14] Friedel-Crafts acylation has been a useful method for the direct formation of conjugated ketones.[15] The acid **5.11** was chlorinated with $SOCl_2$, and the product was reacted with 1,4-bis(trimethylsilyl)-1,3-butadiyne giving ketone **5.12** as an unstable brown oil. The reaction crude was passed through silica plug and the product was used in the next stage without further purification. Reaction of **5.12** under Ramirez' conditions gave dibromide **5.13** as a stable yellow oil in 36% yield over three steps. Selective removal of TMS group afforded **5.14** quantitatively (98%).

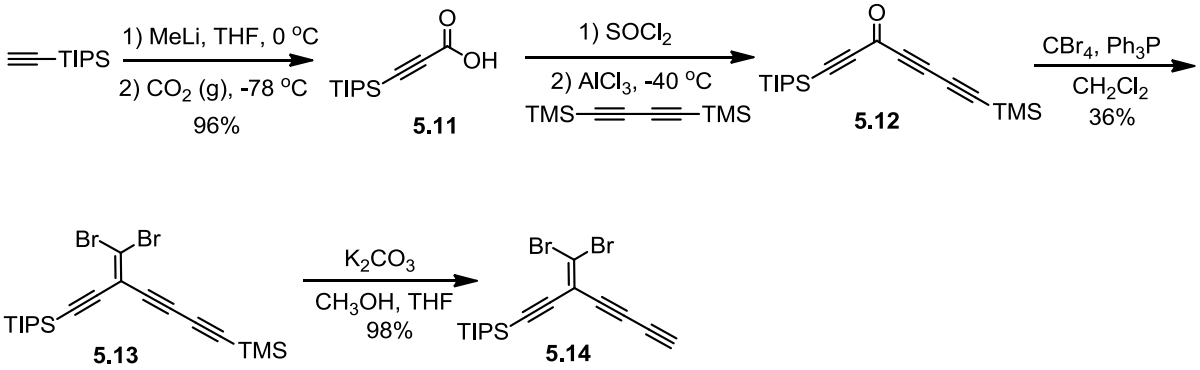

Scheme 5.13 Synthesis of the dibromoolefin **5.14**.

The free butadiyne **5.14** is prone to decomposition in the solid state and deprotection was carried out immediately before the rotaxane synthesis. The CuI·**M4** complex and **5.14** were reacted under homocoupling conditions and after stirring for two days the rotaxane **5d⊂M4** was isolated in 22% yield

(Scheme 5.14). Also, to our surprise, the unthreaded dumbbell **5d** was separated on silica with high yield (59%), thus, in total 81% coupling efficiency was achieved in this reaction. It is the first time that we isolate an unthreaded dumbbell **5d** from a rotaxane reaction mixture of this type.

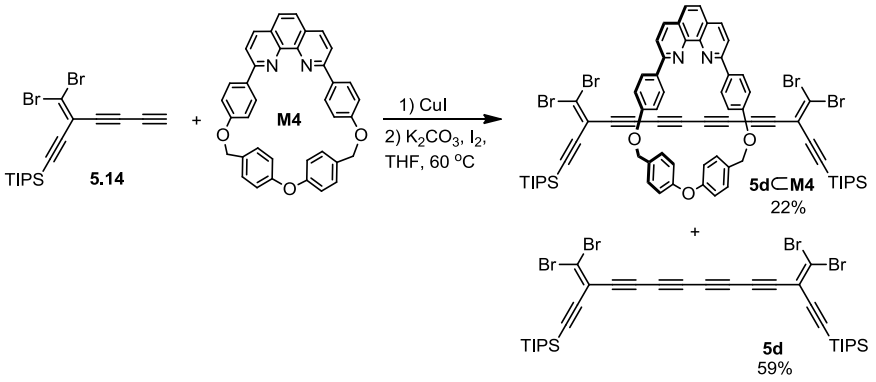

Scheme 5.14 Synthesis of rotaxane **5d⊂M4**. The unthreaded dumbbell **5d** was also isolated from the reaction mixture.

The yield of rotaxane **5d⊂M4** was lower than the yield of rotaxane **5b⊂M1** even though both have the same polyyne framework, and for the latter we never detected the formation of unthreaded dumbbell.

Full deprotection of rotaxane **5d⊂M4** would enable to do valuable chemical modifications on the free acetylenic termini, provided that the macrocycle will not slip out. This would open astonishing opportunities in the synthesis of polyyne rotaxanes. For example, the fully deprotected **5d⊂M4** could be reacted with supertrityl triyne **2.2** under Hay coupling conditions thus constructing a C28 carbon framework. Alternatively, the fully deprotected **5d⊂M4** rotaxane after further transformation of terminal free acetylenes to butadiynes could be used in rotaxane synthesis in the presence of macrocycles to give [4]rotaxanes. However, probably the most spectacular molecular design would be the Hay homocoupling of the fully deprotected **5d⊂M4** rotaxane under diluted conditions to give a cyclic catenane structure, considering the 120° curvature at the ethene moieties which is the perfect geometry for the construction of a hexagonal cycle (Figure 5.7).

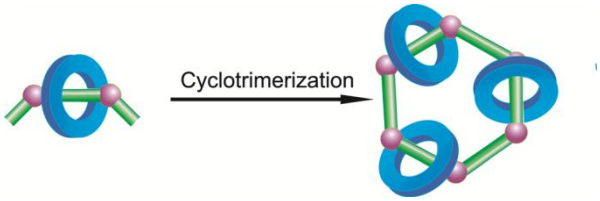

Figure 5.7 Using a dibromoolefin polyyne rotaxane to build up a [4]catenane.

The statistical deprotection of **5d** by TBAF (1.0 eq.) in CH_2Cl_2 afforded a mixture of mono- and bis-deprotected products ***m*-5d** and ***d*-5d** (Scheme 5.15). At the same time, deprotection of the **5d⊂M4** rotaxane under the same conditions resulted in complete disconnection of the rotaxane component, as the CPK modelling predicted.

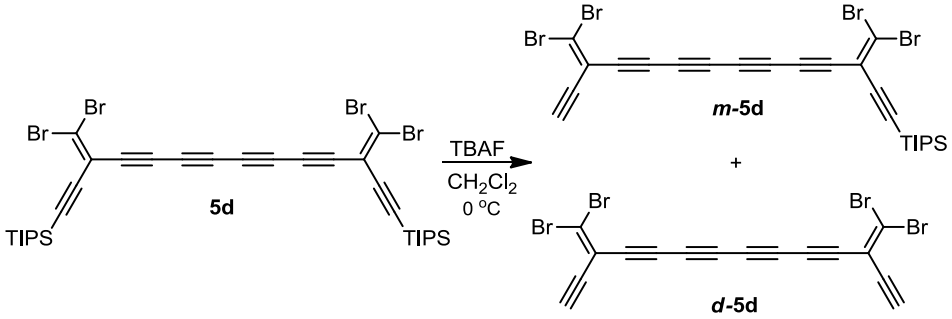

Scheme 5.15 Partial deprotection of the dumbbell **5d** using TBAF in CH_2Cl_2.

The deprotection of **5d** with TBAF was efficient at 0 °C while at room temperature we observed significant decomposition of the reaction compounds. Compounds ***m*-5d** and ***d*-5d** are stable on silica (hexanes) for separation, however, the compounds decomposed upon drying. This did not allow us to calculate the product yields, but we used the solutions of ***m*-5d** and ***d*-5d** for the next step. We were interested in investigating whether it is possible to assemble catenane or non-catenane cyclic structures using ***m*-5d** and ***d*-5d** building blocks. First we tested the oxidative coupling of the ***d*-5d** in diluted CH_2Cl_2 (Hay conditions, CuCl, TMEDA, O_2).[6,11] Unfortunately, all efforts resulted in formation of a black, tar-like precipitate, probably due to polymerization (Scheme 5.16). This is somewhat expected, taking into account the high geometry demand for the construction of a cycle. It is noteworthy to mention that Hay coupling failed for the coupling of monoprotected ***m*-5d** too. It could be that alternative oxidative coupling protocols, like Eglinton-Galbraith coupling ($Cu(AcO)_2 \cdot H_2O$, 2,6-lutidine, MeOH, CH_2Cl_2)[16] could offer better results, however we have not tested this possibility yet.

Next, we reacted fully deprotected ***d*-5d** in the presence of macrocycles **M1** and **M4** under homocoupling conditions. When ***d*-5d** was reacted with the CuI complex of macrocycle **M4** the

consumption of the ***d*-5d** was very slow (at 60 °C, THF) and no rotaxane or catenane was detected in the reaction crude after stirring for 5 days, meanwhile the reaction of ***d*-5d** with the CuI·**M1** complex at 60 °C gave a black carbonaceous precipitate (Scheme 5.16).

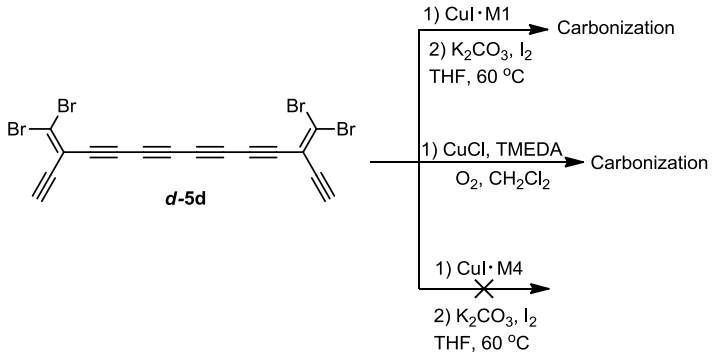

Scheme 5.16 Attempted synthesis of cyclic molecules based on the trimerization of the ***d*-5d** under different conditions.

Although disappointing results were obtained thus far the synthesis of dibromoolefin(polyyne) macrocycles has great interest as precursors for new carbon allotropes in the form of cyclo[n]carbons.[3a,b,17] Further research on the synthesis of these molecules has not been accomplished due to time constrains but its high importance and intriguing outcome is not doubtful.

For catenane synthesis, the rotaxane **5d⊂M4** was unusable in its deprotected form because of dethreading of the macrocycle. An appealing idea to circumvent this problem would be to use a post-synthetic macrocycle modification to tighten its cavity to the size at which the dibromoolefin fragment would prevent dissociation of the thread from the axle. Initially, we prepared the CuI complex of rotaxane **5d⊂M4** and carried out the deprotection of TIPS groups by TBAF in CH_2Cl_2, however the compound decomposed. We did not try to synthesize complexes of the rotaxane **5d⊂M4** with other ions (like Zn^{2+}, Ag^{+}, etc) but rather thought about exploring alternative routes. To our delight, the CPK modelling indicated that the **M2** macrocycle also can be used for the synthesis of TIPS-capped rotaxanes. Its cavity is small, and the TIPS groups are able to prevent the deslipping. More interestingly, if the new rotaxane was synthesized, its Re(I) tricarbonyl complex could be synthesized as shown in Chapter 4. The model of this rotaxane complex showed that the phenanthroline-coordinated bulky $Re(CO)_3Cl$ group occupies most of the macrocycle cavity, leaving just enough space for the polyyne chains. This group should thus enable the dibromoolefins to serve as a stoppering group after TIPS removal.

New rotaxane **5e⊂M2** was synthesized in the conditions shown in Scheme 5.16. The product was isolated in 13% yield. To corresponding Re(I) tricarbonyl complex was synthesized as described in Chapter 4 and the product **$Re(CO)_3Cl$·5e⊂M2** was obtained in 80% yield (Scheme 5.17).

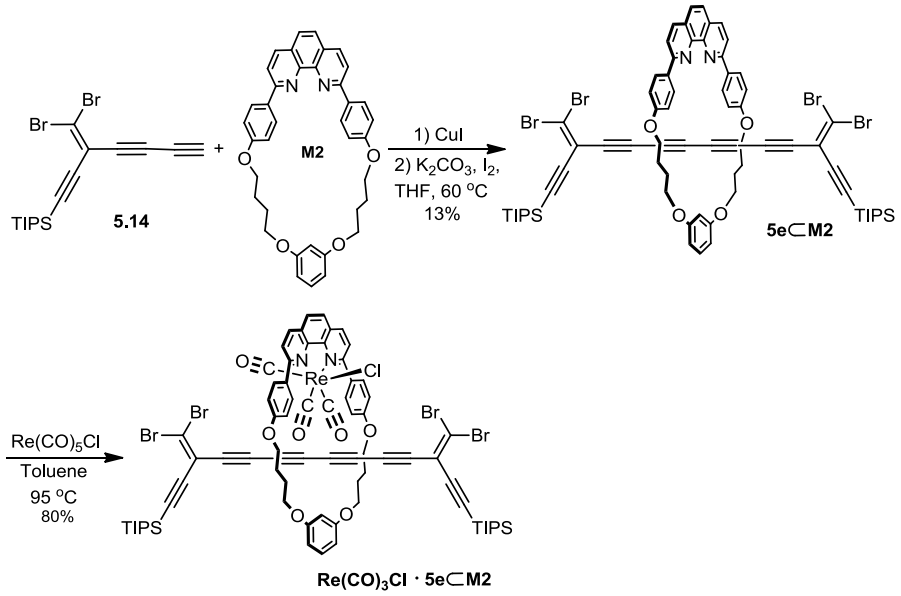

Scheme 5.17 Synthesis of rotaxane **5e⊂M2** and the corresponding **$Re(CO)_3Cl$·5e⊂M2** complex.

The rotaxane **5e⊂M2** was fully characterized (^1H and ^{13}C NMR, MALDI, UV-vis absorption techniques). Because of time restriction we limited the **$Re(CO)_3Cl$·5e⊂M2** complex characterization only to ^1H NMR spectroscopy, which showed similar pattern of proton signal splitting due to the desymmetrization of macrocycle's 'faces' as observed for analogous rotaxane complexes (see Chapter 4).

5.5 Conclusion

The synthesis of *gem*-dibromoolefin masked polyyne rotaxanes was achievable using Tr*- and TIPS-capped precursors. Although a single acetylene bond, pendent to the *gem*-dibromoolefin fragment, allows threading via cross-coupling reactions to give rotaxanes in poor yields, the change from a single acetylene to a terminal butadiyne significantly improved the product yield. However, the final step of rearrangement and polyyne framework build-up has not yet been successful and requires further investigation, like careful screening of the range of reaction temperature, solvents, the source of lithium base, etc. It will also be interesting to study the Re-coordinated rotaxanes which might rearrange more smoothly. The synthesis of TIPS-capped rotaxanes uncovers the potential of polyyne rotaxanes for catenane structure assembly. The novel Re(I) tricarbonyl complex of TIPS rotaxane appears to be a promising building block for this

purpose, however, further investigations and optimization of reaction conditions will be needed before the target catenaned structures will be within reach.

5.6 Experimental Part: General Experimental Procedures

Unless stated otherwise, all reagents and solvents were used as commercially supplied, without further purification. Dry THF was obtained by passing through alumina under N_2 pressure. Column chromatography was carried out using Silica 60A (particle size 35–70 μm, Fisher, UK) as the stationary phase. Where mixtures of solvents were used, ratios reported are by volume. TLC was performed on precoated silica gel plates (0.25 mm thick, 60 F254, Merck, Germany) and visualized under UV light (254 nm). NMR spectra were recorded at 500 MHz using Bruker AVII 500 or at 400 MHz using Bruker DPX 400 instruments at 298 K, unless stated otherwise. Chemical shifts are reported in parts per million (ppm) from low to high frequency and referenced to the residual solvents resonances.[18] Coupling constants (*J*) are reported in hertz (Hz, to an accuracy of ±0.1 Hz). Standard abbreviations indicating multiplicity were used as follows: s = singlet, d = doublet, dd = double doublets, t = triplet, q = quartet, m = multiplet. Melting points (m.p.) were determined by placing the sample between a pair of microscope cover glasses on an electrically heated metal block. MALDI-TOF mass spectrometry was carried out in positive reflectron mode using a Micromass MALDI micro MX spectrometer with dithranol (1,8-dihydroxyanthrone) as a matrix. Low resolution ESI-MS was carried out on a Micromass LCT platform. UV-vis spectra were recorded at ambient temperature on a Perkin-Elmer Lambda 20 or Parkin-Elmer Lambda 25 spectrometers with 1 nm resolution; λ in nm (ε in $L \cdot mol^{-1} \cdot cm^{-1}$). IR spectra were measured by Brucker Tensor 27 spectrometer with ATR accessory.

5.7 Synthesis

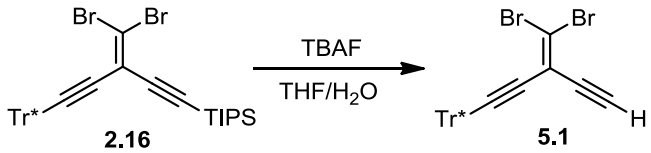

5.1:[6] To a solution of **2.16** (400 mg, 0.413 mmol) in THF (25 ml) water was added (15 mkL) and the mixture cooled down to 0 °C. The TBAF (0.5 mL, 1.0 M in THF, 0.5 mmol) was added dropwise and reaction mixture was allowed to warm up to 20 °C. After 30 min stirring the reaction was quenched by adding saturated NH_4Cl(aq) (10 mL) and the mixture stirred 5 min. The organic layer was collected,

washed with water (50 mL), brine (50 mL) and solvents were removed. Crude product was purified by plug (silica, hexanes/CH_2Cl_2 5:1) to yield the product **5.1** (340 mg, 100%) as a pale yellow solid. R_f = 0.5 (CH_2Cl_2/hexanes 1:10). ^{1}H NMR (400 MHz, $CDCl_3$) δ 7.26 (overlap with solvent residual signal), 6.98 (d, J = 2 Hz, 6H), 3.42 (s, 1H), 1.20 (s, 54H). ^{13}C NMR (100 MHz, $CDCl_3$) δ 149.9, 144.2, 123.9, 120.0, 114.1, 104.4, 83.4, 80.7, 80.3, 57.2, 34.9, 31.5. As in lit.[6b]

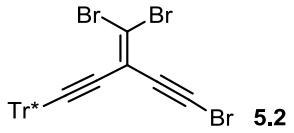

5.2

5.2:[6] This compound is synthesized according the literature procedure.[6] To a mixture of **5.1** (150 mg, 0.37 mmol) in acetone (15 mL) was added *N*-bromosuccinimide (39.8 mg, 0.45 mmol) and $AgNO_3$ (6.2 mg, 0.074 mmol) and the reaction mixture was stirred at 20 °C in darkness for 12 h. The reaction was quenched with water (10 mL) then extracted with hexanes (100 mL). The organic layer was washed with brine (50 mL) and dried over Mg_2SO_4. The solvent was removed *in vacuo* and the crude product purified by passing through a plug (silica, CH_2Cl_2/hexanes 1:10) to yield **5.2** (158 mg, 96%) as a white solid: R_f = 0.52 (CH_2Cl_2/hexanes 1:10). ^{1}H NMR (400 MHz, $CDCl_3$) δ 7.24 (t, J = 2 Hz, 3H), 6.96 (d, J = 2 Hz, 6H), 1.19 (s, 54H). ^{13}C NMR (100 MHz, $CDCl_3$) δ 149.9, 144.1, 123.9, 120.0, 114.5, 107.5, 104.4, 80.5, 77.3, 57.3, 57.2, 34.9, 31.4. As in lit.[6b]

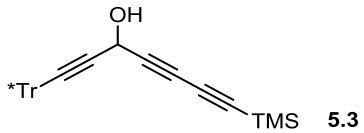

5.3

5.3: To a solution of 1,4-bis(trimethylsilyl)butadiyne (410 mg, 2.11 mmol) in THF (10 mL) cooled to 0 °C under N_2 atmosphere was added MeLi (1.33 mL, 1.6 M in Et_2O, 2.13 mmol) and the mixture was stirred for 30 min. at 20 °C. To this mixture was added a solution of **2.11** (1.25 g, 1.98 mmol) in THF (15 mL) at 0 °C and the reaction stirred at 20 °C for 12 h. The reaction was quenched with saturated aqueous NH_4Cl (20 mL), the aqueous phase was extracted with hexanes (3x30 mL). The organic phase was washed with brine (2x50 mL) and dried over $MgSO_4$. The solvent was removed *in vacuo* and the crude product was purified by column chromatography (silica, gradient with hexanes/EtOAc 50:1 to 20:1) to yield **5.3** (1.0 g, 67%) as a brown oil. ^{1}H NMR (400 MHz, $CDCl_3$) δ 7.26 (t, J = 1.8 Hz, 3H), 6.95 (d, J = 1.8 Hz, 6H), 5.26 (d, J = 8.8Hz, 1H), 2.20 (d, J = 8.3 Hz, 1H), 1.21 (s, 54H), 0.20 (s, 9H). ^{13}C NMR (100 MHz, $CDCl_3$) δ 150.0, 144.5, 123.9, 120.1, 93.1, 88.7, 87.2, 79.6, 74.6, 69.3, 56.3, 53.2, 35.0, 31.6, 0.4.

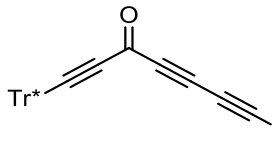

5.4

5.4: To a solution of **5.3** (300 mg, 0.409 mmol) in CH_2Cl_2 (25 mL) was added celite (0.352 g), molecular sieves (0.352 g), and PCC (176 mg, 0.918 mmol) in that order and the reaction stirred at 20 °C under a N_2 atmosphere for 1 d. The mixture was filtered through a plug of silica with CH_2Cl_2 and the solvent removed *in vacuo* to yield **5.4** (286 mg, 93%) as an orange-brown solid. ^{1}H NMR (400 MHz, $CDCl_3$) δ 7.31 (t, J = 2.1 Hz, 3H), 6.95 (d, J = 1.8 Hz, 6H), 1.23 (s, 54H), 0.25 (m, 9H); ^{13}C NMR (100 MHz, $CDCl_3$) δ 159.8, 150.4, 143.0, 123.9, 120.7, 102.7, 98.7, 86.1, 84.7, 75.4, 74.5, 57.0, 35.0, 31.5, 0.6. FTIR 2952, 2900 (w), 2866 (w), 2198, 2098, 1634, 1593 cm^{-1}. EIMS *m/z* 681.3 ([M – (CH_3)$_3$Si]$^+$), 579.4 ([M – (CH_3)$_3$Si(C≡C)$_2$CO(C≡C)]$^+$). As in lit.[6]

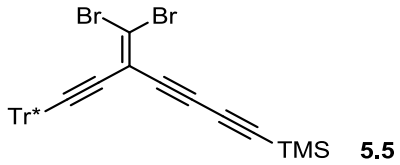

5.5

5.5: To a solution of CBr_4 (243 mg, 0.746 mmol) in CH_2Cl_2 (5 mL) was added PPh_3 (391 mg, 1.492 mmol) and the resulting mixture stirred at 20 °C under a N_2 atmosphere for 3 h. A solution of **5.4** (280 mg, 0.373 mmol) in CH_2Cl_2 (5 mL) was added and the reaction was stirred for 18 h. The reaction mixture was concentrated *in vacuo* and hexanes were added to precipitate the phosphine salts as a white solid along with an oily residue. The supernatant was decanted and filtered through a pad of silica gel (hexane). The oily residue left in the flask was dissolved in minimal CH_2Cl_2 and hexane was added; the heterogeneous mixture was then decanted and the supernatant filtered through silica gel (this procedure was repeated three times). The filtrate was filtered through silica gel until the filtrate remained a clear solution. The solvent was removed *in vacuo* yielding **5.5** (206 mg, 61%) as a brown solid. ^{1}H NMR (400 MHz, $CDCl_3$) δ 7.26 (t, J = 1.7 Hz, 3H), 6.98 (d, J = 1.5 Hz, 6H), 1.22 (s, 54H), 0.22(s, 9H). ^{13}C NMR (100 MHz, $CDCl_3$) δ 150.0, 144.2, 124.0, 120.1, 114.1, 109.2, 105.0, 94.7, 87.5, 80.3, 80.0, 73.0, 57.4, 36.0, 31.6, -0.4. FTIR 2947, 2867, 2362 (vw), 2108 (w), 1461 cm^{-1}.

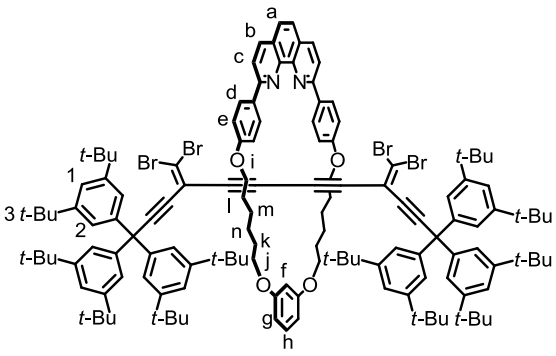

5a⊂M1: To a solution of macrocycle **M1** (29.8 mg, 46.7 μmol) in CH_2Cl_2 (1.5 mL) a solution of CuI (8.9 mg, 46.7 μmol) in CH_3CN (1.5 mL) was added and the mixture was stirred for 1 h at 20 °C. The solvents were removed *in vacuo* and the residue re-dissolved in THF (2 mL). This solution was then added to a mixture of dibromolefine **5.1** (38 mg, 46.7 μmol), dibromolefine bromide **5.2** (50 mg, 56.1 μmol) K_2CO_3 (25.8 mg, 187 μmol) in THF (2 mL). The mixture was flushed with nitrogen, and stirred at 60 °C for 2 d. After cooling to 20 °C, the reaction was quenched by the addition of KCN (12 mg, 187 μmol, in 1 mL H_2O), deluted with CH_2Cl_2 (1 mL), MeCN (1 mL), and stirred at 20 °C for 1 h. More CH_2Cl_2 (5 mL) was added, the organic phase separated, washed with H_2O and the solvents were removed. Column chromatography (silica, hexanes:EtOAc 25:1) afforded the product **5a⊂M1** as a yellow solid (6 mg, 9 %). ^{1}H NMR (500 MHz, CD_2Cl_2) δ 8.55 (d, J = 8.6 Hz, 4H, H_d), 8.30 (br. s, 2H, H_b), 8.14 (d, J = 8.2 Hz, 2H, H_b), 7.78 (s, 2H, H_a), 7.23 (s, 6H, H_1), 7.16 (d, J = 8.8 Hz, 4H, H_e), 7.0 (t, J = 8.2 Hz, 1H, H_h), 6.92 (t, J = 1.5 Hz, 12H, H_2), 6.58 (br. t, J = 1.7 Hz, 1H, H_f), 6.41 (dd, J_1 = 2.2 Hz, J_2 = 6.0 Hz, 2H, H_g), 4.15 (t, J = 7.2 Hz, 4H, H_i), 4.0 (t, J = 6.6 Hz, 4H, H_j), 1.92 (m, 4H, H_k), 1.84 (m, 4H, H_l), 1.61(m, 8H, $H_{m,n}$), 1.14 (s, 108H). ^{13}C NMR (125 MHz, CD_2Cl_2) δ 161.1, 160.9, 156.0, 150.6, 146.3, 144.3, 130.0, 129.4, 127.9, 125.9, 125.3, 124.0, 120.7, 115.2, 114.7, 113.2, 107.9, 105.7, 100.4, 80.1, 79.4, 75.3, 70.1, 68.6, 68.2, 65.4, 57.7, 35.1, 31.5, 30.1, 29.6, 26.4, 26.3. *m/z* (MALDI TOF MS+) calcd. for $C_{140}H_{168}N_2O_4Br_4$ ([M]) 2262.97, found 2261.93, for $C_{140}H_{168}N_2O_4Br_3$ ([M–Br $^-$]$^+$) 2182.06, found 2182.03, for $C_{140}H_{168}N_2O_4Br_2$ ([M–2Br $^-$]$^{2+}$) 2102.14, found 2101.99. UV-vis (THF) λ_{max} / nm (ε / M^{-1} cm^{-1}) 286 (74000), 327 (40000). UV-vis (CH_2Cl_2) λ_{max} / nm (ε / M^{-1} cm^{-1}) 286 (69100), 327 (38800).

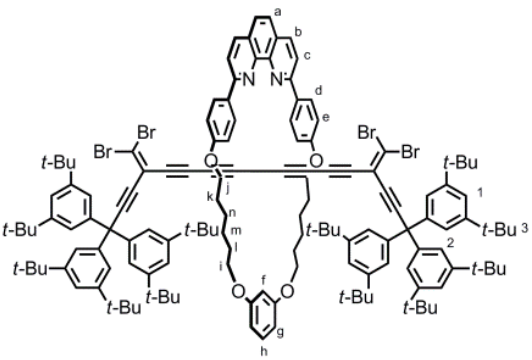

5b⊂M1. To a solution of **5.5** (100 mg, 11 μmol) in THF (7.5 mL) and MeOH (7.5 mL) was added K_2CO_3 (15.2 mg, 11 μmol). After stirring for 1 h, the solvent was removed *in vacuo* and the crude product was purified by passing through silica column (hexanes) to yield deprotected **5.6** (90 mg, 98%) as a white solid. The product was immediately

proceeded for the next step. To a solution of macrocycle **M1** (13.7 mg, 21.5 μmol) in CH_2Cl_2 (1.5 mL) a solution of CuI (4.1 mg, 21.5 μmol) in CH_3CN (1.5 mL) was added and the mixture was stirred for 1 h at 20 °C. The solvent was removed *in vacuo* and the residue re-dissolved in THF (2 mL). This solution was then added to a mixture of **5.6** (45 mg, 53.7 μmol), K_2CO_3 (12 mg, 87 μmol) and I_2 (5.7mg, 22.3 μmol) in THF (2 mL). The reaction mixture was flushed with nitrogen, and stirred at 60 °C for 2 days. After cooling to 20 °C, the reaction was quenched by the addition of KCN (5.8 mg, 89 μmol, in 1 mL H_2O), deluted with CH_2Cl_2 (1 mL), CH_3CN (1 mL), and and stirred at 20 ºC for 2 h. CH_2Cl_2 (5 mL) was added, the organic phase separated, washed with H_2O (10 mL) and the solvents were removed. Column chromatography (silica, hexanes/EtOAc 25 : 1) followed by recrystallization from CH_2Cl_2/MeOH afforded the product **5b⊂M1** as a yellow solid (25 mg, 51.4%). ^{1}H NMR (500 MHz, CD_2Cl_2) δ 8.55 (d, J = 8.3 Hz, 4H, H_d), 8.30 (br. s, 2H, H_b), 7.98 (d, J = 8.2 Hz, 2H, H_c), 7.78 (s, 2H, H_a), 7.23 (br. s, 6H, H_1), 7.16 (d, J = 8.8 Hz, 4H, H_e), 7.0 (t, J = 8.2 Hz, 1H, H_h), 6.93 (d, J = 1.5 Hz, 12H, H_2), 6.58 (br. s, 1H, H_f), 6.41 (dd, J_1 = 2.2 Hz, J_2 = 6.0 Hz, 2H, H_g), 4.13 (t, J = 7.3 Hz, 4H, H_j), 4.0 (t, J = 6.7 Hz, 4H, H_i), 1.93–1.84 (m, 8H, $H_{k,l,}$), 1.61 (br. s, 8H, $H_{m,n}$), 1.14 (s, 108H, H_{11}). ^{13}C NMR (125 MHz, CD_2Cl_2) δ 160.9, 156.0, 150.6, 146.3, 144.3, 137.1, 131.7, 130.0, 129.4, 127.9, 125.9, 125.3, 124.0, 120.6, 119.2, 115.2, 110.2, 114.7, 113.2, 107.9, 105.7, 100.4, 80.1, 79.4, 75.3, 70.1, 68.6, 68.2, 65.4, 57.7, 35.1, 31.5, 30.1, 29.6, 26.4, 26.3. *m/z* (MALDI TOF MS+) calcd. for $C_{144}H_{169}N_2O_4Br_4$ ($[M+H^+]^+$) 2311.97, found 2311.93, for $C_{140}H_{168}N_2O_4Br_2$ ($[M^+–2Br^-]^+$) 2151.06, found 2152.03, for $C_{140}H_{168}N_2O_4Br$ ($[M^+–3Br^-]^+$) 2072.14, found 2071.99. UV-vis (THF) λ_{max} / nm (ε / M^{-1} cm^{-1}) 286 (92000), 340 (52000), 361 (38300), 389 (27000), 421 (18500). UV-vis (CH_2Cl_2) λ_{max} / nm (ε / M^{-1} cm^{-1}) 286 (156000), 340 (88100), 361 (64700), 389 (45500), 421 (22000).

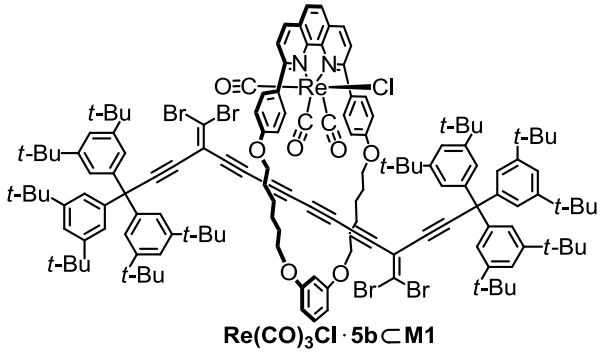

Re(CO)3Cl·5b⊂M1: A solution of **5b⊂M1** (10.0 mg, 4.3 μmol) and rhenium(I) pentacarbonyl chloride (1.7 mg, 4.7 μmol) in toluene (3 mL) was refluxed under nitrogen for 3 h. The solution was cooled to 20 °C, solvent removed and the residue dried under vacuum. Crude product was purified by column chromatography (hexanes:EtOAc 10:1 to EtOAc). The residue was washed with hexanes and recrystallize from CH_3OH afforded the product as a yellow solid (9.3 mg, 80%). ^{1}H NMR (500 MHz, CD_2Cl_2) δ 8.58

(dd, J_1 = 8.3 Hz, J_2 = 1.7 Hz 2H), 8.06 (d, J = 2.8 Hz, 2H), 7.98 (d, J = 8.2 Hz, 2H), 7.72 (br. s, 4H), 7.25–7.23 (m, 6H), 7.13 (br. s, 4H), 6.96 (dd, J_1 =1.7 Hz, J_2 = 6.4 Hz, 12H), 6.84 (d, J = 8.1, 1H), 6.48 (t, J = 2.5 Hz, 1 H), 6.33 (dd, J_1 = 8.0 Hz, J_2 = 3.1 Hz, 2H), 4.23–4.07 (m, 8H), 3.97–3.87 (m, 4H), 1.95–1.76 (m, 8H), 1..14 (d, J_1 = 7.5 Hz, 108H). ^{13}C NMR (125 MHz, CD_2Cl_2)δ193.0, 192.6, 164.1, 161.1, 160.5, 150.2. 150.1, 149.1, 148.9, 144.0, 143.9, 137.9, 134.5, 134,3, 129.7, 129.5, 126.7, 126.0, 124.9, 120.3, 120.2, 114.7, 114.4, 113.4, 113.0, 12.8, 112.8, 107.5, 105.2, 104.7, 100.0, 80.3, 79.9, 79.9, 79.6, 74.2, 73.6, 71.0, 69.4, 68.3, 67.8, 65.3, 64.1, 57.3, 34.7, 31.1, 29.6, 28.7, 25.6, 25.6.

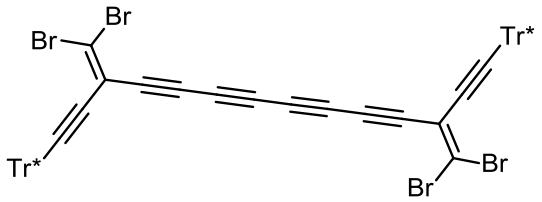

5.b: To a solution of **5.5** (33.0 mg, 35.9 μmol) in a mixture of THF (2 mL) and CH_3OH (2 mL) K_2CO_3 (5 mg, 35.9 μmol) was added and the reaction mixture was stirred for 3 h at 20 °C. The solvent was removed *in vacuo* and the crude product was purified by passing through silica plug (hexanes) to yield deprotected **5.6**To a solution of TMEDA (16 μL, 108 μmol) in CH_2Cl_2 (6 mL) CuCl (3.6 mg, 35.9 μmol) was added and oxygen was bubbled into the solution for 5 min. The deprotected **5.6** was dissolved in CH_2Cl_2 (4 mL) and the solution was transfer to the CuCl-TMEDA mixture. After 5 min stirring (TLC monitoring, hexanes + 10% CH_2Cl_2) the reaction mixture was passed through silica plug (CH_2Cl_2) and the solvent was removed affording the product **5.b** (29.0 mg, 99 %) as a yellow solid. R_f = 0.78 (hexanes + 10% CH_2Cl_2). ^{1}H NMR (500 MHz, CD_2Cl_2) δ 7.32 (t, J = 1.9 Hz, bH), 7.0 (d, J = 1.8 Hz, 12H), 1.22 (s, 108H). ^{13}C NMR (125 MHz, CD_2Cl_2) δ 150.7, 144.3, 124.1, 120.8, 113.7, 112.5, 106.0, 80.4, 79.9, 74.8, 70.3, 64.7.0, 57.8, 35.3, 31.6. Uv-vis (THF) λ_{max} / nm (ε / M^{-1} cm^{-1}) 417 (18000), 387 (27000), 358 (27000), 337 (52000), 315 (45000), 301 (48000), 255 (48000).

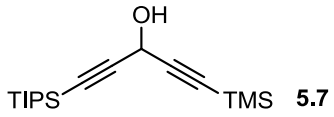

5.7

5.7:[19] To a solution of TIPS-acetylene (0.70 mL, 0.49 g, 4.97 mmmol) in deoxygenated THF (60 mL) *n*-BuLi (2.10 mL, 5.26 mmol, 2.2M in Et_2O) was added at –40 °C under nitrogen. The reaction mixture was cooled down to –78 °C and a solution of TIPS-propargylic aldehyde **2.13** (0.87 g, 4.14 mmol) in THF (10 mL) was added. The reaction mixture was stirred for 3 h upon warming to 20 °C. The reaction was quenched by saturated NH_4Cl(aq) (10 mL), washed with brine (100 mL) and the organic phase was

collected. The solvents were removed and the crude mixture was purified by column chromatography (hexanes:CH_2Cl_2 1:1) affording the product 5.7 (0.90 g, 71%) as a brown oil. Rf = 0.4 (hexanes:CH_2Cl_2 1:1). ^{1}H NMR (400 MHz, $CDCl_3$) δ 5.09 (s, 1H), 2.16 (br. s, 1H), 1.08 (s, 21H), 0.18 (s, 9H). 1^3CNMR (100 MHz, $CDCl_3$) δ 104.1, 102.2, 86.4, 53.1, 18.6, 11.3, -0.3. As in lit.[19]

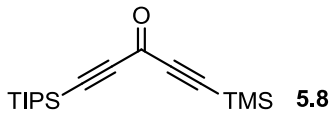

5.8

5.8:[19] To a solution of **5.7** (1.08 g, 3.5 mmol) in CH_2Cl_2 (200 mL) was added celite (3.0 g), molecular sieves (3.0g), and PCC (1.51 g, 7.70 mmol) in that order and the reaction stirred at 20 °C under a N_2 atmosphere for 1 d. The mixture was filtered through a plug of silica with CH_2Cl_2 and the solvent removed *in vacuo* to yield **5.8** (0.90 g, 84%) as an orange-brown oil. ^{1}H NMR (400 MHz, $CDCl_3$) δ 1.09 (s, 21H), 0.23 (s, 9H). ^{13}C NMR (100 MHz, $CDCl_3$) δ 160.3, 105.1, 103.0, 99.5, 98.3, 18.6, 11.2, -0.8. As in lit.[19]

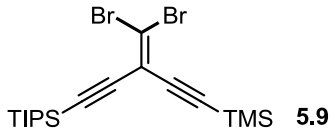

5.9

5.9:[19] To a solution of CBr_4 (1.92 g, 5.88 mmol) in CH_2Cl_2 (5 mL) was added PPh_3 (3.08 g, 11.76 mmol) and the resulting mixture stirred at 20 °C under a N_2 atmosphere for 3 h. A solution of **5.8** (900 mg, 2.94 mmol) in CH_2Cl_2 (5 mL) was added and the reaction was stirred for 24 h. The reaction mixture was concentrated and hexanes were added to precipitate the Ph_3PO as a white solid along with an oily residue. The supernatant was decanted and filtered through a plug of silica gel (hexane). The oily residue left in the flask was dissolved in minimal CH_2Cl_2 and hexane was added; the heterogeneous mixture was then decanted and the supernatant filtered through silica gel (this procedure was repeated three times). The solvent was removed *in vacuo* yielding**5.9** (780 mg, 55%) as a light yellow solid. ^{1}H NMR (400 MHz, $CDCl_3$) δ 1.10 (s, 21H), 0.22 (s, 9H). ^{13}C NMR (100 MHz, $CDCl_3$) δ 114.7, 109.7, 102.5, 102.4, 100.5, 99.9, 18.7, 11.3, -0.3. As in lit.[19]

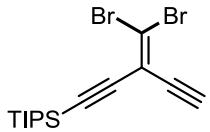

5.10

5.10:[19] To a solution of **5.9** (200 mg, .42 mmol) in THF (10 mL) and MeOH (10 mL) was added K_2CO_3 (69.0 mg, 0.5 mmol). The reaction mixture was stirred for 15 min, the solvent was removed *in vacuo* and the crude product was purified by passing through silica column (hexanes) to yield **5.10** (170 mg, 100%) as a oil. R_f = 0.59 (hexanes). ^{1}H NMR (400 MHz, $CDCl_3$) δ 3.48 (s, 1H), 1.09 (s, 21H). ^{13}C NMR (100 MHz, $CDCl_3$) δ 113.9, 110.7, 101.9, 100.4, 83.7, 80.0, 18.7, 11.3.As in lit.[19]

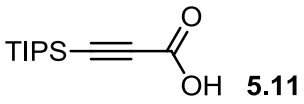

5.11

Triisopropylsilanylpropynoic acid 5.11:[14] A solution of triisopropylsilanylacetylene (3.00 mL, 2.43 g, 13.38 mmol) in THF (100 mL) was cooled under N_2 to 0 °C. A solution of MeLi (1.6 M in ethyl ether, 11.7 mL, 18.73 mmol) was added and the mixture was stirred for 1 h and then cooled to –78 °C and CO_2 gas was bubbled into the solution for 1 h. The reaction mixture was quenched by the slow addition of ~2.0 M aqueous $KHSO_4$ (30 mL), warmed to 20 °C, and extracted with EtOAc. The combined organic layers were washed with brine, dried ($MgSO_4$) and concentrated to a yellow syrup that was diluted with toluene (50 mL), passed through silica plug and eluted with EtOAc (300 mL).The filtrate was concentrated to afford triispropylsilanylpropynoic acid **5.11** (2.9 g, 96%) as yellow syrup that crystallized to a pale yellow solid *in vacuo*. ^{1}H NMR (400 MHz, $CDCl_3$) δ 10.92 (bs, 1 H), 1.21-1.02 (m, 21 H); ^{13}C NMR (100 MHz, $CDCl_3$) δ 157.7, 96.1, 95.1, 18.6, 11.1. As in lit.[14]

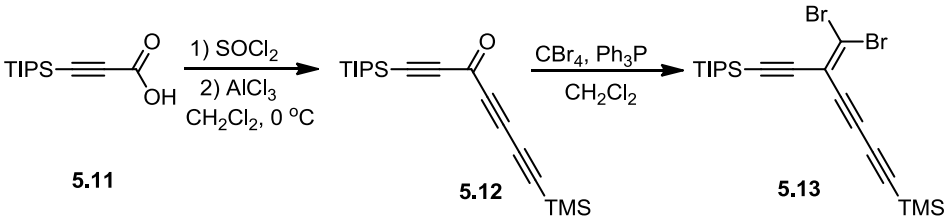

5.11 **5.12** **5.13**

5.13:[5] The compound **5.11** (1.0 g, 4.44 mmol) was dissolved in $SOCl_2$ (2.24 mL, 31.1 mmol) in a flask equipped with $CaCl_2$ drying tube and stirred at 20 ºC for 20 h. The $SOCl_2$ was removed *in vacuo*, 1,2-bis(trimethylsilyl)acetylene (0.912 g, 4.7 mmol) added and the resulting mixture dissolved in dry CH_2Cl_2 (15 mL). To this solution was added slowly $AlCl_3$ (0.712 g, 5.33 mmol) at 0 °C under a N_2 atmosphere and then stirred at 0 °C for 4 h. The reaction was quenched with ice/HCl (10%) (100 mL) at 0 °C and allowed to warm to 20 ºC The organic layer was extratced with Et_2O (150 mL), washed with brine (2 × 50 mL) and dried over $MgSO_4$. The solvent was removed *in vacuo*, the crude product passed through a plug of silica gel (hexane CH_2Cl_2 1:1) and the solvent removed *in vacuo* to yield crude ketone **5.12** (1.27 g, 87%) as a

brown oil which decomposed slowly. Concurrently, to a solution of CBr_4 (6.490 g, 19.57 mmol) in CH_2Cl_2 (200 mL) was added PPh_3 (10.96 g, 41.79 mmol) and the mixture stirred for 1 h under a N_2 atmosphere. The crude ketone was dissolved in CH_2Cl_2 (50 mL), added dropwise, and the mixture stirred at 20 ºC for 2 h under a N_2 atmosphere. The reaction mixture was concentrated *in vacuo* to ca. 50 mL and then hexanes were added to precipitate the phosphine salts as a white solid along with an oily residue. The supernatant was decanted and filtered through a pad of silica. The oily residue left in the flask was dissolved in minimal CH_2Cl_2 and hexanes were added; the heterogeneous mixture was then decanted and the supernatant filtered through silica (this procedure was repeated three times). The solvent was removed *in vacuo* and the crude product purified by column chromatography (silica, hexanes) to yield **5.13** (1.988 mg, 36%) as a brown oil. R_f = 0.59 (CH_2Cl_2/hexanes 1:1); ^{1}H NMR (400 MHz, $CDCl_3$) δ 0.96 (s, 9H), 0.24 (s, 9H), 0.18 (s, 6H). ^{13}C NMR (100MHz, $CDCl_3$) δ 160.1, 103.4, 102.6, 99.4, 98.7, 25.9, 16.8, –0.9, –5.4.

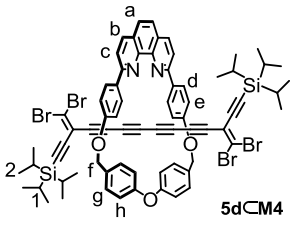

5d⊂M4

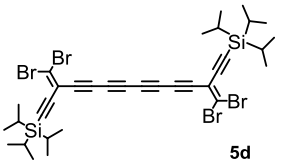

5d

5d⊂M4:To a solution of macrocycle **M4** (55.1 mg, 98.7 μmmol) in CH_2Cl_2 (4 mL) a solution of CuI (18.86 mg, 98.7 μmol) in CH_3CN (4 mL) was added and the mixture was stirred for 1 h at 20 ºC. The solvents were removed *in vacuo* and the residue re-dissolved in THF (4 mL). To the solution of dibromolefine **5.13** (120 mg, 95 μL, 0.247 mmol) in 1:1 mixture of THF and CH_3OH (20 mL) was added K_2CO_3 (34 mg, 0.247 mmol). The reaction mixture was stirred at 20 ºC for 10 min, then the reaction was quenched by addition of saturated NH_4Cl (50 mL), the organic phase was extracted by Et_2O (3 × 50 mL), organic phases were combined, washed with brine (50 mL) and dried over $MgSO_4$. Solvents were removed to the minimum and the mixture was passed through silica plug (hexanes).The solvent volume was reduced to the minimum *in vacuo*, ~ 20 ml THF was added and solvent was removed again to the minimum volume: This procedure was repeated 3 times. In the end this mixture was added to a mixture of CuI·**M4** complex, K_2CO_3 (54.5 mg, 395 μmol) and I_2 (27.8mg, 109 μmol) in THF (4 mL). The reaction mixture was flushed with nitrogen, and stirred in schlenk tube at 65 °C for 2 d. After cooling to 20 ºC, the reaction was quenched by the addition of KCN (25 mg, 384 μmol, in 2 mL H_2O), deluted with CH_2Cl_2 (4 mL) the organic phase separated, washed with H_2O and the solvents were removed. Column chromatography (silica,

hexanes:EtOAc 20 : 1) afforded the product **5d⊂M4** as a dark yellow oil (30 mg, 22%). ^{1}H NMR (500 MHz, $CDCl_3$) δ 8.19 (d, J = 8.3 Hz, 2H, H_b), 7.97 (d, 4H, J = 8.7 Hz, H_d), 7.88 (d, J = 8.4 Hz, 2H, H_c), 7.70 (s, 2H, H_a), 7.31 (q, J = 9.1 Hz, 8H, $H_{g,h}$), 6.93 (d, J = 8.7 Hz, 4H, H_e), 5.31 (s, 4H, H_f), 1.06–1.05 (overlapped s, 42H, $H_{1,2}$). ^{13}C NMR (125 MHz, $CDCl_3$) δ 159.4, 158.4, 157.8, 146.7, 136.3, 134.2, 134.0, 129.9, 127.4, 125.6, 122.4, 120.4, 116.3, 114.5, 113.2, 101.4, 100.6, 80.9, 73.9, 71.5, 70.5, 67.2, 65.6, 18.7, 11.2. *m/z* (MALDI TOF MS+) calcd. for $C_{72}H_{81}N_2O_3Si_2Br_4$ ($[M+H^+]^+$) 1385.15, found 1385.71, for $C_{72}H_{80}N_2O_3Si_2Br_3$ ($[M–Br^-]^-$) 1305.23, found 1304.94, for $C_{72}H_{81}N_2O_3Si_2Br_2$ ($[M+H^+–2Br^-]^{-+}$) 1225.31, found 1225.21. UV-vis (CH_2Cl_2) λ_{max} / nm (ε / M^{-1} cm^{-1}) 244 (72600), 268 (82500), 285 (91500), 321 (69600), 339 (85000), 361 (48500), 389 (25600), 422 (16100). UV-vis (THF) λ_{max} / nm (ε / M^{-1} cm^{-1}) 267 (102000), 278 (98000), 318 (81100), 338 (104000), 3361 (45600), 389 (28000). 422 (18700).

From the silica column yellow fraction was collected before the rotaxane. The NMR analysis confirmed the formation of free dumbbell **5d** (60 mg, 59%).[5] ^{1}H NMR (400 MHz, $CDCl_3$) δ 1.10 (s, 36H), 1.09 (overlapped s, 6H). ^{13}C NMR (100 MHz, $CDCl_3$) δ 114.7, 113.3, 102.0, 100.5, 80.0, 74.1, 70.4, 64.9, 18.7, 11.2. As in lit.[5]

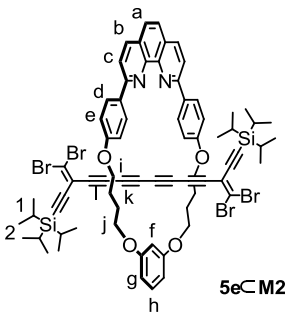

5e⊂M2

5e⊂M2:To a solution of macrocycle **M2** (122.7 mg, 211 μmmol) in CH_2Cl_2 (5 mL) a solution of CuI (40.3 mg, 211 μmol) in CH_3CN (5 mL) was added and the mixture was stirred for 1 h at 20 ºC. The solvents were removed *in vacuo* and the residue re-dissolved in THF (8 mL). To the solution of dibromolefine **5.13** (120 mg, 165 μL, 0.422 mmol) in 1:1 mixture of THF and CH_3OH (40 mL) was added K_2CO_3 (58.3 mg, 0.422 mmol). The reaction mixture was stirred at 20 ºC for 10 min (TLC: hexanes), then the reaction was quenched by addition of saturated NH_4Cl (50 mL), the organic phase was extracted by Et_2O (3 × 100 mL), combined, washed with brine (100 mL) and dried over $MgSO_4$. Solvents were removed to the minimum and the mixture was passed through silica plug (hexanes). The solvent volume was reduced to the minimum *in vacuo*, THF (~ 20 ml) was added and solvent was reduced to the minimum volume: This procedure was repeated 3 times. In the end this mixture was added to a mixture of CuI·**M2** complex, K_2CO_3 (116 mg, 844 μmol) and I_2 (54 mg, 211 μmol) in THF (8 mL). The reaction mixture was flushed with nitrogen, and stirred in schlenk tube at 60 °C. After 24 h stirring TLC showed

unreacted acetylene ans new portion of I_2 (10 mg, 39 μmol) was added and the reaction mixture was stirred additional 24 h. After cooling to 20 ºC, the reaction was quenched by the addition of KCN (25 mg, 384 μmol, in 2 mL H_2O), EDTA (830 mg, 850 μmol) deluted with CH_2Cl_2 (10 mL) the organic phase separated, washed with H_2O and the solvents were removed. Column chromatography (silica, hexanes/EtOAc 20 : 1 to 10 : 1) afforded the product **5e⊂M2** as a yellow oil (40 mg, 13.4%). ^{1}H NMR (500 MHz, $CDCl_3$) δ 8.49 (d, J = 8.8 Hz, 4H, H_d), 8.24 (d, J = 8.4 Hz, 2H, H_b), 8.06 (d, J = 8.4 Hz, 2H, H_c), 7.72 (s, 2H, H_a), 7.19 (d, J = 8.9 Hz, 4H, H_e), 7.14 (t, J = 8.2 Hz, 1H, H_h), 6.72 (t, J = 2.3 Hz, 1H, H_f), 6.52 (dd, J_1 = 8.2, J_2 = 2.3 Hz, 2H, H_g), 4.27 (t, J = 7.8 Hz, 4H, H_i), 4.11 (t, J = 6.4 Hz, 4H, H_j), 2.13 (m, 4H, H_k), 2.01 (m, 4H, H_l), 0.99 (s, 36H, H_1), 0.98 (overlapped s, 6H, H_2). ^{13}C NMR (125 MHz, $CDCl_3$) δ 160.5, 160.3, 156.3, 146.2, 136.6, 132.2, 129.8, 129.3, 127.4, 125.5, 119.1, 116.3, 115.2, 112.7, 107.6, 102.1, 101.9, 100.2, 79.7, 75.0, 70.8, 68.4, 67.8, 65.8, 26.4, 26.1, 18.6, 11.1. *m/z* (MALDI TOF MS+) calcd. for $C_{72}H_{79}N_2O_4\ Si_2Br_4$ ($[M+H^+]^+$) 1409.21, found 1409.48, for $C_{72}H_{79}N_2O_4Si_2Br_3$ ($[M+H^+–Br^-]$) 1330.29, found 1330.68, for $C_{72}H_{79}N_2O_4Si_2Br_2$ ($[M+H^+–2Br^-]^-$) 1249.37, found 1249.94. UV-vis (CH_2Cl_2) λ_{max} / nm (ε / M^{-1} cm^{-1}) 244 (73700), 268 (83700), 285 (92900), 321 (70700), 339 (86300), 361 (49300), 389 (26000), 422 (16400). UV-vis (THF) λ_{max} / nm (ε / M^{-1} cm^{-1}) 245 (77100), 268 (85300), 284 (92100), 321 (69200), 339 (84600), 361 (49000), 389 (25400). 421 (16500).

5.8 References

1. Siemsen, P.; Livingston, R. C.; Diederich, F. *Angew. Chem. Int. Ed*. **2000**, *39*, 2632–2657.
2. Orita, A.; Otera J. *Chem. Rev.* **2006**, *106*, 5387–5412.
3. (a) Rubin, Y.; Kahr, M.; Knobler, C. B.; Diederich, F.; Wilkins, C. L. *J. Am. Chem. Soc.* 1991, *113*, 495–500. (b) Rubin, Y.; Knobler, C. B.; Diederich, F. *J. Am. Chem. Soc.* 1990, *112*, 4966–4968. (c) Tobe, Y.; Fujii, T.; Naemura, K. *J. Org. Chem.* 1994**,** *59*, 1236–1237. (d) Simpkins, S.M. E.; Weller, M. D.; Cox, L. R. *Chem. Commun.* **2007**, 4035–4037.
4. (a) Eisler, S.; Tykwinski, R. R. *J. Am. Chem. Soc*. **2000**, *122*, 10736–10737. **(**b) Eisler, S.; Chahal, N.; McDonald, R.; Tykwinski, R. R. *Chem. Eur. J.* **2003**, *9*, 2542–2550. (c) Shi Shun, A. L. K.; Chernick, E. T.; Eisler, S.; Tykwinski, R. R. *J. Org. Chem.* **2003**, *68*, 1339–1347. (d) Morisaki, Y.; Luu, T.; Tykwinski, R. R. *Org. Lett.* **2006**, *8*, 689–692. (e) Jahnke, E.; Tykwinski, R. R. *Chem. Commun*. **2010**, *46*, 3235–3249.
5. Eisler, S.; Slepkov, A. D.; Elliott, E.; Luu, T.; McDonald, R.; Hegmann, F. A.; Tykwinski, R. R. *J. Am. Chem. Soc.* **2005**, *127*, 2666–2676.
6. (a) Chalifoux, W. A.; Tykwinski, R. R. *Nat. Chem.* **2010**, *2*, 967–971. (b) Chalifoux, W. A. *'Towards Carbyne: Synthesis and Study of Extremely Long Polyynes*' PhD thesis, University of Alberta, Alberta, **2009**.
7. (a) Stephens, R. D.; Castro, C . E. *J. Org. Chem*. 1**963**, *28*, 3313–3315. (b) Kauffmann, T. *Angew. Chem*. 1**974**, *86*, 321–335; *Angew. Chem. Int. Ed. Engl.* 1**974**, *13*, 291–305.
8. (a) Corey, E. J.; Fuchs, P. L. *Tetrahedron Lett.* **1972**, *13*, 3769–3772. (b) N. B. Desai, N. McKelvie, F. Ramirez *J. Am. Chem. Soc.* **1962**, *84*, 1745–1747.
9. Bichler, P.; Chalifoux, W. A.; Eisler, S.; Shi Shun, A. L. K.; Chernick, E. T.; Tykwinski, R. R. *Org. Lett.* **2009**, *11*, 519–522.

10. (a) Fritsch, P. *Liebigs Ann. Chem.* **1894**, *279*, 319–323. (b) Buttenberg, W. P. *Liebigs Ann. Chem.* **1894**, *279*, 324-337. (c) Wiechell, H. *Liebigs Ann.Chem.* **1894**, *279*, 337–344.

11. Hay, S. A. *J. Org. Chem.* **1962**, *27*, 3320–3321.

12. (a) Stang, P. J. *Chem. Rev*. **1978**, *78*, 383–405. (b) van Loon, J.-D.; Seiler, P.; Diederich, F. *Angew. Chem. Int. Ed. Engl.* **1993**, *32*, 1187–1189 (*Angew. Chem*. 1**993**,*105*, 1235–1238). (c) Auffrant, A.; Diederich, F.; Boudon, C.; Gisselbrecht, J.-P.; Gross, M. *Helv. Chim. Acta*, **2004**, *87*, 3085–3105. (d) Kunieda, T.; Takizawa, T. *Chem. Pharm. Bull*. **197**7, *25*,1809–1810.

13. Kuritani, M.; Tashiro, S.; Shionoya, M. *Inorg. Chem*., **2012**, 51, 1508–1515.

14. Wipf, P.; Graham, T. H. *Org. Biomol. Chem.* **2005**, ***3***, 31–35.

15. Walton, D. R. M.; Waugh, F. *J. Organomet. Chem.* **1972**, *37*, 45–56.

16. Eglinton, G.; Galbraith, A. R. *Chem. Ind.(London)* **1956**, 737–738.

17. (a) Diederich, F. ; Rubin, Y.; Knobler, C. B.; Whetten, R. L.; Schriver, K. E.; Houk, K. N. ; Li, Y. *Science*, **1989**, *245*, 1088–1090. (b) Diederich, F.; Rubin, Y. *Angew. Chem., Int. Ed. Engl*. **1992**, *31*, 1101–1124. (c) von Helden, G.; Gotts, N. G.; Bowers, M. T. *J. Am. Chem. Soc*. **1993**, *115*, 4363–4364 (d) Rubin, Y.; Diederich, F. *J. Am. Chem. Soc.* **1989**, *111*, 6870–6871.

18. Fulmer, G. R.; Miller, A. J. M.; Sherden, N. H.; Gottlieb, H. E.; Nudelman, A.; Stoltz, B. M. Bercaw, J. E.; Goldberg, K. I. *Organometallics.* **2010**, *29*, 2176–2179.

19. Anthony, J.; Boldi, A. M.; Rubin, Y.; Hobi, M.; Gramlich, V.; Knobler, C. B.; Seiler, P.; Diederich, F. *Helv. Chim. Acta* **1995**, *78*,13–45.

Chapter 6. General Discussion and Future Directions

Previously, the synthesis of stable polyynes with up to 22 triple bonds has been achieved[1] using the supertrityl end-group, however, the stabilizing effect of the end group decreases upon the elongation of carbon chain, and it seems that new synthetic strategies are necessary to go beyond the stable 44 sp^1 carbon atom chains, in order to approach the properties of carbyne.

This thesis has summarized polyyne rotaxane synthesis showing that rotaxination is an effective way to thread the polyyne chains with a macrocyclic component, creating kind of 'insulated' molecular wires. We demonstrated that the synthesis of rotaxinated polyynes with up to 24 sp^1 carbon atoms on the chain is achievable, however, this approach of mechanical insulation could, in principle, be expanded to the synthesis of longer insulated polyynes. It is expected that mechanical encapsulation will stabilize the polyyne, further enabling the synthesis of carbyne-like insulated molecular wires. Additionally, it has been shown that by applying different synthetic approaches polyyne rotaxanes with different topological order can be prepared.

Another aspect of polyynes discussed in the thesis is the investigation of some photophysical properties of polyyne rotaxanes, particularly *intermolecular* energy transfer in rotaxanes. We have characterized the excited states of polyynes by vibrational and absorption spectroscopy and shown that the polyyne chain is an excellent singlet and triplet excited state energy harvester in rotaxanes. This findings provide more insights into the rich photophysics of polyynes.

The last, fifth chapter of the thesis describes the synthesis of masked polyyne rotaxanes. Unfortunately, this work has not been yet finished due to time restriction, however it encompasses a great potential to prepare insulated cyclocarbons via alkylidene carbenoid rearrangement.[2] Previously, cyclocarbon formation was observed in the gas phase from cyclic precursors.[3] Moreover, it was shown by Diederich and coworkers that in the gas phase the coalescence of cyclocarbons gives fullerenes.[4] The same authors also suggested that in order to obtain stable cyclocarbons, more rigid structures are required, which would not allow the cyclocarbon to undergo fragmentation or rearrangement. Continuing this idea, it seems that the synthesis of polyyne-based catenanes and subsequent reconstruction of polyyne framework could be a promising strategy to isolate the cyclocarbon as a bulk material (Scheme 1).

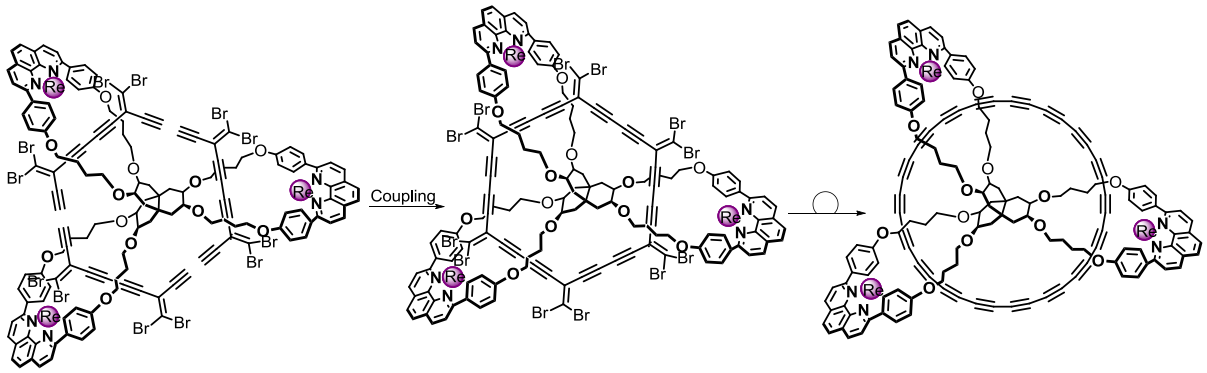

Scheme 1 A possible route towards insulated cyclocarbon.

In chapter 5 we showed that the coordination of Re(I) carbonyl complexes to the macrocycle is a convenient way to reduce the macrocycle cavity size, after rotaxane synthesis. This should allow the dibromoethene moieties to act as a stopper when TIPS or other bulky protective end groups are removed. Then, the terminal acetylene could be threaded through another macrocycle. If the dibromoethene unit can be used as a stopper, then a tripod macrocycle might be used to direct the formation of a catenane, as shown in Scheme 1. The use of tripodal macrocycle (Scheme 1) should provide rigidity to the whole architecture supposedly stabilizing and protecting the reactive cyclocarbon, as it was proposed.

Another interesting strategy towards insulated cyclocarbons could be the development of the chemistry of Pt-polyyne rotaxanes, discussed in Appendix B. So far, all our attempts to make Pt-polyyne rotaxanes were unsuccessful, but it is very attractive to carry out the rotaxination of the planar Pt-polyynes squares[5] (Scheme 2). Using the procedure of reductive elimination of Pt, developed by Bäuele and co-worker,[6] the cyclo[48]carbon-based [5]catenane could be constructed.

Since it was not possible to thread the butadiyne bis(butadiyne)Pt(dppp) complex (Appendix B), it seems reasonable that use of longer derivatives, like the bis(hexatriyne)Pt complex, may result in threading of the terminal alkyne. The same precursor bis(hexatriyne)Pt complex could be used for stepwise construction of the building blocks of the square [5]catenane. The bending of the carbon chain from linearity in the corresponding cyclocarbon-based [5]catenane is small (less than 8° deviation from linearity, based on the polygonal geometry) which implies that strain energy must not have significant destabilizing effect on the cyclocarbon, which, in addition with mechanical insulation, may stabilize the molecule enabling its isolation.

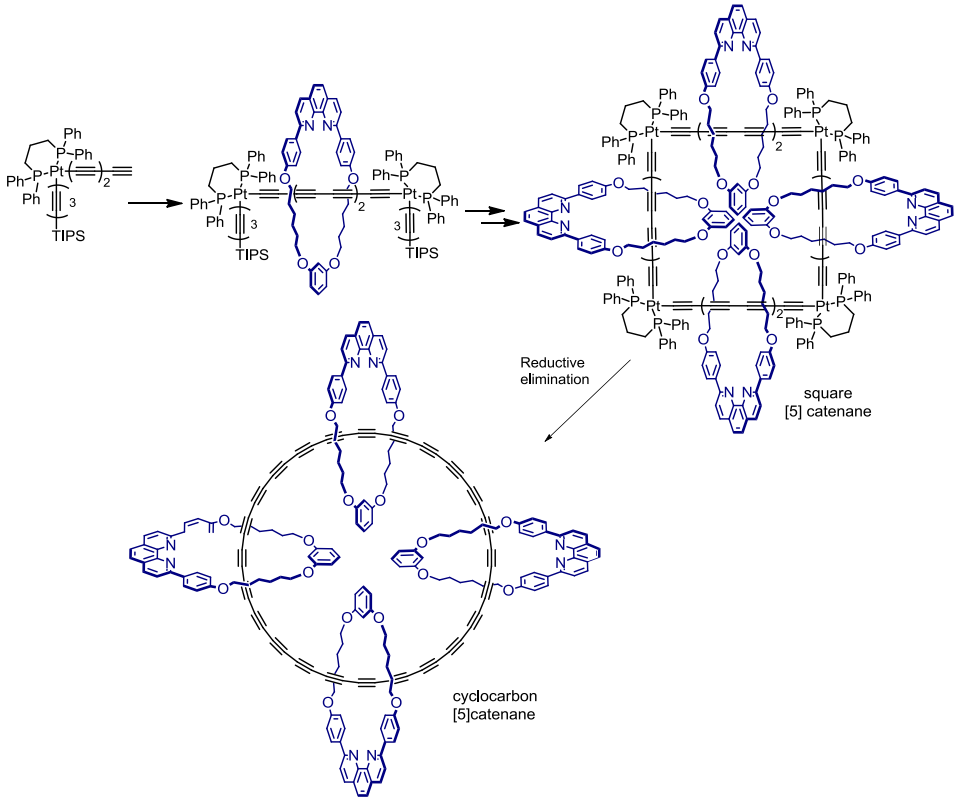

Scheme 2 A possible route to synthesize 48 *sp*[1] carbon-based [5]catenane.

The interest in mechanically insulated polyynes does not concern only the cyclic structures. The route towards the longer linear polyyne rotaxanes can be extended beyond what has been done in this thesis. Particularly, we are interested in preparation of polyyne polyrotaxanes. In the ideal case, we would like to have temporary stoppering group on the terminus of the polyynes. By saying "temporary" we mean a bulky functional group, which can be attached and detached to the polyyne chain at the particular step of the synthesis, without destroying the polyyne chain upon removal. Interestingly, Diederich and Rubin[7] reported a method of clipping the polyyne chains with cobalt carbonyl complexes (Scheme 3).

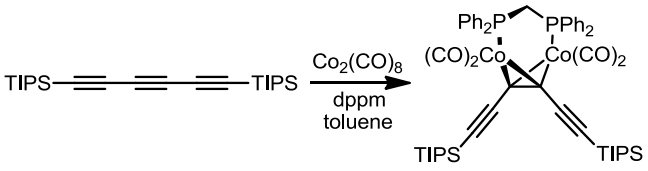

Scheme 3 Synthesis of the cobalt complex reported by Diederich and Rubin (dppm = 1,2-bis(diphenyl-phosphino)methane).[7]

This method could be adopted for the synthesis of polyrotaxanes using the dicobalt complex as a temporary stoppering group. After threading, cobalt could be removed by oxidation, alkyne-ligand exchange or by flash vacuum pyrolysis.[3]

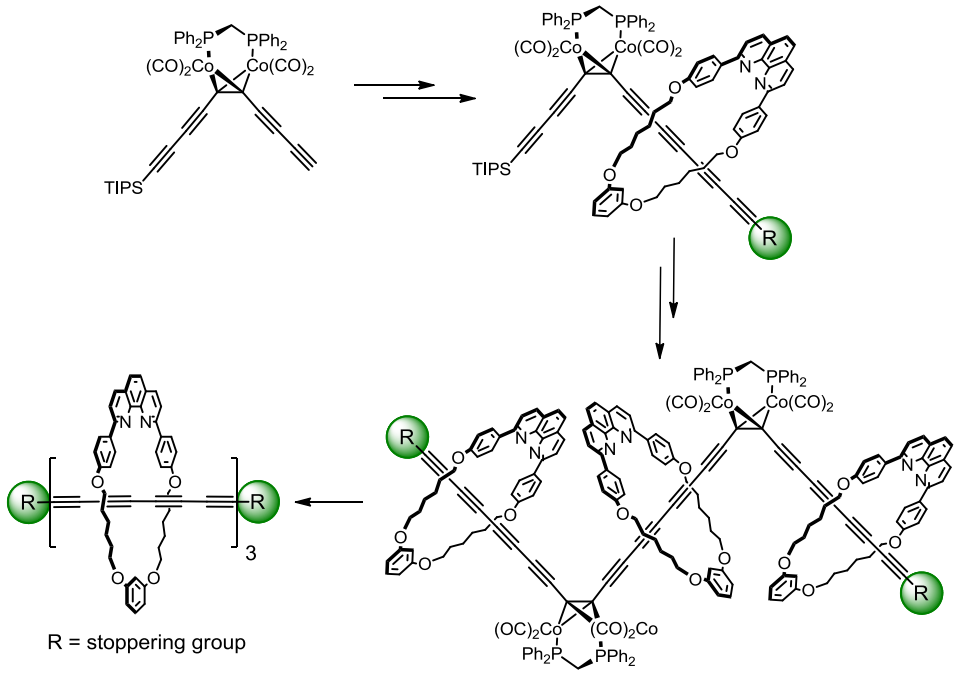

Scheme 4 A suggested synthetic route towards polyyne polyrotaxanes suing clipping strategy.

Dicobalt complexes, bridged with the dppm ligand are stable towards desilylation or coupling reactions, which means that complexes with different alkyne chains can be readily prepared. For example, one of the suggested cobalt complexes could be threaded with a macrocycle from one terminus using another bulky polyyne as a stoppering group (Scheme 4). Farther removal of the second TIPS group and the homocoupling reaction in a presence of the macrocycle would result in the zigzag architecture. The final treatment of the zigzag molecule with suitable oxidant, should give a polyyne polyrotaxane. The Pt complexes, discussed above, also could be exploited for the preparation of polyyne polyrotaxanes in the similar way of chain elongation/threading→Pt elimination.

The discussed approaches and strategies show that this project has much scope for continuation, and the mechanical encapsulation of polyynes has great potential for the design and preparation of fascinating new carbon-rich scaffoldings.

References

1. Chalifoux, W. A.; Tykwinksi, R, R. *Nat. Chem.* **2010**, *2*, 967–971.
2. Tobe, Y.; Umeda, R.; Iwasa, N.; Sonoda, M. *Chem. Eur. J.* **2003**, *9*, 5549–5559.
3. Diederich, F.; Rubin, Y. *Angew. Chem. Int. Ed. Eng*. **1992**, *31*, 1101–1123.
4. McElvany, S. W.; Ross, M. M.; Goroff, N. S.; Diederich, F. *Science* **1993**, *259*, 1594–1596.
5. Janka, M.; Anderson, G. K.; Rath, N. P. *Organometallics* **2004**, *23*, 4382-4390.
6. (a) Fuhrmann, G.; Debaerdemaekerb, T.; Bäuerle, P. *Chem. Commun*. **2003**, 948–949. (b) Bäuerle, P.; Ammann, M.; Wilde, M.; Götz, G.; Mena-Osteritz, E.; Rang, A.; Schalley, C. A. *Angew. Chem. Int. Ed.* **2007**, *46*, 363–368.
7. Rubin, Y.; Knobler, C. B.; Diederich, F. *J. Am. Chem. Soc.* **1990**, *112*, 4966–4968.

Appendix A Photophysics of small $Re(CO)_3Cl$·rotaxane H⊂M2(Re)

As was shown in Chapter 4, the triplet energy transfer from the ^{3}MLCT excited state of $Re(CO)_3Cl$·macrocycle to the ground S_0 state hexayne in the **H⊂M(Re)** takes place by Dexter mechanism. This implies that closer contact between two donor acceptor molecules would increase the overlap of wavefunctions thus increasing the rate of the ^{3}EET. Therefore, we prepared $Re(CO)_3Cl$ complex of **2b⊂M2** rotaxane (see Chapter 2 for the synthesis of **2b⊂M2** rotaxane), in which significantly smaller macrocycle provides tighter contact between CO and C≡C moieties (Figure 1). For convenience, $Re(CO)_3Cl$ complex of **2b⊂M2** rotaxane will be referred as **H⊂M2(Re)**. This new complex was interesting to us for the study of vibrational coupling of rotaxane components[1] using 2D IR spectroscopy.[2] However, the 2D IR spectroscopy of $Re(CO)_3Cl$·rotaxane complexes did not reveal ground state vibrational coupling between polyyne and Re-CO chromophores. We do not show the details of the 2D IR experiments here due to lack of interesting results, but the photophysics of the **H⊂M2(Re)** rotaxane will be discussed.

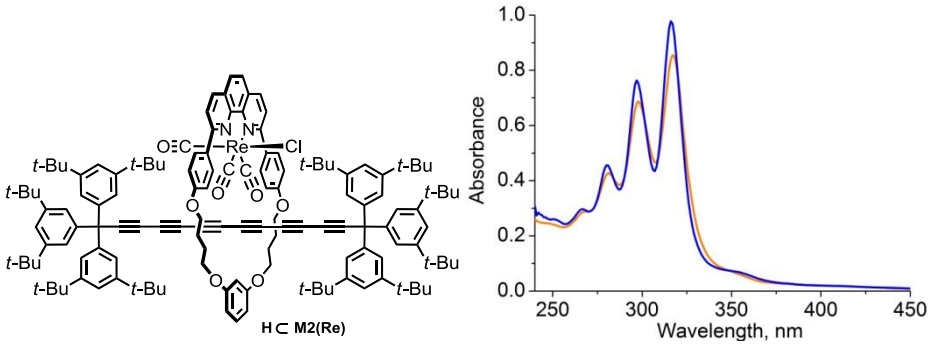

Figure 1 Structure of **2H⊂M2(Re)** rotaxane and the UV-Vis absorption spectrum (orange) in comparison with the absorption spectrum of **H⊂M(Re)** (Chapter 4).

The UV-Vis absorption spectra of both $Re(CO)_3Cl$ rotaxanes are shown in Figure 1. Compared to the **H⊂M(Re)** (Chapter 4), the lowest energy absorption band of hexayne in the spectrum of the **H⊂M2(Re)** rotaxane is 1 nm red-shifted.

The TRIR spectral features of small $Re(CO)_3Cl$·rotaxane **H⊂M2(Re)** are similar to those of **H⊂M(Re)**. When the **B⊂M2(Re)** was excited at 360 nm, the triplet excited $Re(CO)_3Cl$·macrocycle band around ~1450 cm^{-1} decays to give rise to the triplet hexayne band at ~1600 cm^{-1} (Figure 2).

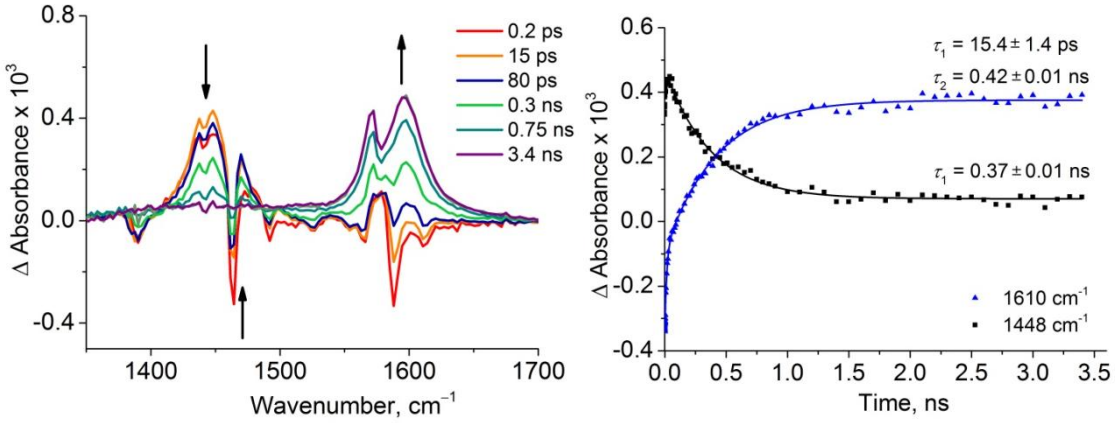

Figure 2 TRIR spectra of **H⊂M2(Re)** in fingerprint region and the kinetics of the ^{3}EET. (Excitation λ = 360 nm, laser energy = 120 nJ)

The negative band at 1464 cm^{-1} recovers within the first 25 ps. The triplet polyyne band at 1610 cm^{-1} rises on the top of the second bleach at 1608 cm^{-1}. Due to the overlap of the two negative and positive bands the growth of the triplet polyyne band seems biexponential fashion: τ_1 = 15.4 ± 1.4 ps (A_1 = 0.34), τ_2 = 0.42 ± 0.01 ns (A_2 = 0.66). The slow component of the kinetics of this band and the rate of the triplet polyyne growth (τ_1 = 0.37 ± 0.01 ns) have similar values.

The bleach recovery rate at 1608 cm^{-1} in both Re(CO)$_3$Cl rotaxanes are similar (^{3}IL→^{3}MLCT conversion, cooling, etc. about 15 ps), which is because the Re-chromophore is the same in both Re(CO)$_3$Cl·rotaxanes. In the small **H⊂M2(Re)** rotaxane the triplet EET is almost 4 time faster (0.42 ns vs.1.5 ns) compared to the **H⊂M(Re)** as it was expected.

The high frequency region of the TRIR spectra show three bleached ground state νCO bands and two transient bands upon excitation (Figure 3). The first transient broad band at 1955 cm^{-1} is predominantly Gaussian by shape, within 25 ps moves to 1969 cm^{-1} and its intensity increases 1.4 times without significant band narrowing. The second broad transient band (Gaussian shape) partially overlaps with A'(1) bleach at 2018 cm^{-1} moves to 2051 cm^{-1}, increases in intensity about 2.1 times and narrows ~70% changing to Lorentzian shape. All this spectral changes are attributed to the ^{3}IL→^{3}MLCT conversion and vibrational energy relaxation.

Another noteworthy feature is that ground state νC≡C stretching is visible as a positive band upon excitation of the Re(CO)$_3$Cl· rotaxane at 350 nm, showing that the excited state Re(CO)$_3$Cl· macrocycle

perturbs the ground state electrons of hexayne π system causing enhanced absorption, similar to the rotaxane **H⊂M(Re)**

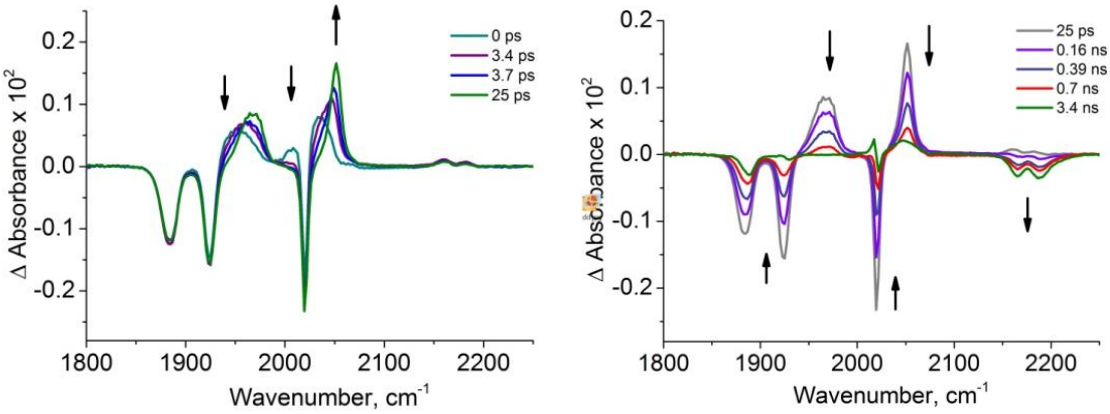

Figure 3 TRIR spectra of **H⊂M2(Re)** in high frequency region at early (left) and late time delay (right). (Excitation λ = 360 nm, laser energy = 120 nJ, Solvent CH_2Cl_2)

Later, the ^{3}MLCT $Re(CO)_3Cl$·macrocycle sensitizes the ground state hexayne. The kinetics of the CO and C≡C bands are depicted below (Figure 4). The excited state $Re(CO)_3Cl$·macrocycle exhibits two bands at 1968 cm^{-1} and 2052 cm^{-1}, with identical decay kinetics (τ ~ 0.4 ns), which matches to the kinetics in fingerprint region.

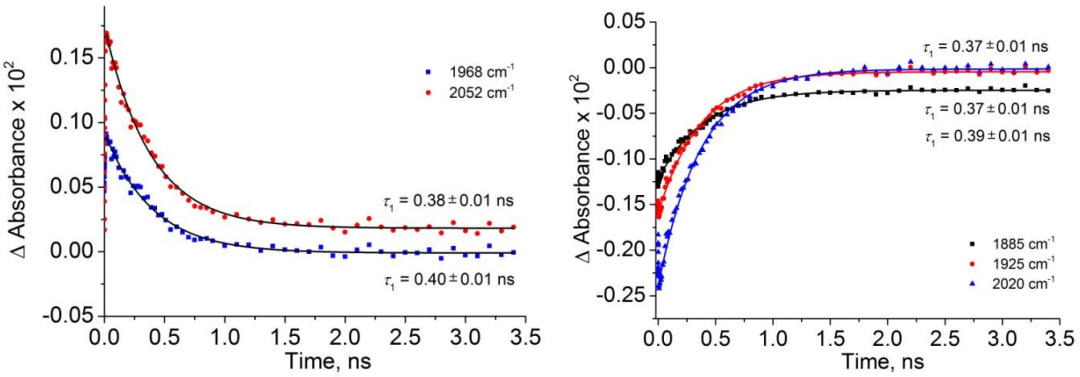

Figure 4 ^{3}EET kinetics in **H⊂M2(Re)** estimated from the transient bands decay (left) and bleached νCO recovery (right).

In the similar way, the recovery of all three νCO bands has the same time evolution with τ value similar to that one of positive bands decay (~ 0.4 ns, Figure 4).

A surprising feature was the rate of the bleaching of the C≡C band: its time constant was 0.48 ns (Figure 5), which is slower than the decay of the triplet state $Re(CO)_3Cl$·macrocycle (0.4 ns, Figure 4).The explanation of this 20% difference in sates is not clear.

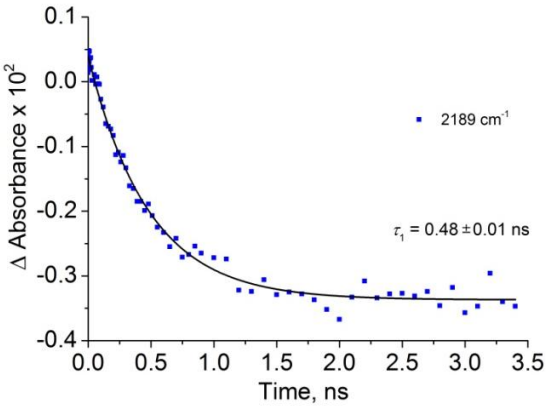

Figure 5 The kinetics of the bleaching of νC≡C band due to ^{3}EET in the **H⊂M2(Re)** rotaxane.

Except this small difference, the general conclusion is that in te small $Re(CO)_3Cl$·rotaxane **H⊂M2(Re)**, the triplet energy transfer is 4 time faster compared to the bigger $Re(CO)_3Cl$· rotaxane **H⊂M(Re)**.

Synthesis of the 2b⊂M2(Re) rotaxane

Rotaxane **2b⊂M2** (16.0 mg, 8.5 μmol) was dissolved in toluene (4 mL) and $Re(CO)_5Cl$ (3.7 mg, 10.2 μmol) was added. The reaction mixture was stirred under reflux 3 h, cooled to 20 ºC and solvent was removed *in vacuo*. The product was purified by column chromatography (silica, hexane/EtOAC = 20:1 gradually to EtOAc) followed recrystallization from hexane which yielded the product as yellow crystalline solid (11 mg, 59 %). R_f = 0.7 (hexane/EtOAc/MeOH = 10:2:1). ^{1}H NMR (500 MHz, 298 K, CD_2Cl_2) 8.6 (d, 2H), 8.06 (s, 2H, Ha), 8.07 (s, 2H), 8.03 (d. 2H), 7.75 (d, 2H), 7.57 (d, 2H), 7.27 (t, 3H), 7.24 (t, 3H), 7.19 (d, 2H) 7.06 (m, 3H), 6.94 - 6.89 (dd, 12H), 6.64 (t, 1H), 6.47–6.46 (dd, 2H), 4.36 (m, 2H), 4.17-3.99 (m, 6H), 2.11–1.82 (m, 8H), 1.53 (s, 8H), 1.17 (s, 54H), 1.12 (s, 54H). ^{13}C NMR (125 MHz, CD_2Cl_2, 298 K) 195.6, 193.6, 164.4, 161.1, 160.8, 150.8. 150.7, 149.4, 143.7, 143.7, 138.2, 134.2, 133,6, 130.3, 130.1, 129.8, 127.0, 125.9, 123.9, 123.9, 121.0, 120.9, 118.3, 112.6, 109.1, 100.4, 86.3, 70.1, 69.5, 68.7, 68.3, 65.0, 64.8, 64.7, 64.1, 64.0, 63.8, 63.2, 63.1, 57.8, 57.7, 35.1, 35.1, 31.5, 31.4, 26.2, 25.2, 23.1, 14.3. UV-vis (CH_2Cl_2) λ / nm (ε / M^{-1} cm^{-1}) 317 (186000), 298 (150000), 280 (93000), 267 (22000); UV-vis (THF) λ / nm (ε / M^{-1} cm^{-1}) 316 (216000), 297 (167000), 280 (101000), 266 (56000).

References

1. (a) Noda, I. *Appl. Spectrosc.* **1990**, *44*, 550–561. (b) Noda, I. *J. Am. Chem. Soc.* **1989**, 111, 8116–8118.
2. Bodis, P.; Panman , M. R.; Bakker , B. H.; Mateo-Alonso, A.; Prato, M.; Jan Buma, W.; Brouwer, A. M.; Kay, E. R.; Leigh, D. A.; Woutersen, S. *Acc. Chem. Res.* **2009**, *42*, 1462–1469.

Appendix B Pt-alkyne complexes for rotaxane synthesis

The Pt(II) phosphine acetylides have been developed for application as molecular wires,[1] luminescent,[2] charge-transport[3] materials, and solar cell dyes.[4] Additionally, *cis*-Pt(alkynide) complexes have been used to prepare carbon-rich molecular squares, such as the complex **B1** (Scheme 1).[5]

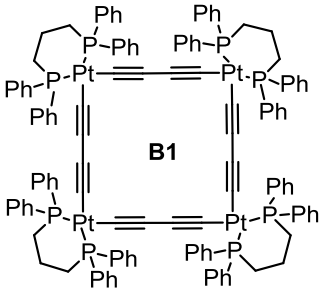

Scheme 1 Structure of Pt-alkyne complex.

There was an interesting report by Bäuerle et al., presenting a Csp-Csp bond formation from Pt σ-acetylide complexes.[6] In their procedure, they carried out 1,1-reductive elimination of the Pt(dppp) "corners" from bismetallacycle **B2** under simultaneous C–C bond formation by treatment with iodine (Scheme 2).

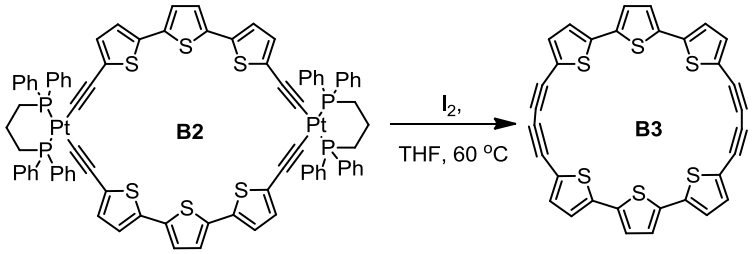

Scheme 2 Bäuerle's methodology of Csp-Csp bond formation from Pt σ-acetylide complex.[6a]

We envisioned that this novel methodology could be exploited in the synthesis of polyyne rotaxanes. The *cis*-Pt-complex with two terminal acetylene chains, readily prepared from *cis*-Pt(Cl)$_2$ complexes **B4**,[7] could perhaps be double threaded, resulting in a right angle complex, the subsequent elimination of metal would give the double-threaded polyyne [3]rotaxane (Figure 1).

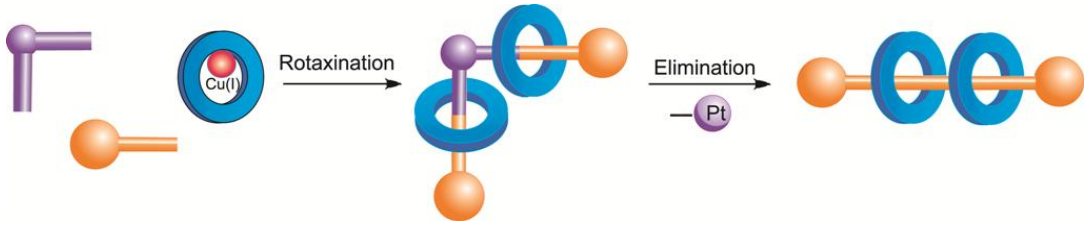

Figure 1 Schematic representation of the synthesis of polyyne [3]rotaxane via elimination of Pt metal.

The cis-$Pt(Cl)_2$ complex B4 was prepared by stirring a suspension of $PtCl_2$ and 1,3-bis(diphenylphosphino)propane (dppp) in $CHCl_3$ at 70 °C.8 The product **B4** was obtained in 92% yield (Scheme 3). The cis-bis(TIPS-acetylide)Pt(dppp) complex **B5** was prepared by reaction of TIPS-acetylene, in presence of Cu(I) salt and Et_3N in CH_2Cl_2, giving the product **B5** in 89% yield (Scheme 3).7

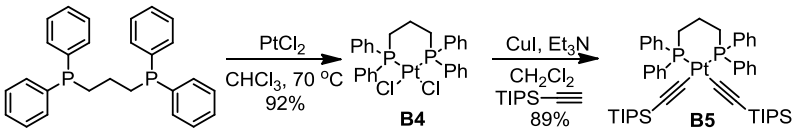

Scheme 3 Synthesis of the **B4** and **B5** complexes.

To our disappointment, all attempts to deprotect **B5** turn to be unsuccessful. First, it was tried by TBAF, stirring the reaction mixture in THF at room temperature (Scheme 4). Even after 24 h stirring the TLC analysis showed no reaction and the starting material was recovered. The same result was obtained when 10-fold excess of TBAF was used at 60 °C.

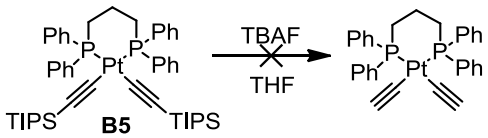

Scheme 4 Attempted deprotection of the **B5**.

Changing the solvent to CH_2Cl_2 did not give a better result. We tested the use of CsF instead of TBAF as a fluorine source, but again no reaction was observed.

It is possible that three bulky isopropyl groups are efficiently shielded by the phenyl groups of dppp moiety, leaving no space for the nucleophylic attack of F^-. An alternative approach could be the synthesis of less bulky, TMS-protected acetylide, however there was little hope that even in the case of successful removal of TMS groups it would be possible to thread the short acetylene end with a macrocycle. Thus, the bis(TMS-butadiyne)Pt(dppp) complex was prepared via lithium-halogen exchange (Scheme 5). The bis(TMS)butadiyne was lithiated by MeLi in THF, then this mixture was transferred through canula to the mixture of **B4**, CuI and Et_3N in deoxygenated THF. After stirring for one day, the reaction was stopped and the crude mixture was purified by column chromatography resulting in di-(**B6**) and monosubstituted (**B7**) complexes in 58% and 18% yield, respectively.

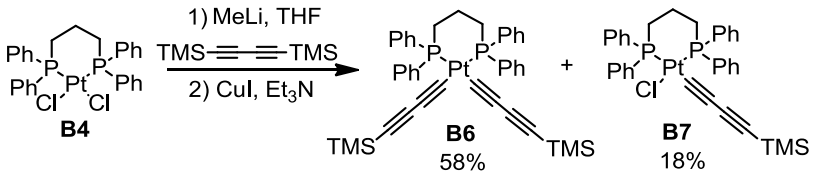

Scheme 5 Synthesis of TMS(butadiyne)Pt(dppp) complexes **B6** and **B7**.

Both **B6** and **B7** complexes can be tested for rotaxane synthesis. For the first trial, the **B7** was deprotected by K_2CO_3 in CH_3OH/THF mixture quantitatively (99%) (Scheme 6). The free butadiyne **B8** then was injected under the rotaxane synthesis conditions using CuI·**M4** macrocycle complex and supertrityl bromotriyne **3.1**. We specially chose cross-coupling reaction conditions (see Chapter 3), escaping from the use of oxidant (I_2) necessary for the homocoupling reaction. The reaction of the **B7** with iodine has not been tested but it was considered that Pt could be easily eliminated as in the case of bis(platinium)-macrocycle **B3** (Scheme 2).[6]

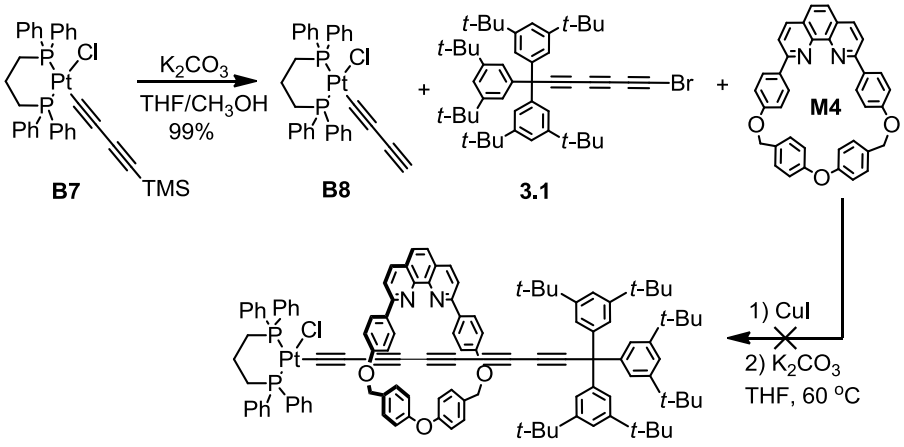

Scheme 6 Attempted synthesis of [2]rotaxane using monobutadiyne **B8**.

After 5 h stirring at 60 °C, the TLC showed complete consumption of **B8** and the reaction was quenched by aqueous KCN. On silica column three fractions were separated, however, none of them was the target rotaxane (analyzed by ^{1}H NMR and MALDI spectra).

Similarly, **B6** complex was deprotected (94%) and the corresponding bis(butadiyne)Pt(dppp) complex **B9** was subjected for the rotaxane synthesis. We tested the cross-coupling reaction with bromotriyne **3.1** using 2 eq. of CuI·macrocycle (**M1** or **M4**) complexes, however, disappointingly, no rotaxane molecule was isolated in either case (Scheme 7) despite complete consumption of the Pt complex **B9**.

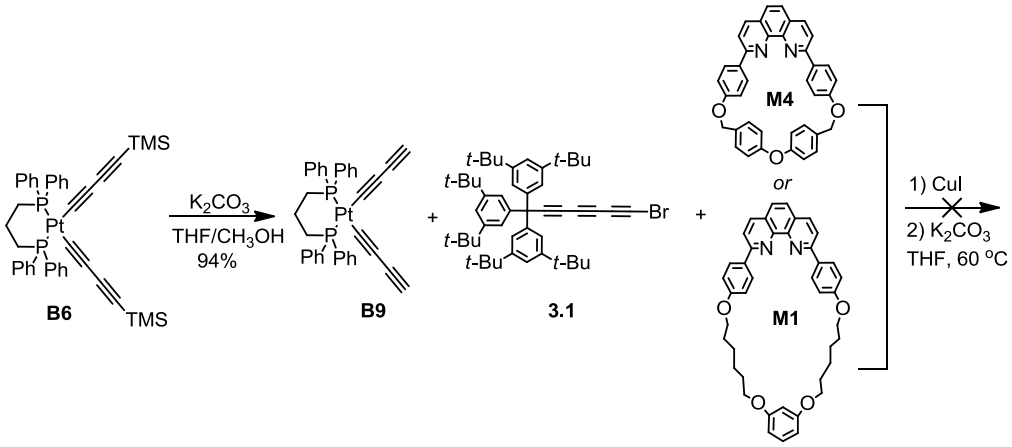

Scheme 7 Attempted synthesis of [3]rotaxane using bis(butadiyne)Pt(dppp) complex **B9**.

The reason for these unsuccessful trials is not understood. It is possible that butadiyne termini are sterically shielded by phenyl groups hindering the threading with the macrocycle. It could be useful to prepare bis(hexatriyne)Pt(dppp) complex in a similar way and test for the cross-coupling reaction with 3.1, but due to time restriction the fully exploration of this interesting route for polyyne rotaxanes has not been accomplished.

Synthesis of compounds

All compounds are characterized by NMR spectroscopy. ^{31}P NMR spectra were measured with proton decoupling.

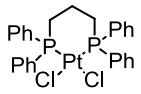

B4

B4: This compound was prepared according to the literature procedure.[8] To a suspension of $PtCl_2$ (0.30 g, 1.13 mmol) in chloroform (40 mL), a solution of dppm (0.465 g, 1.128 mmol) in chloroform (20 mL) was added. The reaction mixture was stirred at reflux for 3 h, and the clear solution turned cloudy. The solvent was removed and the white residue was extracted with CH_2Cl_2 (3 x 50 mL). The organic layers were combined and the solvent was removed giving product **B4** as a white solid (702 mg, 92 %). ^{1}H NMR (400 MHz, $CDCl_3$) 7.65 (q, J_1 = 8.1 Hz, J_2 = 2.8 Hz, 8H), 7.47–7.38 (m, 12H), 2.50 (m, 4H), 2.05 (m, 2H). ^{31}P {^{1}H} NMR (162 MHz, $CDCl_3$) –5.60 (J_{Pt-P} = 3408 Hz). As in lit.[8]

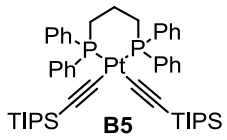

B5

B5: This compound was prepared according to the literature procedure.[7b] To a mixture of Pt(dppp)Cl_2 (**B4**, 50 mg, 73.8 μmol) CuI (5 mg, 26 μmol) and TIPS acetylene (33.6 mg, 41 μL, 184 μmol) in a degassed CH_2Cl_2 (10 ml), dry Et_3N (1 ml) was added under N_2 and the reaction mixture was stirred for 1 d at 20 ºC. To the reaction mixture water (1 mL) was added and the organic layer was separated and solvent was removed. The product **B5** was purified by column chromatography (silica, CH_2Cl_2) and obtained as a white solid (4 mg, 89%). ^{1}H NMR (400 MHz, $CDCl_3$) 7.76 (m, 8H), 7.25 (m, 12H), 2.25 (m, 4H), 1.89 (m, 2H), 074 (s, 6H), 072 (s, 36H). br. s, 8H), 7.32 (t, J = 7.2 Hz, 4H), 7.22 (t, j = 6.4 Hz, 8H), 2.72 (s, 4H), 2.09 (s, 2H), -0.08 (s, 18H). ^{13}C NMR (100 MHz, $CDCl_3$) 133.9, (m) 132.1, (q, J_1 = 9.6 Hz, J_2 = 55.9 Hz,), 130.3, 128.2 (t, $J_{C\text{-}P}$ = 5.2 Hz), 125.0, 124.8, 123.6, 123.4, 108,0, 107.9, 27.2 (pseudo-t, $J_{C\text{-}P}$ = 18.5 Hz), 20.4, 19.0, 11.8. ^{31}P {^{1}H} NMR (162 MHz, $CDCl_3$) –7.56 ($J_{Pt–P}$ = 2136 Hz).As in lit.[8]

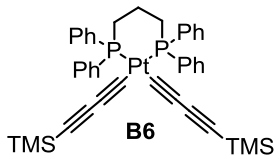

B6

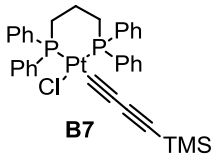

B7

A solution of bis(TMS)butadiyne (35.8 mg, 0.184 mmol) in THF (6 mL) was deoxygenated and LiMe/LiBr (8.4 μL, 0.184 mmol, in 2.2 M Et_2O) was added at 0 °C. The reaction mixture was stirred 30 min, A mixture of Pt(dppp)Cl_2 (**B4**) (50 mg, 73.8 μmol), CuI (5 mg, 26.2 μmol) and Et_3N (1 mL) in degassed THF (6 mL) was added at –40 °C. After stirring 1 day at 20 ºC, the reaction mixture was quenched with water (1 mL), HCl (2 M, 1 mL) and then the aqueous phase was neutralized by saturated aqueous $NaHCO_3$. Organic phase was separated and solvents were removed. The final crude mixture was purified by column chromatography (silica, CH_2Cl_2) affording **B6** (36 mg, 58%) and **B7** (10 mg, 18%) as light yellow solids.

B6: ^{1}H NMR (500 MHz, $CDCl_3$) 7.50 (br. s, 8H), 7.32 (t, J = 7.2 Hz, 4H), 7.22 (t, j = 6.4 Hz, 8H), 2.72 (s, 4H), 2.09 (s, 2H), -0.08 (s, 18H). ^{13}C NMR (125 MHz, $CDCl_3$) 133.7, 130.9, 128.4 (pseudo-t, $J_{C\text{-}P}$ = 5.4 Hz), 101.0 (q, J = 54.4 Hz), 92.7, 78.5, 31.1, 25.2 (pseudo-t, $J_{C\text{-}P}$ = 18.6 Hz), 19.4, 0.2. ^{31}P {^{1}H} NMR (162 MHz, $CDCl_3$) –8.90 ($J_{Pt–P}$ = 2184 Hz).

B7: ^{1}H NMR (500 MHz, CD_2Cl_2) 7.65 (t, J = 9.5 Hz, 8H), 7.48–7.40 (m, 12H), 2.51 (br. s, 4H), 1.99 (m, 2H), 0.09 (s, 9H). ^{13}C NMR (125 MHz, CD_2Cl_2) 133.8, (d, $J_{C\text{-}P}$ = 9.5 Hz), 131.4, 130.6 (q, J = 26.7 Hz), 128.8 (d, $J_{C\text{-}P}$ = 8.5 Hz), 100.2 (q, J = 55.6 Hz), 97.6 (q, J = 55.9 Hz), 92.5-90.8 (m), 79.4, 71.5 (q, J = 13.4 Hz), 68.1, 61.8, 31.01, 25.6 (m), 19.9 (pseudo-t, $J_{C\text{-}P}$ = 6.6 Hz), 0.1. ^{31}P {^{1}H} NMR (162 MHz, $CDCl_3$) –6.0 ($J_{Pt–P}$ = 2172 Hz).

References

1. (a) Diederich, F.; Faust, R.; Gramlich, V.; Seiler, P. *J. Chem. Soc. Chem. Commun*. **1994**, 2045–2046. (b) de Quadras, L.; Hampel, F.; Gladysz, J. A. *Dalton Trans*. **2006**, 2929–2936.

2. (a) Rogers, J. E.; Cooper, T. M.; Fleitz, P. A.; Glass, D. J.; McLean, D. G. *J. Phys. Chem. A* **2002**, *106*, 10108–10115. (b) Tao, C. H.; Zhu, N.; Yam, V. W. W. *Chem. Eur. J*. **2005**, *11*, 1647–1657.

3. Schull, T. L.; Kushmerick, J. G.; Patterson, C. H.; George, C.; Moore, M. H.; Pollack, S. K.; Shashidhar, R. *J. Am. Chem. Soc.* **2003**, 125, 3202–3203. (b) Jones, S. C.; Coropceanu, V.; Barlow, S.; Kinnibrugh, T.; Timofeeva, T.; Bredas, J.-L.; Marder, S. R. *J. Am. Chem. Soc.* **2004**, 126, 11782–11783.

4. Guo, F.; Kim, Y.-G.; Reynolds, J. R.; Schanze, K. S. *Chem. Commun*. **2006**, 1887–1889.

5. Janka, M.; Anderson, G. K.; Rath, N. P. *Organometallics* **2004**, *23*, 4382–4390.

6. (a) Fuhrmann, G.; Debaerdemaekerb, T.; Bäuerle, P. *Chem. Commun*. **2003**, 948–949. (b) Bäuerle, P.; Ammann, M.; Wilde, M.; Götz, G.; Mena-Osteritz, E.; Rang, A.; Schalley, C. A. *Angew. Chem. Int. Ed.* **2007**, *46*, 363–368.

7. (a) Bruce, M. I.; Costuas, K.; Halet, J.-F.; Hall, B. C.; Low, P. J.; Nicholson, B. K.; Skelton, B. W.; White, A. H. *J. Chem. Soc., Dalton Trans*. **2002**, 383–398. (b) Shavaleev, N. M.; Adams, H.; Best, J.; Weinstein, J. A. *J. Organometallic Chem.* **2007**, *692*, 921–925. (c) Sadowy, A. L.; Ferguson, M. J.; McDonald, R.; Tykwinski, R. R. *Organometallics* **2008**, *27*, 6321–6325.

8. Abdullah, B. H.; Abdullah, M. A.; Al-Jibori, S. A; Al-Allaf, T. A. K. *Asian J. Chem.***2007**, *2*, 1334–1340.